ISSN 0021-9673

VOL. 662 NO. 1 FEBRUARY 18, 1994

JOURNAL OF CHROMATOGRAPHY A

INCLUDING ELECTROPHORESIS AND OTHER SEPARATION METHODS

ELSEVIER

JOURNAL OF CHROMATOGRAPHY A

INCLUDING ELECTROPHORESIS AND OTHER SEPARATION METHODS

Scope. The *Journal of Chromatography A* publishes papers on all aspects of **chromatography, electrophoresis** and related methods. Contributions consist mainly of research papers dealing with chromatographic theory, instrumental developments and their applications. In the *Symposium volumes*, which are under separate editorship, proceedings of symposia on chromatography, electrophoresis and related methods are published. *Journal of Chromatography B: Biomedical Applications* —This journal, which is under separate editorship, deals with the following aspects: developments in and applications of chromatographic and electrophoretic techniques related to clinical diagnosis or alterations during medical treatment; screening and profiling of body fluids or tissues related to the analysis of active substances and to metabolic disorders; drug level monitoring and pharmacokinetic studies; clinical toxicology; forensic medicine; veterinary medicine; occupational medicine; results from basic medical research with direct consequences in clinical practice.

Submission of Papers. The preferred medium of submission is on disk with accompanying manuscript (see *Electronic manuscripts* in the Instructions to Authors, which can be obtained from the publisher, Elsevier Science B.V., P.O. Box 330, 1000 AH Amsterdam, Netherlands). Manuscripts (in English; *four* copies are required) should be submitted to: Editorial Office of *Journal of Chromatography A*, P.O. Box 681, 1000 AR Amsterdam, Netherlands, Telefax (+31-20) 5862 304, or to: The Editor of *Journal of Chromatography B: Biomedical Applications*, P.O. Box 681, 1000 AR Amsterdam, Netherlands. Review articles are invited or proposed in writing to the Editors who welcome suggestions for subjects. An outline of the proposed review should first be forwarded to the Editors for preliminary discussion prior to preparation. Submission of an article is understood to imply that the article is original and unpublished and is not being considered for publication elsewhere. For copyright regulations, see below.

Publication information. *Journal of Chromatography A* (ISSN 0021-9673): for 1994 Vols. 652–682 are scheduled for publication. *Journal of Chromatography B: Biomedical Applications* (ISSN 0378-4347): for 1994 Vols. 652–662 are scheduled for publication. Subscription prices for *Journal of Chromatography A*, *Journal of Chromatography B: Biomedical Applications* or a combined subscription are available upon request from the publisher. Subscriptions are accepted on a prepaid basis only and are entered on a calendar year basis. Issues are sent by surface mail except to the following countries where air delivery via SAL is ensured: Argentina, Australia, Brazil, Canada, China, Hong Kong, India, Israel, Japan, Malaysia, Mexico, New Zealand, Pakistan, Singapore, South Africa, South Korea, Taiwan, Thailand, USA. For all other countries airmail rates are available upon request. Claims for missing issues must be made within six months of our publication (mailing) date. Please address all your requests regarding orders and subscription queries to: Elsevier Science B.V., Journal Department, P.O. Box 211, 1000 AE Amsterdam, Netherlands. Tel.: (+31-20) 5803 642; Fax: (+31-20) 5803 598. Customers in the USA and Canada wishing information on this and other Elsevier journals, please contact Journal Information Center, Elsevier Science Inc., 655 Avenue of the Americas, New York, NY 10010, USA, Tel. (+1-212) 633 3750, Telefax (+1-212) 633 3764.

Abstracts/Contents Lists published in Analytical Abstracts, Biochemical Abstracts, Biological Abstracts, Chemical Abstracts, Chemical Titles, Chromatography Abstracts, Current Awareness in Biological Sciences (CABS), Current Contents/Life Sciences, Current Contents/Physical, Chemical & Earth Sciences, Deep-Sea Research/Part B: Oceanographic Literature Review, Excerpta Medica, Index Medicus, Mass Spectrometry Bulletin, PASCAL-CNRS, Referativnyi Zhurnal, Research Alert and Science Citation Index.

US Mailing Notice. *Journal of Chromatography A* (ISSN 0021-9673) is published weekly (total 52 issues) by Elsevier Science B.V., (Sara Burgerhartstraat 25, P.O. Box 211, 1000 AE Amsterdam, Netherlands). Annual subscription price in the USA US$ 4994.00 (US$ price valid in North, Central and South America only) including air speed delivery. Second class postage paid at Jamaica, NY 11431. **USA POSTMASTERS**: Send address changes to *Journal of Chromatography A*, Publications Expediting, Inc., 200 Meacham Avenue, Elmont, NY 11003. Airfreight and mailing in the USA by Publications Expediting.

See inside back cover for Publication Schedule, Information for Authors and information on Advertisements.

0021-9673/94/$07.00

Printed in the Netherlands

VOL. 662, NO. 1 JOURNAL OF CHROMATOGRAPHY A FEBRUARY 18, 1994

CONTENTS

(Abstracts/Contents Lists published in Analytical Abstracts, Biochemical Abstracts, Biological Abstracts, Chemical Abstracts, Chemical Titles, Chromatography Abstracts, Current Awareness in Biological Sciences (CABS), Current Contents/Life Sciences, Current Contents/Physical, Chemical & Earth Sciences, Deep-Sea Research/Part B: Oceanographic Literature Review, Excerpta Medica, Index Medicus, Mass Spectrometry Bulletin, PASCAL-CNRS, Referativnyi Zhurnal, Research Alert and Science Citation Index)

REGULAR PAPERS

Column Liquid Chromatography

Gas Chromatography

(Continued overleaf)

Contents (continued)

JOURNAL OF CHROMATOGRAPHY A

VOL. 662 (1994)

JOURNAL OF CHROMATOGRAPHY A

INCLUDING ELECTROPHORESIS AND OTHER SEPARATION METHODS

ELSEVIER

AMSTERDAM — LONDON — NEW YORK — TOKYO

0021-9673/94/$07.00

Printed in the Netherlands

Journal of Chromatography A, 662 (1994) 1–12
Elsevier Science B.V., Amsterdam

CHROM. 25 717

Computer simulation study of multi-detector size-exclusion chromatography of branched molecular mass distributions

Christian Jackson

E.I. du Pont de Nemours and Company, Central Research and Development, Experimental Station, P.O. Box 80228, Wilmington, DE 19880-0228 (USA)

(First received August 10th, 1993; revised manuscript received October 5th, 1993)

ABSTRACT

Size-exclusion chromatography (SEC) provides a rapid method for determining molecular mass distributions relative to standard calibration materials. If light-scattering and viscosity detectors are used independent measurements of molecular mass and size can be obtained directly, and these can be used to estimate the distribution of branching across the molecular mass distribution. In order to study the effect of branching on the detector signals and the calculated results a computer simulation of the multiple detector SEC analysis of randomly branched polymers was developed. The model is described and results for different amounts of branching, different extents of reaction, and different models of the hydrodynamic size are discussed.

INTRODUCTION

The integration of molecular mass-sensitive detectors with size-exclusion chromatography (SEC) increases the amount of information that can be determined in the analysis. Measurement of the light-scattering intensity and the sample concentration enables the molecular mass distribution (MMD) to be determined directly without column calibration. These data can be combined with the universal calibration curve describing hydrodynamic size as a function of elution volume, to determine the intrinsic viscosity at each elution volume element. Measurement of the specific viscosity, using a continuous viscometer, and sample concentration enables the intrinsic viscosity distribution to be determined directly without column calibration. Universal calibration can then be used to calculate the MMD [1–4].

If light-scattering (LS) and viscosity (Visc) detectors are used, both molecular mass and intrinsic viscosity distributions can be measured directly. This method is particularly suited to the characterization of polymer conformation and branching because the relationship between molecular mass and molecular size, determined from the intrinsic viscosity, is measured across the MMD. Changes in this relationship can be related to the amount of branching or change in conformation [5,6].

Unfortunately, because both branching and molecular mass affect the molecular hydrodynamic size, the one-dimensional size-exclusion separation no longer gives full resolution of the MMD. Instead, only a partial resolution is possible, with the possibility that branched polymer molecules may be unresolved from linear molecules with a different molecular mass, but the same hydrodynamic size.

In addition to the problem of SEC resolution, the LS detector and the viscometer respond differently to branching. In general branching will increase molecular mass and thus the intensity of scattered light; however, the intrinsic viscosity of a branched polymer is less than that of

0021-9673/94/$07.00
SSDI 0021-9673(93)E1177-2

its linear analogue, and so the viscometer response is decreased relative to that for a linear molecule.

In order to gain a better understanding of how these factors affect the experiment and the possible errors involved in the calculated results we developed a computer simulation of the SEC–Visc–LS separation and analysis of a randomly branched condensation polymer.

METHODOLOGY

Molecular mass distribution model

The model MMD used is that developed by Stockmayer and also by Flory [7–9] using a mean-field approach. This model assumes equal intrinsic reactivities and excludes intramolecular reaction between finite species, and more sophisticated treatments have been developed. However, it provides a useful approximation, especially for low degrees of branching. In dilute solution measurements of branching we are interested in comparing the properties of the branched molecule to those of the linear molecule. As the Flory–Stockmayer model reduces to the most probable distribution for linear polymerizations both linear and branched MMDs can be simulated. This makes it preferable to more recent percolation models of branched MMDs [10,11]. The methods for calculating the experimental detector responses follow those developed previously for linear MMDs [12,13].

The model MMD used is for the random condensation of bifunctional monomers with a small amount of trifunctional monomers. This results in structures such as the one shown in Fig. 1.

If the molecular mass of each monomer is considered equal, then the mass fraction of molecules with n trifunctional monomers and l bifunctional monomers is given by

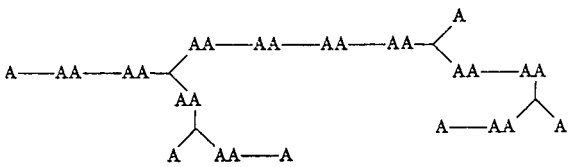

Fig. 1. Typical molecular structure produced by the polymerization model.

$$w_{n,l} = \frac{2(1-p)^2}{p(3-\rho)} \cdot \xi^n \eta^l (n+l)\omega_{n,l} \quad (1)$$

where p is the extent of the reaction, and ρ is the ratio of A groups belonging to branch units to the total number of A groups.

$$\rho = \frac{3N_0}{3N_0 + 2L_0} \quad (2)$$

N_0 and L_0 are the numbers of trifunctional and bifunctional monomers, respectively, and

$$\xi = p\rho(1-p) \quad (3)$$

$$\eta = (1-\rho)p \quad (4)$$

$$\omega_{n,l} = \frac{3(l+2n)!}{l!n!(n+2)!} \quad (5)$$

The monomer molecular mass was set arbitrarily at 100 g/mol. Mass fractions for up to 50 branch points per molecule ($n = 50$) were calculated for each MMD simulated.

If there are no trifunctional monomers eqn. 1 reduces to the equation for the most probable distribution.

$$w_l = (1-p)^2 l p^{(l-1)} \quad (6)$$

Size-exclusion chromatography model

SEC separates the sample by hydrodynamic volume rather than molecular mass, so that the MMD in eqn. 1 needs to be transformed into a hydrodynamic volume distribution [14].

Branching changes the relationship between hydrodynamic volume and molecular mass because a branched molecule is smaller than a linear molecule of the same molecular mass. This decrease in size is described by the branching index, g, which is the ratio of the mean square radius of gyration $\langle R_G \rangle^2$ of the branched molecule to that of the linear molecule with the same molecular mass (M) [15,16],

$$g = \left[\frac{\langle R_G \rangle^2_{\text{branched}}}{\langle R_G \rangle^2_{\text{linear}}} \right]_M \quad (7)$$

This ratio can be directly related to the number of branch points if the radius of gyration is measured under θ conditions, where the effect of excluded volume on the radius of gyration is apparently cancelled by Van der Waals attractions between segments of the chain. For exam-

ple, for a randomly branched polydisperse polymer with trifunctional branch points the weight-average value of g is given by

$$g_w = \frac{3}{n_w}\left(\frac{2+n_w}{n_w}\right)^{1/2} \cdot \ln\left(\frac{(2+n_w)^{1/2}+n_w)^{1/2}}{(2+n_w)^{1/2}-n_w^{1/2}} - 1\right) \quad (8)$$

where n_w is the number of trifunctional branch points per weight-average molecule.

The decrease in the hydrodynamic volume is described by g' which is defined as the decrease in intrinsic viscosity $[\eta]$ at a given molecular mass due to branching

$$g' = \left(\frac{[\eta]_{branched}}{[\eta]_{linear}}\right)_M \quad (9)$$

This is expected to be proportional to the decrease in the radius of gyration

$$g' = g^{\epsilon} \quad (10)$$

In this study it is assumed that the hydrodynamic radius remains proportional to the radius of gyration for branched polymers and so ϵ is set equal to 3/2. Experimentally its value is found to vary from 1/2 to 3/2. The effect of this variation in ϵ on the results is discussed below [17,18].

The SEC experiment is carried out using a thermodynamically good solvent and so it is assumed also that the radii of gyration of the branched and linear polymers have the same expansion factors. This assumes that the relationship between g and the number of branch points is insensitive to solvent quality and that the results based on eqns. 7 and 8 are still valid [19].

For the linear molecules the molecular mass is related to the column elution volume (V) by a calibration curve of the form

$$M_{n=0} = D_1 e^{-D_2 V} \quad (11)$$

where D_1 and D_2 describe the calibration curve for a given column set.

For branched molecules the calibration curve is shifted to larger elution volumes due to the reduction in size of the molecule. This shift is calculated from the equivalence of hydrodynamic sizes at each elution volume and by describing the relationship between intrinsic viscosity and molecular mass by the Mark–Houwink equation. If n is the number of branch points then from eqn. 9, the Mark–Houwink relationship for each n-mer, where an n-mer is the set of molecules with n trifunctional monomers and any number of bifunctional monomers, is given by

$$[\eta]_n = g_n' K M^a \quad (12)$$

where K and a are the Mark–Houwink coefficients for the linear polymer in the solvent. These are set to $1.2 \cdot 10^{-4}$ dl mol g^{-2} and 0.725, respectively, which are typical values for a polymer in a good solvent. The viscometric branching factor g_n' is calculated from eqns. 8 and 10.

The calibration curve for each n-mer can then be written as

$$M_n = [g']^{-1/(a+1)} D_1 e^{-D_2 V} \quad (13)$$

Eqn. 13 can be used to calculate the elution volume of each mass fraction in eqn. 1.

In SEC the mass fraction is measured as a function of the logarithm of molecular mass, so the mass fraction in eqn. 1 is modified to

$$w_{n,l}' = \frac{dM}{d \ln M} w_{n,l} \quad (14)$$

Light-scattering model

In the SEC–LS measurement the polymer can be considered to be at infinite dilution, in which case the intensity of scattered light at zero degrees with respect to the incident beam is directly proportional to the weight-average molecular mass of the polymer at each elution volume

$$I_{\theta=0} = K^* M_w w' \quad (15)$$

where K^* is an optical constant for the scattering system and w' is the mass fraction of all species at a given elution volume. All light scattering tracings shown correspond to the 0° scattering intensity.

Viscosity model

The specific viscosity of the eluting polymer is given by

$$\eta_{sp} = [\eta]_w w' \quad (16)$$

where the intrinsic viscosity of each species is

determined from eqn. 12. The sample is assumed to be at infinite dilution, and the intrinsic viscosity is the weight-average of the intrinsic viscosities of all the species present at a given elution volume.

RESULTS AND DISCUSSION

Results for individual n-mer distributions

The MMD of a branched polymer can be thought of as a set of individual MMDs of each n-mer, *i.e.*, the set of molecules containing n branch points. Fig. 2 shows typical refractometer tracings for fractions with $n = 0$, 1 and 2 branch points per molecule for an MMD with $p = 0.995$ and $\rho = 0.001$. Notice that with increasing number of branch points the mass fraction of n-mer decreases, the average molecular mass increases, and the elution volume decreases. The most highly branched material will be at the high end of the MMD, and the low end in this case is predominantly linear polymer. The molecular mass at each elution volume is also shown for the three fractions. At a given elution volume the n-mer with more branch points has a higher molecular mass than less branched molecules (eqn. 13).

Fig. 3 shows the Mark–Houwink plots for the three fractions. For a given molecular mass value, the intrinsic viscosity decreases with increasing number of branch points. However, according to the Zimm–Stockmayer theory the slope of the calibration curve is independent of the degree of branching for molecules with the same number of branch points but different molecular masses [15].

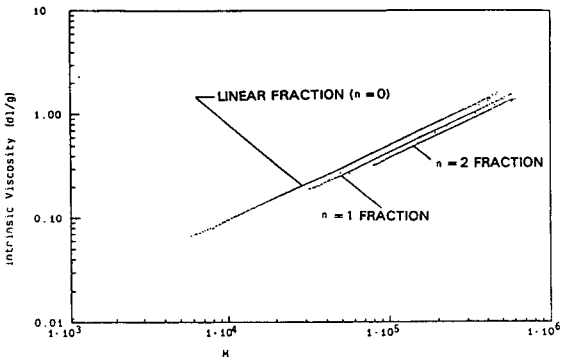

Fig. 3. Mark–Houwink plots of log M_w *vs.* log [η] for the fractions of a branched MMD with 0, 1 and 2 branch points per molecule.

Fig. 4 shows simulated detector tracings for the complete distribution of n-mers for the distribution with $p = 0.995$ and $\rho = 0.001$. For this amount of branching the responses are very similar for each detector and there is little difference between the three peak shapes. As in the study of linear polymers, the LS intensity peak and the specific viscosity peak are both shifted to earlier elution volumes than the refractometer peak as a result of their molecular mass sensitivity. The viscosity peak is not shifted as

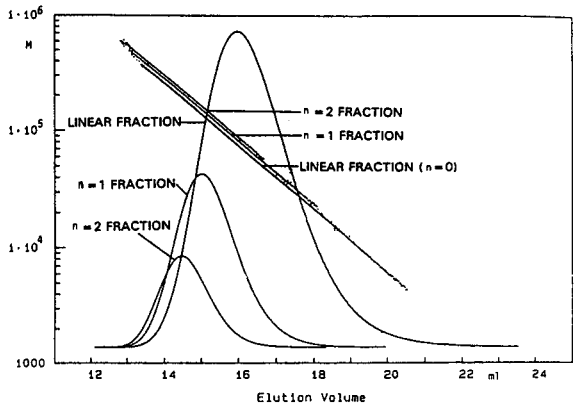

Fig. 2. Concentration detector response as a function of elution volume for fractions with 0, 1 and 2 branch points per molecule in a randomly branched MMD. The corresponding molecular mass calibration curves are also shown.

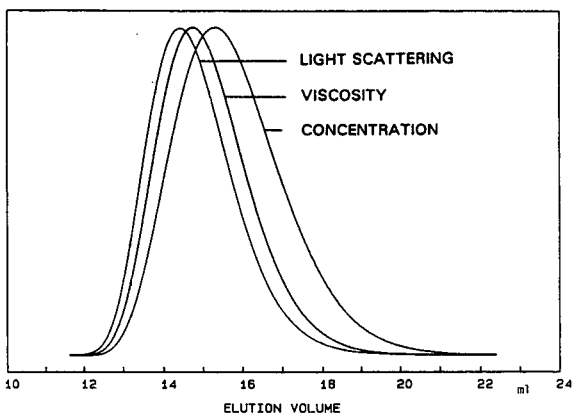

Fig. 4. Simulated tracings from the light-scattering, viscosity and refractive index detectors for a randomly branched MMD ($p = 0.995$, $\rho = 0.001$).

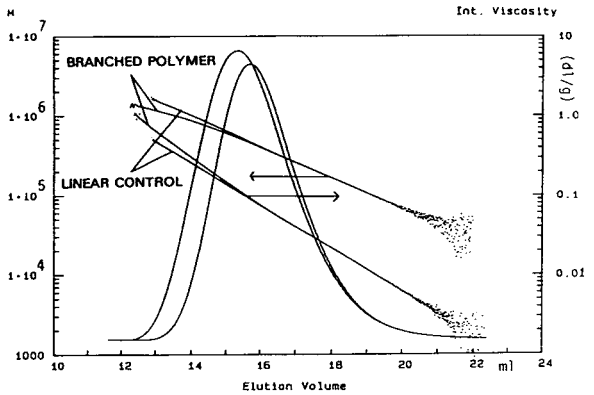

Fig. 5. Comparison of data from linear ($p = 0.995$) and branched ($p = 0.995$, $\rho = 0.001$) MMDs. The concentration detector responses are shown as well as the intrinsic viscosity and molecular mass at each elution volume.

much as the LS peak because it is less sensitive to molecular mass (eqn. 12). Branching causes slight differences in the relationship between the peak shapes and positions compared to those for the linear polymer which are discussed in detail below. However, in general the features for small amounts of branching are very similar to signals from linear MMDs. Fig. 5 shows calculated molecular masses and intrinsic viscosities as a function of elution volume for this distribution compared to a linear polymer at the same extent of reaction.

Fig. 6 shows the Mark–Houwink plot for the data. Although the slope for each fraction is a straight line the complete polymer gives a curved

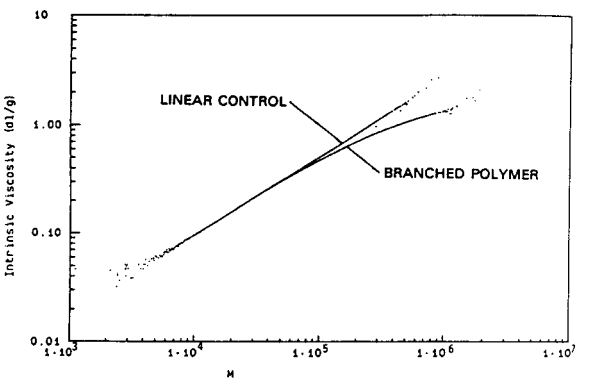

Fig. 6. Comparison of Mark–Houwink plots for the data from the linear and branched MMDs shown in Fig. 5.

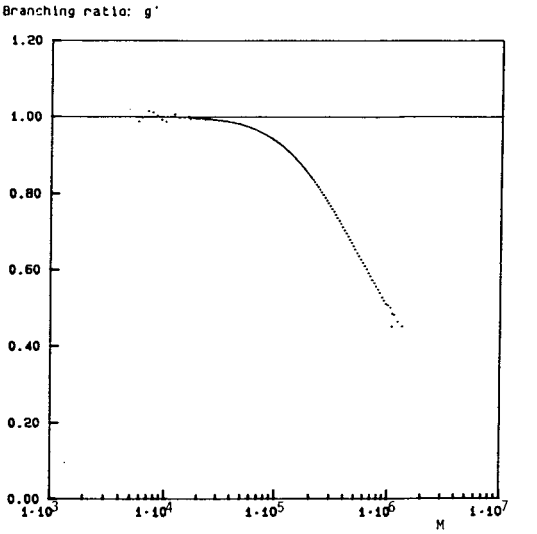

Fig. 7. Branching factor g' as a function of molecular mass for the branched polymer MMD shown in Figs. 3–5.

plot because different degrees of branching are not evenly distributed across the MMD. Fig. 7 shows the branching factor g' as a function of molecular mass. The value of the branching index is unity at the lowest molecular masses, reflecting the presence of predominantly linear polymer and rapidly decreases as molecular mass increases reflecting increased branching at the high end of the MMD.

Effect of extent of reaction

Six sets of data were generated at different extents of reaction ($p = 0.95$, 0.98, 0.99, 0.995, 0.9975 and 0.999) for a branched polymer with $\rho = 0.001$. Figs. 8, 9 and 10 show the refractometer, viscometer and light-scattering detector signals respectively, for the last five of these data sets. In each of the three figures the peak at the lowest elution volume corresponds to the greatest extent of reaction and highest molecular mass, while the peak at the highest elution volume is the lowest extent of reaction and molecular mass ($p = 0.98$). The refractometer tracings clearly show that as the reaction proceeds the MMD is broadened and increasingly skewed to the high-molecular-mass side of the distribution. The areas under the viscometer and LS tracings show the large increase in molecular

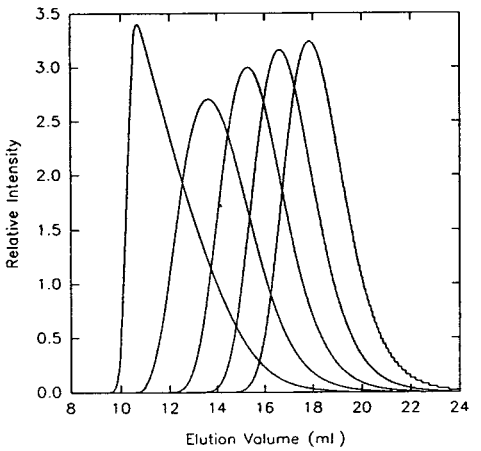

Fig. 8. Concentration detector tracings for branched MMDs at different extents of reaction for a branched polymer MMD with $\rho = 0.001$. From left to right the peaks correspond to $p = 0.999$, $p = 0.9975$, $p = 0.995$, $p = 0.990$ and $p = 0.980$.

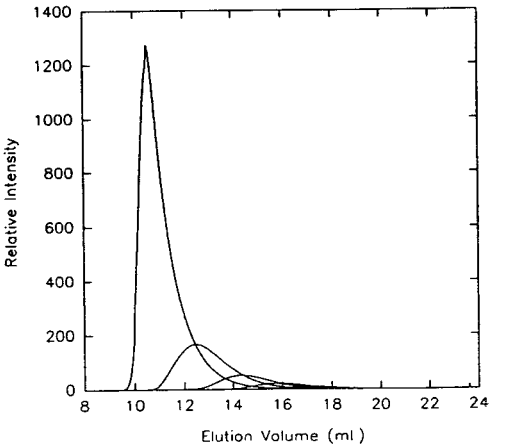

Fig. 10. Light-scattering detector tracings (0°) for branched MMDs at different extents of reaction for a branched polymer MMD with $\rho = 0.001$. From left to right the peaks correspond to $p = 0.999$, $p = 0.9975$, $p = 0.995$, $p = 0.990$ and $p = 0.980$.

mass and intrinsic viscosity of the polymer as the reaction proceeds. The viscosity signal increases less than the LS intensity because of the smaller intrinsic viscosity of branched molecules.

The highly skewed signals from the branched polymer at $p = 0.999$ is due to the proximity of the reaction to the gel point. Gelation occurs for this trifunctional case at a critical extent of reaction p_c given by

$$p_c = \frac{1}{1+\rho} \tag{17}$$

which for $\rho = 0.001$ is 0.999001, only slightly beyond $p = 0.999$. Since the polymer system is close to gelation, a significant mass fraction of the distribution is highly branched high-molecular-mass molecules concentrated at low elution volumes due to the poor resolution of SEC for such a mixture.

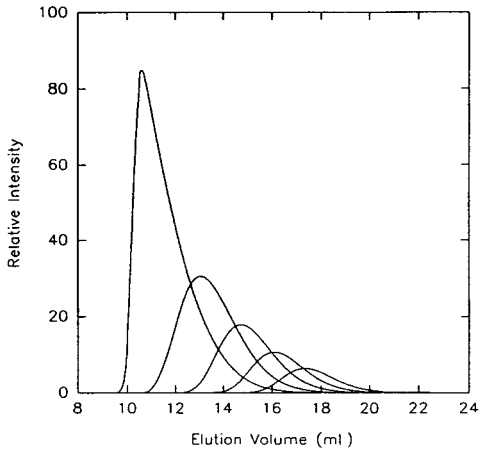

Fig. 9. Viscosity detector tracings for branched MMDs at different extents of reaction for a branched polymer MMD with $\rho = 0.001$. From left to right the peaks correspond to $p = 0.999$, $p = 0.9975$, $p = 0.995$, $p = 0.990$ and $p = 0.980$.

Fig. 11 shows the plots of the branching factor against the same molecular mass scale for the six extents of reaction listed above. As the reaction proceeds the degree of branching increases as does the molecular mass of the branched fractions. However, the slope of the curves at high molecular masses appears to be fairly constant. Table I lists the number-average, weight-average and z-average values of the branching factor for each value of the extent of reaction.

The number-average branching factor is defined as

$$g'_N = \frac{\sum_i N_i g'_i}{\sum_i N_i} \tag{18}$$

the mass-average branching factor is defined as

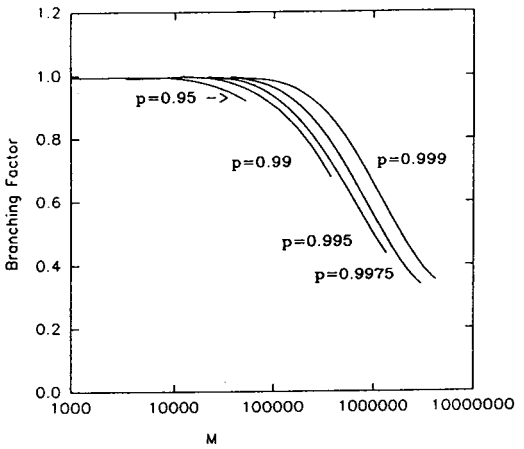

Fig. 11. Branching factor g' as a function of molecular mass for branched polymer MMD with different extents of reaction ($\rho = 0.001$).

$$g'_w = \frac{\sum_i M_i N_i g'_i}{\sum_i M_i N_i} \quad (19)$$

and the z-average branching index is as

$$g'_z = \frac{\sum_i M_i^2 N_i g'_i}{\sum_i M_i^2 N_i} \quad (20)$$

where i is the number of each elution volume element and N_i is the number of molecules in each volume element calculated from

$$N_i = \frac{M_i}{c_i} \quad (21)$$

TABLE I

NUMBER; WEIGHT- AND Z-AVERAGE BRANCHING INDICES FOR MMDs AT DIFFERENT EXTENTS OF REACTION AND $\rho = 0.001$

p	g'_n	g_w'	g'_z
0.9500	0.995	0.991	0.985
0.9800	0.985	0.979	0.950
0.9900	0.978	0.955	0.919
0.9950	0.962	0.908	0.833
0.9975	0.934	0.800	0.645
0.9990	0.874	0.618	0.460

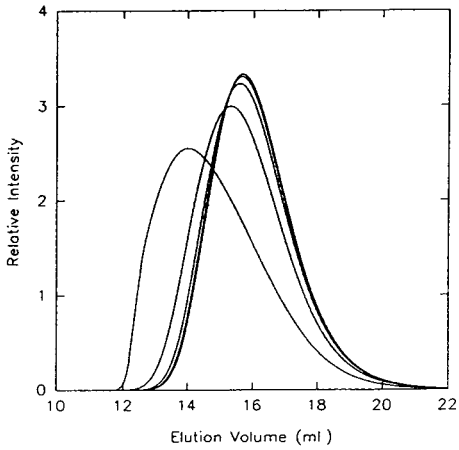

Fig. 12. Concentration detector tracings for branched MMDs with different fractions of branched monomer at extent of reaction $p = 0.995$. From left to right the peaks correspond to $\rho = 0.003$, $\rho = 0.001$, $\rho = 0.0003$, $\rho = 0.0001$ and $\rho = 0.00003$.

where c_i is the concentration of polymer at each volume element.

Effect of the fraction of branched monomers

A second set of data was generated for distributions at the same extent of reaction ($p = 0.995$) but with increasing amounts of branched monomer ($\rho = 0.00003$, 0.0001, 0.0003, 0.001 and 0.003). Figs. 12, 13 and 14 show the signals

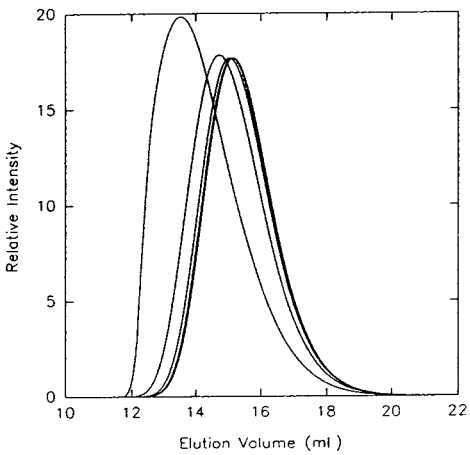

Fig. 13. Viscosity detector tracings for branched MMDs with different fractions of branched monomer at extent of reaction $p = 0.995$. From left to right the peaks correspond to $\rho = 0.003$, $\rho = 0.001$, $\rho = 0.0003$, $\rho = 0.0001$ and $\rho = 0.00003$.

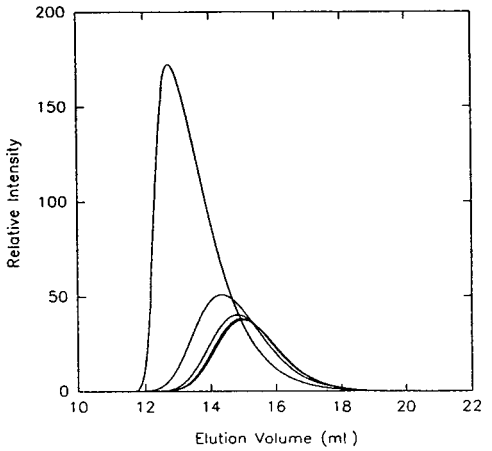

Fig. 14. Light-scattering detector tracings (0°) for branched MMDs with different fractions of branched monomer at extent of reaction $p = 0.995$. From left to right the peaks correspond to $\rho = 0.003$, $\rho = 0.001$, $\rho = 0.0003$, $\rho = 0.0001$ and $\rho = 0.00003$.

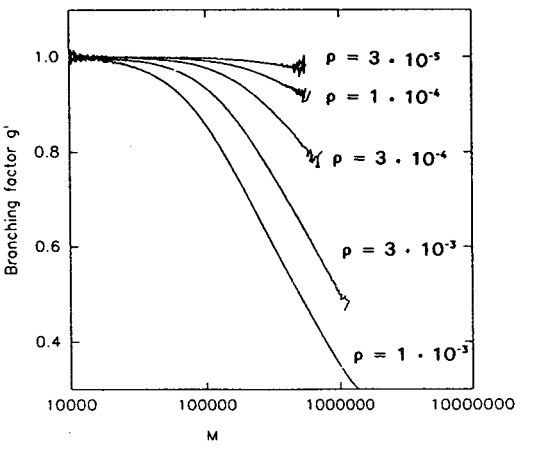

Fig. 15. Branching factor g' as a function of molecular mass for branched polymer MMD with different fractions of branched monomer ($p = 0.995$).

from the refractometer, viscometer and light scattering detector, respectively. In each figure the peak at the lowest elution volume is the one with the greatest amount of branched monomer and the peak at the highest elution volume the one with the least. The refractometer data show the broadening of the MMD and the increased skew, while the viscometer and LS detector data show the increase in intrinsic viscosity and molecular mass in addition to the broadening and skew of the distribution. The changes are qualitatively the same as for increasing extent of reaction.

Fig. 15 shows the plots of the branching factor against molecular mass. As the fraction of branched monomer increases the limiting slope at high molecular masses increases and moves to slightly higher molecular mass values. Table II lists the average g' values for each distribution.

Peak molecular masses

For the Flory–Schulz linear MMD the molecular mass at the elution fraction which gives the peak concentration signal is the weight-average molecular mass. The molecular mass of the elution fraction that gives the peak LS intensity is the z-average molecular mass and the peak viscometer signal is at an elution fraction with a molecular mass between weight- and z-averages, given by

$$M_{\text{Visc peak}} = (1 + a/2)M_w \tag{22}$$

where a is the exponent of the Mark–Houwink equation [7].

Fig. 16 shows the relationship between the concentration detector peak molecular mass and the weight-average molecular mass for both sets of data discussed above. The relationship between the molecular masses at the different detector peaks and the molecular mass moments of the distribution was found to be the same for the data from distributions at different extents of reaction and distributions with different fractions of branched monomer. A least-squares fit to the data gives

$$M_{\text{RI peak}} \approx M_w^{0.98} \tag{23}$$

TABLE II

NUMBER-, WEIGHT- AND z-AVERAGE BRANCHING INDICES FOR MMDs WITH DIFFERENT FRACTIONS OF BRANCHED MONOMERS AND $p = 0.995$

ρ	g'_n	g'_w	g'_z
0.00003	0.994	0.997	0.995
0.0001	0.996	0.991	0.983
0.0003	0.981	0.974	0.952
0.001	0.967	0.908	0.831
0.003	0.842	0.684	0.490

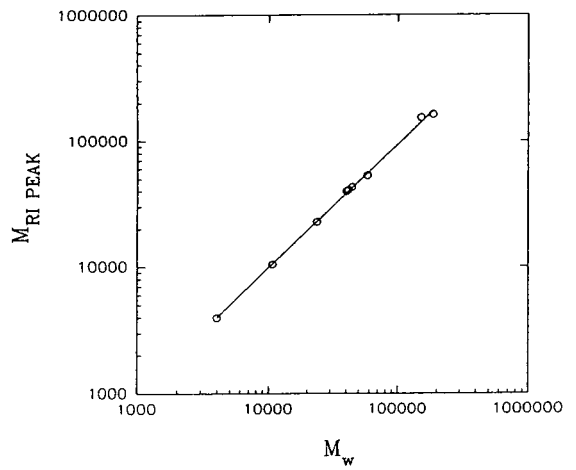

Fig. 16. Correlation of molecular mass at the maximum in concentration detector response with weight-average molecular mass.

The exponent is less than unity because as branching increases the MMD is increasingly dominated by low concentrations of high-molecular-mass, highly branched material. This shifts the weight-average molecular mass to higher values. Because of the relatively low concentration of these species the effect on the position of the maximum concentration signal is less.

Fig. 17 shows the relationship between the molecular mass at the LS intensity peak and the

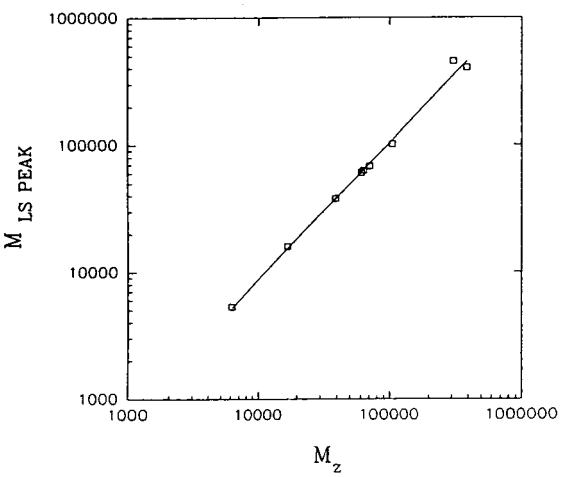

Fig. 17. Correlation of molecular mass at the maximum in light-scattering detector response with z-average molecular mass.

z-average molecular mass. The relationship between the two is

$$M_{\text{LS peak}} \approx M_z^{1.08} \tag{24}$$

The relationship with the weight-average molecular mass is

$$M_{\text{LS peak}} \approx M_w^{1.16} \tag{25}$$

The exponent is greater than unity because of the change in the shape of the distribution. There is a small amount of very-high-molecular-mass material which has a greater effect on the position of the LS intensity maximum than it does on the z-average molecular mass. For these branched MMDs the LS peak reflects a higher moment of the distribution than the z-average molecular mass. Another possible effect is due to molecular mass polydispersity at each elution volume. As branching increases the molecular mass at each elution volume will become increasingly polydisperse leading to an overestimate by light scattering of the number-average molecular mass at a given elution volume. This effect may be pronounced in the high-molecular-mass fraction of the distribution where the molecular mass at each elution volume will be overestimated, although it has little effect on calculations of the molecular mass moments. A manuscript discussing these effects in more detail is forthcoming.

These results are in qualitative agreement with recent studies on branched polymers close to the gel point although the experimental slopes are slightly higher [20–22]. The slope of the simulated data in eqn. 25 is less than the value of 2 predicted by the Flory–Stockmayer theory probably because the SEC model does not give a separation by molecular mass. The slope for the simulated data is expected to be sensitive to the model of the SEC separation of branched polymers used.

Fig. 18 shows the same data as Fig. 17 but for the molecular mass at the elution volume that gives the peak viscosity signal. In this case the situation is complicated because with increasing branching the intrinsic viscosity decreases relative to its value for a linear polymer and so the fit to the data curves slightly downwards at high molecular masses.

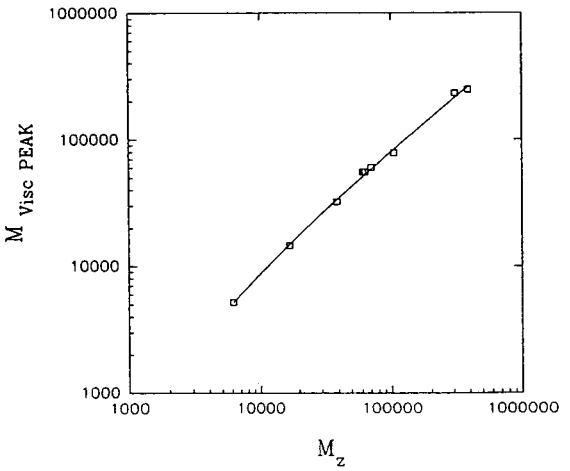

Fig. 18. Correlation of molecular mass at the maximum in viscosity detector response with z-average molecular mass.

Effect of SEC resolution on determination of molecular mass distribution

For a linear polymer there is a single-value relationship between a given hydrodynamic volume and molecular mass. For branched polymers this is no longer the case because a given elution volume from the chromatograph may contain molecules of different molecular masses but the same hydrodynamic radius. In this case we have imperfect resolution and the molecular mass polydispersity will be underestimated.

To study how large this loss of resolution is we calculated the true polydispersity as the MMD was generated, and compared this to the apparent polydispersity after transforming the MMD to the SEC MMD. Tables III and IV show these data for both variations in extent of reaction and variation in number of branch points. M_z/M_w is used as a measure of accuracy because it is the high-molecular-mass end of the distribution that is most sensitive to this loss of resolution.

TABLE III

TRUE AND MEASURED POLYDISPERSITIES, M_z/M_w, OF SAMPLE MMDs WITH $\rho = 0.001$

p ($\rho = 0.001$)	True M_z/M_w	SEC–LS M_z/M_w
0.9500	1.54	1.53
0.9800	1.58	1.57
0.9900	1.64	1.63
0.9950	1.79	1.78
0.9975	2.08	2.06
0.9990	1.72	1.71

TABLE IV

TRUE AND MEASURED POLYDISPERSITIES, M_z/M_w, OF SAMPLE MMDs WITH $p = 0.995$

ρ ($p = 0.995$)	True M_z/M_w	SEC–LS M_z/M_w
0.00003	1.51	1.51
0.0001	1.53	1.53
0.0003	1.59	1.58
0.001	1.79	1.78
0.003	2.04	2.03

The results show that there is very little loss of resolution and that the apparent MMD is very close to the true MMD. This can be understood by considering the elution profiles of different n-mers shown in Fig. 2. The MMDs for different n-mers only partially overlap because the average molecular mass increases greatly with increasing number of branch points. As a result a given elution volume does not contain a wide range of architecturally different molecules, but only a few whose molecular masses are very close. This means that the molecular mass polydispersity at most elution volumes is very small so that the average errors caused by measuring the loss of resolution are insignificant.

Effect of the relationship between the radius of gyration and the hydrodynamic radius

The previous data were generated assuming that the relationship between hydrodynamic radius and radius of gyration is independent of branching. Experimental and theoretical data indicate that the hydrodynamic radius may be less sensitive to branching than the radius of gyration, *i.e.*, for a given number of branch points the reduction in hydrodynamic radius relative to that of the linear polymer of the same molecular mass, is less than the reduction in the radius of gyration.

In order to show how this can affect the data

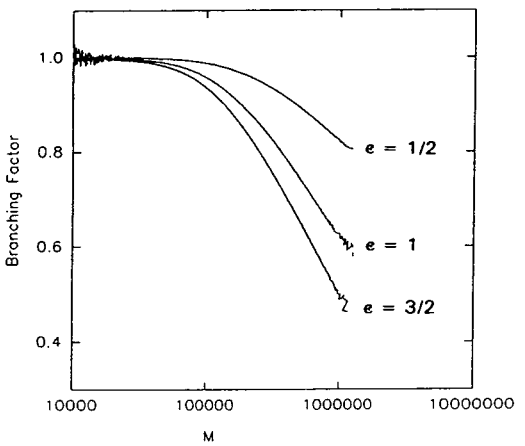

Fig. 19. Branching factor g' as a function of molecular mass for branched polymer MMD with different relationships between radius of gyration and hydrodynamic radius ($p = 0.995$, $\rho = 0.001$).

we generated two additional data sets where the exponent in eqn. 10 was set to 1 and 1/2. Data were generated for MMDs with $p = 0.995$ and $\rho = 0.001$. As the exponent decreases the sensitivity of the hydrodynamic volume to branching also decreases. This means that the chromatographic separation is less affected by branching, but that the size change caused by branching is more difficult to detect.

Fig. 19 shows branching factor plots for the data sets generated with $\epsilon = 1$, and 1/2 compared to 3/2. Table V shows the corresponding change in the average value of g'.

If Fig. 19 is compared with Fig. 15, it can be seen that the effect of changing ϵ is very similar to that of changing the number of branch points. For these reaction conditions changing ϵ from 3/2 to 1/2 has the same effect as decreasing the number of branch points by about an order of magnitude. It is clear that if g' is to be used to estimate the number of branch points in a polymer then ϵ must be determined first for the polymer–solvent system by careful measurements of the radius of gyration and intrinsic viscosity of samples with different amounts of branching. We are currently studying this problem using SEC combined with multi-angle laser-LS and viscosity detectors to measure both the radius of gyration and the intrinsic viscosity distributions of model branched polymers.

TABLE V

ϵ	g'_w
1/2	0.965
1	0.934
3/2	0.908

CONCLUSIONS

The simulation illustrates the expected behavior of the branching index and molecular mass for branched MMDs under different reaction conditions. Branching is greatest at the high-molecular-mass end of the MMD, at low molecular masses the polymer may be predominantly linear. Different averages of the branching index may be calculated, the z-average value is the most sensitive to branching. The relationship between the molecular masses at the peak of the LS tracing and the moments of distributions is in reasonable agreement with experiment. The loss of resolution in determining the MMD caused by branching is very small and is comparable to errors caused by signal noise. A significant problem with branching analysis by SEC with LS and viscosity detectors is determining the relationship between the decrease in intrinsic viscosity caused by branching and the number and functionality of those branches. Future work will look at the radius of gyration as a function of elution volume for the model and also the effect of gelation, and the SEC model used, on the different detector peak elution volumes and molecular masses.

ACKNOWLEDGEMENTS

I thank Howard Barth and the reviewers for numerous stimulating remarks.

REFERENCES

1 W.W. Yau, J.J. Kirkland and D.D. Bly, *Modern Size-Exclusion Chromatography*, Wiley, New York, 1979.
2 H.G. Barth and J.W. Mays (Editors), *Modern Methods of Polymer Characterization*, Wiley, New York, 1991.

3 A.R. Cooper (Editor), *Determination of Molecular Weight*, Wiley, New York, 1989.
4 J.J. Kirkland, S.W. Rementer and W.W. Yau, *J. Appl. Polym. Sci.*, 48 (1991) 39.
5 W.W. Yau, *Chemtracts*, 1 (1990) 1.
6 C. Jackson, H.G. Barth and W.W. Yau, in *Proc. Int. Gel Permeation Chromatography Symposium*, Waters Division of Millipore, Milford, MA, 1991.
7 P.J. Flory, *Principles of Polymer Chemistry*, Cornell University Press, Ithaca, NY, 1953, Ch. 8.
8 W.H. Stockmayer, *J. Chem. Phys.*, 11 (1943) 45.
9 W.H. Stockmayer, *J. Chem. Phys.*, 12 (1944) 125.
10 R.F.T. Stepto, in S.L. Aggarwal and S. Russo (Editors), *Comprehensive Polymer Science; First Supplement*, Pergamon Press, New York, 1992, Ch. 10.
11 D. Stauffer, *Introduction to Percolation Theory*, Taylor & Francis, New York, 1985.
12 C. Jackson and W.W. Yau, *J. Chromatogr.*, 645 (1993) 209.
13 C. Jackson and W.W. Yau, *Polym. Mater. Sci. Eng.*, 69 (1993) 212.
14 H. Benoit, Z. Grubisic, P. Rempp, D. Decker and J.G. Zilliox, *J. Chem. Phys.*, 63 (1963) 1507.
15 B.H. Zimm and W.H. Stockmayer, *J. Chem. Phys.*, 17 (1949) 1301.
16 H. Yamakawa, *Modern Theory of Polymer Solutions*, Academic Press, New York, 1971.
17 J. Roovers, in H.F. Mark (Editor), *Encyclopedia of Polymer Science and Engineering*, Wiley, New York, 2nd ed., 1989.
18 B.H. Zimm and R.W. Kilb, *J. Polym. Sci.*, 37 (1959) 19.
19 J.F. Douglas, J. Roovers and K.F. Freed, *Macromolecules*, 23 (1990) 4168.
20 F. Schosseler, H. Benoit, Z. Grubisic-Gallot, C. Strazielle and L. Leibler, *Macromolecules*, 22 (1989) 400.
21 E.V. Patton, J.A. Wesson, M. Rubinstein, J.C. Wilson and A.E. Oppenheimer, *Macromolecules*, 22 (1989) 1946.
22 J. Bauer, P. Lang, W. Burchard and M. Bauer, *Macromolecules*, 24 (1991) 2634.

Journal of Chromatography A, 662 (1994) 13–26
Elsevier Science B.V., Amsterdam

CHROM. 25 661

Multiple-site binding interactions in metal-affinity chromatography

I. Equilibrium binding of engineered histidine-containing cytochromes *c*

Robert J. Todd, Robert D. Johnson and Frances H. Arnold*

Division of Chemistry and Chemical Engineering, California Institute of Technology, Pasadena, CA 91125 (USA)

(First received August 16th, 1993; revised manuscript received October 18th, 1993)

ABSTRACT

Mechanisms of protein retention in immobilized metal-affinity chromatography (IMAC) have been probed using a set of *Saccharomyces cerevisiae* iso-1-cytochrome *c* histidine variants constructed by site-directed mutagenesis. Proteins containing a single accessible histidine exhibit Langmuir-type isotherms with maximum protein binding capacities between 5 and 10% of the maximum copper loading and the capacity of the support to bind imidazole. A simple model that assumes that the copper sites are densely packed and can be blocked by protein adsorption yields binding constants for single-histidine proteins that are similar to the binding constant for free imidazole. Proteins containing multiple accessible histidines do not exhibit simple Langmuir-type behavior; they appear to interact with the support by simultaneous coordination to more than one metal ion, the result of which is to increase the apparent binding affinity by as much as a factor of 1000. The protein binding constant depends on the availability of copper sites: binding is significantly weaker at low surface concentrations of copper that presumably cannot support multiple-site interactions. The protein binding capacity drops to zero at copper loadings less than one-half the maximum, indicating that immobilized iminodiacetic acid ligands are sufficiently close together that two can coordinate a single copper ion, which precludes its interaction with a protein. Protein adsorption via multiple-site coordination has important consequences for the optimization of IMAC separations and the design of new IMAC supports.

INTRODUCTION

Immobilized metal-affinity chromatography (IMAC) has proven to be a useful and versatile technique for the isolation and purification of proteins. As ligands for affinity separations, metal ion complexes offer important advantages over biological affinity agents such as inhibitors and antibodies [1]. Small, inexpensive metal complexes are stable under a wide range of conditions, can be recycled many times without loss of activity and can be formulated into very-high-capacity chromatographic supports. Elution can be effected under relatively mild conditions, and the columns can be cleaned and regenerated easily, without reduction in protein binding capacity. The selectivity of the separation can be tailored through the choice of metal ion, solvent conditions, or by modification of the target protein (*e.g.*, the addition of histidine-rich affinity "handles"). These advantageous features have driven the recent rapid growth in IMAC applications [2] (for a recent compendium of IMAC applications and methods, see ref. 3).

Rapidly reversible interactions with metal ions

* Corresponding author.

0021-9673/94/$07.00
SSDI 0021-9673(93)E1104-8

immobilized on a hydrophilic chromatographic support (*e.g.*, Cu^{2+} chelated by an iminodiacetate-derivatized resin) result in the retention of proteins with metal-coordinating ligands on their surfaces, primarily histidine at neutral pH. Depending on the elution conditions, selectivity can be derived from the multiplicity or local environment of metal-coordinating residues [4,5]. Thus IMAC is effective for isolating proteins from crude mixtures; it can also be used to effect highly selective separations of closely related proteins.

Despite recent progress in elucidating IMAC adsorption mechanisms and quantifying protein binding behavior [6,7], the precise molecular mechanisms by which proteins are selectively retained on IMAC matrices are not well understood. Equilibrium binding studies have shown that a simple Langmuir-type model may not adequately describe protein binding to IMAC supports: binding heterogeneity as evidenced by non-linear Scatchard plots is often observed for tightly binding proteins [6,7]. Based on these observations, Hutchens *et al.* [6] proposed that protein binding may involve simultaneous interactions between multiple sites on the protein and the IMAC support. The nature of protein binding has important implications for the design of efficient separations as well as for the design of new materials for IMAC supports. Interactions at multiple sites can greatly enhance binding affinity and dramatically alter specificity for certain classes of proteins. This can affect retention profiles and lead to puzzling differences in chromatographic performance on different supports or under different conditions. Multiple-site binding can also provide a basis for the design of materials capable of selective protein recognition. It is possible to target individual molecules by matching the distribution of metal ions to a spatial distribution of metal-coordinating ligands [8], and efforts to prepare new metal-affinity chromatography supports capable of specific multiple-site binding to target molecules are underway [9,10].

Homologous proteins that differ in their histidine contents have proven useful for elucidating molecular bases of IMAC retention [4,11]. The ability to use protein engineering to add or delete specific amino acid residues, while leaving the remaining protein surface unchanged, allows a more complete and unambiguous study of the contributions of individual metal-coordinating sites [5]. In this study, we compare the equilibrium binding isotherms of variants of a small globular protein, iso-1-cytochrome *c* from *Saccharomyces cerevisiae*, on a TSK polymer matrix derivatized with Cu^{2+}–iminodiacetate (Cu^{2+}-IDA). Using these well-characterized protein variants, we are able to evaluate how the number and placement of surface histidines influences binding and IMAC separation. The engineered histidine-containing cytochrome *c* proteins are ideally suited to investigating the extent to which binding to IMAC supports involves coordination at multiple sites. This information is used to develop a simple but useful description of protein binding to IMAC supports that is consistent with our understanding of analogous metal ion complexes in solution.

MATERIALS AND METHODS

Variants of *S. cerevisiae* iso-1-cytochrome *c* ($M_r = 12\,588$) containing different distributions of histidine residues were constructed by site-directed mutagenesis, expressed in yeast and purified as described previously [12,13]. Cytochromes *c* from tuna heart ($M_r = 12\,170$) and horse heart ($M_r = 12\,384$) were purchased from Sigma and used without further purification.

Preparation of metal-affinity gel

TSK Guardgel Chelate-5PW (17-μm macroporous beads) was purchased from Tosohaas. The specific surface area of this polymer-based, hydrophilic support in the swollen state is not known; a pore size of *ca.* 1000 Å is reported by the manufacturer. The immobilizing ligand, iminodiacetic acid (IDA), is attached to the TSK matrix via a spacer. To prepare the support for use in binding studies, the TSK Chelate-5PW was packed into a column (10 cm × 1 cm) and washed extensively with 50 m*M* EDTA, pH 8.0. To obtain the maximum copper loading, the column was equilibrated with 50 m*M* $CuSO_4$. Excess copper was removed by washing with 0.1 *M* sodium acetate, pH 4.0. The gel was then

equilibrated in 50 m*M* sodium phosphate (NaP_i), 0.5 *M* NaCl, pH 7.0 for measurement of binding isotherms. For copper loading less than maximum, the column was equilibrated with 0.1 *M* sodium acetate, pH 4.0, and 2-ml aliquots of the gel were transferred to 50-ml centrifuge tubes. Different copper loadings were obtained by adding limiting amounts of $CuSO_4$ ($< 18.5 \cdot 10^{-3}$ mmol Cu per ml gel) dissolved in 40 ml acetate buffer, followed by rapid vortexing and subsequent mixing by inversion for at least 1 h. The gel was then washed three times with 40 ml of acetate buffer and three times with 40 ml phosphate buffer.

Measurement of copper loading

To quantify copper loading, the TSK gel was resuspended in the equilibration buffer (50 m*M* NaP_i, 0.5 *M* NaCl, pH 7.0; packed volume:total volume = 1:4). A 50 m*M* solution of EDTA, pH 8.0 (600 μl) was added to 400 μl of the gel suspension in a microcentrifuge tube. This suspension was equilibrated for 60 min by inversion and spun at 10 000 rpm (800 *g*) in a microcentrifuge for 5 min. The supernatant was transferred to a fresh tube, and the Cu^{2+}-EDTA concentration was determined, in quadruplicate, by measuring the visible absorbance at 800 nm in comparison with that of Cu^{2+}-EDTA, pH 7.0 ($\epsilon_{800} = 73.6$ cm^{-1} M^{-1}). The maximum copper loading (Cu_{max}) was found to be $18.5 \cdot 10^{-3}$ mmol per ml of packed gel, in agreement with values previously determined by repeated washing with EDTA [12].

Equilibrium binding isotherms

Equilibrium binding isotherms were measured at room temperature using a modified version of the procedure developed by Hutchens and coworkers [6,7]. The TSK gel was loaded with copper ions and resuspended in the equilibration buffer (50 m*M* NaP_i, 0.5 *M* NaCl, pH 7.0; packed volume:total volume = 1:4) as described above. The high ionic strength, sufficient to elute the net positively charged cytochromes *c* from CM-Sephadex cation-exchange resin [12,13], was used to minimize electrostatic interactions during IMAC. Cytochrome *c* (800 μl of 0.4–0.004 m*M* dilutions prepared in the same buffer) was added to 200 μl of the gel suspension in a microcentrifuge tube. This suspension was equilibrated by inversion for 30 min (after which time no further significant adsorption is observed) and spun at 10 000 rpm (800 *g*) in a microcentrifuge for 5 min. The supernatant was transferred to a fresh tube, and the protein concentration was determined, in duplicate, by measuring the visible absorbance at 550 nm ($\epsilon_{550} = 2.76 \cdot 10^4$ cm^{-1} M^{-1}) after reduction with sodium dithionite [14].

Capacities and binding constants from isotherms

Simple Langmuir binding is described by eqn. 1, where Q is the amount of protein adsorbed per ml of packed gel and C is the liquid-phase protein concentration, at equilibrium. The isotherm is fully described by two parameters, a binding constant K and the maximum capacity for the adsorbed protein, Q_{max}.

$$Q = \frac{Q_{max} K C}{1 + KC} \quad (1)$$

This simple model cannot describe the isotherms of the cytochrome *c* variants containing multiple histidines. The simplest model to which these isotherms can be fit is a bi-Langmuir isotherm,

$$Q = \frac{Q_{max,A} K_A C}{1 + K_A C} + \frac{Q_{max,B} K_B C}{1 + K_B C} \quad (2)$$

where K_A and K_B represent the binding constants to two types of binding sites, strong and weak, respectively. The corresponding maximum capacities for binding at these two types of sites are $Q_{max,A}$ and $Q_{max,B}$.

To describe the binding of imidazole to the IMAC support, it is necessary to include the possibility that more than one imidazole will coordinate with different affinities to a single metal. Assuming two imidazoles can coordinate to a single copper, the adsorption isotherm for imidazole to immobilized Cu^{2+}-IDA is described by

$$Q = \frac{Q_{max,A} K_A C + (Q_{max,A} + Q_{max,B}) K_A K_B C^2}{1 + K_A C + K_A K_B C^2} \quad (3)$$

where K_A refers to the first imidazole binding to the coordination sites of Cu^{2+}-IDA and K_B to a second imidazole binding to the remaining

coordination sites. The maximum capacity for imidazole is $Q_{max,A} + Q_{max,B}$.

RESULTS

Cytochrome c surface histidine variants

A series of *S. cerevisiae* cytochromes *c* were designed and constructed for these studies (Table I). The label assigned to each variant in Table I indicates the surface histidines. Mutations made to the wild-type protein and the total number of surface histidines are also listed. Amino acids 4 and 8 were chosen as sites for replacement with histidine, based on their high degree of surface accessibility. In addition, naturally occurring histidines at positions 26, 33 and 39 were replaced with other amino acids in order to determine the contributions these residues make to the protein's interaction with the IMAC matrix. All the natural surface histidines have been replaced by other amino acids in the H(−) control.

In each of the iso-1-cytochrome *c* variants, the lone cysteine at position 102 was replaced by a serine to prevent oxidative dimerization at the surface sulfhydryl group [15]. The structural integrity of each mutant was confirmed by UV–visible spectroscopy, and the histidine content was confirmed by ^{1}H NMR spectroscopy [12,16]. Expression of these variants in a strain of yeast lacking cytochrome *c* guarantees that each is biologically functional, which in turn ensures that a conformation very similar to the native one has been maintained [12,13].

Formation of the ternary IDA-Cu^{2+}–protein complex that leads to retention on the IMAC support is expected to depend on the accessibilities of individual surface histidines. The accessibilities of the ϵ-nitrogens of each histidine residue to a probe approximately the size of Cu^{2+}-IDA (1.93 Å radius) were determined using the coordinates of the crystal structure of *S. cerevisiae* cytochrome *c* [5,17] (Table II). Engineered histidines were incorporated into a modified cytochrome *c* structure using the molecular graphics software Insight (version 2.0). Based on this structure, the histidines at positions 4 and 8 are expected to be fully accessible to Cu^{2+}-IDA. The remaining histidines exhibit varying, lower degrees of accessibility, as indicated in Table II.

TABLE I

ENGINEERED VARIANTS OF *S. CEREVISIAE* ISO-1-CYTOCHROME *c* AND NATIVE CYTOCHROMES *c*

All engineered variants ($M_r \approx 12\,500$) contain the replacement of cysteine by serine at position 102 to prevent dimerization. Remaining mutations alter surface histidine content. Surface histidines of native cytochromes *c* from tuna ($M_r = 12\,170$) and horse ($M_r = 12\,384$) are listed for comparison. Number of surface-accessible histidines includes His 26. C = Cysteine; H = histidine; K = lysine; L = leucine; N = asparagine; Q = glutamine; S = serine; T = threonine.

Label	Amino acid substitutions	Number of surface histidines
H(−)	C102S, H39Q, H33N, H26N	0
H_{26}	C102S, H39Q, H33N	1
H_4	C102S, H39Q, H33N, H26N, K4H	1
H_8	C102S, H39Q, H33N, H26N, T8H	1
$H_{26}H_4$	C102S, H39Q, H33Q, K4H	2
$H_{26}H_8$	C102S, H39Q, H33Q, T8H	2
$H_{26}H_{33}$	C102S, H39Q	2
$H_{26}H_{33}H_{39}$	C102S	3
$H_{26}H_{33}H_4$	C102S, H39Q, K4H	3
$H_{26}H_{33}H_8$	C102S, H39Q, T8H	3
Tuna (H_{26})		1
Horse (H_{26},H_{33})		2

TABLE II

CALCULATED ACCESSIBLE SURFACE AREAS OF ISO-1-CYTOCHROME *c* SURFACE HISTIDINES

Calculations were performed using coordinates from the high-resolution crystal structure of *S. cerevisiae* iso-1-cytochrome *c* [17]. The surface area is reported as the total area at the δ- and ε-nitrogens accessible to a probe the size of Cu^{2+}-IDA (1.93 Å radius) [5]. The percent accessibility is the accessible surface area relative to an unhindered imidazole.

Histidine position	Accessible surface area (Å^2)	Percent accessibility
4	25.7	88
8	25.5	87
26	3.2	11
33	5.1	17
39	20.9	71

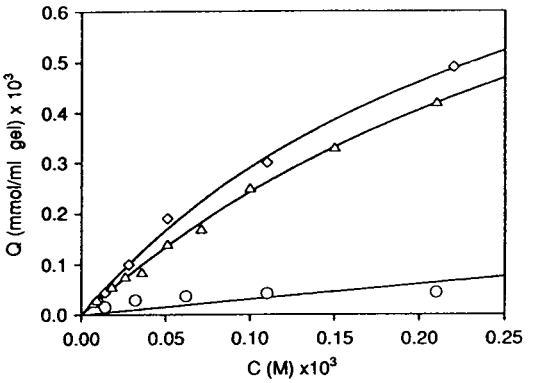

Fig. 1. Equilibrium binding isotherms of weakly binding cytochromes *c*. Solid lines represent fit of Langmuir isotherm (eqn. 1) with parameters given in Table III. (◇) H_{26}; (△) tuna; (○) H(−).

Binding isotherms for single-histidine proteins and imidazole at maximum copper loading

Protein binding isotherms were measured at pH 7.0, where surface histidines are largely unprotonated and free to coordinate to the metal[a]. Isotherms for the H(−) control, H_{26} and tuna cytochrome *c* are shown in Fig. 1. These proteins exhibit simple Langmuir-type binding behavior (linear Scatchard plots), and the capacities and binding constants obtained by fitting these data to the Langmuir isotherm (eqn. 1) are listed in Table III. The H(−) variant with no surface-accessible histidines exhibits almost no affinity for the Cu^{2+}-IDA matrix at pH 7.0. Tuna cytochrome *c* and the H_{26} *S. cerevisiae* variant, both of which have only histidine 26, exhibit similar binding isotherms with apparent binding constants of $2 \cdot 10^3$–$4 \cdot 10^3$ M^{-1}. Their maximum capacities (extrapolated from the data) are *ca.* $1.2 \cdot 10^{-3}$ mmol protein per ml of gel (*ca.* 15 mg/ml).

Equilibrium binding isotherms for the three single-histidine variants shown in Fig. 2 are also adequately described by a simple Langmuir equation. Variants with fully accessible histidines at positions 4 and 8 bind significantly more tightly than H_{26}, whose histidine 26 has less than 10% of the accessibility of histidines 4 and 8 (Table II).

Binding isotherms were also measured for imidazole (data not shown). While histidines at a protein surface are sterically excluded from occupying two coordination sites on one metal, two equivalents of imidazole can bind to matrix-bound Cu^{2+}-IDA. Maximum capacity ($Q_{max,A} + Q_{max,B}$) and binding constants for the first and second imidazoles (K_A and K_B) were obtained by fitting eqn. 3 to the experimental isotherms. The resulting values are reported in Table III. The binding constant K_A for the first imidazole is similar to the binding constant for imidazole to Cu^{2+}-IDA in solution[b] ($3.4 \cdot 10^3$ M^{-1} at 25°C) [18,19]. The observed maximum capacity for imidazole ($Q_{max,A} + Q_{max,B}$) equals twice the copper loading and is much higher than the capacities observed for the single-histidine proteins. In fact, while all of the copper sites are available to imidazole, only 5–10% can be occupied by cytochromes *c* with single histidines.

The apparent binding constants of the single-histidine proteins obtained by fitting eqn. 1 to the isotherms are almost ten times greater than

[a] The pK_a values for the individual surface histidines, measured by ^{1}H NMR spectroscopy, range from 5.4 to 6.5 [12,16].

[b] The reported binding constant of $2.2 \cdot 10^3$ M^{-1} (imidazole–Cu^{2+}-IDA at 35°C) [18] was extrapolated to 25°C using $\Delta H = -7.6$ kcal/mol (imidazole–Cu^{2+} at 25°C) [19].

TABLE III

LANGMUIR BINDING PARAMETERS FOR ISO-1-CYTOCHROME *c* VARIANTS, NATIVE CYTOCHROMES *c* AND IMIDAZOLE TO Cu^{2+}-IDA TSK 5PW

Adsorption isotherms of single-histidine proteins have been fit to the Langmuir model (eqn. 1). Isotherms of multiple-histidine proteins have been fit to the bi-Langmuir model (eqn. 2). Imidazole isotherms have been fit to eqn. 3.

	K_A (M^{-1})	$Q_{max,A}$ (mmol/ml gel) × 10^3	K_B (M^{-1})	$Q_{max,B}$ (mmol/ml gel)x10^3	Initial slope (ml/ml gel)
Imidazole	$5.7 \pm 0.7 \cdot 10^3$	18.0 ± 0.9	$4.0 \pm 3.0 \cdot 10^1$	18.8 ± 0.6	$1.0 \pm 0.1 \cdot 10^2$
H(−)	N.D.[a]	N.D.[a]	–	–	0.3 ± 0.1
Tuna	$2.4 \pm 0.1 \cdot 10^3$	1.25 ± 0.3	–	–	3.0 ± 0.2
H_{26}	$3.5 \pm 0.6 \cdot 10^3$	1.12 ± 0.13	–	–	4.0 ± 0.3
H_4	$5.6 \pm 0.3 \cdot 10^4$	1.15 ± 0.02	–	–	$6.4 \pm 0.2 \cdot 10^1$
H_8	$4.9 \pm 0.5 \cdot 10^4$	1.03 ± 0.04	–	–	$5.0 \pm 0.4 \cdot 10^1$
Horse	$3.8 \pm 0.6 \cdot 10^5$	0.17 ± 0.02	$0.7 \pm 0.3 \cdot 10^4$	1.33 ± 0.34	$7.6 \pm 0.5 \cdot 10^1$
$H_{26}H_4$	$9.0 \pm 1.0 \cdot 10^5$	1.10 ± 0.10	$1.9 \pm 1.0 \cdot 10^4$	0.29 ± 0.10	$1.0 \pm 0.2 \cdot 10^3$
$H_{26}H_8$	$1.0 \pm 0.1 \cdot 10^6$	0.78 ± 0.06	$1.8 \pm 1.0 \cdot 10^4$	0.56 ± 0.09	$7.8 \pm 1.4 \cdot 10^2$
$H_{26}H_{33}$	$7.4 \pm 0.7 \cdot 10^5$	0.52 ± 0.03	$2.4 \pm 0.5 \cdot 10^4$	0.90 ± 0.02	$4.3 \pm 0.4 \cdot 10^2$
$H_{26}H_{33}H_4$	$5.6 \pm 0.8 \cdot 10^6$	1.33 ± 0.13	$4.8 \pm 2.0 \cdot 10^4$	1.08 ± 0.13	$7.6 \pm 1.3 \cdot 10^3$
$H_{26}H_{33}H_8$	$3.6 \pm 0.7 \cdot 10^6$	1.32 ± 0.10	$1.5 \pm 0.8 \cdot 10^4$	0.95 ± 0.11	$4.8 \pm 1.0 \cdot 10^3$
$H_{26}H_{33}H_{39}$	$4.3 \pm 0.4 \cdot 10^6$	1.27 ± 0.04	$2.9 \pm 0.5 \cdot 10^4$	0.96 ± 0.04	$5.3 \pm 0.5 \cdot 10^3$

[a] K and Q_{max} could not be determined independently.

that of imidazole (*e.g.*, $5 \cdot 10^4$ M^{-1} for H_8 *versus* $6 \cdot 10^3$ M^{-1} for imidazole). Similarly low capacities and high apparent binding constants have been reported for lysozyme and ovalbumins binding Cu^{2+}-IDA–Sepharose and Cu^{2+}-IDA–TSK gels [6,20].

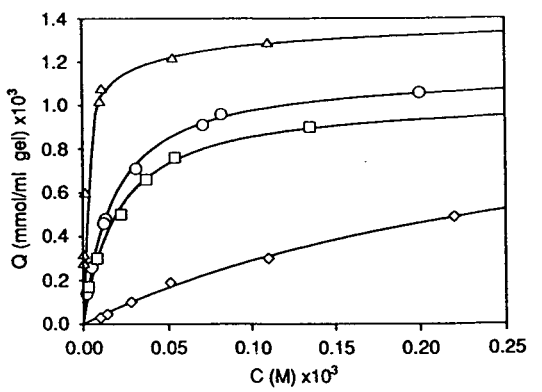

Fig. 2. Equilibrium binding isotherms of iso-1-cytochrome *c* variants. Solid lines through data for H_{26} (◇), H_4 (□) and H_8 (○) variants represent fit of Langmuir isotherm (eqn. 1) with parameters given in Table III. Solid line through data for $H_{26}H_4$ variant (△) represents the fit to a bi-Langmuir model (eqn. 2) using the parameters given in Table III. The initial slope of the isotherm for the two-histidine variant ($H_{26}H_4$) is >10 times larger than the initial slopes of the single-histidine isotherms.

Binding isotherms for multiple-histidine proteins at maximum copper loading

Proteins with multiple exposed histidines bind significantly more tightly and have slightly higher maximum capacities than single-histidine proteins, as shown in Fig. 2 for the $H_{26}H_4$ variant. The sole difference between $H_{26}H_4$ and the H_4 variant, a second histidine only partially exposed on the surface of the protein (histidine 26), increases the initial slope of the binding isotherm by more than a factor of 10 (Table III). Scatchard plots of the isotherm data for the $H_{26}H_4$ and $H_{26}H_8$ two-histidine variants, shown in Fig. 3, indicate at least two modes of binding. Binding data for all the multiple-histidine proteins were fit to the bi-Langmuir isotherm (eqn. 2), and the resulting binding constants and capacities are given in Table III. The first binding constants for the two-histidine variants are approximately 10^6 M^{-1}, while the second binding constants (weak site) are similar to those of

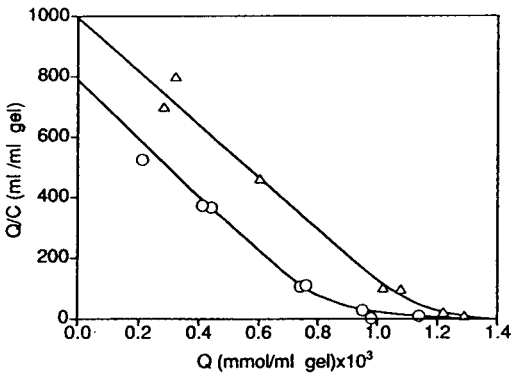

Fig. 3. Scatchard plot of $H_{26}H_4$ (△) and $H_{26}H_8$ (○) equilibrium binding data fit to bi-Langmuir binding isotherm (eqn. 2).

the single-histidine variants (*ca.* 10^4 M^{-1}). The total capacities for the proteins with two surface histidines are approximately 30% greater than the capacities for single-histidine cytochrome *c* variants.

Isotherms of the three-histidine variants also indicate multiple binding modes (data not shown), one of which corresponds to a very strong interaction [12]. Fitting the bi-Langmuir model to the isotherms yields values for the first binding constant of $5 \cdot 10^6$–$10 \cdot 10^6$ M^{-1} and capacities that are approximately twice those of the single-histidine proteins (Table III).

Binding isotherms for a multiple-histidine protein at decreased copper loading

Equilibrium binding isotherms were measured for horse cytochrome *c* on the TSK Guardgel Chelate 5PW at copper loading varying from $18.5 \cdot 10^{-3}$ mmol/ml (Cu_{max}) to $6.1 \cdot 10^{-3}$ mmol/ml (data not shown). At high copper loading ($14.5 \cdot 10^{-3}$–$18.5 \cdot 10^{-3}$ mmol/ml) the adsorption isotherms of this two-histidine protein display multiple binding modes. These data were analyzed using the bi-Langmuir isotherm (eqn. 2), and the binding parameters are presented in Table IV. At lower copper loading ($6.1 \cdot 10^{-3}$–$12.3 \cdot 10^{-3}$ mmol/ml), analysis of the data using the bi-Langmuir model resulted in negligible ($< 2 \cdot 10^{-5}$ mmol/ml) values for $Q_{max,A}$, the strong binding site capacity. The data at these lower loadings were adequately described by the single Langmuir isotherm (eqn. 1).

As the copper loading is decreased, the first binding constant (strong site) of horse cytochrome *c* for the IMAC support decreases rapidly at first, from $4 \cdot 10^5$ M^{-1} at maximum loading to $5 \cdot 10^3$ M^{-1} at two-thirds loading ($12 \cdot 10^{-3}$

TABLE IV

LANGMUIR BINDING PARAMETERS FOR HORSE HEART CYTOCHROME *c* AT DECREASING COPPER LOADING

Adsorption isotherms for horse cytochrome *c* on IDA-TSK 5PW at high copper loading ($14.8 \cdot 10^{-3}$–$18.5 \cdot 10^{-3}$ mmol/ml gel) have been fit to the bi-Langmuir model (eqn. 2). Isotherms at low copper loading have been fit to the simple Langmuir model (eqn. 1).

Cu (mmol/ml gel) × 10^3	K_A (M^{-1})	$Q_{max,A}$ (mmol/ml gel) × 10^3	K_B (M^{-1})	$Q_{max,B}$ (mmol/ml gel) × 10^3	Initial slope (ml/ml gel)
18.5 ± 0.4	$3.8 \pm 0.6 \cdot 10^5$	0.17 ± 0.02	$7.3 \pm 3.0 \cdot 10^3$	1.33 ± 0.34	$7.6 \pm 0.5 \cdot 10^1$
15.6 ± 0.1	$2.1 \pm 0.4 \cdot 10^5$	0.23 ± 0.05	$7.4 \pm 4.9 \cdot 10^3$	0.99 ± 0.35	$5.8 \pm 0.3 \cdot 10^1$
14.8 ± 0.1	$1.2 \pm 0.4 \cdot 10^5$	0.19 ± 0.08	$3.8 \pm 1.9 \cdot 10^3$	1.19 ± 0.18	$2.5 \pm 0.2 \cdot 10^1$
12.3 ± 0.2	$5.0 \pm 1.4 \cdot 10^3$	0.97 ± 0.25	–	–	5.0 ± 0.2
12.0 ± 0.1	$5.3 \pm 0.9 \cdot 10^3$	0.80 ± 0.12	–	–	4.3 ± 0.2
10.5 ± 0.1	$4.2 \pm 1.3 \cdot 10^3$	0.53 ± 0.15	–	–	2.3 ± 0.2
9.5 ± 0.1	$4.0 \pm 3.1 \cdot 10^3$	0.43 ± 0.31	–	–	1.8 ± 0.3
7.6 ± 0.4	$4.3 \pm 2.8 \cdot 10^3$	0.41 ± 0.15	–	–	2.0 ± 0.4
6.1 ± 0.3	N.D.[a]	N.D.[a]	–	–	0.4 ± 0.1

[a] K and Q_{max} could not be determined independently.

mmol/ml). The extrapolated maximum capacity ($Q_{max,A} + Q_{max,B}$) decreases steadily with copper loading, until there is negligible adsorption at one-third the maximum copper loading ($6.1 \cdot 10^{-3}$ mmol/ml).

DISCUSSION

Single-site protein binding

Comparing the isotherms for the H(−) and H_{26} variants (Fig. 1) indicates that a surface histidine is required for any significant binding of cytochrome *c* to the Cu^{2+}-IDA support at pH 7.0. In the absence of accessible histidines, the contributions from the remaining surface residues and the amino terminus in H(−) result in minimal protein adsorption. This observation mirrors those reported for other proteins and other IMAC supports at neutral pH [4,5,8,21]. The free cysteine (C102) on the surface of native yeast cytochrome *c* has been replaced by serine in the variants studied here. When C102 is present, metal affinity chromatography on Cu^{2+}-IDA yields significant amounts of a second protein form which co-elutes with variants containing twice the surface histidine content of the monomer (data not shown). This second form is most likely the disulfide-cross-linked dimer commonly observed for this protein.

Once there is a histidine accessible for coordination to the immobilized copper ions, protein binding is assured. However, the binding behavior of histidine-containing proteins differs from that of imidazole (Table III). While all the immobilized copper ions appear to be accessible to imidazole, only a small fraction ($< 10\%$) can be involved in protein binding. Furthermore, cytochrome *c* variants with fully accessible histidines bind with apparent affinities ten times greater than imidazole. What is the source of this high binding affinity?

A simple model which assumes that protein adsorption blocks access to multiple metal ion sites at the surface of the chromatographic support can explain both the large apparent binding constants for single-histidine proteins and the low protein binding capacities. For a protein with a single histidine, the interaction illustrated in Fig. 4a is described by

$$P + nCu \rightleftharpoons PCu + [(n-1)Cu] \quad K_1 = \frac{[PCu]}{[P][Cu]}$$

where the protein (P) blocks $n-1$ additional copper sites from further interactions (blocked sites designated by brackets) upon coordinating to a metal ion (Cu) on the chromatographic support. This model also results in a Langmuir-type isotherm,

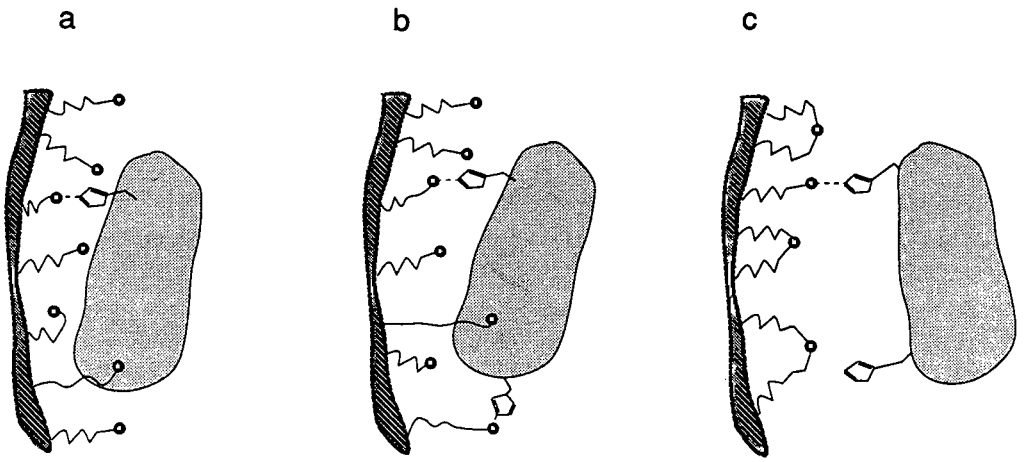

Fig. 4. Proposed binding interactions in IMAC. (a) Protein binds IMAC surface at a single copper site and blocks access to other sites (by protein). (b) Multiple-site binding to IMAC surface: two histidines simultaneously coordinate to separate copper sites. (c) Multiple-histidine protein exhibiting single-site binding to IMAC surface at reduced copper loading. Adjacent immobilizing ligands simultaneously chelate a single metal, preventing interaction with histidine (and other ligands).

$$Q = \frac{Cu_{acc} K_1 C}{1 + nK_1 C} \quad (4)$$

where Cu_{acc} is the total concentration of immobilized copper accessible for protein binding and K_1 is the binding constant for a protein bound to a single copper site via a single histidine. At saturation copper loading, the concentration of accessible copper is assumed equal to the total concentration of immobilized copper ($Cu_{acc} = Cu = Cu_{max}$). Parameters obtained by fitting the isotherms to eqn. 4 are given in Table V. This analysis indicates that adsorption of cytochromes *c* with single histidines blocks *ca.* 16–18 copper sites.

The diameter of hydrated cytochrome *c* is 34 Å [17]. Assuming adsorption does not involve large conformational changes, bound proteins could be expected to block further access to $34^2 = 1156$ Å^2 of surface per molecule. This area corresponds to 16 copper sites at an average spacing of *ca.* 8.5 Å between metal ions. A conceptually similar analysis applied to ion exchange indicates that adsorption of similarly sized proteins can block access to *ca.* 30 salt ions [22].

If protein adsorption only involves coordination of the imidazole ring of a single histidine residue to an immobilized copper ion, then the intrinsic binding constants should not be greater than the binding constant of free imidazole to the IMAC support. If the solvation effects involved in a protein histidine–Cu interaction are the same as for an imidazole–Cu interaction, then free imidazole should in fact provide an upper bound for the contribution of the first fully accessible histidine to protein binding. Binding constants for the H_4 and H_8 variants with fully accessible histidines become comparable to the binding constant for imidazole when the protein adsorption isotherms are fit using eqn. 4, as shown in Table V. The relatively low binding constant for H_{26} can once again be attributed to the low accessibility of its histidine.

A lower bound for the contribution of a fully accessible histidine can be estimated by comparing the binding of the H_4 and H_8 variants to the same protein without surface histidines, H(−). The binding constant of an essentially non-binding protein, H(−), can be estimated from the initial slope of its adsorption isotherm, $Cu_{acc}K_1$. The single histidines in the H_4 and H_8 variants contribute more than a factor of 200 to the binding constant, relative to the H(−) variant (Table V), and >3 kcal mol^{-1} (1 cal = 4.1868 J) to the binding free energy. For comparison, the free energy of binding of a single imidazole to aqueous Cu^{2+}-IDA is 4.8 kcal mol^{-1} at 25°C [18,19].

This simple "site exclusion" model can also explain the seemingly surprising result reported by Hutchens and Yip [20] that free copper does

TABLE V

BINDING PARAMETERS FOR SELECTED ISO-1-CYTOCHROME *c* VARIANTS BASED UPON "SITE-EXCLUSION" MODEL

Adsorption isotherms for single-histidine variants have been fit using eqn. 4. Isotherms for two-histidine proteins have been fit to eqn. 6, using K_1 from analogous single-histidine variants. Total copper loading (Cu_{acc}) is $18.5 \cdot 10^{-3}$ mmol/ml gel.

Variant	K_1 (M^{-1})	*n*	K_2	θ
H(−)	$1.6 \pm 0.4 \cdot 10^1$	N.D.[a]	–	–
H_{26}	$2.2 \pm 0.2 \cdot 10^2$	16 ± 2.2	–	–
H_4	$3.5 \pm 0.1 \cdot 10^3$	16 ± 0.2	–	–
H_8	$2.7 \pm 0.2 \cdot 10^3$	18 ± 0.7	–	–
$H_{26}H_4$	$3.5 \cdot 10^3$	14 ± 0.3	22 ± 3	0.76 ± 0.05
$H_{26}H_8$	$2.7 \cdot 10^3$	15 ± 0.4	27 ± 4	0.58 ± 0.05

[a] *n* cannot be determined.

not influence protein binding to an IMAC support and therefore must differ from immobilized copper in how it interacts with the protein. Free copper at the low concentrations used in those experiments (10–100 μM) would in fact not be expected to influence binding if the intrinsic protein-to-immobilized copper binding constants are only *ca.* $3 \cdot 10^3$ M^{-1} instead of ten times larger. Although free copper may be able to bind at sites not accessible to immobilized copper, its affinity for cytochrome *c* surface histidines is immediately apparent in ^{1}H NMR spectra [23] and is well documented for other proteins [24].

The possibility that protein binding blocks access to other copper sites was first discussed by Belew *et al.* [25], who rejected it in favor of invoking multipoint attachment of the protein to the IMAC matrix via undefined histidine, cysteine or tryptophan residues to explain the apparent high affinities. The cytochromes *c* used in the current studies do not have surface cysteine residues, and the lone surface tryptophan (33) in tuna cytochrome *c* is not present in the proteins from *S. cerevisiae* or horse. While one cannot absolutely rule out other sites (*e.g.* lysines or a free N-terminus) for multipoint attachment of the cytochromes *c* containing only one accessible histidine, the contribution of all the other surface residues is certainly small compared to that of even a poorly accessible histidine. Therefore, we favor the "site-exclusion" explanation, which yields intrinsic protein binding constants that are consistent with analogous IDA-Cu^{2+}–imidazole complexes, both immobilized and in solution. As will be shown below, this framework is also consistent with binding data for multiple-histidine proteins and is further supported by evidence of a high surface density of immobilized metal sites.

Distribution of immobilized copper sites

The Cu^{2+}-IDA complexes must be quite densely packed at the surface of this IMAC support for adsorption of cytochrome *c* to block 16 copper ions. Protein adsorption behavior at decreased copper loading provides strong evidence for this close packing of metal sites. Consider a pair of immobilized IDA ligands, L. Under copper-limited conditions, two ligands will chelate a single copper ion, provided they can both reach the metal. The L–Cu–L complex completely cages the copper, leaving no vacant coordination sites for protein binding:

$$\text{L–Cu} + \text{L} \rightleftharpoons \text{L–Cu–L} \nrightarrow \text{L–Cu–L–P}$$

If the immobilized IDA ligands are close enough together to form L–Cu–L complexes, then the total protein binding capacity should decrease rapidly at copper loadings less than maximum.

Because the metal can coordinate two IDA ligands, a distinction must be made between the concentration of immobilized copper accessible to protein (Cu_{acc}) and the total concentration of immobilized copper (Cu). Assuming equilibrium binding constants of immobilized IDA for copper that are comparable to formation constants for aqueous Cu-IDA species (*ca.* 10^{11} M^{-1} for aqueous Cu^{2+}-IDA and *ca.* 10^{17} M^{-2} for Cu^{2+}-$(IDA)_2$ [19]), all the immobilized copper will be coordinated by a single IDA group at saturation loading ($Cu_{acc} = Cu = Cu_{max}$). At lower copper loading, however, some fraction of the immobilized copper will be in the form of L–Cu–L complexes, precluded from protein interactions ($Cu_{acc} < Cu$). There is in fact no measurable adsorption of horse cytochrome *c* to the TSK IMAC gel at low concentrations of copper ($Cu:Cu_{max} < 1:3$) (Table IV). Significant residual protein binding capacity would be expected if the metal ions were isolated and could remain accessible.

Multiple-site protein binding

The existence of multiple coordinating sites on a protein surface can influence binding affinity in various ways. If two histidines bind *independently* (only one at a time), the apparent binding constant of a two-histidine protein would be twice that of a protein containing only one histidine of comparable accessibility, reflecting the increased availability of binding sites (a statistical effect). If, on the other hand, two histidines (or a histidine and another functional group) can bind *simultaneously* to distinct copper sites on the matrix (two-site binding), the binding constant could be much larger.

Two-site binding, illustrated in Fig. 4b, can be analyzed in a manner analogous to chelation in

small metal ion complexes. The increase in the binding constant for the two-histidine protein compared to a single-histidine protein (Fig. 4a) will depend on the enthalpy gained from forming the second histidine–Cu^{2+}-IDA interaction relative to the entropy lost by further constraining the protein and the metal ion complexes at the support surface. If the entropic losses and the strain introduced upon binding are negligible, the increase in the apparent binding constant can be as large as the increase in affinity of a single-histidine protein over the protein with no histidines: a factor of 10^2–10^3.

Multiple-site binding to a support whose distribution of ligands is essentially random requires that the metal ion sites be densely packed in regions of the matrix accessible to protein. Our observations that *ca.* 16 immobilized copper ions are blocked by adsorption of cytochrome *c* and that the immobilized IDA ligands are close enough to form L–Cu–L complexes indicate a site density on this TSK gel that could support multiple-site binding.

For a protein with two potential binding sites, the reaction represented by eqn. 4 can be extended to include the second interaction,

$$P + nCu \rightleftharpoons PCu + [(n-1)Cu] \quad K_1 = \frac{[PCu]}{[P][Cu]}$$

$$PCu + [(n-1]Cu] \rightleftharpoons PCu_2 + [(n-2)Cu]$$

$$K_2 = \frac{[PCu_2]}{[PCu]}$$

where PCu_2 represents a protein bound to the matrix at two copper sites. As before, n represents the number of copper ions blocked by protein binding. The second binding constant K_2 represents the apparent binding affinity of the second (histidine) side chain for a nearby copper site on the surface, a reaction of zero order in protein concentration. These equilibria yield the modified isotherm of eqn. 5,

$$Q = \frac{Cu_{acc}K_1(1+K_2)C}{1+nK_1(1+K_2)C} \quad (5)$$

Because the distribution of copper ions on the support surface is not uniform, not all proteins adsorbed via a single histidine will find appropriate sites for a second interaction. Assuming that only some fraction θ of the surface sites can accommodate strong two-site binding ($K_2 \gg 1$), while the remainder of the sites can accommodate only single-site binding ($K_2 \approx 0$), eqn. 5 can be extended to a bi-Langmuir-type equation,

$$Q = \frac{\theta Cu_{acc}K_1K_2C}{1+nK_1K_2C} + \frac{(1-\theta)Cu_{acc}K_1C}{1+nK_1C} \quad (6)$$

K_1K_2 is the apparent binding constant for protein binding via two-site interactions.

The binding data for the $H_{26}H_4$ and $H_{26}H_8$ variants can now be analyzed using eqn. 6, where Cu_{acc} equals the total copper loading ($18.5 \cdot 10^{-3}$ mmol/ml) and the binding constants K_1 for fully accessible histidines 4 and 8 are already known from the single-histidine variants H_4 and H_8. The values of K_2, θ and n obtained from the isotherms for the multiple-histidine proteins are given in Table V. Adding histidine 26 to either histidine 4 or 8 results in a 20-fold or greater increase in the apparent binding constant, relative to single-site binding, for 60% of the surface sites. This increase matches the 20-fold increase that histidine 26 provides the H_{26} variant over H(−). Similarly, the 200-fold increase histidines 4 or 8 offer the $H_{26}H_4$ and $H_{26}H_8$ variant over H_{26} is consistent with the increase of at least 200-fold these histidines offer the H_4 and H_8 variants over H(−). Thus a second, fully accessible histidine adds >3 kcal mol^{-1} to the binding energy, compared to a single-histidine protein. The values of n obtained by this analysis are also consistent with those for the single-histidine variants: *ca.* 15 copper sites are blocked by each protein molecule.

Addition of histidine 33 in $H_{26}H_{33}H_4$ variant increases the apparent initial slope by a factor of 8 compared to $H_{26}H_4$ (Table III), indicating the possibility of three-site binding. Although the analysis represented by eqn. 6 could be extended to include simultaneous three-site binding, fitting the isotherms for the three-histidine cytochrome *c* variants leaves indeterminate the three-site binding parameters analogous to θ and K_2 for two-site binding. Because of the high affinity expected for simultaneous three-site binding (*ca.* 10^7 M^{-1}), the initial slope of the adsorption isotherm must be measured accurately at im-

practically low protein concentrations ($< 10^{-7}$ M) to determine these parameters. Nonetheless, the apparent initial slope calculated from the first point on the adsorption isotherm represents a lower bound for the true initial slope. Thus simultaneous three-site binding is estimated to be at least an order of magnitude stronger than two-site binding.

The increased maximum capacity of the three-histidine variants correspondingly decreases the parameter n, the number of copper sites blocked by protein binding, from 16–18 for single-histidine proteins to only 8–10 for three-histidine proteins. The overly simplified model presented here cannot provide a satisfactory explanation for this result. The increased capacity for tighter-binding proteins could reflect a heterogeneous population of sites with different binding affinities, or, possibly, conformational rearrangement (compaction) of proteins adsorbed via high-affinity three-site interactions compared to lower-affinity single-site binding.

Binding mode changes with decreasing copper loading

We would expect binding via multiple-site interactions to depend strongly on the density and distribution of available copper ions at the support surface. While multiple-site binding might occur on a densely-derivatized support, binding should occur via single-site interactions on a support with a low concentration of available metal ions. This can be achieved easily by decreasing the copper loading (Fig. 4c). If the immobilized IDA groups are close enough to simultaneously coordinate a single metal, a decrease in copper loading results in a significant portion of the total immobilized copper sequestered in L–Cu–L complexes. This leads to a more rapid decrease in the concentration of immobilized copper accessible to protein surface groups ($Cu_{acc} < Cu$).

As shown in Fig. 5, the initial slope of the binding isotherm of a two-histidine protein decreases sharply with decreasing copper loading near the maximum ($Cu/Cu_{max} \approx 1$). At these high loadings the protein displays high-affinity binding characteristics of simultaneous, multiple-site interactions (Table IV). According to eqn. 6

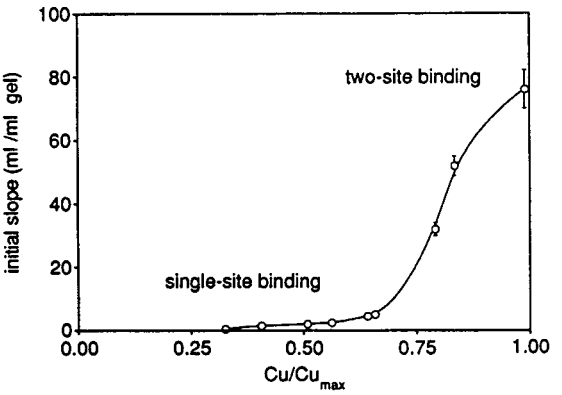

Fig. 5. Initial slopes of adsorption isotherms ($K_A Q_{max,A} + K_B Q_{max,B}$) of horse cytochrome c as a function of the fractional copper loading (Cu/Cu_{max}).

the initial slope of the adsorption isotherm is given by $\theta K_1 K_2 Cu_{acc}$. (This is proportional to protein retention in isocratic chromatography under analytical conditions ($Q \ll \theta Q_{max}/n$).) Decreasing the copper loading lowers the concentration of accessible copper sites (Cu_{acc}), which also affects the value of θK_2.

At lower copper loading ($Cu/Cu_{max} \approx 1/2$), accessible metal sites are much less densely packed, which decreases the likelihood that the surface can support high-affinity two-site binding. At these loadings, this two-histidine protein displays simple isotherms typical of single-histidine proteins (Table IV). The apparent binding constant remains roughly constant with copper concentration and is comparable to that of imidazole ($4 \cdot 10^3$ M^{-1}), suggesting that adsorption is due primarily to single-site binding to isolated copper sites. If so, the initial slope of the adsorption isotherm is $K_1 Cu_{acc}$, where K_1 does not depend on copper concentration. As expected, the initial slope of the horse cytochrome c adsorption isotherm is much less sensitive to the copper concentration in this range.

Implications of changing the binding mode from single to multiple-site interactions

The possibility that proteins can bind at multiple copper sites simultaneously has important implications for the use of existing chromatographic supports as well as the design of new ones. The non-uniform distribution of metals

results in binding sites characterized by a distribution of binding affinities, which can cause peak broadening and reduce the concentration range where linear behavior is observed.

If a protein can interact with the support at more than one metal site, the availability of metals on a particular chromatographic surface will dramatically influence the retention and separation that can be achieved. For example, retention during analytical isocratic chromatography of two proteins is governed by the ratio of the initial slopes of their respective binding isotherms. The initial slope of the isotherm is dominated by multiple-site interactions, as seen for the yeast cytochrome *c* variants with different surface histidines. The extent to which multiple-site interactions can occur is governed in turn by the density and accessibility of immobilized copper. Thus it may be possible to tailor IMAC supports for specific separations of multiple-histidine proteins by controlling the concentration of metal and how it is linked to the support.

For example, to separate a protein containing a single, high-affinity binding site (*e.g.*, a metal-chelating site [1]) from other proteins containing multiple, low-affinity binding sites (*e.g.*, non-chelating histidines), multiple-site interactions should be avoided. Multiple-site interactions are minimized at low loadings, where the metal ions are isolated. Under these conditions protein adsorption would be governed by the sum of single-site binding constants, which favor the single high-affinity site. A support with a low density of immobilized copper ions would efficiently separate a protein containing a dihistidine metal-binding site from other proteins with multiple surface histidines [13]. Because only a small fraction of the metal ions are actually involved in coordinating a protein, this could conceivably be accomplished without a drastic reduction in protein binding capacity.

Conversely, to optimize the separation of two-histidine proteins from those with single histidines, two-site interactions (θK_2) should be maximized relative to single-site interactions (K_1). The product θK_2 is sensitive to the density of copper sites, while the binding constant K_1 for a single histidine protein is not. The high density of immobilized copper sites of this TSK matrix provides for relatively large values of θ and K_2, which translate into efficient separations [16].

A logical extension of this concept is the creation of specific high-affinity binding sites by distributing metals on the chromatographic surface to match the distribution of histidines on a target protein. For example, receptor complexes that position two metals at a fixed distance selectively bind their complementary bis-imidazole "protein analogues" in the presence of other bis-imidazoles [8]. Selective chromatographic supports could be prepared by immobilizing appropriate bis-metal complexes. An alternative approach to preparing such "patterned" supports is template polymerization, in which the target molecule itself acts as a template to correctly position the metal ions in the polymer matrix during synthesis [9].

CONCLUSIONS

Equilibrium binding data for a series of homologous proteins with specifically engineered surface histidines can be interpreted within a framework that yields binding constants consistent with the behavior of analogous imidazole–copper complexes in solution and on IMAC supports. Equilibrium binding of multiple-histidine proteins is significantly tighter than expected based on statistical effects because it involves simultaneous interactions with more than one immobilized metal ion. A consequence of multiple-site interactions is a significant increase in the binding affinity that strongly depends on the metal ion distribution. This principle is not limited to metal-affinity chromatography, but should be applicable to any separation in which multiple-site interactions can dominate binding (*e.g.*, ion exchange [26]). The ability to control multiple-site interactions provides a unique opportunity to tailor IMAC and other chromatographic supports for specific protein separations.

SYMBOLS

C	protein concentration in the liquid phase (M)

K apparent equilibrium binding constant for protein adsorption (M^{-1})

K_A apparent equilibrium binding constant for protein adsorption (strong site) (M^{-1})

K_B apparent equilibrium binding constant for protein adsorption (weak site) (M^{-1})

K_1 equilibrium binding constant for protein adsorption to a single copper site via a single protein binding site (M^{-1})

K_2 equilibrium binding constant to a second copper site via a second protein binding site of an adsorbed protein

n number of copper sites blocked by protein adsorption

θ fraction of copper sites that will support simultaneous two-site binding via two protein binding sites

Cu concentration of immobilized copper (mmol/ml gel)

Cu_{max} concentration of immobilized copper at saturation copper loading (mmol/ml gel)

$Cu_{\widehat{acc}}$ concentration of immobilized copper accessible to protein binding (mmol/ml gel)

Q_{max} maximum capacity for adsorbed protein (mmol/ml gel)

$Q_{max,A}$ maximum capacity for adsorbed protein (strong sites) (mmol/ml gel)

$Q_{max,B}$ maximum capacity for adsorbed protein (weak sites) (mmol/ml gel)

ACKNOWLEDGEMENTS

This research is supported by the National Science Foundation (BCS-9108502) and the Office of Naval research (N00014-92-J-1178). F.H.A. acknowledges a fellowship from the David and Lucile Packard Foundation and a Presidential Young Investigator Award from the National Science Foundation. R.J.T. acknowledges a predoctoral training fellowship in biotechnology from the National Institute of General Medical Sciences, National Research Service Award 1 T32 GM 08346-01 from the Pharmacology Sciences Program. R.D.J. acknowledges a graduate fellowship from Kelco Division of Merck and Co., Inc.

REFERENCES

1 F.H. Arnold, *Bio/Technology*, 9 (1991) 151.
2 J.W. Wong, R.L. Albright and N.-H.L. Wang, *Sep. Purif. Methods*, 20 (1991) 49.
3 F.H. Arnold (Editor), *Methods: A Companion to Methods in Enzymology*, Vol. 4, No. 1, Academic Press, New York, 1992.
4 E.S. Hemdan, Y. Zhao, E. Sulkowski and J. Porath, *Proc. Natl. Acad. Sci. U.S.A.*, 86 (1989) 1811.
5 N.T. Mrabet, *Biochemistry*, 31 (1992) 2690.
6 T.W. Hutchens, T.-T. Yip and J. Porath, *Anal. Biochem.*, 170 (1988) 168.
7 T.W. Hutchens and T.-T. Yip, *Anal. Biochem.*, 191 (1990) 160.
8 S. Mallik, R.D. Johnson and F.H. Arnold, *J. Am. Chem. Soc.*, 115 (1993) 2518.
9 P.K. Dhal and F.H. Arnold, *J. Am. Chem. Soc.*, 113 (1991) 7417.
10 P.K. Dhal and F.H. Arnold, *Macromolecules*, 25 (1992) 7051.
11 Y. Zhao, E. Sulkowski and J. Porath, *Eur. J. Biochem.*, 202 (1991) 1115.
12 R.J. Todd, *Ph.D. Thesis*, California Institute of Technology, Pasadena, CA, 1993.
13 R. Todd, M. Van Dam, D. Casimiro, B.L. Haymore and F.H. Arnold, *Proteins: Struct. Funct. Genet.*, 10 (1991) 156.
14 E. Margoliash and N. Frohwirt, *Biochem. J.*, 71 (1959) 570.
15 S.L. Mayo, W.R. Ellis, Jr., R.J. Crutchley and H.B. Gray, *Science*, 233 (1986) 848.
16 R.J. Todd, R.D. Johnson and F.H. Arnold, unpublished results.
17 G.V. Louie and G.D. Brayer, *J. Mol. Biol.*, 214 (1990) 527.
18 P.C. Sinha, V.K. Saxena, N.B. Nigam and M.N. Srivastava, *Ind. J. Chem.*, 28A (1989) 335.
19 A.E. Martell and R.M. Smith, *Critical Stability Constants*, Vol. 2, Plenum Press, New York, 1975.
20 T.W. Hutchens and T.-T. Yip, *J. Chromatogr.*, 500 (1990) 531.
21 E. Sulkowski, *BioEssays*, 10 (1989) 170.
22 G. Jayaraman, G., S.D. Gadam and S.M. Cramer, *J. Chromatogr.* 630 (1993) 53.
23 J.T. Kellis, Jr., R.J. Todd and F.H. Arnold, *Bio/Technology*, 9 (1991) 994.
24 C.D. Moore, O.N. Al-Misky and J.T.J. Lecomte, *Biochemistry*, 30 (1991) 8357.
25 M. Belew, T.-T. Yip, L. Andersson and J. Porath, *J. Chromatogr.*, 403 (1987) 197.
26 S.D. Gadam, G. Jayaraman and S.M. Cramer, *J. Chromatogr.*, 630 (1993) 37.

Journal of Chromatography A, 662 (1994) 27–35
Elsevier Science B.V., Amsterdam

CHROM. 25 645

Poly(N-vinylpyrrolidone) shielding of matrices for dye-affinity chromatography

Improved elution of lactate dehydrogenase from Blue Sepharose and secondary alcohol dehydrogenase from Scarlet Sepharose

Igor Yu. Galaev and Bo Mattiasson*

Department of Biotechnology, Chemical Centre, Lund University, P.O. Box 124, S-221 00 Lund (Sweden)

(First received August 5th, 1993; revised manuscript received October 4th, 1993)

ABSTRACT

Poly(N-vinylpyrrolidone) (PVP) shielding of Blue Sepharose and Scarlet Sepharose proved to be an efficient method for improving the process of purification of lactate dehydrogenase (LDH) from porcine muscle and secondary alcohol dehydrogenase (SADH) from *Thermoanaerobium brockii*, respectively. PVP shielding of Blue Sepharose resulted in improvement of the efficiency of either specific or non-specific elution of LDH. PVP protection of Scarlet Sepharose resulted in an improvement in the SADH recovery during specific elution and in an improvement in enzyme purity on non-specific elution. The dynamic capacities of the columns were in both cases decreased after PVP shielding. PVP shielding is considered to prevent the matrices from binding foreign proteins and from non-specific binding of nucleotide-dependent enzymes, while not seriously impairing the specific binding of these enzymes to the affinity matrices.

INTRODUCTION

The trend in protein purification is to use affinity-mediated separation fairly early in the purification work [1–3]. Earlier, affinity chromatography was often used towards the end of a tedious purification scheme when only minor contaminants with properties close to those of the target molecule were present. With the development towards the early application of affinity-mediated purification, some constraints are introduced. Stable, small ligands are preferred instead of proteinaceous ligands, even if the former are less specific [4]. This leads to group-specific isolation, and in many cases also some non-specific co-purification. The ligands belonging to this group of stable, small compounds are, *e.g.*, textile dyes [5–11], hydrophobic groups [12–15], chelating ligands [16,17] and boronates [18].

"Dye-affinity" chromatography using triazine dyes coupled to different matrices is widely used for the purification of dehydrogenases and kinases [5–11]. Traditionally these enzymes are eluted either specifically with nucleotide solutions or non-specifically with high salt concentrations [19,20]. Low or moderate recoveries (30–70%) of nucleotide-dependent enzymes by affinity chromatography using Cibacron Blue-substituted matrices [21–25] or Scarlet Red-substituted Sepharose [26] have been reported.

* Corresponding author.

0021-9673/94/$07.00
SSDI 0021-9673(93)E1089-I

Textile dyes have been described as having potential use in the purification of many different proteins [6–11,21–25]. The importance of this group of ligands has led to the development of a range of new synthetic dyes specially designed to become more specific [27].

An alternative mode of operation would be to try to manipulate the binding to the ligand and thereby to reduce the amount of non-specifically bound protein. From earlier model studies we have shown that additions of polymers such as poly(N-vinylpyrrolidone) (PVP) to Cibacron Blue formed complexes that shielded the dye from forming weak interactions with proteins. This resulted in an improved elution of lactate dehydrogenase from PVP-shielded Blue Sepharose. Both specific and non-specific elution were improved [28].

This work was carried out with the aim of investigating the possibility of exploiting the interaction between triazine dyes and PVP to improve the performance in the affinity-mediated separation of enzymes from crude homogenates with the idea that decreased non-specific binding would simplify the overall purification procedure.

EXPERIMENTAL

Lactate dehydrogenase type XXX-S from porcine muscle, β-NADH grade III, β-NADP sodium salt, Cibacron Blue 3GA and PVP K 26-35 with an average molecular mass of 40 000 were purchased form Sigma (St. Louis, MO, USA). Oxamic acid was purchased from BDH (Poole, UK). Blue Sepharose was synthesized by coupling Cibacron Blue 3GA to Sepharose CL-4B according to ref. 29. The Cibacron Blue content determined according to ref. 30 was 4.9 μmol per ml of swollen gel. Scarlet Sepharose was a generous gift from Professor R.K. Scopes (Centre for Protein and Enzyme Technology, La Trobe University, Australia) and was synthesized by coupling of Procion Scarlet H-2G to Sepharose CL-4B according to ref. 31.

Minced pork was purchased in a local shop and homogenized in ice-cold 20 m*M* Tris–HCl buffer (pH 7.3) containing 1 m*M* EDTA (10 ml of buffer per gram of muscle tissue). The homogenate was filtered through a synthetic fibre pad to remove larger particulate matter, centrifuged for 15 min to remove cell debris and the supernatant was filtered through Munktell filter-paper to remove traces of fat. The porcine muscle extract was kept frozen without any loss of LDH activity and was applied directly, after thawing and filtering, to the Blue Sepharose column. The crude extract had an activity of 64 U/ml and a protein content of 5.5 mg/ml (specific activity 11.6 U/mg protein).

The obligate anaerobic thermophilic organism *Thermoanaerobium brockii* was cultured in batch according to ref. 32. Cells were harvested by centrifugation and stored frozen at −18°C. Cells were not maintained under strictly anaerobic conditions during harvesting and storage. Extraction of cells was carried out by sonication in 20 m*M* morpholinopropanesulphonate buffer (pH 6.5) containing 30 m*M* NaCl and 2 m*M* $MgCl_2$ (MES buffer) (4 ml per gram wet mass of cells). Cell debris was removed by centrifugation and the supernatant was applied directly to the column. The crude extract had an activity of 49 U/ml and a protein content of 14.0 mg/ml (specific activity 3.5 U/mg protein).

Chromatographic experiments using Blue Sepharose

All chromatographic experiments with Blue Sepharose were carried out at room temperature using a 9.8 × 0.9 cm I.D. column at a flow-rate of 0.55 ml/min. All solutions introduced to the column were in 20 m*M* Tris–HCl buffer (pH 7.3). The porcine muscle extract was applied to the column until breakthrough of LDH (120–200 ml with the untreated column and 60–70 ml with the PVP-shielded column). The column was washed with buffer until no more protein (monitored as absorbance at 280 nm) was detected in the eluate. Non-specific elution of LDH was performed with 1.5 *M* KCl and specific elution was performed with 10 m*M* oxamate + 0.1 m*M* NADH. Fractions were collected every 20 min when eluted from the untreated column and every 5 min when eluted from the PVP-shielded column. The height equivalent to a theoretical plate (HETP) was calculated as $HETP = L/N$, where L is the bed length and N is the number

of theoretical plates calculated as $N = 5.54 (V/W_{1/2})^2$, where V is the elution volume and $W_{1/2}$ is the peak width at half-height.

Chromatographic experiments using Scarlet Sepharose

All chromatographic experiments with Scarlet Sepharose were carried out at room temperature using a 2.8 × 0.9 cm I.D. column at a flow-rate of 0.09 ml/min. For SADH elution all solutions introduced to the column were in MES buffer. The cell extract was applied to the column until breakthrough of SADH. The column was washed with buffer until no more protein (monitored as absorbance at 280 nm) was detected in the eluate. Non-specific elution of SADH was performed with 1.5 *M* KCl and specific elution with 0.5 m*M* NADP. For LDH elution all solutions introduced into the column were in 20 m*M* Tris–HCl buffer (pH 7.3). The porcine muscle extract was applied to the column until breakthrough of LDH. The column was washed with buffer until no more protein (monitored as absorbance at 280 nm) eluted. Non-specific elution of LDH was performed with 1.5 *M* KCl and specific elution with 10 m*M* oxamate + 0.1 m*M* NADH. Fractions were collected every 15 min.

The PVP shielding of the columns was performed with 1% PVP-40 000 solution followed by washing with 1.5 *M* KCl (pH 3.4) until no PVP was detected in the effluent. This was followed by re-equilibration of the column with an appropriate buffer.

LDH activity was measured in the fractions according to a reported procedure [33]. SADH activity was measured in the fractions according to ref. 26. Concentration of PVP was measured as the absorbance of a polymer–iodine complex at 480 nm, the complex being produced according to ref. 34. Protein was determined according to Lowry *et al.* [35].

Sodium dodecyl sulphate polyacrylamide gel electrophoresis (SDS-PAGE) with 12% gel was performed according to ref. 36 using carbonic anhydrase (M_r 31 000), ovalbumin (M_r 45 000), bovine serum albumin (M_r 66 200) and phosphorylase B (M_r 92 500) as standards.

RESULTS AND DISCUSSION

Application of porcine muscle extract to a fresh Blue Sepharose column until breakthrough resulted in binding of LDH along with a significant amount of foreign proteins, which could not be eluted with the buffer. Non-specific elution with 1.5 *M* KCl resulted first in the elution of foreign proteins followed by LDH with a recovery of 76% as judged from activity measurements (Fig. 1 and Table I). The LDH recovery increased gradually to nearly 100% only after subsequent purification cycles with application of porcine muscle extract to the same column. Thus, pretreatment of Blue Sepharose with the homogenate resulted in masking of sites capable of non-specific irreversible binding of LDH. The same effect occurred during the specific elution of LDH with 0.1 m*M* NADH + 10 m*M* oxamate, but in contrast to non-specific elution foreign proteins adsorbed on the column were not eluted during specific elution. After specific elution the column needed to be regenerated; foreign proteins could be eluted with 1.5 *M* KCl (Fig. 2).

The PVP shielding of the column resulted in a

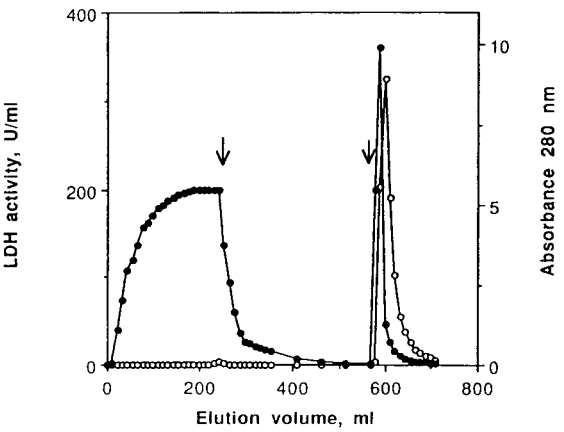

Fig. 1. Elution profile of (○) LDH activity and (●) protein with 1.5 *M* KCl from unmodified Blue Sepharose. Arrows indicate when washing with buffer and elution with 1.5 *M* KCl were begun. Experimental conditions: 9.8 × 0.9 cm I.D. column; the porcine muscle extract was applied to the column until breakthrough of LDH; the column was washed with 20 m*M* Tris–HCl buffer (pH 7.3) until no more protein (monitored as absorbance at 280 nm) eluted; LDH was eluted at a flow-rate of 0.55 ml/min with 1.5 *M* KCl; fractions were collected every 20 min.

TABLE I

LDH PREPARATIONS PRODUCED BY DIFFERENT ELUTION MODES

Material	Mode of chromatography	Enzyme bound (U)	Enzyme eluted (U)	Elution volume (ml)	Activity[a] (U/ml)	Protein[a] (mg/ml)	Specific activity[a] (U/mg)	Recovery (%)	Purification (-fold)[a]
Unmodified Blue Sepharose[b]	Non-specific elution	7120	5410	126.5	325	1.5	216	76	19
	Specific elution	12 100	5590	110	499	2.1	237	46	20
PVP-treated Blue Sepharose[c]	Non-specific elution	4200	4040	11	1160	5.2	223	96	19
	Specific elution	3550	3480	13.8	777	3.8	204	98	18
Unmodified Scarlet Sepharose[b]	Non-specific elution	1360	1280	10.8	760	13.8	55	94	4.7
	Specific elution	903	650	6.8	260	1.6	162	72	14
PVP-treated Scarlet Sepharose[c]	Non-specific elution	616	665	5.4	540	4.3	125	108	11
	Specific elution	375	364	5.4	290	1.6	180	97	15
Commercial sample					597	3.1	192		
Crude extract					64	5.5	11.6		

[a] In the peak fraction.
[b] First run on the newly packed column.
[c] First run on the newly packed and PVP-shielded column.

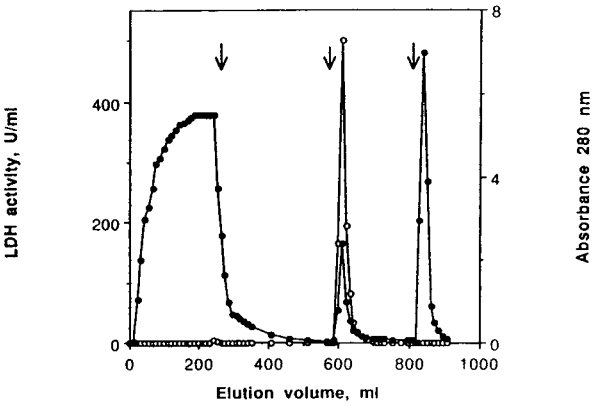

Fig. 2. Elution profile of (○) LDH activity and (●) protein from unmodified Blue Sepharose with 0.1 m*M* NADH + 10 m*M* oxamate, followed by elution with 1.5 *M* KCl. Arrows indicate when washing with buffer, elution with 0.1 m*M* NADH + 10 m*M* oxamate and elution with 1.5 *M* KCl were begun. Experimental conditions as in Fig. 1, except that LDH was eluted with 0.1 m*M* NADH + 10 m*M* oxamate.

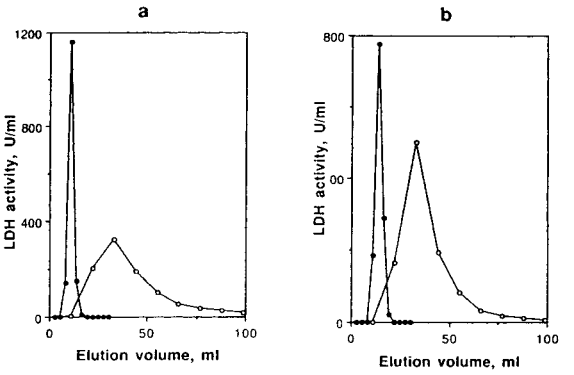

Fig. 3. Elution profile of LDH activity with (a) 1.5 *M* KCl and (b) 0.1 m*M* NADH + 10 m*M* oxamate from (○) unmodified and (●) PVP-treated Blue Sepharose. Experimental conditions: 9.8 × 0.9 cm I.D. column was treated with 1% PVP-40 000 solution followed by washing with 1.5 *M* KCl (pH 3.4) until no PVP was detected in the eluate, and re-equilibration with 20 m*M* Tris–HCl buffer (pH 7.3); the porcine muscle extract was applied to the column until breakthrough of LDH; the column was washed with buffer until no more protein (monitored as absorbance at 280 nm) eluted; LDH was eluted at a flow-rate of 0.55 ml/min with 1.5 *M* KCl or 10 m*M* oxamate + 0.1 m*M* NADH; fractions were collected every 20 min when eluted from the untreated column and every 5 min when eluted from the PVP-protected column. The total amount of LDH eluted from the column was taken as 100% in both instances for the sake of comparison.

significant decrease in binding of foreign proteins and in an improvement in the effectiveness of elution of LDH either specifically or non-specifically (Fig. 3). The decreased binding of foreign proteins with the PVP-shielded column eliminated the need for a regeneration step after the specific elution. The column could be used repeatedly after re-equilibration with buffer. The LDH recovery was about 100% even during the first run on a fresh Sepharose Blue column shielded with PVP. Thus, PVP blocked the sites to which LDH irreversibly bound. Some proteins from the homogenate played the same role during the first application of porcine muscle extract on to a Blue Sepharose column. It is preferable to use PVP to block binding sites on the matrix rather than an unidentified mixture of proteins from the homogenate. PVP is a cheap, stable, non-toxic and highly biocompatible polymer [37]. No polymer was detected in the eluate from the PVP-protected column during chromatography of LDH (the sensitivity of the method of PVP assay being 0.1 mg/ml).

PVP shielding resulted in a significant improvement in the effectiveness of the elution. The HETP for the untreated column was 1.3 cm (non-specific elution) and 0.47 cm (specific elution). PVP shielding decreased the HETP to 0.13 cm for both types of elution. LDH is eluted from the PVP-shielded column as a symmetrical peak and about 95% of eluted enzyme can be collected in a volume of 8 ml. LDH is eluted from an untreated column of the same size with significant tailing, and 95% of eluted LDH can be collected only in a volume of about 100 ml (Fig. 3). A volume decrease is preferable for the further downstream processing because the cost of the purification step is usually proportional to the feed concentration.

PVP shielding with a 1% polymer solution is a relatively inexpensive procedure, and considerably cheaper than, for instance, regeneration of the column with the same volume of 1.5 *M* KCl. The price of PVP-40 000 according to Sigma is $101.2/kg whereas that of KCL is $34.1/kg, but the latter is used at a ten times higher concentration (1.5 *M* KCl corresponds approximately to a 10% solution). Moreover, PVP adheres to the column and can be reused.

TABLE II

SADH PREPARATIONS PRODUCED BY DIFFERENT ELUTION MODES

Material	Mode of chromatography	Enzyme bound (U)	Enzyme eluted (U)	Elution volume (ml)	Activity[a] (U/ml)	Protein[a] (mg/ml)	Specific activity[a] (U/mg)	Recovery (%)	Purification (-fold)[a]
Unmodified Scarlet Sepharose[b]	Non-specific elution	1970	2130	8.1	308	6.1	50.5	108	14
	Specific elution	2525	1790	12.5	174	1.16	150	71	43
	Non-specific elution after specific		910	6.8	156	3.5	44.6	36	1
PVP-treated Scarlet Sepharose[c]	Non-specific elution	371	367	6.8	220	1.8	122	99	35
	Specific elution	240	224	8.1	81	0.5	162	93	46
	Non-specific elution after specific elution		19	6.8	7.8	0.6	13	8	3.7
Crude extract	Non-specific elution				49	14.0	3.5		

[a] In the peak fraction.
[b] First run on the newly packed column.
[c] First run on the newly packed and PVP-shielded column.

The results obtained correspond well with previous data on zonal elution of pure LDH from PVP-shielded Sepharose Blue [28]. PVP, owing to its high affinity to Cibacron Blue ligands, occupied sites capable of non-specific binding of foreign proteins and of irreversible binding of LDH and prevented this binding. LDH is considered to bind to PVP-protected Blue Sepharose only due to specific interactions of Cibacron Blue ligands with nucleotide binding sites of the enzyme. The number of sites suitable for specific binding is less than the total number of specific and non-specific LDH binding sites in unmodified Blue Sepharose. This resulted in a decrease in dynamic capacity from 1150–1950 U/ml swollen gel (230–400 U/mmol Cibacron Blue ligand) for the untreated column to 680–570 U/ml swollen gel (120–140 U/mmol Cibacron Blue ligand) for the PVP-shielded column.

Table I and Fig. 4 show virtually the same purity of LDH samples, obtained as the result of specific and non-specific elution from unmodified and PVP-shielded Blue Sepharose. In all cases, one step purification using dye-affinity chromatography resulted in highly purified preparations.

Application of a *Thermoanaerobium brockii* extract to a Scarlet Sepharose column resulted in adsorption of SADH along with significant amounts of foreign proteins. This behaviour resembled that of LDH binding to Blue Sepharose, but in contrast to the latter case foreign proteins were eluted simultaneously with SADH by 1.5 *M* KCl, resulting in a poor purification (Table II and Fig. 5, lane 2). Specific elution

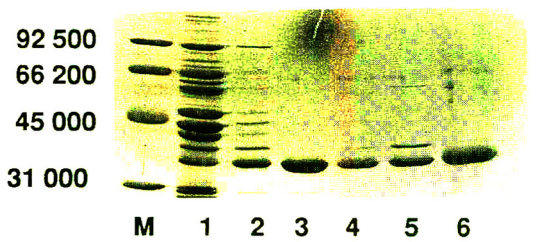

Fig. 4. SDS-PAGE patterns for LDH. Lanes: M = marker proteins; 1 = crude extract; 2 and 4 = elution with 1.5 *M* KCl from unmodified and PVP-treated Blue Sepharose, respectively; 3 and 5 = elution with 0.1 m*M* NADH + 10 m*M* oxamate from unmodified and PVP-protected Blue Sepharose, respectively; 6 = commercial sample.

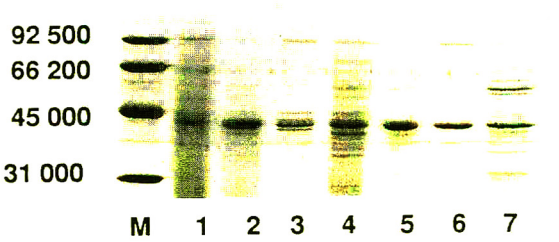

Fig. 5. SDS-PAGE patterns for SADH. Lanes: M = marker proteins; 1 = crude extract; 2 and 5 = elution with 1.5 *M* KCl from unmodified and PVP-treated Scarlet Sepharose, respectively; 3 and 6 = elution with 0.5 m*M* NADP from unmodified and PVP-protected Scarlet Sepharose, respectively; 4 and 7 = elution with 1.5 *M* KCl after elution with 0.5 m*M* NADP from unmodified and PVP-treated Scarlet Sepharose, respectively.

with 0.5 m*M* NADP resulted in more pure enzyme preparation with a recovery of 70%, and the remaining 30% of SADH activity could be eluted together with other adsorbed proteins by 1.5 *M* KCl as crude preparation (Table II and Fig. 5, lanes 3 and 4). The specific elution at lower loadings gave lower recoveries and in the zonal mode SADH was not eluted by 0.5 m*M* NADP at all. The strong binding of SADH to Scarlet Sepharose was also reported by Nagata *et al.* [26], who managed to obtain a 70% recovery only during overloading conditions; with conventional loading, elution with 0.5 m*M* NADP was not successful.

The PVP shielding of Scarlet Sepharose resulted in an improvement in the effectiveness of specific elution and purity of the enzyme preparation, the recovery being 93% (Fig. 5, lane 6, and Fig. 6). Again, as with Blue Sepharose, PVP shielding of Scarlet Sepharose prevented adsorption of foreign proteins and non-specific interaction of SADH with the matrix. The decreased adsorption of foreign proteins resulted in a reasonable purity of SADH even after non-specific elution from the PVP-treated column (Table II and Fig. 5, lane 5). The dynamic capacity of the column was decreased 5.3–10.5-fold after PVP protection.

The non-specific interactions seemed to be more pronounced with Scarlet Sepharose, which bound more foreign proteins than Blue Sepharose did, especially when porcine muscle extract was applied. LDH and SADH are eluted readily

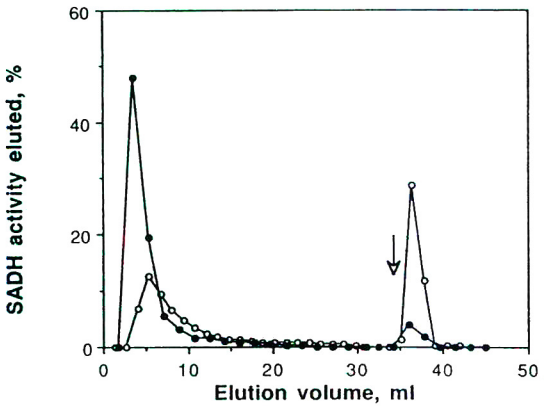

Fig. 6. Elution profile of SADH activity with 0.5 m*M* NADP from (○) unmodified and (●) PVP-treated Blue Sepharose followed by elution with 1.5 *M* KCl. The arrow indicates when elution with 1.5 *M* KCl was begun. Experimental conditions: 2.8 × 0.9 cm I.D. column was treated with 1% PVP-40 000 solution followed by washing with 1.5 *M* KCl (pH 3.4) until no PVP was detected in the eluate, and re-equilibration with 20 m*M* morpholinopropane sulphonate buffer (pH 6.5) containing 30 m*M* NaCl and 2 m*M* $MgCl_2$; the *Thermoanaerobium brockii* extract was applied to the column until breakthrough of SADH; the column was washed with buffer until no more protein (monitored as absorbance at 280 nm) eluted; SADH was eluted at a flow-rate of 0.09 ml/min with 0.5 m*M* NADP; fractions were collected every 15 min. The total amount of SADH eluted from the column was taken as 100% in both instances for the sake of comparison.

from Scarlet Sepharose with 1.5 *M* KCl along with foreign proteins. One could see a deep red ring of haeme-containing proteins on the Scarlet Sepharose column during KCl elution after application of porcine muscle extract, and the LDH-containing eluate fractions were coloured red. A high adsorption of foreign proteins resulted in poor purity of LDH preparations after dye-affinity chromatography on Scarlet Sepharose (Table I). Even in that case, PVP shielding of Scarlet Sepharose improved the purity of LDH preparations, although they had a lower specific activity compared with LDH preparations obtained after elution from untreated and PVP-treated Blue Sepharose.

Thus, PVP protection of dye-affinity matrices significantly decreased the adsorption of foreign proteins and also non-specific binding of the target molecules. The phenomena observed are interpreted as being the result of a shielding effect by PVP of the textile dye and also of non-specific sites of the support. PVP has affinity for the triazine dye, but when a dehydrogenase with higher affinity appears, displacement takes place. Owing to multi-point attachment, this displacement is local and the polymer stays on the column. The shielded ligand dye-affinity chromatographic process is characterized by improved elution effectiveness, facilitated column regeneration if specific elution is used, no decrease in the purity of enzyme preparations and a decrease in the dynamic capacity of the column. This concept of improving the performance of dye-affinity chromatography is now being further evaluated in our laboratory.

ACKNOWLEDGEMENTS

The support of the Swedish Royal Academy of Sciences (KVA), the National Swedish Board for Technical and Industrial Development (NUTEK), the Swedish Agency for Cooperation with Developing Countries (SAREC) and the Swedish Research Council for Engineering Sciences (TFR) is gratefully acknowledged. The authors thank Professor Robert K. Scopes for generously providing Scarlet Sepharose, Nora Perotti for the synthesis of Blue Sepharose, Dr. Olle Holst and Åsa Rosenlund for cultivation of cells, Eva Linné-Larsson for practical advice on electrophoresis and Dr. Rajni Kaul for linguistic advice.

REFERENCES

1 G. Johansson, in H. Walter, D.E. Brooks and D. Fisher (Editors), *Partitioning in Aqueous Two-Phase Systems —Theory, Methods, Uses and Applications to Biotechnology*, Academic Press, New York, 1985, p. 161.
2 R. Kaul and B. Mattiasson, *Bioseparation*, 3 (1992) 1.
3 R.W. Leser and J.A. Asenjo, *J. Chromatogr.*, 584 (1992) 43.
4 C.R. Lowe, in M.A. Vijayalakshmi and O. Bertrand (Editors), *Protein–Dye Interactions: Developments and Applications*, Elsevier Applied Science, London, 1989, p. 11.
5 F. Qadri, *Trends Biotechnol.*, 3 (1985) 7.
6 C.V. Stead, *Bioseparation*, 2 (1991) 129.
7 M.A. Vijayalakshmi, *Trends Biotechnol.*, 7 (1989) 71.

8 T. Makriyannis and Y.D. Clonis, *J. Chromatogr.*, 28 (1993) 179.
9 Y.D. Clonis, T. Atkinson C.J. Bruton and C.R. Lowe (Editors), *Reactive Dyes in Protein and Enzyme Technology*, Macmillan, Basingstoke, 1987.
10 Y.D. Clonis, in M.T.W. Hearn (Editor), *HPLC of Proteins and Polynucleotides*, VCH, New York, 1991, Ch. 13, p. 453.
11 Y.D. Clonis, *CRC Crit. Rev. Biotechnol.*, 7 (1988) 163.
12 A.J. Alpert, *J. Chromatogr.*, 359 (1986) 85.
13 Y. Guan, X.-Y. Wu, T.E. Treffry and T.H. Lilley, *Biotechnol. Bioeng.*, 40 (1992) 517.
14 Y. Kato, T. Kitamura and T. Hashimoto, *J. Chromatogr.*, 298 (1984) 407.
15 Y.L.K. Sing, Y. Kroviarski, S. Cochet, D. Dhermy and O. Bertrand, *J. Chromatogr.*, 598 (1992) 181.
16 E. Sulkowski, *Trends Biotechnol.*, 3 (1985) 1.
17 R. Woker, B. Campluvier and M.-R. Kula, *J. Chromatogr.*, 584 (1992) 85.
18 P.D.G. Dean, F.A. Middle, C. Longstaff, A. Bannister and J.J. Dembinski, in I.M. Chaiken, M. Wilchek and I. Parikh (Editors), *Affinity Chromatography and Biological Recognition*, Academic Press, Orlando, 1983, p. 433.
19 A.A. Glemza, B.B. Baskeviciute, V.LA. Kadusevicius, J.H.J. Pesliaskas and O.F. Sudziusviene, in M.A. Vijayalakshmi and O. Bertrand (Editors), *Protein–Dye Interactions: Developments and Applications*, Elsevier Applied Sci. Publ., London, 1989, p. 107.
20 R.K. Scopes, in M.A. Vijayalakshmi and O. Bertrand (Editors), *Protein–Dye Interactions: Developments and Applications*, Elsevier Applied Sci. Publ., London, 1989, p. 97.
21 A.J. Anderson, *J. Chem. Educ.*, 65 (1988) 901.
22 R. Harkins, J. Black and M. Rittenberg, *Biochemistry*, 16 (1977) 3831.
23 M. Morill, S.T. Thompson and E. Stellwagen, *J. Biol. Chem.*, 254 (1979) 4371.
24 B. Notton, R. Fido and E. Hewitt, *Plant Sci. Lett.*, 8 (1977) 165.
25 C.S. Ramadoss, J. Steczko, J.W. Uhlig and B. Axelrod, *Anal. Biochem.*, 130 (1983) 481.
26 Y. Nagata, K. Maeda and R.K. Scopes, *Bioseparation*, 2 (1992) 35.
27 C.R. Lowe, S.J. Burton, N.P. Burton, W.K. Alderton, J.M. Pitts and J.A. Thomas, *Trends Biotechnol.*, 10 (1992) 442.
28 I.Yu. Galaev and B. Mattiasson, *J. Chromatogr.*, 648 (1993) 367.
29 W. Heyns and P. De Moor, *Biochim. Biophys. Acta*, 358 (1974) 1.
30 G.K. Chambers, *Anal. Biochem*, 83 (1977) 551.
31 R.K. Scopes, *Anal. Biochem.*, 136 (1984) 525.
32 J.G. Zeicus, P.W. Hegge and M.A. Anderson, *Arch. Microbiol.*, 122 (1979) 41.
33 *Worthington Enzymes and Related Biochemicals*, Worthington Biochemical, Freehold, NJ, 1982, p. 109.
34 *European Pharmacopea*, Maisonneuve, Sainte-Ruffine, 1986, 2nd ed., Part I, p. 685-2.
35 O.H. Lowry, N.J. Rosebrough, A.L. Far and R.J. Randall, *J. Biol. Chem.*, 193 (1951) 265.
36 U.K. Laemmli, *Nature*, 227 (1970) 680.
37 H.F. Mark, N.G. Gaylord and N.M. Bikales (Editors), *Encyclopedia of Polymer Science and Technology*, Vol. 14, Wiley, New York, 1971, p. 244.

Journal of Chromatography A, 662 (1994) 37–47
Elsevier Science B.V., Amsterdam

CHROM. 25 637

Preparation and chromatographic properties of uniform size cross-linked macroporous poly(vinyl *p-tert.*-butylbenzoate) beads

Evaluation of preferential retention toward organohalides

Ken Hosoya*, Etsuko Sawada, Kazuhiro Kimata, Takeo Araki and Nobuo Tanaka

Department of Polymer Science, Kyoto Institute of Technology, Matsugasaki, Sakyo-ku, Kyoto 606 (Japan)

(First received February 2nd, 1993; revised manuscript received October 11th, 1993)

ABSTRACT

Uniform size cross-linked macroporous poly(vinyl *p-tert.*-butyl benzoate) beads (VPTBBA) were prepared by a two-step swelling and polymerization method. VPTBBA was obtained in 78% yield and utilized as a packing material in high-performance liquid chromatography. The specific surface area of VPTBBA, which had a polymodal broad pore size distribution, was calculated as 314 m^2/g by the BET method. In the reversed-phase mode, VPTBBA showed preferential retention towards some aromatic and/or aliphatic halogenated compounds. In a comparison of its chromatographic properties with those on other packing materials such as two kinds of poly(vinyl carboxylate)-based beads, poly(styrene–divinylbenzene) beads and poly(methyl methacrylate–ethylene dimethacrylate) beads, and a silica-based monomeric C_{18} stationary phase, the selectivities on VPTBBA can be explained mainly based on both dipole–dipole interactions caused by the π-acidic phenyl group of VPTBBA and preferential retention towards planer solutes. Moreover, the relatively hydrophobic *tert.*-butyl groups contribute to steric selectivity and to the total hydrophobicity of the packing material.

INTRODUCTION

Halogenated organic compounds are one of the most serious environmental contaminants because they possibly cause cancer, deformity or at least health disorders [1–7]. Therefore, attempts have been made to remove organohalides such as dioxins from the environment [8–13]. Toxic chlorinated dibenzo-*p*-dioxins (PCDDs) are photodecomposed using various techniques to produce less toxic compounds [14–20] and the removal of halogenated alkanes or alkenes utilized as dry-cleaning solvents such as chloroform, trichloroethane and tetrachloroethylene from air and environmental water has also been attempted [21], but for efficient operation it is necessary to concentrate these toxic pollutants from the environmental media because their concentrations are usually low, especially in aqueous media [22].

Recently, a slightly cross-linked polymer of vinyl *p-tert.*-butyl benzoate was reported to show preferential absorption of organohalides such as chloroform and tetrachloroethylene [23]. A soft gel, Chloroclean, is now commercially available for the absorption of organohalides. This monomer is chromatographically interesting because it contains an aromatic ester group with a bulky

* Corresponding author.

SSDI 0021-9673(93)E1076-C

and hydrophobic *tert.*-butyl substituent at the *para* position of the phenyl ring.

Here, we report on the preparation of a size monodisperse HPLC packing material of cross-linked poly(vinyl *p-tert.*-butyl benzoate) beads (VPTBBA) utilizing a two-step swelling and polymerization method [24] and its chromatographic properties in comparison with typical polymer packing materials such as poly(styrene–divinylbenzene) particles (ST) and poly(methyl methacrylate–ethylene dimethacrylate) particles (MMA) and also a typical silica-based stationary phase such as a C_{18} phase. Moreover, two other kinds of cross-linked poly(vinyl carboxylate)s were utilized as reference packing materials for comparison of their chromatographic properties with those of VPTBBA.

EXPERIMENTAL

Materials

Vinyl *p-tert.*-butylbenzoate (CAS No. 15484-80-7) and vinyl cyclohexanecarboxylate were gifts from Fuso Chemical (Osaka, Japan) and vinyl benzoate was purchased from Polyscience (Warrington, PA, USA). A methanol solution of standard halogenated compounds, "Organohalides Std. Soln. A", was purchased from Wako (Osaka, Japan) and all other solutes except tetrachlorodibenzo-*p*-dioxins (TCDDs) were purchased from Nacalai Tesque (Kyoto, Japan). Styrene, divinylbenzene (55% grade), methyl methacrylate and ethylene dimethacrylate were also purchased from Nacalai Tesque.

Preparation of six monodisperse polymer beads

Polystyrene seed particles were prepared by an emulsifier-free emulsion polymerization method reported elsewhere [25]. A two-step swelling and polymerization method took place using dibutyl phthalate as an activating solvent (first-step swelling) followed by further swelling with monomers including porogenic solvent (second-step swelling) at room temperature [26]. The ratio of monomer, cross-linking agent and porogenic solvent was 25:25:50 (v/v/v). Polymerization was carried out at 80°C under an argon atmosphere for 24 h and extraction of porogenic solvent (toluene or cyclohexanol) was carried out by repeated washing with methanol, tetrahydrofuran and toluene. The specific surface area was measured by a Porous Materials automated BET machine and the mercury intrusion method was examined using a Porous Materials Model 60K-A-1 automated porosimeter. These measurements were carried out at the Department of Chemistry, Cornell University (Ithaca, NY, USA) with the permission of Professor Jean M.J. Fréchet.

Chromatography

All chromatographic solvents were purchased from Nacalai Tesque and used without further purification. The polymer particles were packed into a stainless-steel column 100 or 150 mm × 4.6 mm I.D.) using the slurry method. HPLC was performed with a Jasco, 880-PU intelligent pump or a Shimadzu, LC-4A ternary gradient pump equipped with a Rheodyne Model 7125 valve loop injector. Peak monitoring was carried out with a Jasco UVIDEC-100-III or a Shimadzu SPD-2A UV detector set at 254 or 280 nm and with a refractive index detector. Peak information was recorded with Shimadzu C-R4A and C-R3A Chromatopacs. The reproducibility of retention time in duplicate was better than 2%. Polystyrene standard samples for size-exclusion chromatography were purchased from Polymer Laboratories.

Separation of tetrachlorodibenzo-p-dioxins (TCDDs)

Separations of TCDDs were carried out at the Centers for Disease Control (CDC) (Atlanta, GA, USA) using a Waters HPLC system and detection was carried out at 230 nm. All the TCDDs were used with permission of Dr. Donald G. Patterson, Jr. (CDC).

RESULTS AND DISCUSSIONS

Preparation of size monodisperse particles

In addition to the poly[vinyl *p-tert.*-butylbenzoate (1)–ethylene dimethacrylate] packing (VPTBBA), poly[vinyl benzoate (2)–ethylene dimethacrylate] (VBA) and poly[vinyl cyclohexanecarboxylate (3)–ethylene dimethacrylate] packings (VCHA) were also prepared as refer-

TABLE I

CHEMICAL YIELDS OF THE PREPARED PARTICLES

Monomer	Cross-linker	Porogen	Yield (%)	Abbreviation
1[a]	EDMA[b]	Toluene	78	VPTBBA
2[a]	EDMA[b]	Toluene	79	VBA
3[a]	EDMA[b]	Toluene	72	VCHA
Styrene	DVB[c]	Cyclohexanol	91	ST
Methyl methacrylate	EDMA[b]	Cyclohexanol	95	MMA

[a] See Fig. 1.
[b] Ethylene dimethacrylate.
[c] Divinylbenzene.

ence packing materials. The structures of the monomers utilized are depicted in Fig. 1. The volume ratio of monomers, porogen and other additives and the polymerization conditions were identical. However, with vinyl *p-tert.*-butylbenzoate, it took 24 h to complete the swelling, whereas with vinyl benzoate and vinyl cyclohexanecarboxylate only 2–4 h were required.

Yields calculated based on the amounts of the monomers including cross-linking agent utilized in the swelling step were less than 80% (Table I). These yields are relatively lower than those of the prepared poly(styrene–divinylbenzene) particles (ST) or poly(methyl methacrylate–ethylene dimethacrylate) particles (MMA), which gave quantitative yields [27]. These findings can be explained by the difference in copolymerization reactivity ratio between ethylene dimethacrylate and vinyl carboxylates. For example, the copolymerization reactivity ratio between a monomer with methyl methacrylate (M_1) and vinyl *p-tert.*-butylbenzoate (M_2) are reported to be 20.07 and 0.0565 for r_1 and r_2, respectively [23]. The difference means that at an early stage of the polymerization, preferential polymerization between ethylene dimethacrylates as depicted in eqn. 1 [28] takes place, resulting in a low content of vinyl *p-tert.*-butylbenzoate in the cross-linked polymer.

vinyl *p-tert.*-butylbenzoate •

+ ethylene dimethacrylate (easy)

vinyl *p-tert.*-butylbenzoate •

+ vinyl *p-tert.*-butylbenzoate (difficult)

ethylene dimethacrylate •

+ vinyl *p-tert.*-butylbenzoate (difficult)

ethylene dimethacrylate •

+ ethylene dimethacrylate (easy) (1)

On the basis of elemental analysis data (Table II), the experimentally obtained mole ratio of

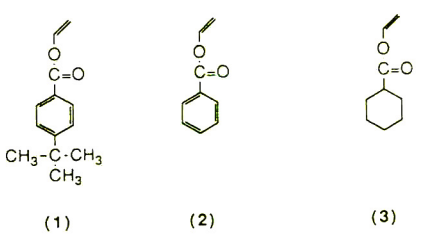

Fig. 1. Structures of monomers.

TABLE II

ELEMENTAL ANALYSIS OF PARTICLES

Packing material	H (%)	C (%)	O (%)
VPTBBA	7.34	64.08	28.58
VBA	6.48	62.97	30.55
VCHA	7.71	62.20	30.09
ST	8.08	90.65	–
MMA	7.37	59.03	33.60

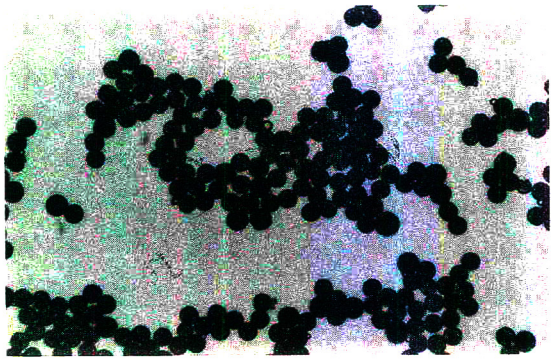

Fig. 2. Optical micrograph of VPTBBA (×450).

the polymerized vinyl *p-tert.*-butylbenzoate and ethylene dimethacrylate was calculated as 3:7. As the theoretical mole ratio should be 5:5, a loss of vinyl *p-tert.*-butylbenzoate resulted in relatively low yield of VPTBBA. Good monodispersity of VPTBBA was obtained as shown in Fig. 2. The estimated particle diameter of VPTBBA was *ca.* 5.6 μm.

Surface area and pore size

The specific surface areas of the three particles measured by the BET method are summarized in Table III. All three particles were found to have similar specific surface areas. The calculated average pore size of VPTBBA measured by the mercury intrusion method is around 80 Å, but the volume percentage of the pores smaller than 100 Å was about 50%, as depicted schematically in Fig. 3. Interestingly, the mercury porosimetry also suggested that VPTBBA also involved very large pores up to 2000 Å, the volume percentage of the pores between 500 and 2000 Å being calculated as 30% (Fig. 3). These findings suggest that VPTBBA has a polymodal relatively broad pore size distribution, which is the cause of the very rough surface observed in the SEM picture of VPTBBA (Fig. 4). This polymodal broad pore structure may be explained also based on the difference in copolymerization reactivity ratio as described in the previous section. In the early stage of polymerization, primary globules with a greater extent of cross-linking were produced. Then, as polymerization proceeded, lower cross-linked polymers including more vinyl *p-tert.*-butylbenzoate were formed

TABLE III

PHYSICAL PROPERTIES OF PARTICLES

Measured by BET method.

Particle	Surface area (m^2/g)	Average pore diameter (Å)
VPTBBA	313.9	60.3
VBA	344.4	61.1
VCHA	410.9	60.3

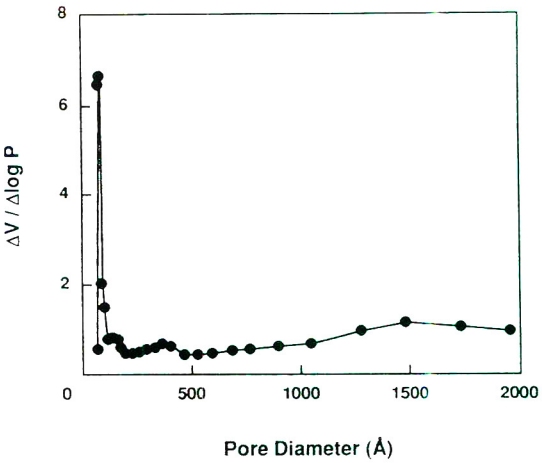

Fig. 3. Pore size distribution of VPTBBA measured by mercury intrusion method.

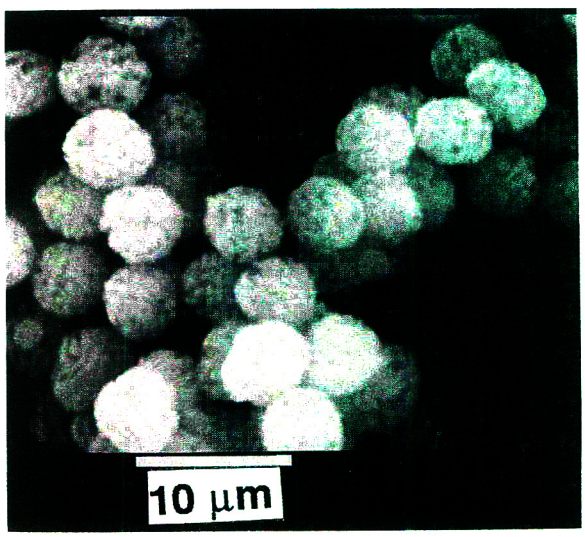

Fig. 4. Scanning electron micrograph of VPTBBA.

to afford the secondary beads which might produce the relatively broad pore size distribution of VPTBBA.

The BET and a mercury intrusion method are usually carried out under dry conditions. Therefore, sometimes, these tend to be incompatible with the results determined by size-exclusion chromatography, which is performed in a swollen condition. This time, tetrahydrofuran (THF) was utilized as the solvent in size-exclusion chromatography. A calibration graph obtained with polystyrene standards and alkylbenzenes on VPTBBA confirms the relatively broad pore size and pore size distribution (Fig. 5) which is basically compatible with the BET and mercury intrusion methods.

Selectivity in reversed-phase mode

VPTBBA separated alkylbenzenes well using 60% aqueous acetonitrile with a 100-mm column, as shown in Fig. 6. If the hydrophobic selectivity of VPTBBA in terms of the increase in retention caused by one methylene group of an alkylbenzene, $\alpha(CH_2)$, is compared with those of VBA, VCHA, ST and MMA [29], VPTBBA has an intermediate hydrophobicity between those of ST and MMA (Table IV). This finding can be expected from elemental analysis data because VPTBBA also has an intermediate carbon content between those of ST and MMA. Interestingly, VPTBBA has almost the same $\alpha(CH_2)$ value as VCHA with a lower carbon content, but a higher $\alpha(CH_2)$ value than VBA. These findings may be explained based on the

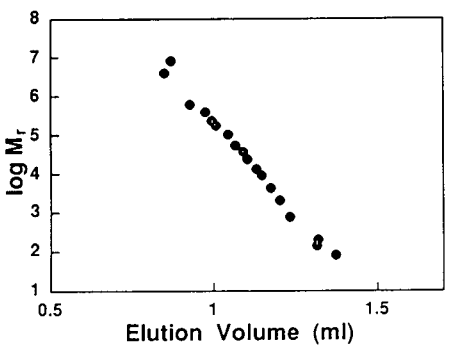

Fig. 5. Calibration graph for VPTBBA. Mobile phase, tetrahydrofuran; flow-rate, 0.5 ml/min; detection, UV at 254 nm. Samples: polystyrene standards and alkylbenzenes.

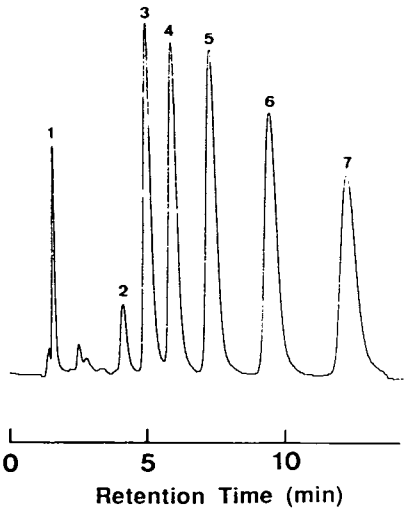

Fig. 6. Separation of alkylbenzenes on VPTBBA. Mobile phase, 60% aqueous acetonitrile; flow-rate, 0.8 ml/min; column, 100 mm × 4.6 mm I.D.; detection, UV at 254 nm. Samples: 1 = uracil; 2 = benzene; 3 = toluene; 4 = ethylbenzene; 5 = propylbenzene; 6 = butylbenzene; 7 = amylbenzene.

difference in contributions between the hydrophobicity of the aromatic ring of VPTBBA and that of the aliphatic ring of VCHA, which is usually more hydrophobic than corresponding aromatic group [30] and the relatively hydrophobic *tert.*-butyl substituent on VPTBBA. Therefore, the *tert.*-butyl substituent is found to contribute the hydrophobicity of the packing material, as expected from a hydrophobic substituent.

On the other hand, steric selectivity in terms of the α value of the planar triphenylene and sterically bulky and similarly hydrophobic *o*-terphenyl (T/O) [29] suggests that VPTBBA shows a much higher steric selectivity than VCHA and MMA, which do not contain a phenyl ring. The α value of VPTBBA is smaller than that of ST because ST includes an aromatic cross-linking agent (divinylbenzene) in addition to the monomer, but the phenyl ring of VPTBBA clearly enhances the steric selectivity. Interestingly, the *tert.*-butyl substituent on VPTBBA also contributes steric selectivity to give a higher α value than VBA. Although micropores have been reported to affect preferential retention towards planar compounds [31], this time VPTBBA,

TABLE IV

CHROMATOGRAPHIC PROPERTIES OF POLYMER BEADS

Mobile phase, 60% acetonitrile; flow-rate, 0.8 ml/min; detection, UV at 254 nm.

Parameter	VPTBBA	VBA	VCHA	ST	MMA
$\alpha(CH_2)^a$	1.31	1.27	1.32	1.49	1.23
T/O^b	2.13	2.03	1.62	2.79	1.27

[a] k'(amylbenzene)/k'(butylbenzene).
[b] k'(triphenylene)/k'(*o*-terphenyl).

VBA and VCHA, which were prepared using almost the same reaction conditions, all produced similar pore structures judging from BET measurements (Table III), and therefore the higher steric selectivity on VPTBBA may be due to not only the phenyl ring but also a contribution of the *tert.*-butyl substituent. Although a *tert.*-butyl substituent is sterically bulky, this finding can be understood if the bulky substituent tends to prevent self-stacking of phenyl rings but enhances interactions between the stationary phase and solutes.

The retention selectivity of VPTBBA in 60% aqueous acetonitrile was compared with those of other packing materials including a silica-based monomeric C_{18} stationary phase (Fig. 7). VPTBBA showed a similar selectivity to VCHA, as expected from the similar $\alpha(CH_2)$ values, except for alkyl alcohols. Although VCHA had almost the same $\alpha(CH_2)$ value as VPTBBA, the preferential retention toward alkyl alcohols on VCHA is probably due to the higher content of hydrophilic oxygen atoms of VCHA than that of VPTBBA. On the other hand, VPTBBA was found to show preferential retention towards hydrophobic solutes such as alkylbenzenes, alkyl bromides and alkanes compared with VBA. This is due to the hydrophobic aliphatic substituent (*tert.*-butyl group) of VPTBBA, as suggested before.

ST showed a longer retention towards all the alkyl alcohols, alkylbenzenes and alkyl bromides tested, including other halogenated compounds (Organohalides Std. Soln. A), which will be described later. However, VPTBBA showed a relatively preferential retention toward hydrophilic alkyl alcohols in comparison with another hydrophobic solutes, which was a different phenomenon from the relationship with the other four stationary phases. As mentioned before, VPTBBA includes an oxygen atom in its structure and this may produce this selectivity. Both MMA and C_{18} stationary phases showed much longer retention toward alkyl alcohols; on the other hand, VPTBBA showed preferential retention towards hydrophobic solutes compared with MMA and C_{18} stationary phases, especially towards alkyl bromides. Interestingly, the retentions of halogenated solutes in Organohalides Std. Soln. A were found to be similar on both VPTBBA and C_{18}, in contrast to those of alkyl alcohols. This finding supports the reported characteristics of VPTBBA described in the Introduction. This kind of tendency was also found between VPTBBA and MMA. In addition, the shorter alkyl chain in the alkyl bromides, the more preferential is the retention shown by VPTBBA. This finding means VPTBBA potentially has a preferential retention with the bromine substituent itself.

Retention selectivity on VPTBBA for substituted benzene derivatives is depicted in Fig. 8 in a comparison with that on ST. Although the phenyl ring of VPTBBA involves both an electron-withdrawing group, a carbonyl group and an electron-donating group (*tert.*-butyl), VPTBBA showed preferential retention towards electron-rich substituted benzene derivatives such as phenol and bromobenzene. On the other hand, ST involving an electron-rich phenyl ring showed preferential retention toward relatively electron-poor substituted benzene derivatives

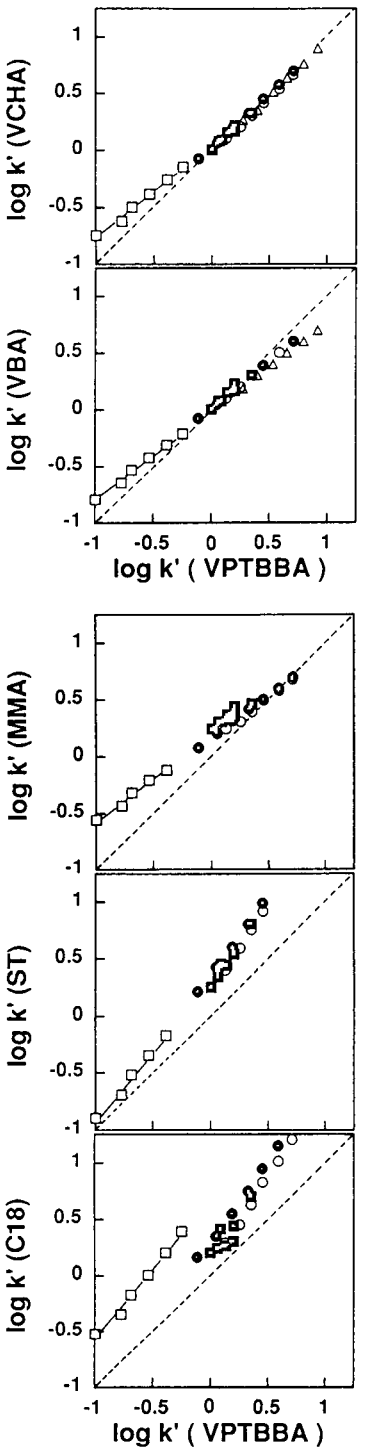

Fig. 7. Selectivity of VPTBBA. Chromatographic conditions in Fig. 6. Samples: □ = alkyl alcohols; ○ = alkylbenzenes; ● = alkyl bromides; ■ = organohalides; △ = alkanes.

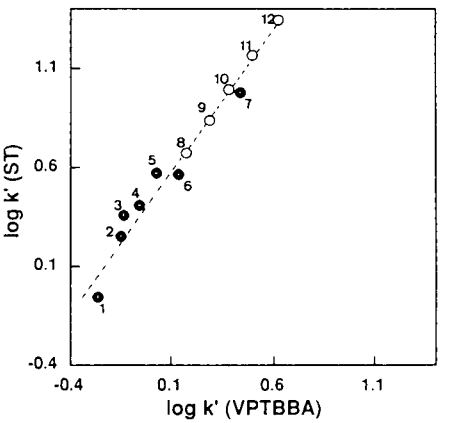

Fig. 8. Selectivity of VPTBBA. Chromatographic conditions as in Fig. 6. Samples: 1 = phenol; 2 = aniline; 3 = acetophenone; 4 = benzonitrile; 5 = methyl benzoate; 6 = nitrobenzene; 7 = bromobenzene; 8 = benzene; 9 = toluene; 10 = ethylbenzene; 11 = propylbenzene; 12 = butylbenzene.

such as acetophenone, benzonitrile and methyl benzoate, with the only exception of nitrobenzene. These findings suggest that VPTBBA tends to act as a stationary phase with an alternatively π-acidic characteristic ligand.

Separation selectivity with organohalides

Retentions of halogenated organic compounds contained in commercial Organohalides Std. Soln. A are summarized in Table V. The standard solution includes seven organohalides with different concentrations which is usually utilized as a standard for gas chromatographic analyses. The compounds are arranged in order of increasing k' values on VPTBBA.

The k' values increased with increase in the number of halogen substituents and carbons of the solutes. Hence chloroform showed the smallest k' value, while tetrachloroethylene gave the largest k' value on every stationary phase. As expected, ST and C_{18} stationary phases showed longer retentions toward all the halogenated compounds owing to their highly hydrophobic characteristics; in addition, interestingly, MMA also showed longer retentions than the more hydrophobic VPTBBA. However, the ratio between k'(chloroform) and k'(tetrachloroethylene) was 1.71 on MMA, which was the smallest selectivity observed. This finding means that

TABLE V

RETENTION PROPERTIES OF ORGANOHALIDES IN ORGANOHALIDES STD. SOLN. A

Mobile phase: 60% aqueous acetonitrile; flow-rate, 0.8 ml/min; detection, refractive index.

No.	Solute	k'					
		VPTBBA	VBA	VCHA	ST	MMA	C_{18}
1	Chloroform	1.02	0.99	1.00	1.72	1.70	1.59
2	Bromodichloromethane	1.21	1.18	1.18	2.14	1.99	1.71
3	1,1,1-Trichloroethane	1.25	1.16	1.19	2.83	1.98	2.55
4	Chlorodibromomethane	1.43	1.40	1.40	2.69	2.31	1.82
5	Trichloroethylene	1.61	1.44	1.46	3.38	2.21	2.70
6	Bromoform	1.67	1.65	1.60	3.35	2.68	1.93
7	Tetrachloroethylene	2.35	2.01	2.07	6.35	2.91	5.02
	α (7/1)[a]	2.30	2.03	2.07	3.69	1.71	3.15
	α (5/3)[b]	1.29	1.24	1.22	1.19	1.11	1.06

[a] k'(tetrachloroethylene)/k'(chloroform).
[b] k'(trichloroethylene)/k'(1,1,1-trichloroethane).

MMA has a relatively preferential retention with the halogenated organic compounds, but the retention selectivity is poor, which should lead to poor resolution. Although ST and C_{18} showed a larger ratio than VPTBBA between k'(chloroform) and k'(tetrachloroethylene), both VBA and VCHA showed smaller ratios than VPTBBA.

The C_{18} stationary phase can separate the halogenated compounds well, except for 1,1,1-trichloroethane and trichloroethylene, as depicted in Fig. 9. These two compounds involve

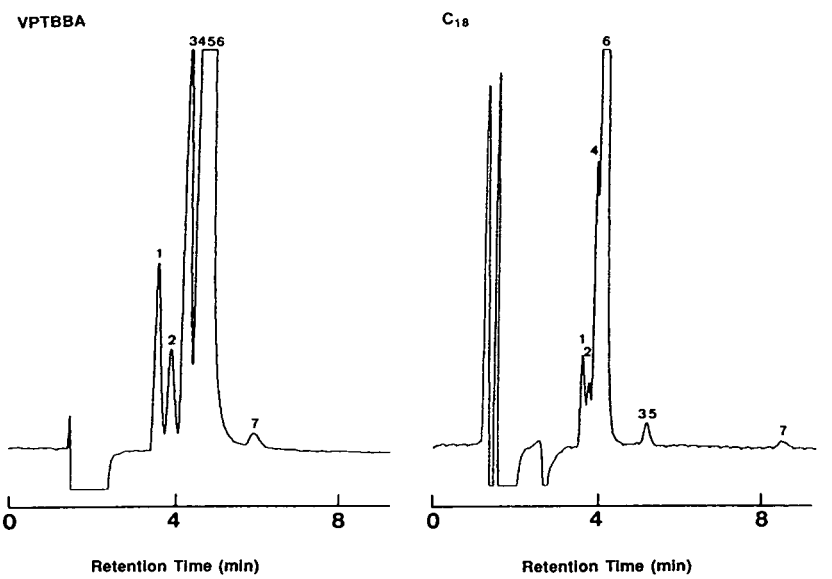

Fig. 9. Separation of organohalide standards. Chromatographic conditions as in Fig. 6, except detection (refractive index). Samples: 1 = chloroform (2 mg/ml); 2 = bromodichloromethane (1 mg/ml); 3 = 1,1,1-trichloroethane (0.1 mg/ml); 4 = chlorodibromomethane (4 mg/ml); 5 = trichloroethylene (0.5 mg/ml); 6 = bromoform (20 mg/ml); 7 = tetrachloroethylene (0.2 mg/ml).

the same number of chlorine substituents but a difference is found in the planarity of the compounds. As the C_{18} stationary phase can separate solutes mainly due to the difference in their hydrophobicity, in this instance a poor resolution of above two compounds is obtained. On the other hand, VPTBBA separated the two compounds well (Fig. 9). If the ratios between k'(1,1,1-trichloroethane) and k'(trichloroethylene) are compared, VPTBBA shows the highest ratio with all six stationary phases. In summary, VPTBBA has a better steric selectivity with a moderate absolute retention towards the halogenated compounds.

Separations of tetrachlorodibenzo-*p*-dioxins (TCDDs) were carried out utilizing acetonitrile as mobile phase. This mobile phase is too strong to separate TCDDs on the usual silica-based stationary phases [32], and therefore polymer-based separation media potentially have longer retentions with TCDDs, so it is suitable for the concentration of TCDDs from aqueous media. As shown in Fig. 10, VPTBBA could separate a synthetic isomer pair, 1,2,3,7-TCDD and 1,2,3,8-TCDD, which are usually difficult to separate, whereas ST could not separate them with much longer retention times. As we reported previously [32], silica-based stationary phase with a π-acidic phenyl ring such as a nitrophenyl group (NPE phase) could separate this isomer pair with the same elution order,

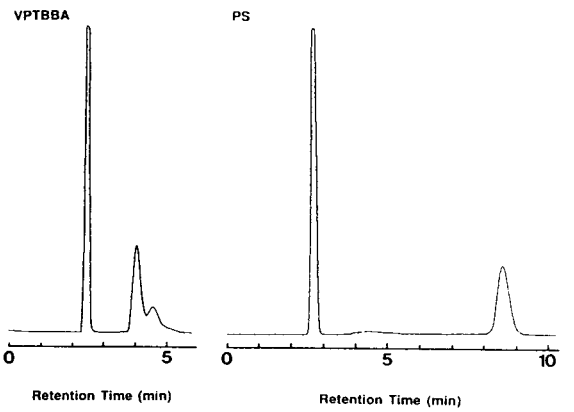

Fig. 10. Separation of a TCDD isomer pair. Mobile phase, acetonitrile; flow-rate, 1 ml/min; detection, UV at 230 nm; column, 150 mm × 4.6 mm I.D. Samples: 1,2,3,7- and 1,2,3,8-TCDD isomer pair.

whereas that with a π-basic ligand such as a pyrenyl group (PYE phase) could not separate them. In this way, as described in the previous section (Fig. 8), VPTBBA acts as a stationary phase with a π-acidic ligand whereas ST has a π-basic ligand.

The retention selectivities of 22 isomers of TCDDs are summarized in Table VI. Although VPTBBA only separated the isomer pair of 1,2,3,7- and 1,2,3,8-TCDDs, ST separated other isomer pairs with much longer retention times. As described before, the selectivity on ST is very similar to those on a silica-based PYE phase and a C_{18} stationary phase but not the same, whereas VPTBBA shows a similar selectivity to silica-based NPE stationary phase in the case of only the isomer pair of 1,2,3,7- and 1,2,3,8-TCDDs. Interestingly, VCHA showed a very similar selec-

TABLE VI

SEPARATION OF TCDDS ON POLYMER-BASED COLUMNS

Mobile phase, acetonitrile; flow-rate, 1 ml/min; detection, UV at 230 nm.

TCDD	k'		
	VPTBBA	ST	VCHA
1234	0.98	4.38	0.8
1236	1.11	4.71	0.97
1239		4.13	
1237	1.21	4.86	1.04
1238	1.55		1.33
1246	0.94	4.09	0.86
1249			
1247	1.05	4.62	0.94
1248			
1267	0.92	4.55	0.98
1289		4.06	
1268	1.10	4.78	0.97
1279		4.19	
1368	1.07	4.27	0.94
1379		4.99	
1469	0.78	3.21	1.06
1269	0.94	3.82	0.84
1478	1.10	4.77	0.97
1278	1.29	6.24	1.08
1369	0.94	4.07	0.86
1378	1.26	5.75	1.05
2378	1.42	4.97	1.12

tivity to VPTBBA. As VCHA does not contain a phenyl ring, the similar selectivities found on both VPTBBA and VCHA suggest that polar ester groups which are involved in the structure of both packing materials play an important role in the retention selectivity for TCDDs on VPTBBA. On silica-based NPE stationary phase, TCDDs having higher dipole moments tended to be retained longer, but this rule could not be applied to VPTBBA. On VPTBBA, 1,4,6,9-TCDD had the smallest k' value, whereas 2,3,7,8-TCDD was retained with the second largest k'. This is very interesting because 2,3,7,8-TCDD, which is reported to have the strongest toxicity [33,34], is a planar TCDD and 1,4,6,9-TCDD may have a staggered structure because of steric repulsion of two pairs of two chlorine atoms and an oxygen atom between the two chlorine atoms (Fig. 11). This means that VPTBBA can recognize the planarity of the TCDDs also. A typical case is the separation of the isomer pair of 1,2,6,7- and 1,2,8,9-TCDDs (Fig. 11). On silica-based NPE stationary phase, these two isomers could be well separated based on the difference in their dipole moments [32]. As 1,2,6,7- and 1,2,8,9-TCDDs have dipole moments of 0.023 and 4.220 D [35], respectively, 1,2,8,9-TCDD is retained longer on the NPE stationary phase. On the other hand, on VPTBBA, these two isomers could not be separated at all, probably because 1,2,8,9-TCDD has more staggered structure than 1,2,6,7-TCDD owing to the two chlorine atoms at the 1- and 9-positions and the selectivity caused by the steric selectivity and dipole moment may offset their selectivities on VPTBBA. Moreover, on VPTBBA, the six TCDDs which have k' values smaller than 1.0 (1,2,3,4-, 1,2,4,6-, 1,2,6,7-, 1,4,6,9-, 1,2,6,9- and 1,3,6,9-) involve at least two chlorine atoms at the 1-,4-,6- or 9-positions, which may decrease their planarity, whereas the five TCDDs with k' larger than 1.2 (1,2,3,7-, 1,2,3,8-, 1,2,7,8-, 1,3,7,8- and 2,3,7,8-) involve only one or no chlorine atom at these positions. These findings also strongly suggest that steric selectivity is one of the most important retention parameters on VPTBBA. A combination of these two major selectivities can determine the separation selectivity on VPTBBA, and therefore the selectivities on the three different stationary phases are not identical, but if the ratios between k' of 1,4,6,9- and 2,3,7,8-TCDDs are compared, it is interesting that VPTBBA has a value of 1.82 whereas ST and VCHA have values of 1.76 and 1.06, respectively. These high steric selectivities found on VPTBBA are consistent with those in the previous sections.

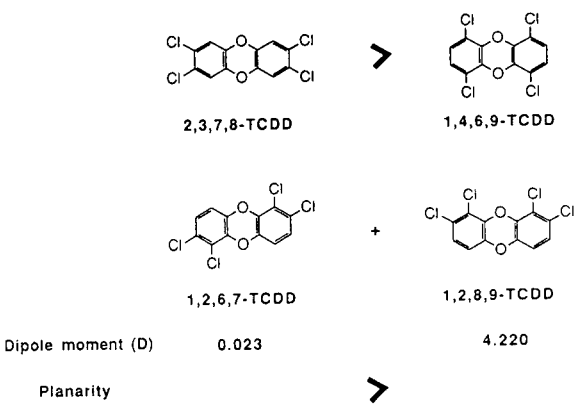

Fig. 11. Retention selectivity of VPTBBA toward TCDDs.

CONCLUSIONS

VPTBBA prepared with ethylene dimethacrylate as cross-linking agent showed a bimodal broad pore size distribution because of the difference in copolymerization reactivity ratio. In a comparison of its chromatographic properties with those of a silica-based stationary phase C_{18}, VPTBBA showed preferential retention toward chlorinated aliphatic compounds with much higher steric selectivity, whereas it has a π-acidic ligand compared with the retention selectivity of a poly(styrene–divinylbenzene) particle. In the separation of TCDDS, VPTBBA retained planar isomers preferentially and dipole–dipole interactions sometimes offset this high steric selectivity, resulting in poor resolution.

In comparison with the chromatographic properties of two other poly(vinyl carboxylate)s, VBA and VCHA, the *tert.*-butyl substituent contributed the hydrophobicity of the particles and also enhanced the steric selectivity. Although the separations of TCDDs are relatively poor on polymer-based separation media, those polymer-

based separation media are effective for the concentration of TCDDs from aqueous mobile phases, because they show much longer retention times than silica-based separation media. Although the quantitative introduction of vinyl *p-tert.*-butylbenzoate could not be achieved, VPTBBA is potentially a good separation medium and absorption medium and its moderate hydrophobicity makes it possible to apply it for the practical concentration of organohalides from aqueous environments.

ACKNOWLEDGEMENTS

This work was partly supported by a grant for the International Joint Research Program from the Japanese Ministry of Education, Science and Culture (03044089 and 05044054). The authors thank Professor Jean M.J. Fréchet and Dr. D.G. Patterson, Jr., for BET and mercury intrusion measurements and TCDD samples, respectively.

REFERENCES

1 J.F. Moore, *Ann. N.Y. Acad. Sci.*, 320 (1979) 151.
2 G.M. Decad, L.S. Birnbaum and H.B. Mattews, *Toxicol. Appl. Pharmacol.*, 57 (1981) 231.
3 J. McKinney and E. McConnell, *Chlorinated Dioxin and Related Compounds—Impact on the Environment*, Pergamon Press, Oxford, 1982, p. 367.
4 B.A. Schwetz, J.M. Morris, G.L. Sparschu, V.K. Rowe, P.J. Gehring, J.L. Emerson and C.G. Gerbin, *Environ. Health Perspect.*, 5 (1973) 87.
5 E.E. McConnell, J.A. Moore, J.K. Haseman and M.W. Harris, *Toxicol. Appl. Pharmacol.*, 44 (1978) 335.
6 K.D. Courtney and J.A. Moore, *Toxicol. Appl. Pharmacol.* 20 (1971) 396.
7 D. Neubert, P. Zens, A. Rathenwallner and H.-J. Merker, *Environ. Health Perspect.*, 5 (1973) 67.
8 F. Matsumara, J. Quensen and G. Tsushimoto, *Environ. Sci. Res.*, 26 (1983) 191.
9 G.M. Klecka and D.T. Gibson, *Appl. Environ. Microbiol.*, 39 (1980) 288.
10 G.M. Klecka and D.T. Gibson, *Biochem. J.*, 180 (1979) 639.
11 M. Philippi, J. Schmid, H.K. Wipf and R. Hutter, *Experientia*, 38 (1982) 659.
12 J.A. Bumpus, M.T.D. Wright and S.D. Aust, *Science*, 228 (1985) 1434.
13 J.A. Bumpus and S.D. Aust, *Am. Chem. Soc.*, 338 (1987) 340.
14 M.P. Esposito, T.O. Tiernan and F.E. Dryden, *Dioxins, EPA-600/2-80-197*, Environmental Protection Agency, Washington, DC, 1980, p. 233.
15 M. Koshioka, T. Yamada, J. Kanazawa and T. Murai, *Chemosphere*, 19 (1989) 684; *J. Pestic. Sci.*, 15 (1989) 39.
16 D. Crosby, A.S. Wong, J.R. Plimmer and E.A. Woolson, *Science*, 173 (1971) 748.
17 C. Botre, A. Memoli and F. Alhaique, *Environ. Sci. Technol.*, 12 (1978) 335.
18 D. Crosby and A.S. Wong, *Science*, 195 (1977) 1337.
19 G.A. Epling, Q. Qiu and A. Kumar, *Chemosphere*, 18 (1989) 329.
20 H. Muto, M. Shinada and Y. Takizawa, *Environ. Sci. Technol.*, 25 (1991) 316.
21 Kurita Industry, Japan, unpublished results.
22 W.Y. Shiu, W. Doucette, F.A.P.C. Gobas, A. Andren and D. Mackay, *Environ. Sci. Technol.*, 22 (1988) 651.
23 Fuso Chemical, Osaka, unpublished communications.
24 F.K. Hansen and J. Ugelstad, *Makromol. Chem.*, 80 (1979) 737.
25 V. Smigol, F. Svec, K. Hosoya, Q. Wang and J.M.J. Fréchet, *Angew. Makromol. Chem.*, 195 (1992) 151.
26 K. Hosoya, Y. Kishii, N. Tanaka, K. Kimata, S. Maruya, T. Araki and J.M.J. Fréchet, *Chem. Lett.*, (1992) 1145.
27 K. Hosoya and J.M.J. Fréchet, *J. Polym. Sci., Part A*, 31 (1993) 2129.
28 G. Odian, *Principles of Polymerization*, Wiley, New York, 3rd ed., 1991, p. 456.
29 K. Kimata, K. Iwaguchi, S. Ohnishi, K. Jinno, R. Eksteen, K. Hosoya, M. Araki and N. Tanaka, *J. Chromatogr. Sci.*, 27 (1989) 721.
30 N. Tanaka, K. Sakagami and M. Araki, *J. Chromatogr.*, 199 (1980) 327.
31 K. Hosoya, S. Maruya, K. Kimata, H. Kinoshita, T. Araki and N. Tanaka, *J. Chromatogr.*, 625 (1992) 121.
32 K. Kimata, K. Hosoya, N. Tanaka and T. Araki, *J. Chromatogr.*, 595 (1992) 77.
33 S. Safe, *Chemosphere*, 16 (1987) 791.
34 S. Safe, T. Zacharewski, L. Safe, M. Harris, C. Yao and M. Holcomb, *Chemosphere*, 18 (1989) 941.
35 C.J. Koester and R.A. Hites, *Chemosphere*, 17 (1988) 2355.

Journal of Chromatography A, 662 (1994) 49–60
Elsevier Science B.V., Amsterdam

CHROM. 25 652

Hydrophobicity parameters determined by reversed-phase liquid chromatography

VIII. Hydrogen-bond effects of ester and amide groups in heteroaromatic compounds on the relationship between the capacity factor and the octanol–water partition coefficient

Chisako Yamagami*, Miho Yokota and Narao Takao

Kobe Women's College of Pharmacy, Motoyamakita-machi, Higashinada, Kobe 658 (Japan)

(First received August 3rd, 1993; revised manuscript received October 15th, 1993)

ABSTRACT

The logarithms of the capacity factors, log k', for several heteroaromatic systems (furan, pyrrole, benzofuran, indole, benzene and their alkyl, ester and amide derivatives) were determined on a Capcell Pak C_{18} column using methanol–buffer (pH 7.4) mobile phases of different compositions. These results and the log k_w values, derived by a linear extrapolation of the plot of log k' against the volume fraction of methanol to 0% methanol, were correlated with experimental log P values by taking into account the hydrogen-acceptor and hydrogen-donor effects. Whereas the hydrogen-donor effect was found to be minimized by using the log k_w parameter, the hydrogen-acceptor effect was found to become insignificant in an eluent containing 50% methanol. Isocratic data determined at this eluent composition gave the simplest and best correlation.

INTRODUCTION

The logarithm of the 1-octanol–water partition coefficient, log P, is a widely used hydrophobicity parameter in quantitative structure–activity relationship (QSAR) studies [1,2]. For compounds without hydrogen-bonding functional groups, their log P values can often be calculated by taking account of the additive property of substituent hydrophobicity constants, π. However, if the compounds include polar groups, such calculations tend to yield erroneous log P values [3–5], and the use of experimental values is required. Recently, reversed-phase liquid chromatographic (RPLC) techniques have found utility in predicting log P values in place of the standard shake-flask method. Extensive examples where the log P value is estimated from the logarithm of the capacity factor, log k', obtained under various chromatographic conditions, have been reported [6–9]. Although the RPLC method is convenient and simple to treat, a universal procedure, including the RPLC conditions, for simulating log P does not seem to have been established.

In our continuing fundamental work on physico-chemical parameters used in QSAR, we have systematically investigated log P values in some heteroaromatic series, such as pyridines and diazines, and have found that the partition

* Corresponding author.

0021-9673/94/$07.00
SSDI 0021-9673(93)E1096-I

behaviour is greatly affected by the hydrogen-bond abilities of the ring heteroatom(s) and the substituent on the hetero-ring [5,10]. In order to examine whether the RPLC method can be utilized for determining log P under such circumstances, we have also studied the relationship between log P and log k' obtained with a Capcell Pak C_{18} column and methanol–buffer (pH 7.4) eluents [11–14]. It was demonstrated that the log k_w value (log k' extrapolated to 0% organic modifier) gives accurate estimates of log P for compounds free from strong hydrogen bonders [14], whereas it tends to overestimate the log P value of hydrogen acceptors (H-acceptors) and underestimate that of hydrogen donors (H-donors) [12–14]. In particular, our results obtained so far for several series of compounds ArX (X = variable substituent) have shown that ester groups (CO_2R), being strong hydrogen acceptors, are usually deviants from log P–log k_w relationships, in contrast to other weak hydrogen-accepting substituents such as OR, SR and NMe_2, which lie close to the calibration line [11]. The amide group ($CONH_2$, CONHR) is another functional group of interest. As they are expected to show amphiprotic characters, their log k_w values would involve an overestimating factor as an H-acceptor as well as an underestimating factor as an H-donor.

Keeping the above in mind, we attempted to extend our investigations to a larger number of compounds with such substituents. In this work, we prepared several systematic series of ester and amide derivatives of typical heteroaromatic compounds as shown below, and measured their capacity factors. The relationships between log P and log k_w (log k') were compared with those for the parents and their alkylated compounds to survey the hydrogen-bond effects of ester and amide groups in both chromatographic and octanol–water partitioning systems.

EXPERIMENTAL

Compounds

The compounds used are given in Table I. Some of them have been used previously [13]. The others, if not commercially available, were prepared as described previously [13].

Partition coefficients

Some of the 1-octanol–water log P values were taken from our previous papers [5,13]. Those for the others were measured in this study at 25°C by the conventional shake-flask method. For the measurement of volatile compounds the concentration was determined in both phases by RPLC according to the previous procedure [16].

RPLC procedure

The apparatus and the procedure used were the same as described previously [16]. Commercial Capcell Pak C_{18} columns [17,18] (5 or 25 cm × 4.6 mm I.D.) (Shiseido) were used without further treatment (silanol effects were demonstrated to be negligible in previous and preliminary work [11]). Commercial HPLC-grade methanol and water were used. As an aqueous phase, 0.01 M phosphate buffer (pH 7.4) was used. The methanol–buffer eluents were prepared by volume. Samples were dissolved in methanol (about 0.5%) and 1-2 μl was injected at 25°C. The flow-rate was 0.5–2.0 ml/min. The capacity factor, k', was determined from the retention time of the sample, t_R, by the equation $k' = (t_R - t_0)/t_0$, where the t_0 value is the retention time of methanol. Solutes were chromatographed on the 5-cm column for an eluent containing 15% methanol and on the 25-cm column for eluents containing 30, 50 and 70% methanol.

RESULTS OF REGRESSION ANALYSES

Relationship between log k_w and log P

The compounds examined were furan (Fr), benzofuran (BF), pyrrole (Pyr), 1-methylpyrrole (1-Me-Pyr), indole (In), 1-methyl-indole (1-Me-In), benzene (Bz) and their alkyl, ester and amide derivatives. The 1-Me-Pyr and 1-Me-In series were studied to examine the hydrogen-donor effect of the acidic hydrogen attached to the ring-N atom (N*H*). Although some of them were studied in previous work [13,14], measurements were made for all compounds in this work under the same conditions. As one of the most widely used chromatographic parameters for predicting log P, log k_w values were derived by linear extrapolations using log k' values deter-

mined at methanol concentrations ranging from 30 to 70%:

$$\log k' = \log k_w - SX \quad (1)$$

where X represents the volume fraction of methanol in the mobile phase. In previous work it was shown that the log k_w value obtained in this way correlates better with log P than log k_w values obtained otherwise [12]. Although retention data in an eluent containing 15% methanol were also measured, they tended to deviate from the linear line. Therefore, the data in this eluent were excluded from the analyses. The log k_w values are given in Table I together with the log P values.

It is known empirically that the log k_w value derived for the methanol–water mobile phase system with a C_{18}-modified stationary phase can be a direct measure of log P for certain compounds (log k_w method) [6,11]. Although the correlation between log k_w and log P for compounds given in Table I is fairly good ($r = 0.98$, Fig. 1), close examination of the differences between log k_w and log P show the following tendencies in accordance with those observed in our previous work [14]: (i) the log k_w values for Fr, BF, 1-Me-Pyr, 1-Me-In, Bz and their alkyl derivatives, which are non-hydrogen bonders or very weak H-acceptors, agreed well with log P; (ii) for Pyr, In and their alkyl derivatives, classified as H-donors, the log k_w method tended to underestimate the log P values, *i.e.*, log $k_w <$ log P; (iii) for esters with the parent nucleus noted in (i), classified as strong H-acceptors, the log k_w method overestimated the log P values, *i.e.*, log $k_w >$ log P.

For the compounds not included in (i)–(iii), the relationship between log P and log k_w was more complicated because those compounds contain various combinations of H-donating, H-accepting and amphiprotic substituents. To separate these hydrogen-bond effects, the compounds were divided into subgroups depending on the hydrogen-bond types as follows: system N, parent compounds: Fr, BF, 1-Me-Pyr, 1-Me-In and their alkyl derivatives, and substituents (subgroups): CO_2R (E), CONHR and $CONH_2$ (AM); and system H, parent compounds: Pyr, In and their alkyl derivatives, and substituents (subgroups) CO_2R (E), CONHR and $CONH_2$ (AM), where in system H the aromatic rings have H-donors and in system N the aromatic rings are non-hydrogen-bonders or very weak H-acceptors. Alkyl derivatives were included in the parent compounds because they exhibit no hydrogen-bond effect. Classification of the furan ring into this group is rationalized also by a theoretical approach: preliminary semi-empirical molecular orbital calculations by the PM3 method suggested that the interaction energy between furan and water molecules is relatively insignificant. Analyses were made by using the hydrogen-bond indicator variables as follows: $HB_H = 1$ for compounds of system H, $HB_H = 0$ for those of system N; $HB_E = 1$ for esters, $HB_E = 0$ for the others; and $HB_{AM} = 1$ for amides, $HB_{AM} = 0$ for the others. The parameter used are listed in Table II

First, pre-analyses in terms of eqn. 2 were made step by step on the assumption that the hydrogen-bond effects attributable to each functional group are additive:

$$\log k_w = a \log P + \sum_i b_i HB_i + c \quad (2)$$

where HB_i represents one of the HB parameters given above. The coefficients and constant values can be obtained by regression analyses. By this treatment, the b_i value should reflect the hydrogen-bond effect contributed from each hydrogen-bonding group.

Effect of the ring NH (H-donor effect). To see the H-donor effect attributable to the ring N*H* atom, we tried the analysis for the parent compounds of both N and H systems, yielding an excellent correlation, with an improvement of eqn. 4 compared with the single correlation (eqn. 3):

$$\log k_w = 1.023 \log P - 0.190$$

$$n = 15,\ r = 0.990,\ s = 0.101,\ F = 627 \quad (3)$$

$$\log k_w = 1.012 \log P - 0.152 HB_H - 0.097$$

$$n = 15,\ r = 0.997,\ s = 0.062,\ F = 843 \quad (4)$$

In these equations and throughout this work, n is the number of compounds used for calculations, r is the correlation coefficient, s is the standard

TABLE I

RETENTION PARAMETERS AND 1-OCTANOL–WATER LOG *P* VALUES

Compound	System	Log P^a	Log $k_w{}^b$	S^b	r^c
Furan (Fr)	*N*	1.34	1.17	1.88	0.998
-2-Me		1.85	1.79	2.41	1.000
-2-Et		2.40	2.39	2.92	1.000
-2-CO_2Me		1.00	1.32	2.50	1.000
-2-CO_2Et		1.50	1.84	2.96	1.000
-2-CONHMe		0.23	0.45	2.07	0.999
-2-CONHEt		0.61	0.82	2.32	0.999
-2-CONHPr		1.10[d]	1.28	2.66	0.999
-2-$CONH_2$		−0.11	0.19	2.05	0.999
-3-CO_2Me		1.28	1.52	2.59	1.000
-3-CO_2Et		1.78	2.07	3.07	1.000
-3-CO_2Pr		2.36[d]	2.66	3.58	1.000
-3-CONHMe		0.34	0.43	1.95	1.000
-3-CONHEt		0.72	0.75	2.15	1.000
-3-CONHPr		1.20[d]	1.19	2.49	1.000
-3-$CONH_2$		0.09	0.22	1.94	1.000
Benzofuran (BF)	*N*	2.67	2.72	3.43	1.000
-2-CO_2Me		2.53	2.83	3.79	0.999
-2-CO_2Et		3.05[d]	3.37	4.27	0.999
-2-CONHMe		1.85[d]	2.00	3.34	0.999
-2-CONHEt		2.22[d]	2.34	3.62	0.999
-2-CONHPr		2.65[d]	2.80	4.04	0.998
-2-$CONH_2$		1.54[d]	1.79	3.24	0.999
Pyrrole (Pyr)		0.75	0.52	1.62	0.999
-2-Et		1.59	1.42	2.36	1.000
-2,5-di-Me		1.47	1.30	2.25	1.000
-2-CO_2Me		1.27[d]	1.40	2.67	1.000
-2-CO_2Et		1.73[d]	1.90	3.09	1.000
-2-CONHMe		0.42[d]	0.44	2.03	0.999
-2-CONHEt		0.80[d]	0.79	2.28	0.999
-2-CONHPr		1.25[d]	1.25	2.62	0.999
-2-$CONH_2$		0.09[d]	0.22	2.00	0.999
1-Me-pyrrole (1Me-Pyr)	*N*	1.15	1.06	1.72	0.999
-2-CO_2Me		1.80[d]	2.06	3.04	1.000
-2-CONHMe		0.71[d]	0.88	2.32	0.999
-2-CONHEt		1.09[d]	1.21	2.55	0.999
-2-CONHPr		1.63[d]	1.65	2.91	0.999
-2-$CONH_2$		0.45[d]	0.72	2.32	0.999
Indole (In)	*H*	2.14	1.90	2.88	1.000
-2-Me		2.53	2.31	3.22	1.000
-3-Me		2.80	2.50	3.34	0.999
-5-Me		2.68	2.45	3.32	1.000
-2-CO_2Me		2.78[d]	2.84	3.94	1.000
-2-CO_2Et		3.22[d]	3.35	4.39	1.000
-2-CONHMe		1.90[d]	1.85	3.24	0.999
-2-CONHEt		2.32[d]	2.17	3.49	0.999
-2-CONHPr		2.80[d]	2.59	3.87	0.999
-2-$CONH_2$		1.61[d]	1.69	3.17	1.000
-3-CO_2Me		2.57[d]	2.54	3.83	0.999
-3-CO_2Et		3.04	3.07	4.32	0.999

TABLE I (*continued*)

Compound	System	Log P^a	Log k_w [b]	S^b	r^c
-3-CONHMe		1.25[d]	1.35	2.96	0.999
-3-CONHEt		1.62[d]	1.71	3.24	0.999
1-Me-indole (1Me-In)	*N*	2.64	2.60	3.27	1.000
Benzene (Bz)		2.13	1.99	2.48	0.999
-Me		2.69	2.59	2.99	1.000
$-CO_2Me$		2.12	2.34	3.23	1.000
$-CO_2Et$		2.67	2.90	3.73	0.999
-CONHMe		0.90[d]	1.00	2.42	0.999
-CONHEt		1.28[d]	1.29	2.61	0.999
-CONHPr		1.72[d]	1.70	2.95	0.999
$-CONH_2$		0.64	0.86	2.42	0.999

[a] Taken from refs. 13 and 14, unless indicated otherwise.
[b] See eqn. 1.
[c] Correlation coefficient.
[d] This work.

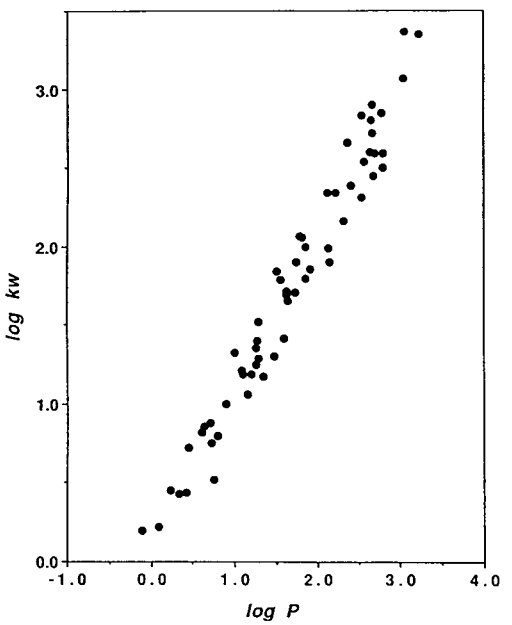

Fig. 1. Relationship between log k_w and log P for all compounds given in Table I.

deviation and F is the value of the F-ratio between regression and residual variances.

Effect of the ester group (H-acceptor effect). To estimate the contribution of the H-acceptor effect attributable to the ester group, analyses for the parent compounds and the esters of system N were carried out and eqns. 5 and 6 were obtained:

$$\log k_w = 0.938 \log P + 0.223$$

$$n = 16,\ r = 0.948,\ s = 0.191,\ F = 124 \quad (5)$$

$$\log k_w = 1.019 \log P + 0.351HB_E - 0.097$$

$$n = 16,\ r = 0.995,\ s = 0.061,\ F = 674 \quad (6)$$

Addition of the parent and ester compounds of system H to the above data set gave the following correlations:

$$\log k_w = 0.998 \log P + 0.042$$

$$n = 31,\ r = 0.956,\ s = 0.210,\ F = 309 \quad (7)$$

$$\log k_w = 0.990 \log P + 0.334HB_E - 0.175HB_H - 0.041$$

$$n = 31,\ r = 0.997,\ s = 0.059,\ F = 1437 \quad (8)$$

In eqn. 8, the coefficients of the *HB* terms are very close to those in eqns. 4 and 6.

Effect of the amide group (amphiprotic effect). Similarly, the contribution of amide groups was described by eqn. 10, derived from the parent compounds and the amide derivatives of system N:

TABLE II

OBSERVED AND CALCULATED HYDROPHOBICITY PARAMETERS AND HYDROGEN-BOND PARAMETERS

Compound	Log k_w (Δ^b) calcd.[a]	Log k'_{M50} obsd.	Log k'_{M50} (Δ^d) calcd.[c]	Log P (Δ^e) calcd.[c]	HB_E	HB_{AM}	HB_H	HB_D
Furan (Fr)	1.29 (−0.12)	0.259	0.25 (0.01)	1.37 (−0.03)	0	0	0	0
-2-Me	1.78 (0.01)	0.599	0.54 (0.06)	1.96 (−0.11)	0	0	0	0
-2-Et	2.31 (0.08)	0.926	0.84 (0.09)	2.54 (−0.14)	0	0	0	0
-2-CO_2Me	1.31 (0.01)	0.043	0.06 (−0.02)	0.99 (0.02)	1	0	0	0
-2-CO_2Et	1.79 (0.05)	0.351	0.34 (0.01)	1.53 (−0.03)	1	0	0	0
-2-CONHMe	0.41 (0.04)	−0.609	−0.57 (−0.04)	0.18 (0.05)	0	1	0	1
-2-CONHEt	0.77 (0.05)	−0.359	−0.36 (0.00)	0.62 (−0.01)	0	1	0	1
-2-CONHPr	1.24 (0.04)	−0.072	−0.08 (0.01)	1.13 (−0.03)	0	1	0	1
-2-$CONH_2$	0.08 (0.11)	−0.847	−0.76 (−0.09)	−0.24 (0.13)	0	1	0	1
-3-CO_2Me	1.58 (−0.06)	0.223	0.22 (0.00)	1.30 (−0.02)	1	0	0	0
-3-CO_2Et	2.06 (0.01)	0.528	0.50 (0.03)	1.84 (−0.06)	1	0	0	0
-3-CO_2Pr	2.61 (0.05)	0.858	0.82 (0.04)	2.42 (−0.06)	1	0	0	0
-3-CONHMe	0.51 (−0.08)	−0.561	−0.51 (−0.05)	0.27 (0.07)	0	1	0	1
-3-CONHEt	0.88 (−0.13)	−0.335	−0.30 (−0.04)	0.67 (0.06)	0	1	0	1
-3-CONHPr	1.34 (−0.15)	−0.066	−0.03 (−0.04)	1.14 (0.06)	0	1	0	1
-3-$CONH_2$	0.27 (−0.05)	−0.756	−0.65 (−0.11)	−0.08 (0.17)	0	1	0	1
Benzofuran (BF)	2.57 (0.15)	0.992	1.00 (−0.01)	2.65 (0.02)	0	0	0	0
-2-CO_2Me	2.78 (0.05)	0.912	0.92 (−0.01)	2.51 (0.02)	1	0	0	0
-2-CO_2Et	3.28 (0.09)	1.198	1.21 (−0.01)	3.02 (0.03)	1	0	0	0
-2-CONHMe	1.96 (0.04)	0.293	0.34 (−0.05)	1.77 (0.08)	0	1	0	1
-2-CONHEt	2.32 (0.02)	0.494	0.55 (−0.06)	2.12 (0.10)	0	1	0	1
-2-CONHPr	2.73 (0.07)	0.733	0.79 (−0.06)	2.54 (0.11)	0	1	0	1
-2-$CONH_2$	1.66 (0.13)	0.135	0.16 (−0.03)	1.49 (0.05)	0	1	0	1
Pyrrole (Pyr)	0.58 (−0.06)	−0.279	−0.28 (0.00)	0.76 (−0.01)	0	0	1	1
-2-Et	1.39 (0.03)	0.236	0.19 (0.05)	1.67 (−0.08)	0	0	1	1
-2,5-di-Me	1.27 (0.03)	0.178	0.12 (0.06)	1.57 (−0.10)	0	0	1	1
-2-CO_2Me	1.42 (−0.02)	0.048	0.01 (0.04)	1.34 (−0.07)	1	0	1	1
-2-CO_2Et	1.86 (0.04)	0.331	0.27 (0.06)	1.84 (−0.11)	1	0	1	1
-2-CONHMe	0.44 (0.00)	−0.600	−0.66 (0.06)	0.54 (−0.12)	0	1	1	2
-2-CONHEt	0.80 (−0.01)	−0.362	−0.45 (0.09)	0.96 (−0.16)	0	1	1	2
-2-CONHPr	1.24 (0.01)	−0.086	−0.20 (0.11)	1.45 (−0.20)	0	1	1	2
-2-$CONH_2$	0.13 (0.09)	−0.804	−0.85 (0.05)	0.18 (−0.09)	0	1	1	2
1-Me-pyrrole (1Me-Pry)	1.11 (−0.05)	0.184	0.14 (0.04)	1.23 (−0.08)	0	0	0	0
-2-CO_2Me	2.08 (−0.02)	0.521	0.51 (0.01)	1.83 (−0.03)	1	0	0	0
-2-CONHMe	0.87 (0.01)	−0.303	−0.30 (−0.00)	0.72 (−0.01)	0	1	0	1
-2-CONHEt	1.23 (−0.02)	−0.086	−0.09 (0.00)	1.10 (−0.01)	0	1	0	1
-2-CONHPr	1.75 (−0.10)	−0.169	0.21 (−0.04)	1.55 (0.08)	0	1	0	1
-2-$CONH_2$	0.62 (0.10)	−0.458	−0.45 (−0.01)	0.45 (0.00)	0	1	0	1
Indole (In)	1.92 (−0.02)	0.474	0.50 (−0.03)	2.09 (0.05)	0	0	1	1
-2-Me	2.29 (0.02)	0.708	0.72 (−0.01)	2.50 (0.03)	0	0	1	1
-3-Me	2.55 (−0.05)	0.866	0.87 (−0.00)	2.78 (0.02)	0	0	1	1
-5-Me	2.43 (0.02)	0.797	0.80 (−0.00)	2.66 (0.03)	0	0	1	1
-2-CO_2Me	2.87 (−0.03)	0.849	0.86 (−0.01)	2.75 (0.03)	1	0	1	1
-2-CO_2Et	3.29 (0.06)	1.126	1.11 (0.02)	3.23 (−0.01)	1	0	1	1
-2-CONHMe	1.86 (−0.01)	0.212	0.17 (0.04)	1.97 (−0.07)	0	1	1	2
-2-CONHEt	2.27 (−0.10)	0.393	0.40 (−0.01)	2.29 (0.03)	0	1	1	2
-2-CONHPr	2.73 (−0.14)	0.630	0.67 (−0.04)	2.70 (0.10)	0	1	1	2
-2-$CONH_2$	1.58 (0.11)	0.085	0.00 (0.09)	1.75 (−0.14)	0	1	1	2

TABLE II (*continued*)

Compound	Log k_w (Δ^b) calcd.[a]	Log k'_{M50} obsd.	Log k'_{M50} (Δ^d) calcd.[c]	Log P (Δ^e) calcd.[c]	HB_E	HB_{AM}	HB_H	HB_D
-3-CO_2Me	2.67 (−0.13)	0.589	0.74 (−0.15)	2.29 (0.28)	1	0	1	1
-3-CO_2Et	3.12 (−0.05)	0.865	1.01 (−0.15)	2.78 (0.27)	1	0	1	1
-3-CONHMe	1.24 (0.11)	−0.163	−0.20 (0.04)	1.31 (−0.06)	0	1	1	2
-3-CONHEt	1.60 (0.11)	0.053	0.01 (0.04)	1.69 (−0.07)	0	1	1	2
1-Me-indole (1Me-In)	2.54 (0.06)	0.967	0.98 (−0.01)	2.61 (0.03)	0	0	0	0
Benzene (Bz)	2.05 (−0.06)	0.766	0.69 (0.08)	2.26 (−0.13)	0	0	0	0
-Me	2.59 (0.00)	1.109	1.01 (0.10)	2.86 (−0.17)	0	0	0	0
-CO_2Me	2.38 (−0.04)	0.706	0.69 (0.02)	2.15 (−0.03)	1	0	0	0
-CO_2Et	2.91 (−0.01)	1.006	1.00 (0.01)	2.68 (−0.01)	1	0	0	0
-CONHMe	1.05 (−0.05)	−0.240	−0.20 (−0.04)	0.83 (0.07)	0	1	0	1
-CONHEt	1.42 (−0.13)	−0.047	0.02 (−0.07)	1.17 (0.11)	0	1	0	1
-CONHPr	1.84 (−0.14)	0.200	0.26 (−0.06)	1.61 (0.12)	0	1	0	1
-$CONH_2$	0.80 (0.06)	−0.377	−0.34 (−0.04)	0.59 (0.05)	0	1	0	1

[a] Calculated by eqn. 14.
[b] Difference between observed and calculated log k'_w values by eqn. 14.
[c] Calculated by eqn. 21.
[d] Difference between observed and calculated log k'_{M50} values by eqn. 21.
[e] Difference between observed and calculated log P values by eqn. 21.

$$\log k_w = 0.918 \log P + 0.186$$

$$n = 28,\ r = 0.990,\ s = 0.111,\ F = 1306 \quad (9)$$

$$\log k_w = 0.976 \log P + 0.181HB_{AM} - 0.020$$

$$n = 28,\ r = 0.994,\ s = 0.089,\ F = 1026 \quad (10)$$

Addition of the corresponding compounds of system H produced eqns. 11 and 12:

$$\log k_w = 0.895 \log P + 0.166$$

$$n = 45,\ r = 0.987,\ s = 0.129,\ F = 1555 \quad (11)$$

$$\log k_w = 0.957 \log P + 0.173HB_{AM} - 0.140HB_H + 0.010$$

$$n = 45,\ r = 0.995,\ s = 0.081,\ F = 1327 \quad (12)$$

Again, the coefficients in eqn. 12 are very close to those in eqns. 4 and 10.

As the pre-analyses gave very stable correlations, we attempted analyses with the combined data set including all the compounds studied and obtained an excellent correlation (eqn. 14), which was much improved in comparison with eqn. 13:

$$\log k_w = 0.950 \log P + 0.145$$

$$n = 61,\ r = 0.981,\ s = 0.165,\ F = 1478 \quad (13)$$

$$\log k_w = 0.960 \log P + 0.340HB_E + 0.178HB_{AM} - 0.147HB_H + 0.008$$

$$n = 61,\ r = 0.996,\ s = 0.077,\ F = 1759 \quad (14)$$

As shown in Table II and Fig. 2, the log k_w values calculated by eqn. 14 agreed well with the observed values.

Relationship between the S parameter and log P

Several investigators [9,20] have found that the S parameter also correlates well with log P. The relationship between S and log P is shown in Fig. 3 for all the compounds studied. The correlation was poor ($r = 0.84$). It should be noted that the ester and amide derivatives behaved differently from the parent compounds in such a manner that esters and amides gave greater S values than parent compounds under the equivalent log P values. Chen *et al.* [20] have investigated in detail the properties of the S parameter. They demonstrated that the S value for a given solute is nearly constant regardless of the differ-

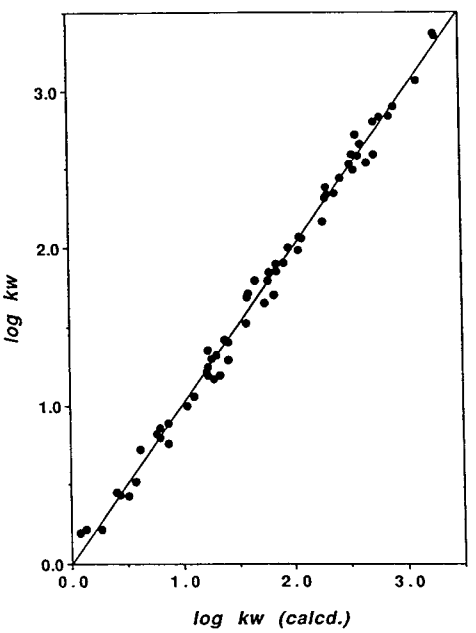

Fig. 2. Relationship between log k_w and the calculated log k_w values (eqn. 14).

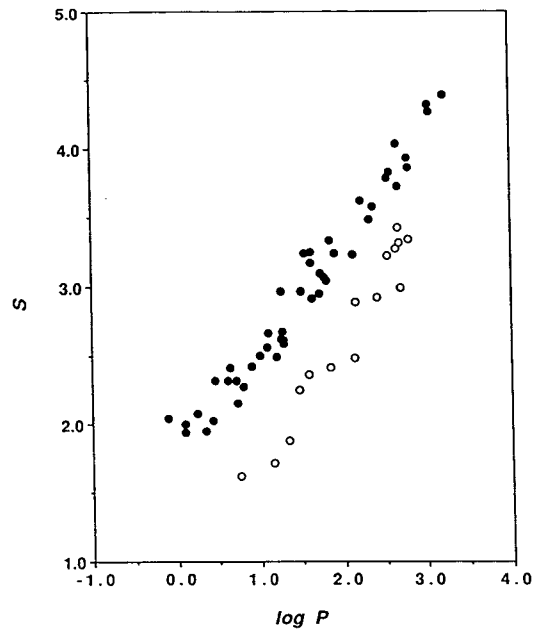

Fig. 3. Relationship between the S parameter (eqn. 1) and log P for all compounds given in Table I. ○ = Parent compounds; ● = ester and amide derivatives.

ent C_{18} packing agents, and concluded that the S value is determined mainly by the interaction between the solute and the mobile phase, meaning that the S value derived from the same mobile phase system reflects the nature of the solute. To confirm this point in our case, we determined the S values for the parent and ester compounds (31 compounds) with a Chemcopac ODS-H column and obtained results that agreed well with the S values in Table I with an average deviation of ±0.06. The features shown in Fig. 3 indicate that the retention of esters and amides is more dependent on the mobile phase composition, in other words, the hydrogen-bond ability of ester and amide groups is more sensitive to changes in the surrounding medium.

Relationship between isocratic log k' and log P

The results presented above strongly suggest that the log k' *vs.* log P relationship varies with the methanol content in the mobile phase. Therefore, isocratic retention data were similarly analysed at 30, 50 and 70% methanol concentrations (M30, M50 and M70). Excellent correlations corresponding to eqn. 14 were obtained, as shown by eqns. 16, 18 and 20 in Table III.

It is of interest that the HB_E term was found to be insignificant in the correlation in the M50 eluent (eqn. 18), while the HB_{AM} term was found to be insignificant in the M30 eluent (eqn. 16). As the coefficients of the HB_{AM} and HB_H terms agreed within a 95% confidence interval in eqn. 18, we attempted to combine both terms into a common hydrogen-donor parameter HB_D:

$$\log k_{M50} = 0.561 \log P - 0.198HB_D - 0.503$$

$$n = 61,\ r = 0.995,\ s = 0.055,\ F = 2898 \qquad (21)$$

where HB_D ($=HB_H + HB_{AM}$) takes the values 0, 1 and 2 depending on the number of H-donating sites contained in the molecule, that is $HB_D = 1$ for compounds with –CONH– or ring-N*H*, $HB_D = 2$ for those with both –CONH– and ring-N*H*, and $HB_D = 0$ for the others. As shown in Fig. 4 and Table II, eqn. 21, the simplest correlation obtained in this work, could predict the log P values satisfactorily. This treatment may be rationalized by the reason given later.

TABLE III

COEFFICIENTS FOR CORRELATIONS OBTAINED BY EQN. 2 AT EACH MOBILE PHASE COMPOSITION

Log $k' = a$ log $P + b_E HB_E + b_{AM} HB_{AM} + b_H HB_H + c$.

Mobile phase	Term					n	r	s	F	Eqn. No.
	Log P	HB_E	HB_{AM}	HB_H	c					
M0[a]	0.950				0.145	61	0.981	0.165	1478	13
	0.960	0.340	0.178	−0.147	0.008	61	0.996	0.077	1759	14
M30	0.743				−0.372	61	0.983	0.121	1675	15
	0.729	0.167	(0)[b]	−0.163	−0.332	61	0.997	0.053	2959	16
M50	0.604				−0.746	61	0.967	0.140	838	17
	0.549	(0)	−0.229	−0.174	−0.476	61	0.996	0.052	2117	18
	0.466				−1.072	61	0.925	0.166	351	19
M70	0.399	−0.119	−0.335	−0.187	−0.696	61	0.989	0.065	653	20

[a] Figures after M represent the volume-% of methanol
[b] Statistically insignificant.

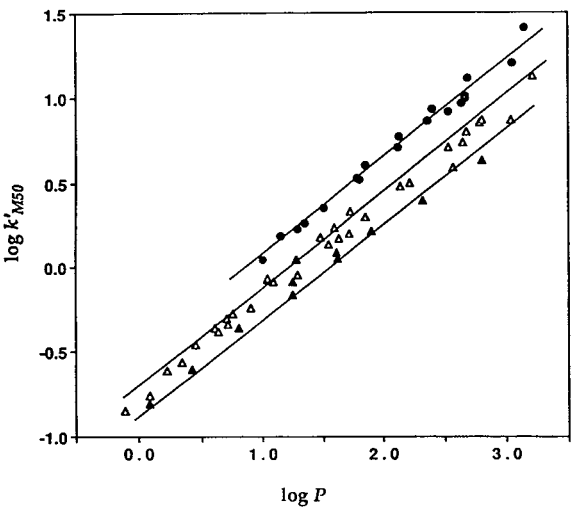

Fig. 4. Relationship between log k' and log P by eqn. 21. ○ = parent compounds ($HB_D = 0$); △ = compounds with $HB_D = 1$; ▲ = compounds with $HB_D = 2$.

DISCUSSION

It is known that an HPLC system using an alkyl-bonded stationary phase often discriminates among solutes according to the hydrogen-bond properties. Usually, log k'–log P plots give a good linear relationship among the same congeners, but tend to give separate correlations for different groups of congeners [6,7,9,21–24]. The procedure employed in this work is based on this fact. Our results revealed that the relationship between hydrohobicity indices derived from RPLC and octanol–water systems can be excellently expressed, as a first approximation, by the general eqn. 2 as far as the compounds studied are concerned. This means that the hydrogen-bond effects attributed to ester, ring-N*H* and amide groups are approximately additive. The fact that discrete type parameters, *HB*, worked well suggests that the same type of substituents (*e.g.*, CO_2R) have comparable hydrogen bond abilities regardless of the kind of aromatic system to which they are attached. This reasoning may be rationalized by considering that H-acceptor abilities, β, for $ArCO_2R$ are approximately equivalent [25].

When the corresponding coefficients of each term were compared as a function of the mobile phase composition, systematic changes were observed. The coefficients of log P, HB_E and HB_{AM} terms were seen to decrease linearly with increase in methanol concentration. Especially the plot of the coefficient of log P against the volume fraction of methanol showed perfect linearity with a correlation coefficient better than 0.999,

yielding an intercept of 0.97, which is very close to unity. A similar plot with the c values gave an intercept close to zero. These results demonstrate not only that the log k_w parameter can be a direct indication of the log P value for non-hydrogen bonders, but also that the hydrophobic component (log P term) can be successfully separated from other correction terms ($\Sigma\, b_i HB_i$), if required, supporting the validity of eqn. 2.

As is clear in eqn. 14, the log k_w value involves a positive contribution from the ester group (H-acceptor) and a negative contribution from the ring N*H* group (H-donor), leading to overestimated log P values for esters and underestimated values for compounds with the ring-N*H* group, if we estimate log P values from their log k_w values. The amide group (amphiprotic group) made a small positive contribution for the reason described below. The overall hydrogen-bond effect of amides could be treated as the sum of effects of –C(=*O*)*N*H– (H-acceptor) and –C(=O)N*H*– (H-donor) moieties. It is interesting that the sum of the coefficients of HB_E and HB_H terms is approximately equivalent to the coefficient of the HB_{AM} term in all eluents. This finding led us to hypothesize that the H-accepting ability of –C(=*O*)*O*R is similar to that of –C(=*O*)*N*H– and also the H-donating ability of the ring N*H* is similar to that of –C(=O)N*H*–. Thus, the fact that the HB_{AM} term is insignificant at 30% MeOH concentration, as shown in eqn. 16, would be explained by considering that the H-acceptor and H-donor abilities of the amide group are compensated around this eluent composition (note that the coefficients of HB_E and HB_H are similar values of opposite signs). In more water-rich eluents, the H-acceptor effect probably exceeds the H-donor effect in the amide group, judging from the HB_E and HB_H values for M0, thereby yielding a positive coefficient of the HB_{AM} term. This is the case observed in eqn. 14.

As for the HB_H term, the change in coefficient was very small and fairly constant, and the more important is that the coefficient of the HB_H term was negative in all the equations obtained. This is a phenomenon usually observed [7,9,16,24,26, 29] and thought to be inevitable so long as alkyl-bonded stationary phases are used because H-donors are more hydrophobic relative to non-H-donors in the octanol–water system than the RPLC system owing to the higher basicity of octanol than methanol and stationary phases. An explanation regarding this problem was given in detail in a previous paper [11].

As mentioned above, the M50 eluent hardly differentiated H-acceptors from non-hydrogen bonders. Under this condition, the amide group is thought to behave as an H-donor. This is the reason why the two parameters HB_H and HB_{AM} could be reasonably unified into HB_D. We have already reported [11,13] analogous findings that H-acceptors and non-hydrogen bonders give a single log k'–log P linearity in the M50 eluent. The utility of this mobile phase composition was further verified by applying eqn. 21 to other H-acceptors not included in Table II. The compounds tested and the results of analyses are summarized in Table IV.

Pyrazine has two strong H-accepting sites in the aromatic nucleus whereas the $CONMe_2$ substituent is a stronger H-acceptor than CO_2R [25,27,28]. It is clearly shown that the log P values calculated by eqn. 21 agreed with the log P values fairly well whereas their log k_w values gave overestimated values. Several other investigators [29–32] have reported that isocratic log k' data determined in eluents containing around 50% MeOH yield a better correlation with log P than the log k_w data do.

The ester effect was observed in a similar manner when we compared octanol–water log P values (log P_{oct}) of monosubstituted diazines with those determined from the chloroform–water partition system (log P_{CL}) [15]. The plot of log P_{CL} against log P_{oct} (Fig. 1 in ref. 15) presents a good linear relationship through the points for substituents such as H, alkyl, OR, NMe_2, SMe with CO_2R as positive deviants, presenting a feature which is very similar to the corresponding log k'–log P plot in water-rich eluents (Fig. 1 in ref. 11). We have explained this result in terms of stronger H-accepting ability of CO_2R groups than other well behaved substituents and of the number of hydrogen-bondable sites [15]. We tried the same treatment on a furan series consisting of furan, alkylated furans

TABLE IV

APPLICATION OF EQN. 21 TO OTHER COMPOUNDS CONTAINING STRONG H-ACCEPTORS

Compound	Log P^a	Log k_w [b]	Δ^c	Log k'_{M50} obsd.	Log k'_{M50} (Δ^e) calcd.[d]	Log P (Δ^f) calcd.[d]	HB_D
FR-2CONMe$_2$	0.41	0.92	0.51	−0.311	−0.27 (−0.04)	0.36 (0.05)	0
FR-3CONMe$_2$	0.24	0.81	0.57	−0.380	−0.37 (−0.01)	0.24 (−0.00)	0
BF-2CONMe$_2$	1.85[g]	2.42	0.57	0.535	0.54 (−0.01)	1.85 (−0.00)	0
In-2CONMe$_2$	1.96[g]	2.40	0.44	0.518	0.40 (0.12)	2.16 (−0.21)	1
In-3-OAc	2.03[g]	2.30	0.27	0.494	0.44 (0.05)	2.12 (−0.09)	1
1Me-In-2CO$_2$Me	3.37[g]	−[h]	−	1.447	1.39 (0.06)	3.45 (−0.08)	0
BZ-CONMe$_2$	0.62	1.42	0.80	−0.026	−0.16 (0.13)	0.86 (−0.24)	0
BZ-Ac	1.58	1.78	0.20	0.347	0.38 (−0.03)	1.52 (0.06)	0
Pyrazine (Pr)	−0.26	0.15	0.41	−0.590	−0.65 (0.06)	−0.13 (−0.13)	0
Pr-Me	0.21	0.49	0.28	−0.383	−0.39 (0.01)	0.24 (−0.03)	0
Pr-Et	0.69	1.02	0.33	−0.084	−0.12 (0.04)	0.76 (−0.07)	0

[a] Taken from refs. 5 and 13 unless indicated otherwise.
[b] Derived by eqn. 1.
[c] Difference between log k_w and log P values.
[d] Calculated by eqn. 21.
[e] Difference between observed and calculated log k'_{M50} values.
[f] Difference between observed and calculated log P values.
[g] This work.
[h] Not obtained because the retention time was too long in the eluent containing 30% MeOH.

and ester derivatives. Here again, esters and non-hydrogen-bonding substituents gave separate plots, reflecting the difference in association of the CO_2R moiety with octanol relative to that with $CHCl_3$ (not shown). These results confirm that the partition of ester derivatives, being strong H-acceptors, varies more sensitively with the change in the partitioning system. All those described above led us to conclude that the outstanding behaviour exerted by the ester group is ascribed to the solute–solvent interaction and not phenomena characteristic of the chromatographic retention process. The fact that the parameters S for esters are larger relative to the parent compounds confirms this argument.

The log k_w parameter is preferred by most investigators in predicting log P [6,9,21,33,34]. The merits pointed out are that the selective solute–solvent interactions can be eliminated [6] and the hydrogen-bond effects are reduced by using log k_w [23]. On the other hand, other results demonstrate that isocratic log k' data yield improved correlations. We can obtain an insight into this problem from the present results. Inspection of Table III reveals that the optimum mobile phase composition would vary depending on the hydrogen-bond properties of solutes. If a data set contains no hydrogen-donor components, an isocratic method with the use of an eluent containing about 50% methanol, yielding a single linear relationship, would be recommended. On the other hand, for a data set without H-acceptors, the log k_w method would improve the correlation because the contribution of the hydrogen-donor effect becomes minimal at 0% methanol concentration. As amphiprotic solutes can be treated as the sum of H-donor and H-acceptor components, the overall effect should depend on the relative hydrogen-bond ability of H-donating and H-accepting sites in the substituent. There would be cases where the log k_w parameter can be a good indication of log P

without corrections. This is probably because an over-estimating effect of H-accepting site(s) is almost cancelled by an under-estimating effect of H-donating site(s) in the log k_w value. Such examples can be found in practice in this work. When the difference between two opposite effects is not so large, the log k_w method might apparently work.

If the data set consists of solutes with different hydrogen-bond properties, our systematic studies dealing with simple O- and N-containing aromatic systems revealed that an eluent containing around 50% methanol, in which amphiprotic solutes are expected to behave only as H-donors, would give the simplest correlation with log P, permitting reliable log P values to be derived, provided that the hydrogen-donating components are treated separately as shown by eqn. 21. Further investigations will be needed to elucidate the hydrogen-bond effects of amphiprotic solutes on the correlation between chromatographic hydrophobicity and octanol–water partition coefficients. Our future work will deal with this problem.

REFERENCES

1 T. Fujita, J. Iwasa and C. Hansch, *J. Am. Chem. Soc.*, 86 (1964) 5175.
2 A. Leo, C. Hansch and D. Elkins, *Chem. Rev.*, 71 (1971) 525.
3 T. Fujita, *Prog. Phys. Org. Chem.*, 14 (1983) 75.
4 S.J. Lewis, M.S. Mirrless and P.J. Taylor, *Quant. Struct.–Act. Relat.*, 2 (1983) 1.
5 C. Yamagami, N. Takao and T. Fujita, *Quant. Struct.–Act. Relat.*, 9 (1990) 313.
6 Th. Braumann, *J. Chromatogr.*, 373 (1986) 191; and references cited therein.
7 H. Terada, *Quant. Struct.–Act. Relat.*, 5 (1986) 81, and references cited therein.
8 R. Kaliszan, *Quantitative Structure–Chromatographic Retention Relationships*, Wiley, New York, 1987.
9 D.J. Minick, J.H. Frenz, M.A. Patrick and D.A. Brent, *J. Med. Chem.*, 31 (1988) 1923; and references cited therein.
10 C. Yamagami, N. Takao and T. Fujita, *J. Pharm. Sci.*, 80 (1991) 772.
11 C. Yamagami, T. Ogura and N. Takao, *J. Chromatogr.*, 514 (1990) 123.
12 C. Yamagami and N. Takao, *Chem. Express*, 6 (1991) 113.
13 C. Yamagami and N. Takao, *Chem. Pharm. Bull.*, 40 (1992) 925.
14 C. Yamagami and N. Takao, *Chem. Express*, 7 (1992) 385.
15 C. Yamagami, N. Takao and T. Fujita, *J. Pharm. Sci.*, 82 (1993) 155.
16 C. Yamagami and N. Takao, *Chem. Pharm. Bull.*, 41 (1993) 694.
17 Y. Ohtsu, H. Fukui, T. Kanda, K. Nakamura, M. Nakano, O. Nakata and Y. Fujiyama, *Chromatographia*, 24 (1987) 380.
18 Y. Ohtsu, Y. Shiojima, T. Okumura, J. Koyama, K. Nakamura, O. Nakata, K. Kimata and N. Tanaka, *J. Chromatogr.*, 481 (1989) 147.
19 M. Kuchař, E. Kraus and M. Jelinková, *J. Chromatogr.*, 557 (1991) 399.
20 N. Chen, Y. Zhang and P. Lu, *J. Chromatogr.*, 606 (1992) 1.
21 W.E. Hammers, G.J. Meurs and C.L. de Ligny, *J. Chromatogr.*, 247 (1982) 1.
22 Th. Braumann, G. Weber and L.H. Grimme, *J. Chromatogr.*, 261 (1983) 329.
23 K. Miyake, N. Mizuno and H. Terada, *J. Chromatogr.*, 439 (1988) 227.
24 C. Yamagami, H. Takami, K. Yamamoto, K. Miyoshi and N. Takao, *Chem. Pharm. Bull.*, 32 (1984) 4994.
25 M.J. Kamlet, R.M. Doherty, M.H. Abraham, Y. Marcus and R.W. Taft, *J. Phys. Chem.*, 92 (1988) 5244.
26 N. Tanaka, H. Goodell and B. Karger, *J. Chromatogr.*, 158 (1978) 233.
27 R.W. Taft, D. Gurka, L. Joris, P. von R. Schleyer and J.W. Rakshys, *J. Am. Chem. Soc.*, 91 (1969) 4801.
28 M.H. Abraham, P.P. Duce, D.V. Prior, D.G. Barratt, J.J. Morris and P.J. Taylor, *J. Chem. Soc., Perkin Trans. 2*, (1989) 1355.
29 J.E. Haky and A.M. Young, *J. Liq. Chromatogr.*, 7 (1984) 675.
30 M. Kuchař, V. Rejholec, E. Kraus, V. Miller and V. Rábek, *J. Chromatogr.*, 280 (1983) 279.
31 T.L. Hafkenscheid and E. Tomlinson, *Int. J. Pharm.*, 16 (1983) 225.
32 A. Bechalacy, A. Tsantili-Kakoulidou, N. El. Tayar and B. Testa, *J. Chromatogr.*, 541 (1991) 221.
33 N. El. Tayar, H. van de Waterbeemd and B. Testa, *Quant. Struc.–Act. Relat.*, 4 (1985) 69.
34 J.L.G. Thus and J.C. Kraak, *J. Chromatogr.*, 320 (1985) 271.

Journal of Chromatography A, 662 (1994) 61–69
Elsevier Science B.V., Amsterdam

CHROM. 25 635

Solution properties of polyelectrolytes

X☆. Influence of ionic strength on the electrostatic secondary effects in aqueous size-exclusion chromatography

Rosa García, Iolanda Porcar, Agustín Campos, Vicente Soria and Juan E. Figueruelo*

Departament de Química Física, Universitat de València, E-46100 Burjassot, València (Spain)

(First received June 17th, 1993; revised manuscript received October 8th, 1993)

ABSTRACT

The retention behaviour of polyelectrolytes in aqueous size-exclusion chromatography (SEC), where electrostatic repulsion is the main secondary effect affecting to the separation mechanism, was investigated. A theoretical treatment was developed in order to establish the influence of the mobile phase ionic strength on calibration graphs, often used for the characterization of polyions by SEC. A master equation, derived in closed form, involving two terms related to the net charge of polyion and the residual surface charge on the gel packing, was derived. The formalism provides the basis for a more detailed analysis of chromatographic retention data in electrostatic interaction systems. Moreover, the introduction of some approximations in the original equation served to obtain an equivalent expression that is easier to use, and in which the functionality with respect to the ionic strength, I, remains unaltered. Reported data on the elution of sodium polystyrene sulphonate and poly(L-glutamic acid) from both organic and silica-based packings were used to test the goodness of the predictions carried out with the above-mentioned equations.

INTRODUCTION

Partially or totally dissociated ionic polymers in aqueous media display electrolyte behaviour. Localized positive and/or negative charges on the lateral groups of the polymer chain confer on polyelectrolytes specific properties different to those of uncharged polymers. In this context, whereas size-exclusion chromatography (SEC) of synthetic polymers in organic solvents is a useful tool for the evaluation of their molecular mass averages and molecular mass distributions, difficulties arise [1] when it is intended to evaluate those properties of polyelectrolytes from aqueous SEC. In order to obtain compatibility between a gel and water, the gels used in aqueous SEC exhibit ionic or strongly polar groups. These groups on the gel surface and the ionic atmosphere surrounding the macroion are the origin of the above difficulties [2]. Although the size-exclusion effect is the main separation mechanism in SEC, when the solute is a polyelectrolyte, interactions between its ionic atmosphere and the polar groups on the inner surface of pores interfere with the SEC process and cause secondary effects.

The distribution of polyelectrolytes inside

* Corresponding author.
☆ For Part IX, see ref. 9.

0021-9673/94/$07.00
SSDI 0021-9673(93)E1091-D

charged pores is a relatively recent and interesting topic from both the theoretical and experimental points of view. Dubin and co-workers [3–5] developed a model to predict the ion exclusion effect. Their model calculates the pore volume "forbidden" to the polyion, or repulsion volume, as a function of the electrostatic potential of the stationary phase. In this context, Mori [6] proposed an empirical correlation between the repulsion volume and the ionic strength of the eluent. On the other hand, Styring *et al.* [7] focused their attention on the electrostatic behaviour of the ionic atmosphere of polyelectrolytes without paying attention to the residual charge of the gel.

On the other hand, the elution behaviour of synthetic polyelectrolytes and biopolymers has often been treated as if there were an exponential dependence of retention on salt concentration. In this context and following previous work on the SEC of polyanions [8,9], we present here a theoretical treatment of the influence of ionic strength (I) on calibration graphs in aqueous SEC. The recently proposed functionality on I^{-1}, in contrast to that on $I^{-1/2}$ suggested by other workers [7], is analysed and tested using previously reported chromatographic data [6–10].

EXPERIMENTAL

Samples and solvents

The standards of uncharged polymers used were dextran samples from Pharmacia (Uppsala, Sweden) with nominal molar masses of 10 000, 17 700, 40 000, 66 900, 83 300, 170 000, 500 000 and 2 000 000 g mol^{-1} and poly(ethylene oxide) (PEO) from Fluka (Darmstadt, Germany) with molar masses 2000 and 4000 g mol^{-1} in order to cover the chromatographic low-molar-mass range. The polyelectrolytes tested were samples of poly(L-glutamic acid) (PGA) from Sigma (St. Louis, MO, USA) and sodium poly(styrene sulphonate) (PSS) from Pressure Chemical (Pittsburgh, PA, USA). Their nominal molar masses (in g mol^{-1}) and the abbreviations used are 13 600 (PGA-1), 43 000 (PGA-2), 77 800 (PGA-3), 1600 (PSS-1), 16 000 (PSS-2), 31 000 (PSS-3), 88 000 (PSS-4) and 177 000 (PSS-5). All samples showed polydispersities lower than 1.1.

The solvents used for viscometric measurements and as eluents in SEC were buffers made up from NaH_2PO_4 and Na_2HPO_4 for pH 7.0 and from NaOAc and HOAc for pH 5.0. The desired ionic strengths were adjusted from 0.005 to 0.10 *M*. Reagents used in the preparation of buffers were of analytical-reagent grade from Merck (Darmstadt, Germany).

Viscosities

Intrinsic viscosity values $[\eta]$ for uncharged polymers in pure water at 25.0 ± 0.1°C were evaluated through their viscometric equations given in refs. 8 and 9. Viscosity measurements on polyelectrolyte samples at 25.0 ± 0.1°C were performed with an AVS 440 automatic Ubbelohde-type capillary viscometer from Schott Geräte (Hofheim, Germany). The details of the experimental conditions and procedure have been reported previously [8].

Chromatography

The liquid chromatographic equipment has been described elsewhere [8]. The columns used were Ultrahydrogel 250 (UHG-250) packed with hydroxylated polymethacrylate-based gel of 250 Å nominal pore size (30×0.78 cm I.D.) from Waters Assoc. (Milford, MA, USA), and Spherogel TSK PW4000 packed with hydroxylated polyether copolymer of 500 Å nominal pore diameter (30×0.75 cm, I.D.) from Beckman Instruments (Galway, Ireland). The exclusion and total column volumes were 5.48 and 10.46 ml, respectively, for the UHG-250 column and 5.15 and 10.40 ml, respectively, for the TSK column, as determined with blue dextran (molar-mass = 2 000 000 g mol^{-1}) and ^2H_2O, respectively. Other experimental details were as used previously [8].

RESULTS AND DISCUSSION

In the SEC of uncharged polymers it has been widely demonstrated that the elution volume data fit well the so-called universal calibration function [11]:

$$\log M[\eta] = a - bV_e \quad (1)$$

where M, $[\eta]$ and V_e are the molar mass, intrinsic viscosity and peak elution volume of the polymer, respectively, and a and b are calibration constants. The slope, b, can be expressed in terms of column set characteristics as

$$b = \frac{a}{V_0 + V_p + V_a} \quad (2)$$

where V_0, V_p and V_a are the void volume, the available pore volume and a residual volume specified graphically in Fig. 1, respectively. The insertion of b from eqn. 2 into eqn. 1 yields

$$V_e = V_0 + V_a + V_p - k_{UC} \log M[\eta] \quad (3)$$

Note that k_{UC} denotes the inverse of b according to the terminology used by Styring *et al.* [7].

The same considerations can be extended to charged polymers, so that

$$V'_e = V_0 + V'_a + V'_p - k'_{UC} \log M[\eta]_I \quad (4)$$

where V'_e is the peak elution volume of the polyion, $[\eta]_I$ its intrinsic viscosity at a given ionic strength, I, k'_{UC} the inverse of the slope of the particular calibration plot of $\log M[\eta]_I$ *vs.* V'_e, and the remaining parameters are as specified in Fig. 1.

The elution volume of an uncharged polymer can be expressed as a function of the distribution coefficient, K_{SEC}, through

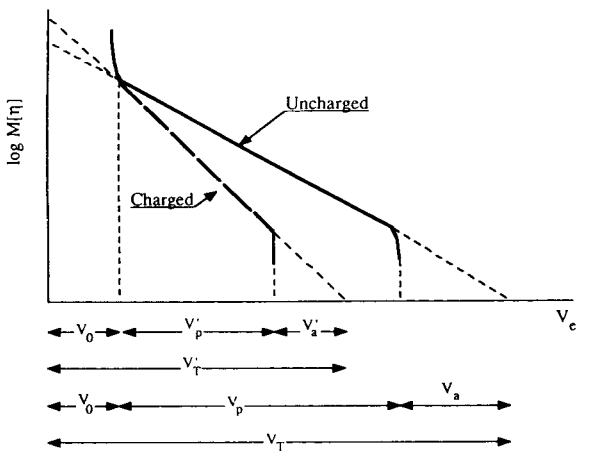

Fig. 1. Depiction of the different chromatographic volumes, appearing throughout the paper, placed on a calibration plot.

$$V_e = V_0 + K_{SEC}V_p \quad (5)$$

and for a polyelectrolyte [10,12] as

$$V'_e = V_0 + K_{SEC}V'_p \quad (6)$$

where $V'_p = V_p - V_r$ is the virtual pore volume available to the polyelectrolyte, *i.e.*, the difference between the pore volume given by the supplier and the "repulsion volume" impenetrable to the polyion by charge repulsion. The V'_p value is always lower that V_p when polymer–gel electrostatic repulsion takes place.

In addition, the elution volumes of polyelectrolytes depend strongly on the mobile phase ionic strength, as has been evidenced experimentally in several contributions dealing with the SEC of polyanions [3–9,10,12–14]. In this context, Styring and co-workers [7,13] explored this effect quantitatively and proposed the following empirical relationship:

$$V'_e = V_\infty - k_{el}I^{-1/2} \quad (7)$$

where V_∞ is the elution volume of a polyanion when $I \rightarrow \infty$, denoting an ionic strength high enough to screen their charges or to cancel the solute–gel repulsive interactions, and k_{el} is a constant accounting for electrical and geometrical features of both the polyion and gel support [7]. However, some discrepancies arose when the above equation was used to fit experimental data. For this reason, we have recently proposed an alternative semi-empirical correlation for the V'_e dependence on I, namely [9]

$$V'_e = V_e - k_{el}I^{-1/2} + K''I^{-1} \quad (8)$$

where V_e has the same meaning as V_∞ in eqn. 7, and the coefficient K'' also takes into account polymer–gel electrostatic interactions. For more precise information about this coefficient see eqn. 7 in ref. 9.

So far, we have presented basic equations for the SEC of charged and uncharged polymers and a recently reported empirical correlation of I with V_e. We now proceed to combine the above equations in order to obtain an expression that could take into account the influence of ionic strength on the calibration graphs of polyions. For this purpose, the insertion of the expressions

for V_e and V'_e given by eqns. 5 and 6, respectively, into eqn. 8, after some rearrangement yields

$$V'_p - \frac{K''}{K_{SEC}} \cdot I^{-1} = V_p - \frac{k_{el}}{K_{SEC}} \cdot I^{-1/2} \quad (9)$$

and inserting into eqn. 9 the V_p and V'_p expressions derived from eqns. 3 and 4, respectively, and coupling with some algebra, the following equation can be written:

$$V'_e + \log\left\{\frac{(M[\eta]_I)^{k'UC}}{(M[\eta]_\infty)^{k_{UC}}}\right\} + V_a - V'_a = V_e - \frac{k_{el}}{K_{SEC}} \cdot I^{-1/2} + \frac{K''}{K_{SEC}} \cdot I^{-1} \quad (10)$$

Note that $[\eta]_\infty$ has been used instead of $[\eta]$ because eqn. 3 is also valid for polyions when $I \rightarrow \infty$, that is, when they behave as uncharged polymers.

A tentative effort to analyse quantitatively the secondary electrostatic effects in aqueous SEC of polyions can be performed by means of eqn. 10. Nevertheless, we must previously proceed to express the above relationship in a more convenient form. First, note that most of the magnitudes involved in this equation are often handled by chromatographers, except the difference $V_a - V'_a$, which can be replaced with an equivalent term extracted from Fig. 1 and expressed as $V_T - V'_T - V_p + V'_p$. Moreover, recalling eqn. 9 and neglecting the numerical value of the difference $V_a - V'_a$, the above relationship could be written as

$$V'_e + \log\left\{\frac{(M[\eta]_I)^{k'UC}}{(M[\eta]_\infty)^{k_{UC}}}\right\} + V_p - V'_p = V_e \quad (11)$$

In the light of this equation, two terms account for specific contributions to the secondary electrostatic effects in aqueous SEC. The first one, $\log\{(M[\eta]_I)^{k'UC}/(M[\eta]_\infty)^{k_{UC}}\}$ takes into account the influence of eluent ionic strength on the $M[\eta]$ as representative of the shape and size of the polyion. Of course, when $I \rightarrow \infty$, $[\eta]_I \rightarrow [\eta]_\infty$ and $k'_{UC} \rightarrow k_{UC}$ and this term will be cancelled out. The second term refers to the pore volume inaccessible to polyions owing to the electrostatic potential of the stationary phase. Its value is $V_p - V'_p = V_r = A\chi_e$, where A is the area of the inner surface of the pores and χ_e the width of the electrostatic barrier created by the surface potential [3,10]. In fact, as χ_e is proportional to the Debye length, when $I \rightarrow \infty$, $\chi_e \rightarrow 0$, and this term will also be cancelled out.

We next proceed to verify the validity of eqn. 11. For this purpose, we selected previously reported chromatographic systems [6–10]. In order to make this equation manageable, a final transformation was carried out, yielding

$$V'_e + \Delta V' = V_e - k'_{UC} \log [\eta]_I \quad (12)$$

where $\Delta V' = \log\{M^{k'UC}/(M[\eta]_\infty)^{k_{UC}}\} + V_p - V'_p$. Consequently, a plot of $V'_e + \Delta V'$ *vs.* $k'_{UC} \log [\eta]_I$ should allow one to obtain by extrapolation V_e data that will serve to compare them with the corresponding experimental values.

In Figs. 2, 3 and 4 are depicted the plots of eqn. 12 for the systems: PGA–Spherogel TSK PW4000, PGA–UHG-250 and PSS–UHG-250, respectively, in eluents with different I and pH values. All data necessary to apply this equation

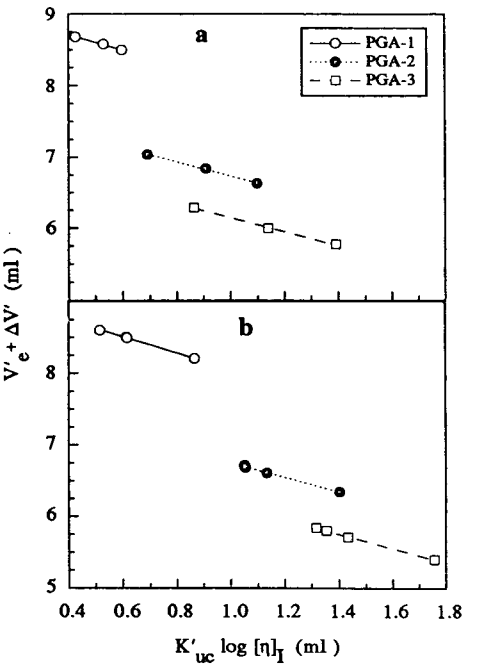

Fig. 2. Plot of eqn. 12 for poly(L-glutamic acid) (PGA)–Spherogel TSK PW4000 in the eluents (a) acetate buffer (pH 5.0) and (b) phosphate buffer (pH 7.0). Ionic strength range, 5–50 m*M*. Data from refs. 8 and 9.

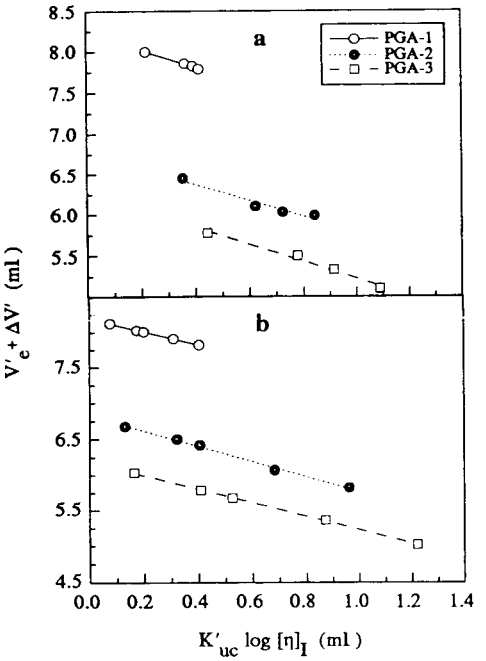

Fig. 3. Plot of eqn. 12 for poly(L-glutamic acid) (PGA)–Ultrahydrogel (UHG-250) in the eluents (a) acetate buffer (pH 5.0) and (b) phosphate buffer (pH 7.0). Ionic strength range, 5–100 m*M*. Data from refs. 8 and 9.

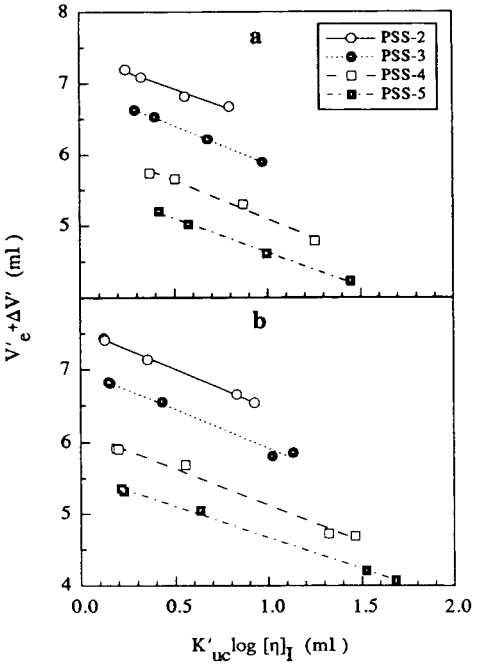

Fig. 4. Plot of eqn. 12 for sodium poly(styrene sulphonate) (PSS)–UHG-250 in the eluents (a) acetate buffer (pH 5.0) and (b) phosphate buffer (pH 7.0). Ionic strength range, 5–50 m*M*. Data from refs. 8 and 9.

have recently been reported [8,9]. Good linear fits with slope values close to unity are observed in all instances, consistent with the proposed functionality. From a quantitative point of view, the predicted V_e values for each sample and system agree very well with those from dextrans, as can be seen in Table I. From the comparison between both sets of V_e data, a slight deviation within the experimental error is observed. The same trend has been evidenced for other systems reported by different workers [6,7,10], as can be seen in Figs. 5–7 and Table II.

In spite of the formal importance of eqn. 12, it is scarcely useful in practice because its application demands a knowledge of an excessive number of data from both charged and uncharged polymers. In order to surmount this drawback, an approximate form of the original eqn. 10 was derived assuming that $k'_{UC} \approx k_{UC}$ and $V_a - V'_a \approx 0$:

$$V'_e + \Delta V^* = V_e - \frac{k_{el}}{K_{SEC}} \cdot I^{-1/2} + \frac{K''}{K_{SEC}} \cdot I^{-1} \quad (13)$$

where $\Delta V^* = k'_{UC}$ log $([\eta]_I/[\eta]_\infty)$. Several comments should be made about this simplified version: (a) the assumptions made to derive eqn. 13 are less drastic as the divergence between the calibration graphs for both charged and uncharged polymers vanishes (see Fig. 1); (b) for practical purposes, this equation is workable using as input data those obtained from charged polymers exclusively; and (c) in addition to the introduced approximations, the functionality of V'_e on $I^{-1/2}$ remains unaltered, being a second-order polynomial with respect to $I^{-1/2}$, whereas Styring *et al.*'s model [7] predicts a linear dependence expressed as

$$V'_e + \Delta = V_e - k_{el} I^{-1/2} \quad (14)$$

where $\Delta = k_{UC}$ log $([\eta]_I/[\eta]_\infty)$.

Eqns. 13 and 14 were tested with the same chromatographic systems as mentioned above. As an example, Figs. 8 and 9 depict plots of eqn. 13 (parts a) and eqn. 14 (parts b) for PSS–UHG-250–buffer (pH 7.0) [8,9] and PSS–CPG–buffer

TABLE I

DATA ON ELUTION VOLUMES FOR UNCHARGED POLYMERS [8,9] AND VALUES FOR CHARGED POLYMERS PREDICTED THROUGH EQNS. 12, 13 AND 14

System	Sample	V_e (ml)			
		Eqn. 12	Eqn. 13	Eqn. 14	Uncharged
PGA–TSK–buffer (pH 5.0)	PGA-1	9.14	9.42	10.26	9.12
	PGA-2	7.73	7.99	8.27	7.75
	PGA-3	7.12	7.42	7.87	7.15
PGA–TSK–buffer (pH 7.0)	PGA-1	9.20	9.43	8.56	9.12
	PGA-2	7.76	8.05	7.48	7.75
	PGA-3	7.15	7.20	7.21	7.15
PGA–UHG–buffer (pH 5.0)	PGA-1	8.23	7.81	7.61	8.21
	PGA-2	6.77	6.95	6.54	6.82
	PGA-3	6.26	6.14	6.12	6.21
PGA–UHG–buffer (pH 7.0)	PGA-1	8.20	8.48	7.59	8.21
	PGA-2	6.83	6.80	6.50	6.82
	PGA-3	6.19	6.31	6.14	6.21
PSS–UHG–buffer (pH 5.0)	PSS-1	9.42	9.60	9.29	9.40
	PSS-2	7.40	7.93	7.53	7.51
	PSS-3	6.95	7.01	6.82	6.97
	PSS-4	6.18	6.03	6.23	6.12
	PSS-5	5.57	5.89	5.93	5.55
PSS–UHG–buffer (pH 7.0)	PSS-1	9.36	9.75	9.14	9.40
	PSS-2	7.55	7.99	7.15	7.51
	PSS-3	6.98	7.25	6.58	6.97
	PSS-4	6.14	6.29	6.07	6.12
	PSS-5	5.55	6.01	5.89	5.55

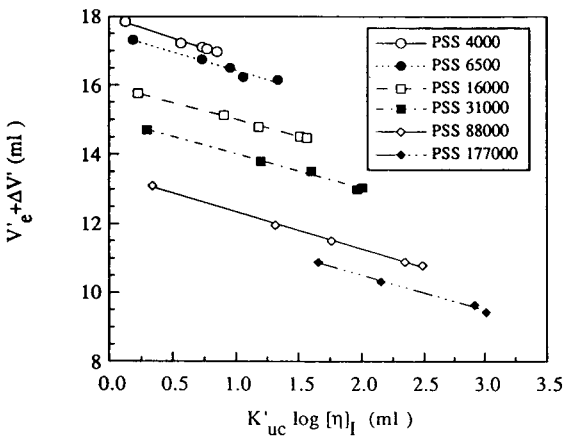

Fig. 5. Plot of eqn. 12 for PSS–FPG(500 + 170) in buffer of pH 8.0 as eluent. Ionic strength covering the range 14–270 m*M*. Data from ref. 6.

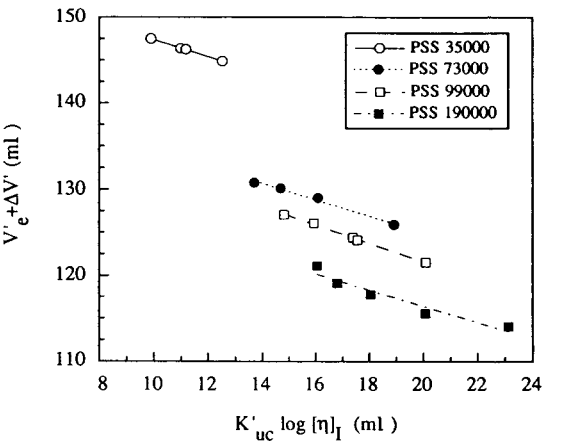

Fig. 6. Plot of eqn. 12 for PSS–glass beads in buffer of pH 6.0 as eluent. Ionic strength covering the range 12–100 m*M*. Data from ref. 7.

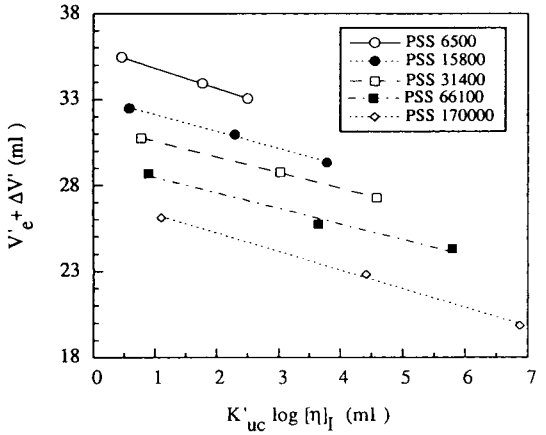

Fig. 7. Plot of eqn. 12 for PSS–CPG in buffer of pH 8.0 as eluent. Ionic strength covering the range 1.2–500 m*M*. Data from ref. 10.

(pH 8.0) [10] systems, respectively. Good fits of eqn. 13 are clearly observed in all instances, whereas the corresponding fits of eqn. 14 show discrepancies with respect to the linear correla-

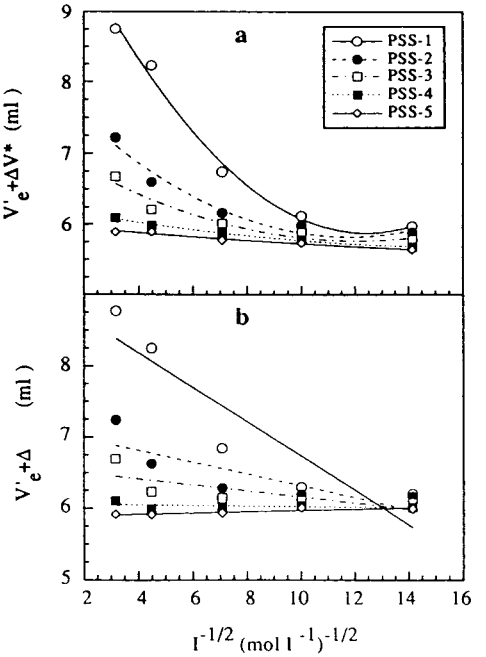

Fig. 8. Comparison between (a) eqn. 13 and (b) eqn. 14 for PSS–UHG-250–buffer (pH 7.0). Ionic strength range, 5–100 m*M*.

TABLE II

DATA ON ELUTION VOLUMES FOR UNCHARGED POLYMERS [6,7,10] AND VALUES FOR CHARGED POLYMERS PREDICTED THROUGH EQNS. 12, 13 AND 14

System	Sample	V_e (ml)			
		Eqn. 12	Eqn. 13	Eqn. 14	Uncharged
PSS–FPG [6]	PSS 6500	17.51	16.29	14.36	17.49
	PSS 16 000	15.97	16.13	13.50	15.96
	PSS 31 000	15.01	15.77	12.78	15.03
	PSS 88 000	13.43	13.94	11.36	13.44
	PSS 177 000	12.56	12.46	10.76	12.38
PSS–glass beads [7]	PSS 35 000	157.5	156.1	152.1	156.4
	PSS 73 000	144.0	143.7	144.2	144.5
	PSS 99 000	142.9	140.1	139.6	140.9
	PSS 190 000	135.2	134.3	134.6	134.3
PSS–CPG [10]	PSS 6500	35.98	37.70	33.68	35.83
	PSS 15 800	33.12	34.77	29.66	33.11
	PSS 31 400	31.46	33.44	28.74	31.55
	PSS 66 100	29.37	31.70	27.11	29.68
	PSS 170 000	27.38	27.25	24.75	27.10

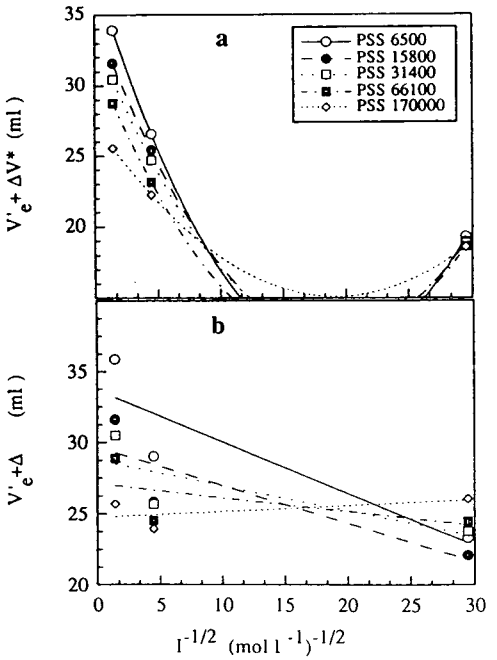

Fig. 9. Comparison between (a) eqn. 13 and (b) eqn. 14 for PSS–CPG–buffer (pH 8.0). Ionic strength range, 1.2–500 m*M*.

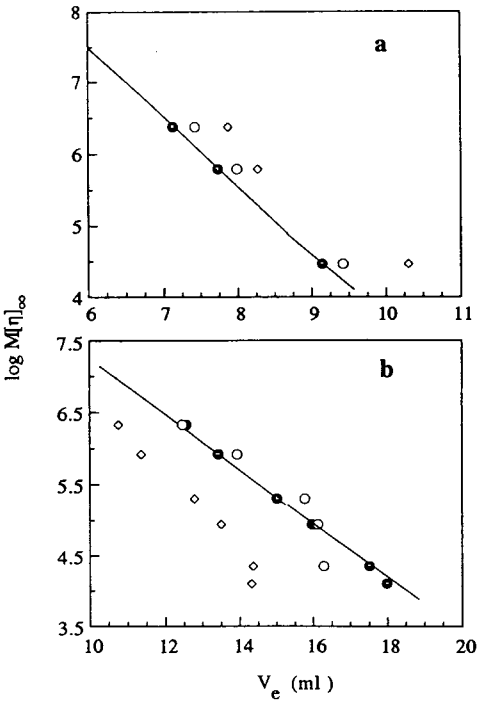

Fig. 10. Comparison between the calibration graphs for uncharged (solid lines) and charged polymers (symbols) predicted with (●) eqn. 12, (○) eqn. 13 and (◇) eqn. 14 for (a) PSS–UHG-250–buffer (pH 7.0) and (b) PSS–CPG–buffer (pH 8.0) chromatographic systems.

tion, being more pronounced as the polyion molar mass decreases. The extrapolated V_e values for these systems and for others, not plotted here for simplicity, are also given in Tables I and II. The comparison between V_e values from eqn. 13 and those for uncharged polymers reveals a good agreement in general, the deviation being *ca.* 4.0% for the most unfavourable cases. This small deviation validates the proposed eqn. 13, at least for the systems selected here, and the assumptions made to derive it. In contrast, the V_e values predicted through eqn. 14 show poor agreement when compared with the experimental elution volumes for uncharged polymers, the deviation being *ca.* 14% in some instances.

In order to complete our test on the predictions carried out with the proposed equations, we have built up current plots more suitable for the SEC characterization of polymers. Thus, Fig. 10 depicts the comparison between the calibration graph obtained for uncharged polymers (solid line) and those predicted by means of eqns. 12, 13 and 14 (symbols) for (a) PGA–TSK–buffer (pH 5.0) and (b) PSS–FPG–buffer (pH 8.0) chromatographic systems. The values of $[\eta]_\infty$ were determined with the equation $[\eta]_I = [\eta]_\infty + SI^{-1/2}$ (see eqn. 1 in refs. 8 and 9). As can be seen, the V_e values predicted through eqn. 12, considered as a closed form, fit the reference calibration graph well, whereas those obtained from eqns. 13 and 14 exhibit deviations, which are pronounced when using eqn. 14.

CONCLUSIONS

We have developed a formalism to predict the effect of the mobile phase ionic strength on the calibration graphs for the SEC of polyions in aqueous media by means of some fundamental equations combined with a recently proposed semi-empirical correlation between I and V_e. It should be emphasized that this treatment infers nothing about the influence of ionic strength on

the elution behaviour of polyelectrolytes when other separation mechanisms, such as adsorption, hydrophobic interactions or hydrogen bonding, take place.

The proposed master equation (eqn. 10 or 12) and the simplified version (eqn. 13) derived from the former making some plausible assumptions, display two terms accounting for the influence of I on the size and shape of the polyion and on the width of the electrostatic barrier on the gel surface. The simultaneous inclusion of these effects in a unique expression allow the quantitative evaluation of both contributions to the elution volume of a given polyion in aqueous SEC.

The predictions made using eqns. 12 and 13 support the proposed formalism, and comparison with eqn. 14 reveals that at high polymer molar masses both functionalities, on $I^{-1/2}$ from Styring *et al.* [7] and on I^{-1} proposed here, work well. However, at low molar masses or when the divergence between the charged and uncharged calibration graphs is more pronounced, the equations reported here yield more accurate predictions.

SYMBOLS

I ionic strength
M molar mass
$[\eta]_I$ intrinsic viscosity of a polyion at a given ionic strength
$[\eta]_\infty$ intrinsic viscosity of a polyion at $I \rightarrow \infty$ (high enough to screen its charges)
V_e elution volume of an uncharged polymer
V'_e elution volume of a polyelectrolyte
V_0 interstitial or void volume
V_p available pore volume for an uncharged polymer
V'_p available pore volume for a polyelectrolyte at a given I
V_T total pore volume for an uncharged polymer
V'_T total pore volume for a polyelectrolyte
$V_a = V_T - (V_0 + V_p)$
$V'_a = V'_T - (V_0 + V'_p)$
k_{UC} inverse of the slope of the uncharged polymer calibration graph
k'_{UC} inverse of the slope of the polyelectrolyte calibration graph
K_{SEC} distribution coefficient accounting for size-exclusion mechanism
k_{el} constant accounting for electrical and geometrical parameters
K'' constant accounting for chromatographic packing features

$$\Delta V' = \log \frac{M^{k_{UC}}}{(M[\eta]_\infty)^{k_{UC}}} + V_p - V'_p$$

$$\Delta V^* = k'_{UC} \log \left(\frac{[\eta]_I}{[\eta]_\infty} \right)$$

$$\Delta = k_{UC} \log \left(\frac{[\eta]_I}{[\eta]_\infty} \right)$$

ACKNOWLEDGEMENTS

This work was partially supported by Grant No. PB91-0808 from DGICYT (Spain). One of the authors (I. P.) is also grateful to the Ministerio de Educación y Ciencia (Spain) for a long-term fellowship.

REFERENCES

1 A.E. Hamielec and M.G. Styring, *Pure Appl. Chem.*, 57 (1985) 955.
2 F. Oosawa, *Polyelectrolytes*, Marcel Dekker, New York, 1971.
3 P.L. Dubin, C.M. Speck and J.I. Kaplan, *Anal. Chem.*, 60 (1988) 895.
4 P.L. Dubin and J.M. Principi, *Macromolecules*, 22 (1989) 1891.
5 P.L. Dubin, R.M. Larter, C.J. Wu and J.I. Kaplan, *J. Phys. Chem.*, 94 (1990) 7243.
6 S. Mori, *Anal. Chem.*, 61 (1989) 530.
7 M.G. Styring, H.H. Teo, C. Price and C. Booth, *Eur. Polym. J.*, 24 (1988) 333.
8 R. García, I. Porcar, A. Campos, V. Soria and J.E. Figueruelo, *J. Chromatogr.*, 655 (1993) 191.
9 R. García, I. Porcar, A. Campos, V. Soria and J.E. Figueruelo, *J. Chromatogr.*, 655 (1993) 3.
10 P.L. Dubin and M.M. Tecklenburg, *Anal. Chem.*, 57 (1985) 275.
11 H. Benoit, Z. Grubisic, P. Rempp, D. Decker and J.G. Zilliox, *J. Chim. Phys.*, 63 (1966) 1507.
12 E. Pérez-Payá, L. Braco, C. Abad, V. Soria and A. Campos, *J. Chromatogr.*, 548 (1991) 93.
13 M.G. Styring, C.J. Davison, C. Price and C. Booth, *J. Chem. Soc., Faraday Trans.*, 80 (1984) 3051.
14 M.G. Styring, C. Price and C. Booth, *J. Chromatogr.*, 319 (1985) 115.

Journal of Chromatography A, 662 (1994) 71–76
Elsevier Science B.V., Amsterdam

CHROM. 25 602

Monitoring the products of acetylation, sulphonation and condensation of 2,4-diaminobenzenesulphonic acid by high-performance liquid chromatography☆

Sajid Husain*, R. Narsimha, S.N. Alvi and R. Nageswara Rao

Analytical Division, Indian Institute of Chemical Technology, Hyderabad 500 007 (India)

(First received August 9th, 1993; revised manuscript received September 29th, 1993)

ABSTRACT

A simple and rapid high-performance liquid chromatographic method was developed for the separation and determination of 2,4-diaminobenzenesulphonic acid (DASA) in acetylation, sulphonation and condensation products. The separation was achieved on a reversed-phased μBondapak C_{18} column using 0.15 *M* ammonium sulphate–acetonitrile (80:20, v/v) as the eluent. The method was used not only for quality assurance but also for process development of 2,4-DASA and was validated using several industrial samples. The mean recovery of DASA from authentic samples was 99.86 ± 1.54% and the limit of detection was $5 \cdot 10^{-9}$ g.

INTRODUCTION

2,4-Diaminobenzenesulphonic acid (DASA) is an important intermediate in the manufacture of dyes for cotton, wool, leather and cosmetics [1]. It is produced in large amounts by the sulphonation of 2,4-dinitrochlorobenzene (DNCB) followed by reduction using iron and hydrochloric acid [2,3]. It yields valuable products such as 2-amino-4-acetanilidobenzenesulphonic acid (AASA), 2,4-diaminobenzenedisulphonic acid (DADA) and 4-aminobenzamide-N-(3-aminobenzene-4-sulphonic acid) (ABSA) on acetylation, sulphonation and condensation respectively [4–6]. Unreacted DASA is generally present in small amounts as an impurity of these compounds, reducing the quality of the finished products significantly. Owing to the similarities in solubility characteristics and chemical properties it is difficult to separate and determine DASA. The separation and determination of DASA are therefore important not only for quality assurance of these products but also for their process development.

A literature search revealed that no method has been reported for the quality assurance of DASA, AASA, DADA and ABSA. Chemical methods of analysis based on diazotization and coupling suffer from interferences from impurities and isomerization. Paper and thin-layer chromatographic methods have been widely used, but are qualitative in nature [7,8]. High-performance liquid chromatography is the method of choice for the separation of aromatic sulphonic acids [9,10]. Cellulose- and polystyrene-based ion-exchange columns have been used extensively to study the behaviour of aromatic sulphonic acids [11], but the separations on these columns have been found to be unsatisfactory because of the poor recovery of analytes due to strong adsorptions and hydrophobic inter-

* Corresponding author.
☆ IICT Communication No. 3259.

0021-9673/94/$07.00
SSDI 0021-9673(93)E1033-V

actions. Zou *et al.* [12] were successful in overcoming these difficulties using ion-pair reagents in reversed-phase liquid chromatography. However, the use of ion-pair reagents such as tetrabutylammonium hydrogensulphate and cetyltrimethylammonium bromide should generally be avoided not only because of the added complexity of the mobile phase but also because of baseline artifacts, irregular peak shapes and widths, marked sensitivity of separations to temperature and slow equilibration of the column before and after ion-pair chromatography [13]. Jandera *et al.* [14,15] reported reproducible and more economical separations using reversed-phase columns with aqueous inorganic salts as mobile phases. In this investigation we extended this idea to the determination of the title compounds not only for quality assurance but also for process development.

In this paper, we describe a simple and rapid high-performance liquid chromatographic method for the separation and determination of small amounts of DASA in reaction mixtures and final products of DADA, AASA and ABSA using a μBondapak C_{18} column and an eluant containing 0.15 *M* ammonium sulphate at ambient temperature.

EXPERIMENTAL

Materials and reagents

All reagents were of analytical-reagent grade unless stated otherwise. Glass-distilled water, HPLC-grade acetonitrile (Spectrochem, Bombay, India) and ammonium sulphate (BDH, Poole, UK) were used. DASA was prepared by heating 2,4-dinitrochlorobenzene with sodium sulphite and then reducing it with iron and hydrochloric acid. AASA, DADA and ABSA were prepared by acetylation, sulphonation and condensation of DASA with acetic anhydride, sulphuric acid and 4-nitrobenzoyl chloride, respectively. Technical-grade samples of DASA, DADA, AASA and ABSA were obtained from Orchem Intermediates (Hyderabad, India).

Apparatus

A high-performance liquid chromatograph (Shimadzu, Kyoto, Japan) with a 20-μl loop injector having a six-way high-pressure valve was used. A Shimadzu SPD-6AV variable-wavelength UV–Vis spectrophotometric detector was connected after the column. A μBondapak C_{18} (Waters Assoc., Milford, MA, USA) column (300 mm × 3.5 mm I.D.; particle size 10 μm) was used for separation. The chromatograms and the integrated data were recorded with a Chromatopac C-R3A processing system.

Chromatographic conditions

The mobile phase was 0.15 *M* ammonium sulphate–acetonitrile (80:20, v/v). Samples were dissolved in the mobile phase. The analysis was carried out under isocratic conditions at a flow-rate of 1 ml/min and a chart speed of 5 mm/min at room temperature (27°C). Chromatograms were recorded at the corresponding absorption maxima (λ_{max}) of the eluting compounds using a wavelength-programmable UV detector.

Analytical procedure

Samples (10 mg) were dissolved in the mobile phase (100 ml) and a 20-μl volume of each sample was injected and chromatographed under the above conditions. Synthetic mixtures and technical and commercial formulations were analysed under identical conditions. The percentage of DASA was calculated from the peak area.

RESULTS AND DISCUSSION

The structures of the compounds under investigation are given in Table I. Fig. 1 shows the reaction pathways followed for preparation of DASA, DADA, AASA and ABSA.

Quality assurance of DASA

The HPLC separation of DASA and its impurities is shown in Fig. 2. The peaks were identified by injecting the individual compounds. It can be seen that DASA is well resolved from the process reactants, *i.e.*, 2,4-DNCB and DNSA. Impurities, *i.e.*, 2,6-DNCB and 2,6-DASA do not interfere in the determination as they elute at 14.50 and 7.12 min, respectively. Acetonitrile was used as an organic solvent modifier to improve the separation. Earlier attempts using different columns, *i.e.*, μBondapak

TABLE I

CHEMICAL STRUCTURES AND ABBREVIATIONS OF THE COMPOUNDS UNDER INVESTIGATION

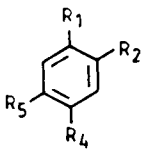

Compound	Abbreviation	R_1	R_2	R_4	R_5
2,4-Dinitrochlorobenzene	DNCB	Cl	NO_2	NO_2	H
Sodium 2,4-dinitrobenzenesulphonate	DNSA	SO_3Na	NO_2	NO_2	H
2,4-Diaminobenzenesulphonic acid	DASA	SO_3H	NH_2	NH_2	H
2,4-Diaminobenzene-1,5-disulphonic acid	DADA	SO_3H	NH_2	NH_2	SO_3H
2-Amino-4-acetanilidobenzenesulphonic acid	AASA	SO_3H	NH_2	$NHCOCH_3$	H
2,4-Diacetanilidobenzenesulphonic acid	DABA	SO_3H	$NHCOCH_3$	$NHCOCH_3$	H
4-Aminobenzamide-N-(3-aminobenzenesulphonic acid)	ABSA	SO_3H	NH_2	$NHCOC_6H_4NH_2$	H

C_8 and μBondapak CN, with aqueous triethylamine and acetonitrile resulted in overlapping of the peaks of DNSA and DNCB.

The effect of temperature on the separation was studied at 20, 25 and 30°C. It was found that a change in the temperature of the column of ±5°C has no significant effect on either the retention capacity or the resolution obtained between DASA and DNSA. However, the elution time of 2,4-DNCB was found to be reduced by 1.5 min per 5°C raise in temperature, resulting in a low resolution ($\alpha_{20°C} = 3.72$, $\alpha_{25°C} = 3.25$ and $\alpha_{30°C} = 2.69$) between DNSA and 2,4 DNCB.

The wavelengths of maximum absorption and retention times for DASA, DNSA and DNCB are given in Table II. Three different wavelengths, *i.e.*, 220 nm for 5 min, 252 nm for 10 min and then 245 nm were used for detection, not only because the detection of each component is ensured but also because good linearity between mass and integral response is obtained. The response data for these compounds are included in Table II. When the UV detector is

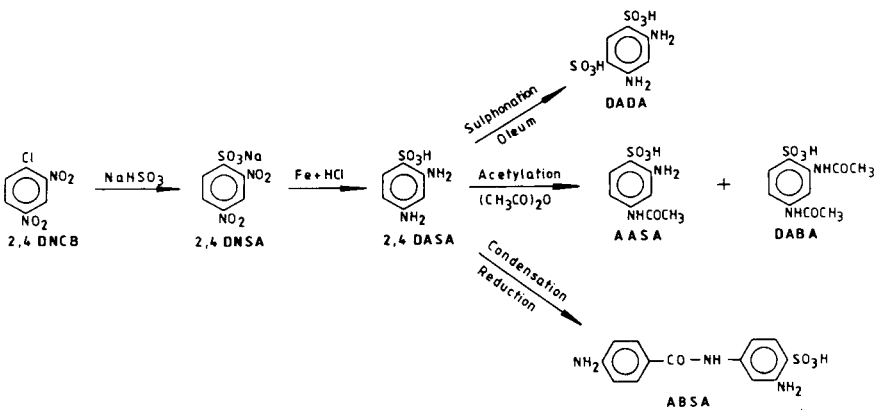

Fig. 1. Preparation of 2,4-diaminobenzenesulphonic acid (DASA) and its products of sulphonation, acetylation and condensation.

TABLE II

RETENTION TIMES (t_R), RELATIVE RESPONSE FACTORS (*RF*), WAVELENGTHS OF MAXIMUM ABSORPTION (λ_{max}) AND LINEARITY DATA FOR DASA, DNSA AND DNCB

Compound	t_R (min)	*RF*	λ_{max} (nm)	Linearity data	
				Regression equation[a]	Correlation coefficient
DASA	4.88	1.29	220	$y = 0.976x + 0.035$	0.998
DNSA	6.07	1.00	252	$y = 0.998x - 0.012$	0.995
DNCB	12.43	2.33	245	$y = 0.979x + 0.023$	0.997

[a] x = Amount taken; y = amount found.

set at 0.001 AUFS the limit of detection for DASA is $5.0 \cdot 10^{-9}$ g with a signal-to-noise ratio of 4.0.

Standards containing known amounts of DASA, DNSA and DNCB were prepared and analysed by HPLC. The accuracy of the method was determined by the standard addition technique. Subsequent additions of small amounts of the impurities were accurately reflected in their peak heights. The measured amounts agreed well with the actual values within 1.45%. The response factors for 1 μg each of all the compounds were determined and used to establish the composition of samples obtained during process development.

The method was applied to monitor the process conditions. The yield of DNSA in the first step was studied. It was separated by adding salts slowly to the mother liquor. The recovery was found to be around 72%. The filtrate containing unrecovered DNSA, unreacted DNCB and salts is called the "effluent" and it is generally disposed of to the environment after treatment in industry. These effluents were collected and analysed by HPLC. It was found that DNSA is present in the effluent in significant amounts and it has to be recovered economically from the effluent. This may be accomplished either by solid-phase extraction or by adjusting the pH. DNSA is further reduced to DASA using iron and hydrochloric acid. It may contain 2-nitro-4-aminobenzenesulphonic acid as an impurity.

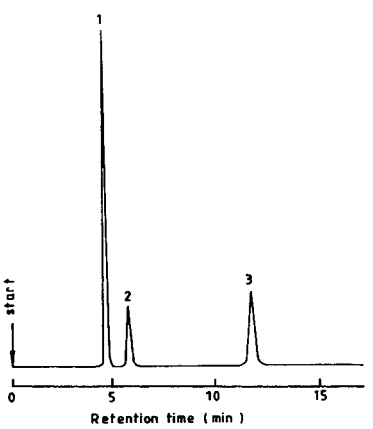

Fig. 2. Chromatogram of a typical mixture containing (1) DASA (20 μg), (2) DNSA (10 μg) and (3) DNCB (10 μg).

The quality of DASA was thoroughly checked on several lots of samples received from industry. The concentrations of various impurities were determined by HPLC and the purity of DASA was calculated. The results are given in Table III and show that the method is precise and accurate. Similar calculations were also

TABLE III

ANALYTICAL DATA FOR TYPICAL SAMPLES OF DASA RECEIVED FROM INDUSTRY

Sample	Assay (%)	S.D.[a] (%)
OIPL/1/92	0.972	1.26
OIPL/2/92	0.986	1.52
OIPL/1/93	0.989	1.07
OIPL/2/93	0.995	1.43

[a] $n = 3$.

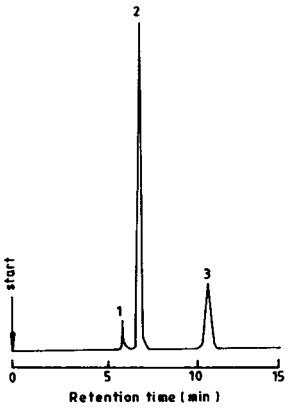

Fig. 3. Chromatogram of a typical mixture containing (1) DASA (2 μg), (2) AASA (20 μg) and (3) DABA (5 μg).

carried out for quality assessment of acetylation, sulphonation and condensation products of DASA. The precision of the purity values thus obtained was found to be good (within 1.63%) in all instances.

Acetylation of DASA

DASA was reacted with acetic anhydride to yield AASA (Fig. 1). Depending on the conditions of the reaction, it generally contains DABA as a by-product and DASA as an unreacted impurity. HPLC separation of these compounds is shown in Fig. 3. The retention data are presented in Table IV. The levels of DASA in reaction mixtures and the final product were determined by HPLC. The results are recorded in Table V. It can be seen that DASA levels as low as 0.1% can be determined accurately by HPLC.

TABLE IV

RETENTION TIMES (t_R), DETECTOR RESPONSES AND WAVELENGTHS OF ABSORPTION MAXIMA (λ_{max}) OF DASA, AASA AND DABA

Compound	t_R (min)	Relative response factor	λ_{max} (nm)
DASA	5.75	1.00	220
AASA	6.68	1.13	228
DABA	10.27	1.96	238

Sulphonation of DASA

DASA was treated with oleum to obtain DADA. The reaction mixture was collected and analysed by HPLC. The HPLC profile is shown in Fig. 4. The peaks were identified by injecting individual authentic compounds. DASA and DADA were found to elute at 5.41 and 8.43 min, respectively. Other reagents, *viz.*, chlorosulphonic acid and sulphuryl chloride, were also tried for sulphonation of DASA and the products obtained were analysed by HPLC. The results are given in Table V.

Condensation of DASA

Initially DASA was condensed with *p*-nitrobenzoyl chloride and then reduced to ABSA using iron and hydrochloric acid. All the reactants of this process were subjected to HPLC and their separation is shown in Fig. 5. It can be clearly seen that DASA is well separated not only from ABSA but also from other impurities, *viz.*, PNBC and NBSA. The method has been well standardized and used for process development. It has been found to be helpful not only for monitoring the reactions but also for improving significantly the yield and purity of ABSA (Table V).

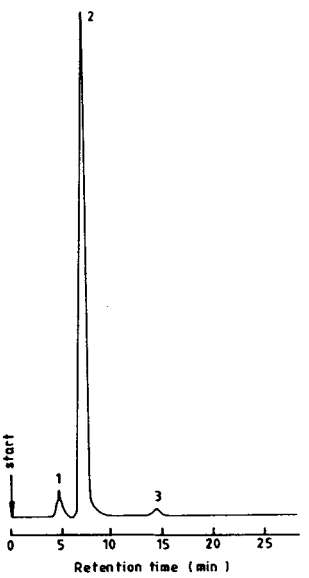

Fig. 4. Chromatogram of the product obtained on sulphonation of DASA. Peaks: 1 = DASA; 2 = DADA; 3 = unknown.

TABLE V

LEVELS OF DASA DETERMINED IN SAMPLES OF AASA, DADA AND ABSA BY HPLC

Sample	DASA concentration (%)	R.S.D.[a] (%)
AASA, Expt. 1	0.34	2.45
AASA, Expt. 2	1.93	2.08
AASA, Expt. 3	3.47	1.59
AASA, Expt. 4	5.45	1.23
DADA, Expt. 1	0.37	2.73
DADA, Expt. 2	0.72	2.15
DADA, Expt. 3	1.83	1.98
ABSA, Expt. 1	0.78	2.80
ABSA, Expt. 2	1.58	1.97

[a] $n = 3$.

CONCLUSIONS

A simple and rapid HPLC method employing a reversed-phase C_{18} column has been developed for monitoring the acetylation, sulphonation and condensation products of DASA. It is precise and accurate for the separation and determination of small amounts of DASA in several of the dye intermediates, *viz.*, AASA, DADA and ABSA. The method is suitable not only for process development but also for quality assurance of DASA and related products.

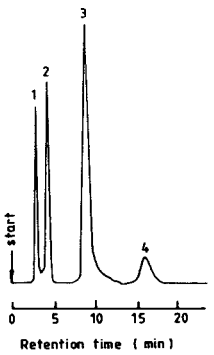

Fig. 5. Chromatogram of the reaction mixture collected during the course of condensation followed by reduction of DASA. Peaks: 1 = DASA; 2 = ABSA; 3 = PNBC; 4 = NBSA.

ACKNOWLEDGEMENT

The authors thank Mrs. Usha Rao (Orchem Industries, Hyderabad) for providing technical samples.

REFERENCES

1 K. Venkataraman, in L.M. Fieser and M. Fieser (Editors), *The Chemistry of Synthetic Dyes*, Academic Press, New York, 1952, pp. 528–529.
2 H.E. Fierz-David and L. Blangley, *Fundamental Processes of Dye Chemistry*, Interscience, New York, 1949, pp. 103–104.
3 L. Hartmut, H. Alfred and P. Manfred, *Eur. Pat. Appl.*, EP 285 972 (1988); *C.A.*, 110 (1989) 134882.
4 J.R. Hzaen, *Eur. Pat. Appl.*, EP 168 680 (1986); *C.A.*, 104 (1986) 224734.
5 R.N. Shreve, *Dyes Classified by Intermediates*, Chemcial Catalog, New York, 1922.
6 E.J. Vandenberg, W.R. Divelye, L.J. Filar, S.K. Patel and H.G. Barth, *J. Polym. Sci., Part A*, 27 (1989) 3745.
7 A. Cee and J. Gasparic, *Mikrochim. Acta*, 1 (1966) 295; *C.A.*, 65 (1966) 7983.
8 L. Lepri, P.G. Desideri and V. Coas, *J. Chromatogr.*, 88 (1974) 331.
9 C. Prandi and T. Venturini, *J. Chromatogr. Sci.*, 19 (1981) 308.
10 U. Streule and A.V. Waltenwyl, *Chromatographia*, 12 (1979) 25.
11 Y. Yoshii, A. Ito and O. Manabe, *Bunseki Kagaku*, 26 (1977) 179.
12 H. Zou, Y. Zhang and P. Lu, *J. Chromatogr.*, 545 (1991) 59.
13 P. Jandera and J. Churacek, *J. Chromatogr.*, 197 (1980) 181.
14 P. Jandera and H. Engelhardt, *Chromatographia*, 13 (1980) 18.
15 P. Jandera, J. Churacek and B. Taraba, *J. Chromatogr.*, 262 (1983) 121.

Journal of Chromatography A, 662 (1994) 77–85
Elsevier Science B.V., Amsterdam

CHROM. 25 665

Methylation, acetylation and gel permeation of hydrolysable tannins

Carole Viriot and Augustin Scalbert*

Laboratoire de Chimie Biologique (INRA), INA–PG, 78850 Thiverval-Grignon (France)

Catherine L.M. Hervé du Penhoat and Christian Rolando

Laboratoire de Chimie, Ecole Normale Supérieure, 24 Rue Lhomond, 75231 Paris (France)

Michel Moutounet

Laboratoire des Polymères et des Techniques Physico-Chimiques (INRA), Institut des Produits de la Vigne, 2 Place Viala, 34060 Montpellier Cedex 1 (France)

(Received August 16th, 1993)

ABSTRACT

Different derivatization methods for hydrolysable tannins were compared and assessed for calibration of gel permeation systems. Methylation of ellagitannins such as vescalagin or castalagin with either diazomethane or dimethyl sulphate yields small amounts of the expected permethylated products together with several by-products resulting from the cleavage of some ester bonds. Acetylation with acetic anhydride–pyridine mixture of the same ellagitannins gives a unique product from each compound, which is partially degraded if the excess of reagent is destroyed by addition of water or methanol. In contrast, application of the same methods to β-penta-O-galloyl-D-glucose and gallic acid gives a unique permethylated product or a relatively more stable peracetate. The best calibration graph for gel chromatography on Styragel columns with tetrahydrofuran as eluent was obtained with peracetylated derivatives.

INTRODUCTION

Tannins are usually considered to be water-soluble polyphenols of molecular mass varying between 500 and 3000. They can be classified in two groups: proanthocyanidins (condensed tannins) and hydrolysable tannins. Hydrolysable tannins include galloyl esters (gallotannins) and hexahydroxydiphenoyl esters (ellagitannins) [1]. The molecular mass upper limit value of 3000 is probably largely underestimated as proanthocyanidin polymers with a degree of polymerization as high as 50 ($M_r = 15\,000$) have been described [2]. The largest molecules of hydrolysable tannins which have been characterized are tetramers ($M_r = 4000$) [3,4]. It is unknown if larger polymeric hydrolysable tannins exist naturally in plants.

The structural characterization of such complex molecules often requires derivatization by either methylation or acetylation. Phenolic and aliphatic hydroxyl groups react with methyl donors to form methoxyl groups. The methylated derivatives, much less reactive than the crude tannins, have been used in chemical degradation studies in which ester bonds of

* Corresponding author.

0021-9673/94/$07.00
SSDI 0021-9673(93)E1114-F

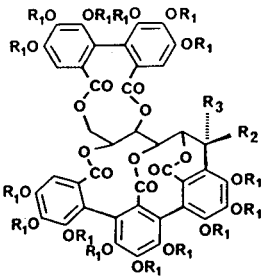

1 (R_1 = H, R_2 = H, R_3 = OH)
2 (R_1 = H, R_2 = OH, R_3 = H)
3 (R_1 = Me, R_2 = H, R_3 = OH)
4 (R_1 = Me, R_2 = H, R_3 = OMe)
5 (R_1 = Ac, R_2 = H, R_3 = OAc)
6 (R_1 = Ac, R_2 = OAc, R_3 = H)

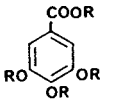

7 (R = H)
8 (R = Me)

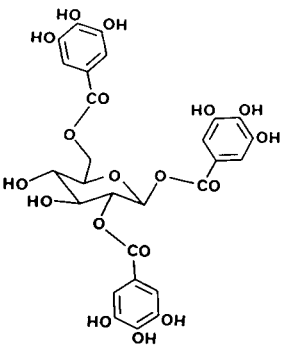

9

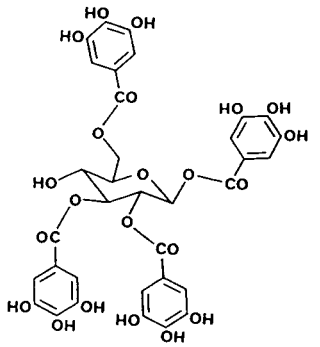

10

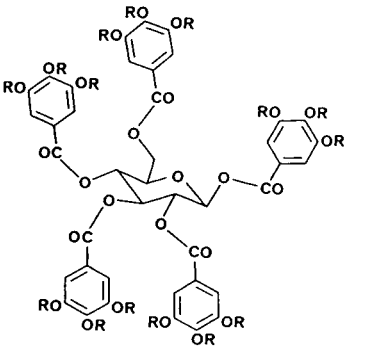

11 (R = H)
12 (R = Me)

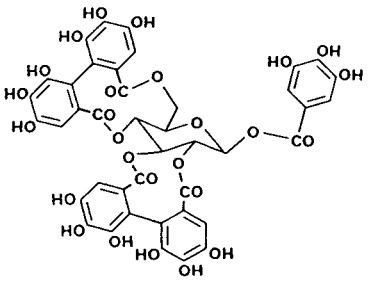

13

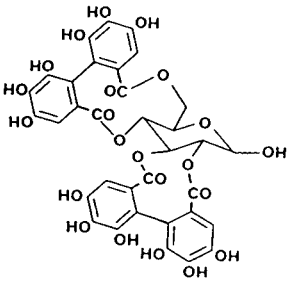

14

hydrolysable tannins are cleaved by methanolysis [5].

Methylation (by diazomethane) followed by acetylation can be used to determine the number of phenolic and aliphatic hydroxyl groups in a purified molecule [5,6].

Methylation and acetylation are often used to modify the solubility properties of tannins. Such reactions limit tailing effects in chromatography on silica (purification) [6] or styrene–divinylbenzene copolymers (gel permeation) [7].

Various methods have been proposed for determining the molecular masses of tannins. Fast atom bombardment mass spectrometry is undoubtly the most accurate method for pure compound or simple mixtures of a few compounds [8,9]. Other methods such as ebulliometry [10], ultracentrifugation [11,12], ^{13}C NMR spectroscopy [13], vapour pressure osmometry [14], low-angle laser scattering [14] and chemical methods [15,16] have been used to determine average molecular masses or molecular mass distributions of more complex mixtures of condensed tannins.

Normal-phase high-performance liquid chromatography with a mixture of hexane, methanol (or isopropyl alcohol), tetrahydrofuran (THF) and formic acid as eluent usually gives a positive and linear relationship between molecular mass and retention time for condensed [17] and hydrolysable [3,18,19] tannins. It requires proper tannin standards and can probably be used exclusively for the comparison of closely related molecules. This method has so far been applied to the comparison of purified tannins and to the analysis of simple mixtures of structurally well defined tannins with molecular masses not exceeding 4000. It is unlikely that such a method could be applied to higher molecular mass tannins, particularly those of indefinite polymeric structure. For these reasons, gel permeation is often preferred for studies of molecular mass distributions of condensed [7] and hydrolysable tannins [19,30].

In this paper, particular problems arising with the methylation, acetylation and gel permeation of hydrolysable tannins are reported and partially solved.

EXPERIMENTAL

Materials

The following C-glucosidic ellagitannins were purified from oak heartwood: four monomers [castalagin (**1**), vescalagin (**2**), grandinin and roburin E] and four dimers (roburin A, B, C and D) [21,22]. The structures of C-glucosidic ellagitannins given here have been revised according to refs. 23 and 24. β-1,2,6-Tri-O-galloyl-D-glucose (**9**), β-1,2,3,6-tetra-O-galloyl-D-glucose (**10**), β-penta-O-galloyl-D-glucose (**11**) and galloyl methyl ester were purified from methanolysed tannic acid (Fluka) [25,26]. Tellimagrandin II (**13**) and pedunculagin (**14**) were purified from oak leaves [27–29]. The identities of all the tannins were established by comparison of their ^{1}H and ^{13}C NMR spectra with those in the literature.

Methylation with diazomethane

Diazomethane was generated by reaction of N-methyl-N-nitroso-*p*-toluenesulphonamide (Aldrich) (2 g in 20 ml of diethyl ether) with potassium hydroxide [5 g in 18 ml of 55% (v/v) aqueous methanol] and recovered by distillation. The etheral solution of diazomethane was added to a methanolic solution (1 ml) of pure tannin (2 mmol of diazomethane per 1–5 mg of tannin). After standing overnight, the mixture was directly analysed by HPLC.

Methylation with dimethyl sulphate

Castalagin (56 mg), K_2CO_3 (550 mg) and dimethyl sulphate (0.5 ml) were added to acetone (3 ml) and refluxed for 3.5 h under nitrogen. The mixture was filtered. The reaction products in the filtrate were dried under reduced pressure.

Acetylation

Tannins (1 mg) were acetylated with acetic anhydride–pyridine (1:1) (500 μl) at room temperature overnight. Reagents were removed under reduced pressure after addition of toluene.

Analytical HPLC

Non-derivatized, permethylated and peracetylated tannins were analysed on a 10-μm μPorasil column (300 mm × 3.9 mm I.D.) (Waters). The elution conditions were as follows: linear gradient from 0 to 95% B from 0 to 30 min, solvent A = hexane–MeOH–THF (72:21:7), solvent B = MeOH–THF (75:25) with citric acid (0.25%) added to both solvent mixtures; flow-rate, 1 ml/min; detection, UV at 280 nm.

Purification of methylated tannins by preparative HPLC

Castalagin (50 mg) was methylated with diazomethane as above and fractionated on a 7-μm LiChrosorb Si 60 column (25 cm × 25 mm I.D.) (Merck). Elution was carried out in the isocratic mode with hexane–MeOH–THF (72:21:7) at a flow-rate of 20 ml/min and the eluate was monitored at 280 nm. Compounds eluted with the three main peaks were collected (5.0, 8.4 and 7.5 mg).

Castalagin (56 mg) permethylated with dimethyl sulphate as above was fractionated by HPLC under the same conditions. Two fractions (15.4 and 32.5 mg) were collected.

Gel permeation chromatography

Polystyrenes and acetylated tannins (1–2 mg/ml in THF, injection volume 20 μl) were analysed on two columns of Ultrastyragel, 500 and 1000 Å (300 mm × 7.8 mm I.D.) (Waters), connected in series. THF (Chromasol SDS) was delivered at a flow-rate of 1 ml/min. Detection was carried out at 280 nm.

Mass spectroscopy

Mass spectroscopy was carried out on a Nermag R 10.10C instrument operating in the chemical ionization mode. The reagent gas was ammonia, the source temperature was 80°C and the pressure of the ionization chamber was 10^{-4} Torr (1 Torr = 133.322 Pa).

^{1}H NMR spectroscopy

Spectra were measured on a Bruker AM 400-MHz spectrometer in a quantitative manner (acquisition time, 1.14 s; recycle time, 61 s) with DMSO-d_6 as the solvent. Galloyl methyl ester, δ 7.16 (s, 2H), 3.96 (s, 3H); tetra-O-methyl gallate (**8**), δ 7.46 (s, 3H), 4.06 (s, 3H), 4.05 (s, 6H), 3.95 (s, 3H).

RESULTS

Methylation

When gallic acid (**7**) and a galloyl ester, β-penta-O-galloyl-D-glucose (**11**), are methylated with diazomethane in a diethyl ether–methanol mixture, they give a unique product as seen by HPLC on a silica column (Fig. 1a). These products were identified by mass spectrometry as the tetra-O-methyl gallate (**8**) and pentadeca-O-methylpentagalloylglucose (**12**).

When castalagin (**1**), an ellagitannin, is methylated under the same conditions, it gives several products (Fig. 1b). The chromatographic profile was not changed by repeated methylations. Similar results were obtained with vescalagin (**2**).

In order to check that the multiple products were not due to incomplete methylation (of either phenolic or aliphatic hydroxyl groups), other reagents known to methylate both phenolic and aliphatic hydroxyl groups were tested. Neither the addition of $BF_3 \cdot Et_2O$ nor $HBF_4 \cdot Et_2O$ catalysts to diazomethane or the use of dimethyl

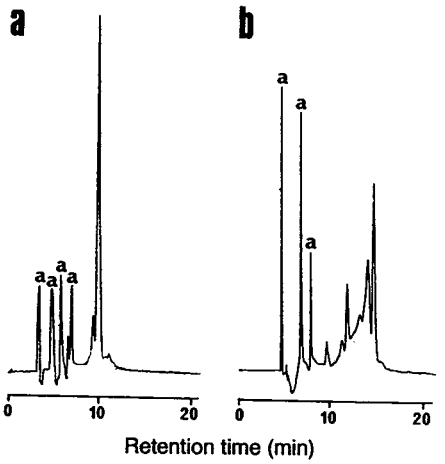

Fig. 1. Normal-phase HPLC of reaction mixtures after diazomethane methylation of hydrolysable tannins. (a) β-Penta-O-galloyl-D-glucose; (b) castalagin. a = Artefacts due to the chromatographic system.

sulphate resulted in the formation of a unique product.

The crude mixture obtained by diazomethane methylation of castalagin was analysed by mass spectroscopy. A complex spectrum was obtained (Fig. 2) which shows the formation of several compounds, most of them having a molecular mass higher than that of the expected pentadeca-O-methyl derivative of castalagin (**3**) (M_r = 1144).

The various products obtained by methylation of castalagin with diazomethane were partially purified by preparative HPLC on silica. Three fractions were obtained. Three products could be detected in the first fraction, with molecular masses of 1144 [m/z 1144 (M^+), 1162 ($M + NH_3 + H)^+$], 1190 [m/z 1190 (M^+), 1208 ($M + NH_3 + H)^+$] and 1208 [m/z 1208 (M^+), 1226 ($M + NH_3 + H)^+$]. The second fraction contained a producet with a molecular mass of 1190 together with one of molecular mass 1176 [m/z 1176 (M^+), 1194 ($M + NH_3 + H)^+$]. The mass spectrum of the third fraction showed only the presence of the compound with a molecular mass of 1176. Analysis by ^1H NMR spectroscopy showed that this compound has 16–17 methoxyl groups with signals varying from 3.52 to 4.14 ppm. Such methoxyl groups might be attached to aromatic or carbonyl carbons [see proton chemical shifts of galloyl methyl ester and tetra-O-methyl gallate (**8**) under Experimental].

Dimethyl sulphate methylation of castalagin also resulted in a complex mixture which was again fractionated by preparative HPLC on silica. Two main fractions were obtained. The first showed major ions corresponding to a compound of molecular mass 1202 [m/z 1202 (M^+), 1220 ($M + NH_3 + H)^+$] and minor ions corresponding to the expected hexadeca-O-methyl derivative (**4**) of castalagin with a molecular mass of 1158 [m/z 1158 (M^+), 1176 ($M + NH_3 + H)^+$]. The second fraction contained two species, a major one of molecular mass 1144 and a minor one of molecular mass 1190 (molecular ions as above).

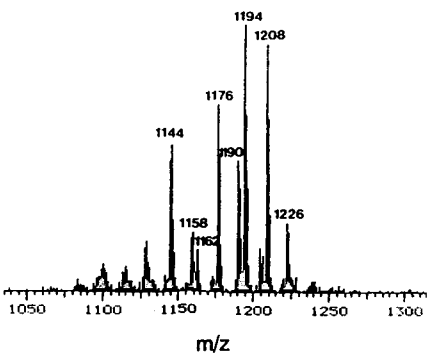

Fig. 2. Mass spectrum of diazomethane-permethylated castalagin.

Acetylation

Acetylation with acetic anhydride in pyridine gave only one product for all the compounds tested, *viz.*, gallic acid (**7**), β-penta-O-galloyl-D-glucose (**11**), castalagin (**1**) or vescalagin (**2**) (Fig. 3). The stability of the resulting acetates varies markedly, however. When the excess of acetic anhydride was destroyed by addition of water or methanol, gallic acid and β-penta-O-galloyl-D-glucose peracetates were not affected; castalagin peracetate (**5**) was partially degraded by the treatment as shown by the several peaks observed by HPLC (Fig. 4a). A decrease in temperature during the degradation of acetic anhydride did not lead to better results.

The best way to remove the reagents was finally found to be direct evaporation under vacuum. Under these conditions only one peak was observed by HPLC of the peracetylated castalagin (Fig. 4b).

Gel permeation

The different tannins and their permethylated and peracetylated derivatives were analysed by gel permeation chromatography on Styragel columns with THF as the eluent. The variations in the retention times of the underivatized tannins, monomers (15.4–15.6 min) and dimers (15.7–15.9 min), were too small to be used for molecular mass determination. Chromatography of dimethyl sulphate permethylated tannins gave a better separation of dimers from monomers (not shown). However, the best results were obtained with peracetylated tannins (Fig. 5): a linear relationship between retention times and the logarithms of molecular masses was obtained for peracetates of castalagin (**5**), vescalagin (**6**) and

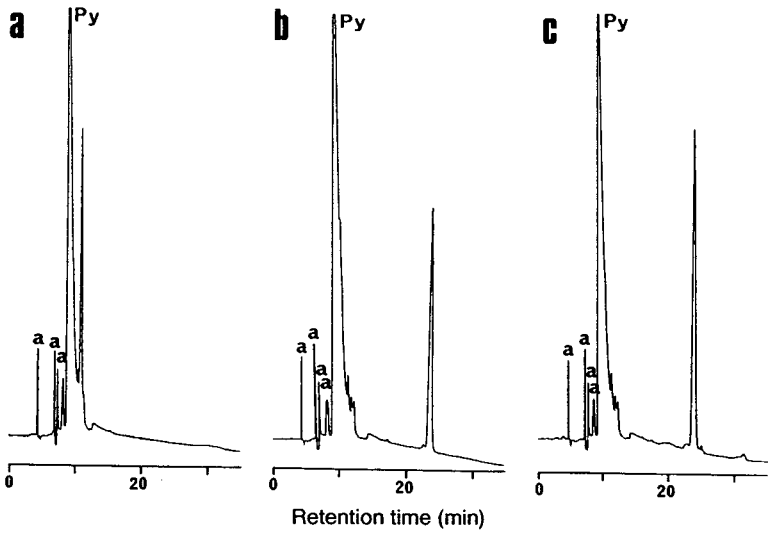

Fig. 3. Normal-phase HPLC of reaction mixtures after acetylation of hydrolysable tannins and derivatives. (a) Gallic acid; (b) β-penta-O-galloyl-D-glucose; (c) castalagin. Py = Pyridine; a = artefacts due to the chromatographic system.

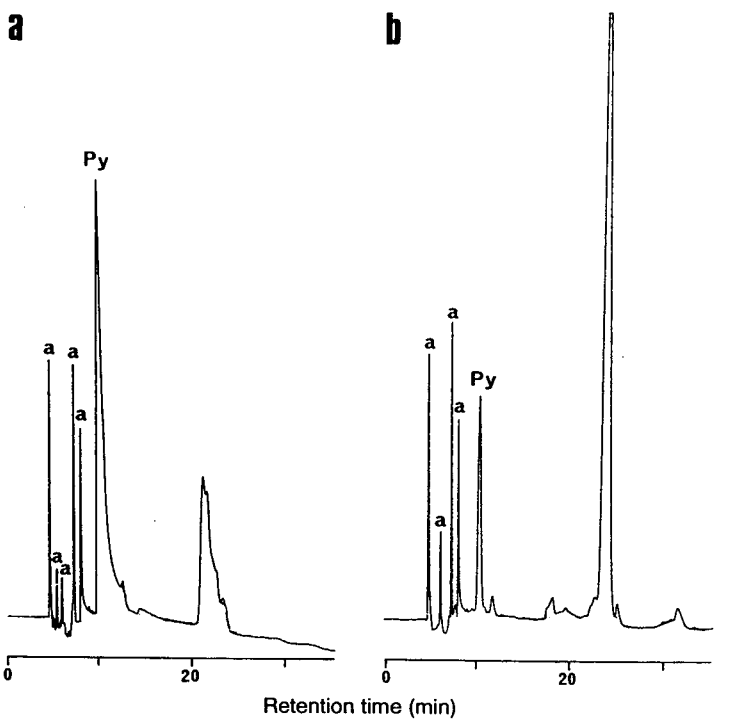

Fig. 4. Normal-phase HPLC of peracetylated castalagin (a) after addition of water to the acetylation reaction mixture and (b) after removal of reagents by evaporation and dissolution in chloroform. Py = Pyridine; a = artefacts due to the chromatographic system.

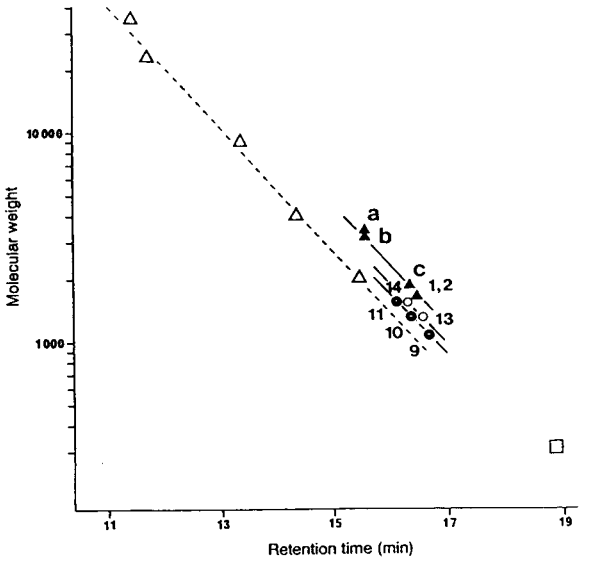

Fig. 5. Calibration graphs for gel permeation of peracetylated hydrolysable tannins on a Styragel column with THF as the eluent. △ = Polystyrenes; □ = galloyl methyl ester peracetate; ● = gallotannin peracetates; ▲ = C-glucosidic tannin peracetates; ○ = other ellagitannin peracetates. Numbers refer to the structures shown in the text; a = roburin B and C; b = roburin A and D; c = roburin E and grandinin.

six of their derivatives, monomers or dimers (all C-glucosidic ellagitannins with a carbon–carbon linkage between the first carbon of the aliphatic chain and one aromatic carbon). The plot is parallel to but not identical with that obtained with polystyrenes.

Gallotannins **9**, **10**, **11** and other ellagitannins [tellimagrandin II (**13**) and pedunculagin (**14**)] gave, for a given molecular mass, retention times intermediate between those of polystyrenes and C-glucosidic ellagitannins.

DISCUSSION

Methylation

Several methods of methylation have been applied previously to hydrolysable tannins. Some of these methods will methylate both phenolic and aliphatic hydroxyl groups (dimethyl sulphate [30], methyl iodide with silver oxide [31], diazomethane with boron trifluoride [30,32]) and others will only methylate phenolic hydroxyl groups (diazomethane) [5] or hemiacetal hydroxyl groups (methyl carbonate) [30]. In general, these methods when applied to ellagitannins give a crude oil composed of several permethylated products.

Permethylation of castalagin (**1**) with diazomethane gave low yields of the pentadeca-O-methyl derivative **3** ($M_r = 1144$), together with several other products. Most of them differ from the pentadeca-O-methyl derivative by a mass increment of 32 ($M_r = 1176$, one extra methoxyl group observed in the ^{1}H NMR spectra) or 2×32 ($M_r = 1208$). These products result from methanolysis of one or two ester linkages. Similar side-reactions have been reported previously with diazomethane methylation of ellagitannins [32]. Partial methylation of the aliphatic hydroxyl group is also observed; the resulting hexadeca-O-methyl derivative **4** ($M_r = 1158$) is eventually degraded by methanolysis of one ester linkage ($M_r = 1190$).

Methanolysis of ellagitannins has been explained by the presence of water in the diazomethane reaction mixture and avoided by carefully drying the solvents (methanol and diethyl ether) [32]. Here, methylation of castalagin, either as a powder or in methanol solution, with diazomethane in diethyl ether gave the same mixture of products as observed by HPLC.

Permethylation of castalagin with dimethyl sulphate gave small amounts of the hexadeca-O-methyl derivative **4** ($M_r = 1158$) together with significant amounts of the pentadeca-O-methyl derivative **3** ($M_r = 1144$), resulting from difficulties met in methylating the aliphatic hydroxyl group. By-products were also formed. The mass 1190 (1158 + 32) can be explained by methanolysis of one ester bond in the hexadeca-O-methyl derivative. Similar by-products have previously been encountered in the permethylation of ellagitannins with dimethyl sulphate [33,34] and the yields were not improved by using dry acetone and anhydrous potassium carbonate [35].

Acetylation

Acetylation of tannins is generally performed with an acetic anhydride–pyridine mixture and the excess of reagent is destroyed by addition of

water. Incomplete acetylation or partial deacetylation has not been previously reported and most workers have not reported any particular problems with the acetylation of flavonoids [35] and proanthocyanidins [7]. With gallic acid (**7**), β-penta-O-galloyl-D-glucose (**11**) or ellagitannins such as castalagin (**1**) or vescalagin (**2**), acetylation is apparently complete as only one product is observed by HPLC. However, HPLC shows the formation of several peaks on addition of water to the ellagitannin reaction mixtures. This can be explained by the relative instability of castalagin and vescalagin peracetates (**5** and **6**) compared with peracetates of gallic acid or β-penta-O-galloyl-D-glucose. A suitable method for the removal of reagents was found to be their direct evaporation under reduced pressure.

Gel permeation

Several gel permeation systems have been used for the determination of molecular mass distributions of tannins. Most workers use divinylbenzene polymer (Shodex K [36]) or styrene–divinylbenzene copolymer columns (TSK-H type [3], HSG-15 [37], Styragel [7]) with THF as the eluent for the analysis of either underivatized [36], permethylated [3] or peracetylated [7] tannins.

When applied to pure underivatized monomeric and dimeric ellagitannins, no significant separation according to molecular mass was observed. The best results were obtained with peracetylated ellagitannins.

The application of such a method to the determination of molecular masses requires proper standards for calibration. The calibration graph established with acetylated hydrolysable tannins differs significantly from that obtained with polystyrenes. The use of polystyrenes as standards will result in a 40% underestimation of the molecular mass of some ellagitannins, particularly those of the C-glucosidic type.

The retention time depends on the structure of hydrolysable tannins. It increases with the degree of oxidation of the tannin molecule (number of biphenyl bonds between aromatic rings), as illustrated with the three following hydrolysable tannins of nearly identical molecular mass; 16.10 min for β-penta-O-galloyl-D-glucose (no biphenyl bond), 16.37 min for tellimagrandin II (one biphenyl bond) and 16.48 min for castalagin (three biphenyl bonds).

Biphenyl linkages decrease the conformational mobility of hydrolysable tannins and reduce their apparent hydrodynamic radii. As a result, for a given molecular mass, gallotannins (with no biphenyl linkage) have relatively short retention times when compared with ellagitannins and flexible linear polystyrenes are particularly ill-suited for calibration of oxidized ellagitannins.

The range of calibration with ellagitannins has been limited to dimers (this work) or to tetramers. No larger molecule has so far been purified and characterized [38]. Determinations of molecular masses higher than those of tetramers by gel chromatography relies on extrapolation of the calibration graph and should thus be interpreted with care [39].

ACKNOWLEDGEMENTS

We sincerely thank the Remy-Martin Company for financial support via a studentship (C.V.) and Nicole Morin for the mass spectroscopy analyses.

REFERENCES

1 E. Haslam, *Plant Polyphenols, Vegetable Tannins Revisited*, Cambridge University Press, Cambrdige, 1989.
2 J. Porter, in R.W. Hemingway and P.E. Laks (Editors), *Plant Polyphenols, Synthesis, Properties and Significance*, Plenum Press, New York, 1992, p. 245.
3 T. Tanaka, G. Nonaka and I. Nishioka, *J. Chem. Res. (M)*, (1985) 2001.
4 T. Okuda, T. Yoshida and T. Hatano, *Heterocycles*, 30 (1990) 1195.
5 T. Okuda, T. Yoshida, M. Ashida and K. Yasaki, *J. Chem. Soc., Perkin Trans. 1*, (1983) 1765.
6 K. Weinges, W. Kaltenhauser, H.-D. Marx, E. Nader, F. Nader, J. Perner and D. Sieler, *Justus Liebigs Ann. Chem.*, 711 (1968) 184.
7 V.M. Williams, L.J. Porter and R.W. Hemingway, *Phytochemistry*, 22 (1983) 569.
8 R. Self, J. Eagles, G.C. Galletti, I. Mueller-Harvey, R.D. Hartley, A.G.H. Lea, D. Magnolato, U. Richli, R. Gujer and E. Haslam, *Biomed. Environ. Mass Spectrom.*, 13 (1986) 449.
9 D.F. Barofsky, in R.W. Hemingway and J.J. Karchesy (Editors), *Chemistry and Significance of Condensed Tannins*, Plenum Press, New York, 1989, p. 175.

10 S.R. Evelyn, *J. Soc. Leather Trades Chem.*, 38 (1954) 309.
11 S.R. Evelyn, *J. Polym. Sci.*, 33 (1958) 53.
12 W.T. Jones, R.B. Broadhurst and J.W. Lyttleton, *Phytochemistry*, 15 (1976) 1407.
13 Z. Czochanska, L.Y. Foo, R.H. Newman and L.J. Porter, *J. Chem. Soc., Perkin Trans. 1*, (1980) 2278.
14 L.J. Porter, *Aust. J. Chem.*, 39 (1986) 557.
15 L.G. Butler, *J. Agric. Food Chem.*, 30 (1982) 1090.
16 H. Kolodziej, *Phytochemistry*, 23 (1984) 1745.
17 E.L. Wilson, *J. Sci. Food Agric.*, 32 (1981) 257.
18 M. Verzele, P. Delahaye and F. van Damme, *J. Chromatogr.*, 362 (1986) 363.
19 T. Okuda, T. Yoshida and T. Hatano, *J. Nat. Prod.–Lloydia*, 52 (1989) 1.
20 T. Yoshida, T. Hatano, T. Okuda, M.V. Memon, T. Shingu, K. Inoue and K. Fukushima, *Tenne Yuki Kagobutsu Toronkai Koen Yushishu*, 26 (1983) 158.
21 A. Scalbert, L. Duval, S. Peng, B. Monties and C. du Penhoat, *J. Chromatogr.*, 502 (1990) 107.
22 C.L.M. Hervé du Penhoat, V.M.F. Michon, S. Peng, C. Viriot, A. Scalbert and D. Gage, *J. Chem. Soc., Perkin Trans. 1*, (1991) 1653.
23 G. Nonaka, T. Sakai, T. Tanaka, K. Mihashi and I. Nishioka, *Chem. Pharm. Bull.*, (1990) 2151.
24 T. Yoshida, H. Ohbayashi, K. Ishihara, W. Ohwashi, K. Haba, Y. Okano, T. Shingu and T. Okuda, *Chem. Pharm. Bull.*, (1991) 2233.
25 E. Haslam, R.D. Haworth, S.D. Mills, H.J. Rogers, R. Armitage and T. Searle, *J. Chem. Soc.*, (1961) 1836.
26 E.A. Haddock, S.M.K. Al-Shafi, R.K. Gupta, D. Magnolato and E. Haslam, *J. Chem. Soc., Perkin Trans. 1*, (1982) 2515.
27 A. Scalbert and E. Haslam, *Phytochemistry*, 26 (1987) 3191.
28 C.K. Wilkins and B.A. Bohm, *Phytochemistry*, 15 (1976) 211.
29 O.T. Schmidt, L. Würtele and A. Harreus, *Justus Liebigs Ann. Chem.*, 690 (1965) 150.
30 T. Yoshida, Y. Maruyama, M.U. Memon, T. Shingu and T. Okuda, *Phytochemistry*, 24 (1985) 1041.
31 M. Nishizawa, T. Yamagishi, N. Genichiro and I. Nishioka, *J. Chem. Soc., Perkin Trans. 1*, (1983) 961.
32 T. Okuda, T. Yoshida and T. Hatano, *J. Chem. Soc., Perkin Trans. 1*, (1982) 9.
33 T. Yoshida, T. Okuda, M.U. Memon and T. Shingu, *J. Chem. Soc., Perkin Trans. 1*, (1985) 315.
34 T. Yoshida, Z.-X. Jin and T. Okuda, *Phytochemistry*, 30 (1991) 2747.
35 M.V. Piretti and P. Doghieri, *J. Chromatogr.*, 514 (1990) 334.
36 T. Matsuo, K. Tamaru and S. Itoo, *Agric. Biol. Chem.*, 48 (1984) 1199.
37 T. Yoshida, T. Hatano, T. Okuda, M.V. Memon, T. Shingu, K. Inoue and K. Fukushima, *Symposium papers of the 26th Symposium on Chemistry of Natural Products, Kyoto*, 1983, p. 158.
38 T. Okuda, T. Yoshida and T. Hatano, *Phytochemistry*, 32 (1993) 507.
39 J. Klumpers, A. Scalbert and G. Janin, Phytochemistry.

Journal of Chromatography A, 662 (1994) 87–93
Elsevier Science B.V., Amsterdam

CHROM. 25 674

Resolution and sensitive detection of carboxylic acid enantiomers using fluorescent chiral derivatization reagents by high-performance liquid chromatography

Kazuo Iwaki*, Toyohiko Bunrin, Yuuko Kameda and Mitsuru Yamazaki

School of Pharmacy, Hokuriku University, Ho-3, Kanagawa-machi, Kanazawa-shi, Ishikawa 920-11 (Japan)

(First received July 27th, 1993; revised manuscript received October 22nd, 1993)

ABSTRACT

Chiral derivatization reagents possessing a dansyl (N-dimethylaminoaphthalene-5-sulphonyl) moiety as fluorophore were developed for the separation and sensitive detection of carboxylic acid enantiomers by high-performance liquid chromatography (HPLC). Synthesis of *d*- and *l*-1-(4-dansylaminophenyl)ethylamine (DAPEA) from easily obtained starting materials by simple four-step reactions gave satisfactory yields. The reagents reacted with carboxylic acid enantiomers such as anti-inflammatory drugs in the presence of condensing agents (2,2′-dipyridyl disulphide and triphenylphosphine) at room temperature for 2.5 h to give corresponding diastereomeric amide derivatives quantitatively. The fluorescence characteristics of the amide formed from DAPEA with 2-phenylpropionic acid enantiomer (DAPE-PPA) were hardly affected by the pH and water content of the mobile phase in the range commonly used for reversed-phase HPLC. The diastereomeric pairs formed from five anti-inflammatory drugs and phenylpropionic acid with DAPEA were efficiently separated by reversed-phase HPLC. The detection limit (signal-to-noise ratio = 3) of DAPE-PPA, when the resulting derivatization reaction mixture was directly injected on to the column, was 170 fmol per injection.

INTRODUCTION

The chiral derivatization method is one of the methods used for the separation of racemic compounds by high-performance liquid chromatography (HPLC). This method requires derivatization steps for the formation of diastereomers from target enantiomers with a chiral reagent prior to separation. This causes the method to be tedious compared with the related chiral stationary phase and chiral mobile phase methods, which can give the direct resolution of enantiomers. However, when the enantiomers have reactive functional groups and no useful chromophores to be detected, this disadvantage becomes a great advantage with respect to the sensitivity and selectivity for the detection of enantiomers, because this diastereomeric method is able to form diastereomers and introduce the appropriate chromophore at the same time. Therefore, numerous chiral derivatization reagents have been developed for the separation of racemic amino and carboxylic acid compounds [1–7].

The dansyl (N-dimethylaminonaphthalene-5-sulphonyl) residue, possessing both fluorescent and chemiluminescent moieties, is a very useful chromophore. For this reason, it has not only been used for the labelling of amino compounds as dansyl chloride, but also recently applied to chromophores of many labelling reagents for trace analysis by HPLC *e.g.*, 4-dansylaminophenyl isothiocyanate [8], dansylsemipiperazine [9], monodansylcadaverine [10] and N-bromoacetyl-N′-dansylpiperazine [11].

* Corresponding author.

0021-9673/94/$07.00
SSDI 0021-9673(93)E1122-G

This paper deals with the synthesis of chiral derivatization reagents having a dansyl residue to give fluorescent diastereomers by reaction with carboxylic acid enantiomers. Reaction conditions for the derivatization of arylpropionic acids were optimized, and the fluorescence characteristics of the resulting diastereomeric amide compound were investigated. The separation of the diastereomers by reversed-phase HPLC is also demonstrated.

EXPERIMENTAL

Reagents

Dansyl chloride (Dns-Cl), enantiomeric 1-(4-nitrophenyl)ethylamine hydrochloride, diethyl phosphorocyanidate (DEPC), 2,2′-dipyridyl disulfide (DPDS) and triphenylphosphine (TPP) were obtained from Tokyo Kasei (Tokyo, Japan), racemic ibuprofen, sodium acetate and 5% palladium–carbon (Pd–C) from Wako (Osaka, Japan), enantiomeric ibuprofen and *d*-naproxen from Funakoshi (Tokyo, Japan) and Sigma (St. Louis, MO, USA), respectively, and di-*tert*.-butyl dicarbonate [$(Boc)_2O$], isomeric 2-phenylpropionic acid (PPA) and N,N′-dicyclohexylcarbodiimide (DCC) from Nacalai Tesque (Kyoto, Japan). Racemic and isomeric pranoprofen, racemic and isomeric flurbiprofen and racemic phenoprofen were donated by Yoshitomi Pharmaceutical (Osaka, Japan), Kaken Pharmaceutical (Tokyo, Japan) and Yamanouchi Pharmaceutical (Tokyo, Japan), respectively, and *l*-naproxen was kindly supplied by Dr. Toshimasa Toyo'oka (National Institute of Hygienic Science, Tokyo, Japan). Acetonitrile was of HPLC grade. Water was purified by distillation, followed by final clean-up through a Milli-Q Labo system (Nihon Millipore, Tokyo, Japan). All other reagents were of analytical-reagent grade.

Apparatus

All melting-points (m.p.) were taken on a Yanagimoto (Tokyo, Japan) micro-m.p. apparatus and are uncorrected. Proton nuclear magnetic resonance (NMR) spectra were measured on a Jeol (Tokyo, Japan) PMX60SI instrument at 60 MHz using tetramethylsilane as an internal standard; abbreviations used are *s* for singlet, d for doublet, t for triplet, q for quartet and m for multiplet. Mass spectrometry (MS) was carried out on a Jeol DX-300 mass spectrometer with 70-eV electron-impact ionization (EI). Optical rotations were recorded on a Jasco (Tokyo, Japan) DIP-370 digital polarimeter equipped with a 100×3.5 mm I.D. cylindrical cell. Fluorescence characteristics were measured on a Hitachi (Tokyo, Japan) F-1200 spectrofluorimeter fitted with a 1-cm silica cell unit.

The HPLC system consisted of an L-6200 delivery system (Hitachi), a Model 7125 loop injector (Rheodyne, Cotati, CA, USA), an ODS-80TM (5 μm) (Tosoh, Tokyo, Japan) prepacked column (150×4.6 mm I.D.) and an L-1200 spectrofluorimeter (Hitachi) fitted with a 12-μl flow cell unit. The column was operated at room temperature. The detector excitation and emission wavelengths were set at 338 and 535 nm, respectively. Results were recorded on a D-2500 chromato-integrator (Hitachi). The flow-rate of the mobile phase was maintained at 1.0 ml/min.

Synthesis of the fluorescent chiral derivatization reagents (Fig. 1)

N - tert. - Butoxycarbonyl - 1 - (4 - nitrophenyl) - ethylamine (II). To a stirred acetonitrile solution (20 ml) of optically active 1-(4-nitrophenyl)ethylamine hydrochloride (**I**) (2.0 g, 10 mmol) and triethylamine (1.1 g, 11 mmol) in ice-bath was added dropwise $(Boc)_2O$ (2.2 g, 10 mmol). The mixture was stirred at room temperature for 1 h and then evaporated *in vacuo*. The residue was dissolved in ethyl acetate (50 ml). This solution was washed with 10% aqueous citric acid and water, dried over anhydrous sodium sulphate and evaporated *in vacuo* gave **II** (2.4 g, 90%) as white crystals, m.p. 85–87°C for the *R*-configuration and 86–89°C for the *S*-configuration. EI-MS, *m/z* 266 (M^+). NMR (ppm) in C^2HCl_3, 8.38 (2H, d, $J = 9$ Hz, Ar–H), 7.35 (2H, d, $J = 9$ Hz, Ar–H), 4.82 (1H, q, $J = 7$ Hz, CH), 1.53 (3H, d, $J = 7$ Hz, CH_3), 1.40 [9H, s, $C(CH_3)_3$].

N-Boc-1-(4-aminophenyl)ethylamine (III). To a solution of **II** (2.0 g, 6.6 mmol) in methanol (40 ml) was added 0.2 g of Pd–C. The suspen-

sion was stirred for 3 h while hydrogen gas was passed through at room temperature. After the Pd–C had been filtered off, evaporation of the filtrate *in vacuo* gave **III** (1.4 g, 79%) as a colourless oil. This was identified only by MS. EI-MS, *m/z* 236 (M^+).

N - Boc - 1 - (4 - dansylaminophenyl)ethylamine (IV). Isomeric **III** (1.4 g, 5.9 mmol) was dissolved in the mixture of acetonitrile (10 ml) and 0.1 *M* sodium hydrogencarbonate (pH 9.0, 50 ml). The solution was stirred during dropwise addition of dansyl chloride (1.9 g, 7.1 mmol) dissolved in acetonitrile (30 ml). The pH of the mixture was kept at 9.0 with 1.0 *M* sodium hydroxide solution. The resulting mixture was stirred for 20 min at room temperature and further for 2 h at 45°C, cooled to room temperature and extracted with ethyl acetate (3 × 30 ml). The extracts were combined, dried over anhydrous sodium sulphate, and evaporated *in vacuo*. Crystallization of the residue from benzene–hexane gave **IV** (2.2 g, 81%) as pale yellow crystals, m.p. 97–100°C for the *R*-configuration and 97–101°C for the *S*-configuration. EI-MS, *m/z* 469 (M^+). NMR (ppm) in C^2HCl_3, 6.8–8.8 (10H, m, Ar–H), 4.85 (1H, q, $J = 7$ Hz, CH), 2.93 [6H, s, $N(CH_3)_2$], 1.37 [9H, s, $C(CH_3)_3$], 1.20 (3H, d, CH_3).

1 - (4 - Dansylaminophenyl)ethylamine (DAPEA, V). To a solution of **IV** (1.5 g, 3.2 mmol) in methanol (10 ml) was added concentrated HCl (2ml). The mixture was stirred at room temperature for 30 min and evaporated *in vacuo*. The residue was dissolved in water (30 ml), the pH was adjusted to 8.0 with sodium hydrogencarbonate and the solution was extracted with ethyl acetate (3 × 30 ml). The extracts were combined, dried over anhydrous sodium sulphate and evaporated *in vacuo*. Recrystallization of the resulting powder from ethanol gave DAPEA (**V**) (1.0 g, 85%) as pale yellow crystals, m.p. 159–161°C for the *R*-configuration and 157–160°C for the *S*-configuration. EI-MS, *m/z* 369 (M^+). NMR (ppm) in $C^2H_3O^2H$, 6.9–8.6 (10H, m, Ar–H), 3.90 (1H, q, $J = 7$ Hz, CH), 2.80 [6H, s, $N(CH_3)_2$], 1.27 (3H, d, $J = 7$ Hz, CH_3). $[\alpha]_D$, 11.0° for the *R*-configuration (28°C) and −11.1° for the *S*-configuration (28°C), $c = 0.2$ in acetonitrile. Calculated for $C_{20}H_{23}N_3O_2S$, C 65.02, H 6.27, N 11.37; found for *R*-configuration, C 65.01, H 6.21, N 11.23%, and for *S*-configuration, C 65.13, H 6.30, N 11.27%.

Synthesis of the diastereomeric amide compound (R)-1-(4-dansylaminophenyl)-N-[(S)-2-phenylpropionyl]ethylamine (DAPE-PPA)

To a stirred solution of *d*-PPA (0.5 g, 3.3 mmol) and *d*-DAPEA (1.2 g, 3.3 mmol) in acetonitrile (30 ml) was added DPDS (1.1 g, 5.0 mmol) and TPP (1.3 g, 5.0 mmol). The mixture was stirred for 3 h at room temperature, evaporated *in vacuo* and the residue dissolved in ethyl acetate (50 ml). This solution was washed with saturated aqueous sodium hydrogencarbonate and water, dried over anhydrous sodium sulphate and evaporated *in vacuo*. The oily residue was purified by column chromatography. Elution with benzene–acetone gave DAPE-PPA (1.0 g, 60%) as a pale yellow oil. EI-MS, *m/z* 500 [$(M - H)^+$]. NMR (ppm) in C^2HCl_3, 6.9–8.7 (15H, m, Ar–H), 4.98 (1H, q, $J = 7$ Hz, 1–H), 3.53 (1H, q, $J = 7$ Hz, 2″–H), 2.85 [6H, s, $N(CH_3)_2$], 1.43 (3H, d, $J = 7$ Hz, 1–CH_3), 1.20 (3H, d, $J = 7$ Hz, 2″–CH_3). Calculated for $C_{29}H_{31}N_3O_3S$, C 69.44, H 6.23, N 8.38; found, C 69.52, H 6.21, N 8.37%.

Measurement of fluorescence characteristics of DAPE-PPA in aqueous medium

A solution of DAPE-PPA in acetonitrile (0.01 mg/ml) was diluted with a ninefold volume of 50 m*M* sodium acetate–acetonitrile (50:50–10:90, v/v) or of 50 m*M* acetate buffer (pH 3–9)–acetonitrile (50:50, v/v). The maximum wavelength and relative fluorescence intensity for each acetonitrile concentration or pH value were measured with the use of a 1-cm quartz cell.

Derivatization procedures for carboxylic acid enantiomers with DAPEA

In a brown micro test-tube, to 100 μl of sample solution in acetonitrile were added 100 μl of 2 m*M* DAPEA solution in acetonitrile, 100 μl of 3 m*M* DPDS solution in acetonitrile and 100 μl of 3 m*M* TPP solution in acetonitrile, successively. The tube was vortex mixed and allowed to stand for 3 h at room temperature. An aliquot

(5 μl) of the resulting mixture was injected on to the HPLC column.

RESULTS AND DISCUSSION

Synthesis of the fluorescent chiral amine

1-Substituted ethylamines with a bulky residue such as phenyl, naphthyl or dimethylaminonaphthyl have mainly been used as chiral derivatization agents for carboxylic acid enantiomers. Because these agents have the chiral centre directly bonded with both the bulky residue and the reactive functional residue for the carboxyl group, the resulting diastereomers derived from the reagent with enantiomers can form an advantageous rigid conformation for separation by conventional HPLC. 1-(4-Nitrophenyl)ethylamine (**I**) is a 1-substituted ethylamine that can be easily obtained as an optically active compound, and the presence of the nitro residue, easily modified to a primary amino group, is of great advantage for the introduction of a dansyl residue. Optically active DAPEA as a 1-substituted ethylamine having a more useful fluorophore was synthesized from optically active **I**.

The synthesis of DAPEA in satisfactory yields was accomplished by very simple four-step reactions as shown in Fig. 1. In order to determine the optical purity of two chiral DAPEAs, the amide compounds, which were derivatized from each DAPEA with N-carbobenzoxy-L-phenylalanine (optical purity ≥99.9%) (Peptide Institute, Osaka, Japan), were injected into the

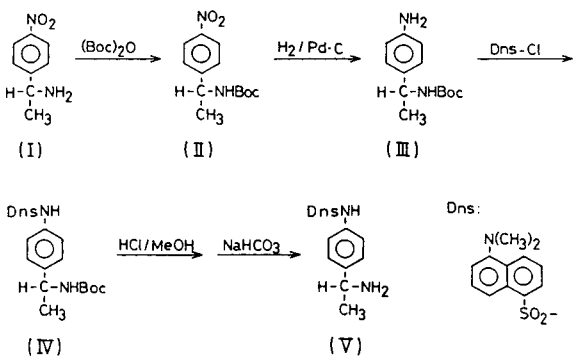

Fig. 1. Reaction course for synthesis of DAPEA from 1-(4-nitrophenyl)ethylamine.

HPLC system. Calculated from the peak areas their optical purity was >99.5%.

Fluorescence characteristics of DAPE-PPA

In order to examine the fluorescence properties of the amide compound derived from a carboxylic acid with DAPEA in aqueous media commonly used in reversed-phase HPLC, the maximum excitation and emission wavelengths and the fluorescence intensities of DAPE-PPA were measured in solutions with various acetonitrile concentrations and pH values. Acetonitrile concentrations in the range 50–90% (v/v) did not affect the excitation wavelength. With increase in acetonitrile content, the emission wavelength was slightly shifted and the intensity was increased by about 30% (Table I). These variations hardly influence the practical detection of the derivatives by HPLC. In the pH range 3–9, all three factors were almost constant (Table II). The diastereomer of DAPE-PPA (synthesized from *d*-DAPEA with *l*-PPA) indicated almost same fluorescence characteristics. The results suggest that the mobile phase used for the detection of the derivatives is not limited in the above range. In the subsequent HPLC studies described below, a neutral pH (6.5) was selected to maintain the column lifetime.

Optimization of derivatization reaction

Fig. 2 shows the derivatization reaction of the arylpropionic acids with DAPEA. Three reagents, DCC [12], DEPC [13] and DPDS–TPP

TABLE I

COMPARISON OF WAVELENGTH MAXIMA AND FLUORESCENCE INTENSITIES IN WATER–ACETONITRILE OF THE AMIDE DERIVED FROM *d*-PPA AND *d*-DAPEA

Acetonitrile (% v/v)	Wavelength (nm)		Relative fluorescence intensity (%)
	λ_{ex}	λ_{em}	
50	335	542	71.5
60	339	536	79.3
70	339	539	86.9
80	339	531	95.2
90	339	526	100.0

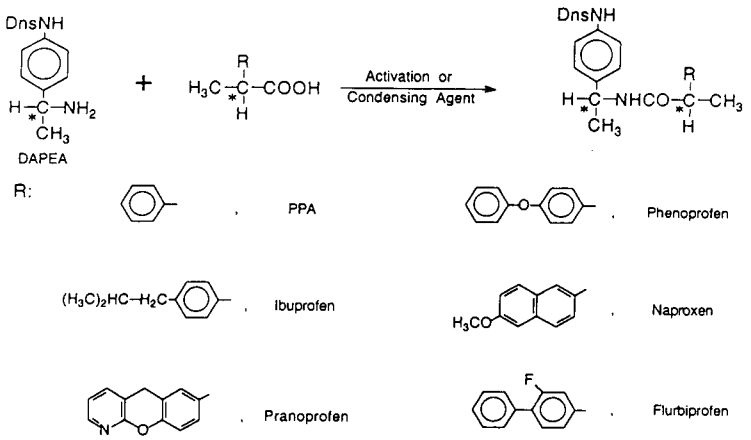

Fig. 2. Derivatization reaction of the arylproprionic acids with DAPEA in the presence of the activation or condensing agents.

[14], as activation or condensing agents for the reaction, were tested. After *d*-PPA (0.1 mg/ml) had reacted with 2 m*M* *d*-DAPEA for 20 min at room temperature in the presence of 5 m*M* of each reagent, the peak height of DAPE-PPA produced from the each reaction was compared with that of authentic DAPE-PPA. DCC and DEPC gave yields of only ≤10% and were discarded. In contrast, DPDS–TPP gave yields of ≥80% under very mild reaction conditions. Therefore, this system was extremely useful and was adopted for the derivatization.

In order to optimize the concentrations of the agents, the peak heights of DAPE-PPA derived from *d*-PPA (0.1 mg/ml) with *d*-DAPEA (1–5 m*M*) using various concentrations of the agents (1–5 m*M*, reaction time 20 min) were measured. When the concentration of DAPEA was ≥2 m*M* and those of DPDS and TPP were each ≥3 m*M*, the maximum peak height was obtained (Fig. 3) and the concentrations specified under Experimental were selected. Under these conditions, the time course of the derivatization was investigated. The reaction proceeded quantitatively for 2.5 h at room temperature, and subsequently DAPE-PPA was stable for at least 24 h in the resulting reaction mixture. The same studies were also carried out with *l*-PPA to compare the reactivity and similar results were obtained; the details are therefore omitted.

Hence the derivatization conditions as given under Experimental were established. The derivatization of *d*-PPA in the range 0.02–10 μg/

TABLE II

COMPARISON OF WAVELENGTH MAXIMA AND FLUORESCENCE INTENSITIES AT VARIOUS pH VALUES OF THE AMIDE DERIVED FROM *d*-PPA AND *d*-DAPEA

pH	Wavelength (nm)		Relative fluorescence intensity
	λ_{ex}	λ_{em}	
9	341	536	96.6
8	339	533	96.3
7	337	536	96.5
6	337	532	99.0
5	338	532	99.0
4	338	529	99.9
3	338	530	100.0

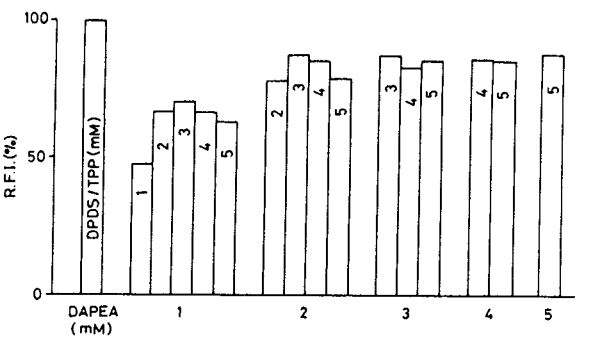

Fig. 3. Effect of reagent concentrations on the formation of the diastereomeric amide. Sample concentration, 125 ng per injection. R.F.I. = Relative fluorescence intensity.

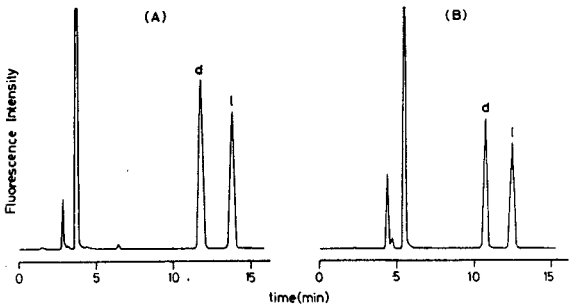

Fig. 4. Chromatographic profiles of the diastereomers derived from *l*-DAPEA with (A) ibuprofen and (B) pranoprofen. Mobile phase, 50 m*M* sodium acetate (pH 6.5)–acetonitrile [(A) 30:70 and (B) 45:55]. Each peak corresponds to 125 ng of enantiomeric ibuprofen and pranoprofen.

ml showed sufficient linearity ($r = 0.9994$), the reproducibility (relative standard deviation) was 2.2% (1.0 μg/ml PPA, $n = 7$) and the detection limit (signal-to-noise ratio = 3) by direct injection of the reaction mixture was 170 fmol per injection (derivatized to 12.5 ng/ml *d*-PPA).

Separation of diastereomers derived from carboxylic acid enantiomers with DAPEA

Separation of the diastereomers derived from six arylpropionic acid enantiomers with DAPEA using the proposed derivatization method was investigated by reversed-phase HPLC. Fig. 4 shows the chromatographic profiles of the diastereomers derivatized from ibuprofen and pranoprofen with *l*-DAPEA, and separation data for the six arylpropionic acids are given in Table III. All of the enantiomeric pairs were excellently separated in 10–15 min without any special techniques for elution. In this work, as optically active compounds of flurbiprofen and phenoprofen could not be obtained, elution orders of enantiomeric pairs were not identified. However, the elution orders probably the same as for the other four compounds. Because the order may depend on the absolute configuration around the asymmetric carbon of the arylpropionic acids (*d*-isomers of the all the arylpropionic acids in Table III are of *S*-configuration and the *l*-isomers are of *R*-configuration). *l*-DAPEA derivatives of

TABLE III

HPLC SEPARATION OF DIASTEREOMERS DERIVED FROM *l*- OR *d*-DAPEA WITH 2-ARYLPROPIONIC ACID DERIVATIVES

$t_0 = 1.4$ min; k', α and R_s refer to the capacity factor, separation factor and resolution, respectively, for a pair of diastereomers. Mobile phase, 50 m*M* sodium acetate (adjusted to pH 6.5)–acetonitrile; flow-rate, 1.0 ml/min; amount injected, 250 ng of each racemic carboxylic acid.

Carboxylic acid	Enantiomer	*l*-DAPEA			*d*-DAPEA			Acetonitrile concentration in eluent (% v/v)
		k'	α	R_s	k'	α	R_s	
PPA	*d*	8.45	1.15	3.53	9.74	1.14	3.45	55
	l	9.69			8.52			
Ibuprofen	*d*	7.44	1.20	4.53	8.74	1.20	4.48	70
	l	8.90			7.29			
Flurbiprofen[a]	*d*	8.71	1.21	4.85	10.57	1.21	4.85	65
	l	10.57			8.71			
Pranoprofen	*d*	6.76	1.18	3.81	8.07	1.19	3.95	55
	l	8.01			6.80			
Phenoprofen[a]	*d*	8.29	1.18	4.18	9.75	1.18	4.20	65
	l	9.76			8.27			
Naproxen	*d*	4.52	1.21	4.01	5.53	1.21	4.28	60
	l	5.45			4.57			

[a] Elution order is estimated.

d-isomers were eluted faster than those of *l*-isomers and *d*-DAPEA derivatives were eluted in the reverse order. However, the configuration of DAPEA did not affect the retention and resolution values. This suggests that the elution order is freely changed for the determination of one enantiomer in a large excess of the other enantiomer.

CONCLUSIONS

The convenient synthesis of fluorescent chiral derivatization agents, *d*- and *l*-DAPEA, was achieved by conventional four-step reactions. The derivatization procedures for carboxylic acid enantiomers using these agents for chromatographic separation and sensitive detection by reversed-phase HPLC, which have applicability in the analysis of biological samples, were achieved. This suggests that the proposed method may serve for the determination of arylpropionic acids in biological fluids for pharmacokinetic studies. In addition, an increase in detectability can be expected, as the chemiluminescence yield of the dansyl moiety by the peroxyoxalate chemiluminescence reaction is extremely high. In order to confirm these expectations, the determination of arylpropionic acids in biological fluids by HPLC with chemiluminescence detection is under study.

ACKNOWLEDGEMENTS

We thank Dr. Toshimasa Toyo'oka of the National Institute of Hygienic Sciences (Tokyo, Japan) for kindly donating *l*-naproxen. This work was supported in part by the Special Research Fund of Hokuriku University.

REFERENCES

1 J. Goto, N. Goto, A. Hikichi, T. Nishimaki and T. Nambara, *Anal. Chim. Acta*, 120 (1980) 187.
2 N. Nimura, Y. Kasahara and T. Kinoshita, *J. Chromatogr.*, 213 (1981) 327.
3 J. Goto, M. Ito, S. Katsuki, N. Saito and T. Nambara, *J. Liq. Chromatogr.*, 9 (1986) 683.
4 N. Nimura and T. Kinoshita, *J. Chromatogr.*, 352 (1986) 169.
5 S. Einarsson, B. Josefsson, P. Moller and D. Sanchez, *Anal. Chem.*, 59 (1987) 1191.
6 K. Iwaki, S. Yoshida, N. Nimura, T. Kinoshita, K. Takeda and H. Ogura, *Chromatographia*, 23 (1987) 899.
7 T. Toyo'oka, M. Ishibashi and T. Terao, *Analyst*, 117 (1992) 727.
8 S.-W. Jin, G.-X. Chen, Z. Palacz and B. Wittmann-Liebold, *FEBS Lett.*, 198 (1986) 150.
9 I. Yanagisawa, M. Yamane and T. Urayama, *J. Chromatogr.*, 345 (1985) 229.
10 Y.M. Lee, H. Nakamura and T. Nakajima, *Anal. Sci.*, 5 (1989) 209.
11 P.J.M. Kwakman, H.-P. van Schaik, U.A. Th. Brinkman and G.J. de Jong, *Analyst*, 116 (1991) 1385.
12 J.C. Sheehan and G.P. Hess, *J. Am. Chem. Soc.*, 77 (1955) 1067.
13 S. Yamada, Y. Kasai and T. Shioiri, *Tetrahedron Lett.*, (1973) 1595.

Journal of Chromatography A, 662 (1994) 95–99
Elsevier Science B.V., Amsterdam

CHROM. 25 682

High-performance liquid chromatographic separation of nucleic acids on a fluorocarbon-bonded silica gel column

Hiroko Itoh, Toshio Kinoshita and Noriyuki Nimura*

School of Pharmaceutical Sciences, Kitasato University, 9-1 Shirokane-5, Minato-ku, Tokyo 108 (Japan)

(First received March 9th, 1993; revised manuscript received October 19th, 1993)

ABSTRACT

The separation of nucleic acids and related compounds was investigated using high-performance liquid chromatography on a new fluorocarbon-bonded silica gel column. The polyadenylate enzymic partial hydrolysate sample and a mixture of various polynucleotide samples were sufficiently separated in the reversed-phase mode using gradient elution with aqueous ammonium acetate–acetonitrile. A mixed-mode separation on the fluorinated phase coated with a tetraalkylammonium salt was also examined for the separation of various polynucleotides, including tRNAs.

INTRODUCTION

Various types of material have been developed for column packings in HPLC. Some fluorinated packing materials [1,2], organic fluoropolymers and their derivatives, as well as silicas with fluorocarbon-bonded phases, have also been investigated. A fluoropolymer, Kel-F (polychlorotrifluoroethylene) [3–5], has been found to be a useful support for the preparation of alkyl- or aryl-bonded polymer beads as a packing material for liquid chromatography. RPC-5 [6] or Neosorb-LC-N [7], which is also based on a polychlorotrifluoroethylene bead coated with a tetraalkyl quaternary ammonium salt, has been used for mixed-mode LC separation of nucleic acids.

On the other hand, materials higher selective towards fluorine-containing solutes have been reported for fluorocarbon-bonded silica gel columns [8–10]. Reversed-phase separation of small molecules on the fluorinated silica columns has been compared with separation on conventional non-fluorine-containing alkylsilyl-bonded silica columns. The capacity factors (k') of small molecules on the C_{10} fluorocarbon-bonded phase, heptadecafluorodecylsilyl silica gel, were found to be approximately the same as those on the C_3 alkylsilyl-bonded silica column [8]. However, there have been few applications for the separation of polar biomolecules on fluorocarbon-bonded silicas. Reversed-phase separation of proteins on the C_{10} fluorocarbon-bonded silica column was reported by Xindu and Carr [11].

Recently, a new fluorocarbonaceous packing material, 1H,1H,2H,2H,3H,3H-tridecafluoro-(4,4-dimethylheptyl)silyl (F_{13}/C_9) bonded spherical microporous silica gel, was prepared for HPLC by Konakahara *et al.* [12]. We have been evaluating this bonded phase for the HPLC analysis of biological substances.

In the present study, F_{13}/C_9 bonded macroporous (pore size 30 nm) silica gel (Fig. 1) was freshly prepared, and the separations of polynucleotides and tRNAs on the fluorinated silica column were investigated in the reversed-phase

* Corresponding author.

0021-9673/94/$07.00
SSDI 0021-9673(93)E1157-U

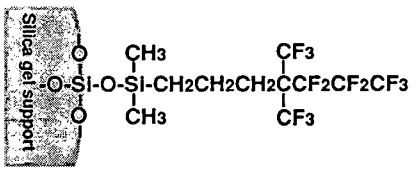

Fig. 1. Structural formula of the fluorocarbon-bonded phase.

mode as well as in the mixed mode. The mixed-mode separation included both an anion exchange mode and a reversed-phase mode on the trioctylmethylammonium chloride-coated fluorinated silica column.

EXPERIMENTAL

Reagents

Polyadenylate sodium salt [poly(A)] and nuclease P1 were purchased from Yamasa Shoyu (Chiba, Japan). Various tRNAs were obtained from Boehringer Mannheim Yamonouchi (Tokyo, Japan). HPLC-grade acetonitrile and other reagents were purchased form Kanto Chemical (Tokyo, Japan) and Wako (Osaka, Japan), respectively. Water was purified by passing it through a Milli-R/Q system (Millipore, Bedford, MA, U.S.A.).

Sample preparation

Poly(A) (100 ml, 30 mg per ml of 0.3 *M* citrate buffer, pH 6) was digested by nuclease P1 (5 ml, 50 mg/ml) containing magnesium chloride (10 ml, 6 mg/ml) at 37°C for 60 min. Crude tRNA and other purified tRNAs were dissolved in concentrations of 1 mg/ml and 1 unit/200 μl, respectively. Both the polynucleotide sample and the tRNA solutions were stored at −18°C until they were used. They were diluted 10–20 times prior to use, and an aliquot of the mixture (10–20 μl) was injected into the HPLC system.

Packing materials

The fluorinated silica gel used in the present study was prepared by NEOS (Shiga, Japan). Macroporous silica gel (mean particle diameter 5 μm; mean pore size 30 nm) was silylated with 1H,1H,2H,2H,3H,3H - tridecafluoro(4,4 - dimethylheptyl)dimethylchlorosilane (NEOS) and then end-capped with trimethylchlorosilane. The resulting material was slurry-packed into a 150 mm × 4.6 mm I.D. stainless-steel column tube for the reversed-phase separation.

For the mixed-mode separation, the fluorinated silica gel was coated with triotylmethylammonium chloride (TOMAC) as follows. The fluorinated silica gel (4 g) was suspended in a chloroform solution of TOMAC (500 mg/50 ml) *in vacuo* in an ultrasonic bath, and then the chloroform was evaporated to dryness. The resulting TOMAC-coated silica material (*ca.* 1.5 g) was suspended with aqueous ammonium acetate as a slurry solvent, and then slurry-packed into a 50 mm × 6.0 mm I.D. stainless-steel column tube at a constant pressure of 300 kg/cm^2.

HPLC apparatus

The high-pressure gradient HPLC system used in this study consisted of two 880-PU HPLC pumps (Jasco, Tokyo, Japan) equipped with an ERC-3510 degasser (Erma, Tokyo, Japan), an 880-30 solvent mixing module (Jasco) and a Model 7125 injector (Rheodyne, Cotati, CA, USA). All the samples were detected with an 875-UV spectrophotometric detector (Jasco) operated at 260 nm. The chromatograms were recorded and processed by a C-R6A Chromatopac integrator (Shimadzu, Kyoto, Japan.).

Chromatographic conditions

The mobile phases, gradient conditions and other chromatographic conditions that were used are given in the text and figure legends. All HPLC separations were performed at room temperature. Since a liquid chromatograph generally contains some dead volumes, a lag time occurs during the running of a gradient. Sample injections, therefore, were made to coincide with commencement of the gradient. The actual gradient delay was previously determined by a tracer technique to draw a gradient curve using a mobile phase B containing a UV-absorbing solvent, such as acetone.

RESULTS AND DISCUSSION

Reversed-phase systems have been used for the separation of oligonucleotides [13,14].

Chemically bonded alkylsilyl silica gels, such as ODS (octadecylsilyl) silica, with an acetonitrile gradient were mainly used for the purpose. A column packed with uncoated Kel-F82 (polychlorotrifluoroethylene) particles was used for the reversed-phase separation of oligonucleotides by Usher [15]. In the field of LC separation of nucleic acids, the separation is not so efficient in the reversed-phase mode as in the ion-exchange mode [16]. However, reversed-phase separation is suitable for preparative use because volatile solvents are used as the mobile phase.

We first examined the reversed-phase separation of various nucleotides on the present fluorinated macroporous silica gel column. A linear gradient elution system with aqueous ammonium acetate and acetonitrile was used. Fig. 2 shows a reversed-phase chromatographic profile of oligoadenylates, which were prepared by the partial digestion of poly(A) with nuclease P1. Oligoadenylates up to the 30-mer were separated sufficiently within 30 min. The separation was satisfactory compared with the previous separation data obtained on a conventional alkylsilyl-bonded silica column. In 1980, Berendsen *et al.* [8] investigated the reversed-phase separation of a number of fluorinated and non-fluorinated solutes on a heptadecafluorodecyl-bonded silica column. Although separation could be carried out with mobile phases containing over 40% (v/v) methanol, the column's performance deteriorated rapidly when the methanol content decrease below this point. Mobile phases with a high aqueous content were completely unusable because they did not wet the bonded phase. Regenerating the column required pure methanol. In contrast, the present separations carried out under highly aqueous conditions containing only a few percent of acetonitrile provided good results. In appears that the fluorocarbon-bonded phase is useful for the separation of polar compounds, such as nucleotides, even if an aqueous mobile phase is used.

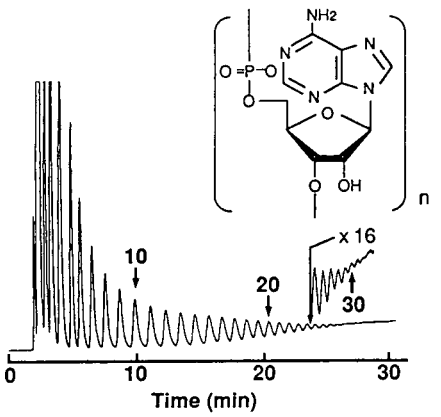

Fig. 2. Reversed-phase HPLC separation of poly(A) enzymic partial hydrolysate on a fluorinated silica column. Eluent A, 0.1 *M* ammonium acetate; eluent B, 10% aqueous acetonitrile; linear gradient from 5% B to 30% B in 60 min; flow-rate, 1.0 ml/min; sample volume, 20 μl.

Next we investigated mixed-mode separation on the fluorocarbon-bonded silica gel. Mixed-mode separations [6,7,17] of nucleic acids and related compounds have previously been performed either on a fluoropolymer gel coated with tetraalkylammonium salt or on an alkylsilyl-bonded silica gel. The separation was based on both an anion-exchange mode and a reversed-phase mode [17]. TOMAC and aqueous sodium perchlorate containing ethylenediamine tetraacetate have generally been used as the coating cationic salt and the mobile phase, respectively. Accordingly, the present coating and separation procedures described in the Experimental section referred to the previous methods.

Fig. 3 shows the mixed-mode separation of poly(A) enzymic hydrolysate on the TOMAC-coated fluorinated silica column. Oligoadenylates

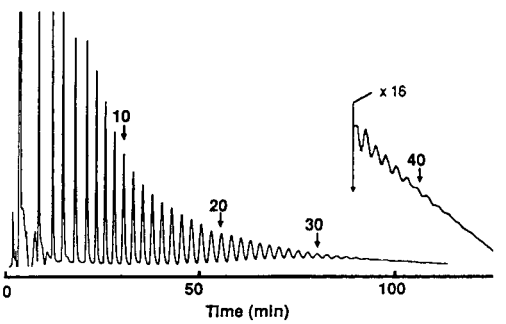

Fig. 3. Mixed-mode HPLC separation of poly(A) enzymic partial hydrolysate on a TOMAC-coated fluorinated silica column. Eluent A, 10 m*M* sodium perchlorate +10 m*M* Tris–acetate buffer (pH 7.5) +1 m*M* Na_2EDTA; eluent B, 0.5 *M* sodium perchlorate +10 m*M* Tris–acetate buffer (pH 7.5) +1 m*M* Na_2EDTA; linear gradient from 0% B to 100% B in 150 min; flow-rate, 1.0 ml/min; sample volume, 15 μl.

up to the 40-mer that were eluted with the perchlorite gradient were efficiently separated within 120 min. Other types of oligonucleotide, such as the oligocytidylates and oligodeoxynucleotides, were also well separated in the mixed mode. Furthermore, tRNAs were also satisfactorily separated on a TOMAC-coated fluorinated silica column by mixed-mode chromatography. Fig. 4 shows the chromatographic profiles of the crude mixture of tRNAs from *Escherichia coli* and purified tRNAs that are specific for amino acids. The present separation of tRNAs with this mixed-mode material equals or surpasses those obtained with RPC-5-like or TOMAC-coated ODS silica gel material [18,19].

The column performance of the TOMAC-coated fluorinated silica was good, and the coating was found to be extremely stable. The lifetime of the fluoropolymer column coated with alkylammonium salt was generally not so long. It has been reported that the polymer-based mixed-mode columns could be used up to several tens of times, but their lifetimes were shorter than those of alkylsilyl-bonded phase columns [6,7]. On the other hand, we have continuously used one of the TOMAC-coated columns for more than a year, for several hundred gradient runs,

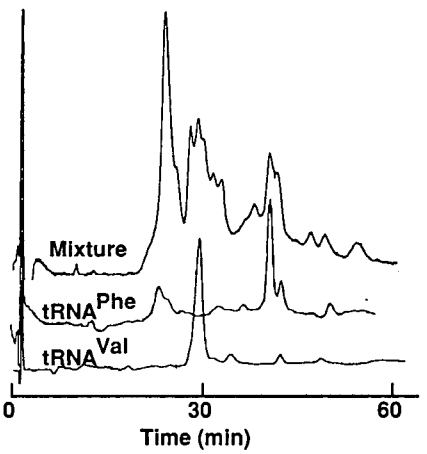

Fig. 4. Mixed-mode HPLC profiles of tRNAs (*E. coli*) on a TOMAC-coated fluorinated silica column. Eluent A, 10 m*M* sodium perchlorate +10 m*M* Tris–acetate buffer (pH 7.5) +1 m*M* Na_2EDTA; eluent B, 0.2 *M* sodium perchlorate +10 m*M* Tris–acetate buffer (pH 7.5) +1 m*M* Na_2EDTA; linear gradient from 15% B to 100% B in 60 min; flow-rate, 1.0 ml/min; sample volume, 10 μl.

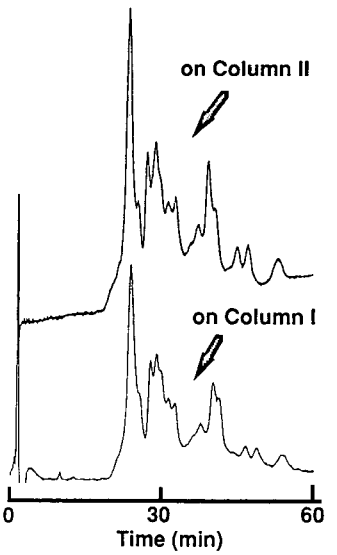

Fig. 5. Mixed-mode HPLC profiles of tRNAs (crude mixture form *E. coli*) on two TOMAC-coated fluorinated silica columns prepared separately. All the conditions were same as in Fig. 4.

with no decrease in the efficiency of the column. It appears that some attracting force other than hydrophobic interaction is occurring between the fluorocarbon phase and the TOMAC, possibly some ionic adsorption of TOMAC on the exposed silanol groups; however, we currently cannot explain this observation. The reproducibility of the coating procedure was also sufficient (Fig. 5); several TOMAC-coated columns showed equal performance and life-time.

The present separation system using the new fluorinated silica gel column may be useful for the separation of nucleic acids in the fields of organic synthesis and biochemistry.

ACKNOWLEDGEMENT

The authors thank NEOS Co. Ltd. for helping to prepare the fluorinated silica packing material.

REFERENCES

1 P. Varughese, M.E. Gangode and R.K. Gilpin, *J. Chromatogr. Sci.*, 26 (1988) 401.

2 N.D. Danielson, L.G. Beaver and J. Wangsa, *J. Chromatogr.*, 544 (1991) 187.
3 T.A. Zwier and M.F. Burke, *Anal. Chem.*, 53 (1981) 812.
4 J.A. Huth and N.D. Danielson, *Anal. Chem.*, 54 (1982) 930.
5 R.W. Siergiej and N.D. Danielson, *Anal. Chem.*, 55 (1983) 17.
6 R.L. Pearson, J.F. Weiss and A.D. Kelmers, *Biochim. Biophis. Acta*, 228 (1971) 770.
7 H. Sawai, *J. Chromatogr.*, 481 (1989) 201.
8 G.E. Berendsen, K.A. Pikaart, L. de Galan and C. Olieman, *Anal. Chem.*, 52 (1980) 1990.
9 H.A.H. Billiet, P.J. Schoenmakers and L. de Galan, *J. Chromatogr.*, 218 (1981) 443.
10 P.C. Sadek and P.W. Carr, *J. Chromatogr.*, 288 (1984) 25.
11 G. Xindu and P.W. Carr, *J. Chromatogr.*, 269 (1983) 96.
12 T. Konakahara, S. Okada, T. Monde, N. Nakayama, J. Furuhashi and J. Sugaya, *Nippon Kagaku Kaishi*, (1991) 1638.
13 K. Makino, H. Ozaki, H. Imaishi, T. Takeuchi, T. Fukui and H. Hatano, *Chromatographia*, 23 (1987) 247.
14 H. Moriyama and Y. Kato, *J. Chromatogr.*, 445 (1988) 225.
15 D.A. Usher, *Nucleic Acid Res.*, 6 (1979) 2289.
16 Y. Baba, T. Matsuura, K. Wakamoto and M. Tsuhako, *J. Chromatogr.*, 558 (1991) 273.
17 L.W. Mclaughlin, *Chem. Rev.*, 89 (1989) 309.
18 R. Bischoff and L.W. McLaughlin, *Anal. Biochem.*, 151 (1985) 526.
19 L.W. McLaughlin and R. Bischoff, *J. Chromatogr.*, 418 (1987) 51.

Journal of Chromatography A, 662 (1994) 101–112
Elsevier Science B.V., Amsterdam

CHROM. 25 583

Isolation and high-performance liquid chromatographic analysis of thearubigin fractions from black tea

R.G. Bailey* and H.E. Nursten

Department of Food Science and Technology, University of Reading, Whiteknights, Reading RG6 2AP (UK)

I. McDowell

Natural Resources Institute, Central Avenue, Chatham Maritime, Kent ME4 4TB (UK)

(First received April 26th, 1993; revised manuscript received August 30th, 1993)

ABSTRACT

Fractions consisting of black tea pigments were isolated and analysed by reversed-phase HPLC. The fractions were shown to be mixtures of the same pigments that had been observed previously, on the HPLC chromatograms of black tea liquor. The thearubigin fractions isolated by Roberts (Roberts' SI and SII thearubigins) were shown to be mixtures of pigments previously classified as group I, II, and III pigments (pigments excluded from, resolved by, and remaining unresolved by HPLC, respectively), showing that the pigments in these three groups were similar to those in groups previously designated as thearubigins by Roberts. The SI and SII fractions were distinguishable by HPLC, and SI-like and SII-like fractions could be isolated by methods different from those of Roberts (*e.g.*, a Sep-Pak C_{18} cartridge). Fractions enriched in group I pigments were isolated using a Bond-Elut SCX cation-exchange cartridge (and on a larger scale on a column of Amberlite CG-120 cation-exchange resin). These fractions were shown by paper chromatography and HPLC to be mixtures of "anthocyanidin" pigments of various molecular masses. HPLC and mass spectrometry showed that an anthocyanidin, designated by Roberts as tricetinidin, was present in the mixture.

INTRODUCTION

The reversed-phase HPLC of black tea liquor was described in previous publications [1–3]. The black tea pigments were classified into three groups, group I being excluded from the columns, group II being resolved by the columns and group III remaining unresolved [2]. The group II (resolved) pigments were classified, by their photodiode-array spectra, into two types [2]. Type I resolved pigments, being yellow, showed an absorption maximum at, or just below, 400 nm, and type II resolved pigments, being brown, showed absorption that tailed off into the visible region. In subsequent publications, the isolation and analysis of a fraction of group III pigments, designated the theafulvins, was described [4,5], and mixtures of pigments from groups I, II and III have been produced by the chemical oxidation of individual catechins [6]. ^{13}C NMR spectroscopy showed the theafulvins to be flavanol polymers with different inter-monomer linkages to proanthocyanidin polymers [4]. In this paper a description is given of the isolation of further pigment fractions and their analysis by the new HPLC methods. This was done to explore methods for isolating new pigment fractions from black tea, and to apply the new HPLC methods comparatively to the analysis of these fractions and of fractions previously designated as thearubigins.

* Corresponding author.

0021-9673/94/$07.00
SSDI 0021-9673(93)E1013-P

To place our work within the older literature, it was decided to compare the HPLC of black tea liquor with that of Roberts' SI and SII thearubigin fractions [7]. Roberts *et al.* [8] separated thearubigins into ethyl acetate-soluble (SI) thearubigins and butanol-soluble (SII) thearubigins. The HPLC of the SI and SII thearubigin fractions was of great interest for two main reasons: (1) the chromatograms would help to identify thearubigins on tea chromatograms, and (2), if distinctive enough, the chromatograms would be useful for classifying other thearubigin fractions as SI-like or SII-like. The SI and SII fractions were isolated by Roberts' method [8] and analysed by HPLC. Also, other pigment fractions from black tea, "polar" and "non-polar" fractions, isolated using a Sep-Pak C_{18} cartridge by a method of Wellum and Kirby [9], were analysed by HPLC. The fractions were distinguishable by HPLC, the former being SII-like and the latter SI-like.

The group I pigments were of interest because they are excluded from all the HPLC columns. The exclusion could be due to molecular size, the material being either of high molecular mass or in a highly associated form, or to the charge carried. Four approaches for their isolation were explored: (1) exclusion from a Sep-Pak C_{18} cartridge, (2) exclusion from a column of Sephadex LH-20, (3) selective adsorption on a column of cellulose and (4) concentration by cation exchange, using cartridges and a column of resin. The fractions were analysed using our HPLC methods in conjunction with photodiode-array detection and LC–MS.

MATERIALS AND METHODS

Sep-Pak C_{18} cartridges (100 mg/1 ml) were obtained from Millipore Waters Chromatography (Watford, UK) and Bond-Elut SCX and CBA cartridges (100 mg/1 ml) from Jones Chromatography (Hengoed, UK). Chromatographic grade Amberlite 120 ion-exchange resin (CG-120) was obtained from BDH (Poole, UK) and Sephadex LH-20 from Pharmacia (Milton Keynes, UK). Whatman CF1 and microcrystalline chromatographic grade cellulose and 3MM chromatography paper were obtained from Whatman (Maidstone, UK).

The HPLC methods and the preparation of the tea liquor were as described previously [1,2]. Aqueous acetic acid was used with an untreated, 25 × 0.49 cm, 5 μm Hypersil ODS and a 15 × 0.49 cm, 5 μm Hamilton PRP-1 column, and an aqueous citrate buffer with an EDTA–citrate treated, 25 × 0.49 cm, 5 μm Hypersil ODS column. Chromatograms were monitored at 280 and 460 nm, the former wavelength being used to detect all phenolics and the latter to detect coloured compounds. In this paper, a chromatogram monitored at either of these wavelengths is referred to as a "280 nm chromatogram" or a "460 nm chromatogram", respectively. UV–Vis spectra were run on a Perkin-Elmer Lambda 5 spectrophotometer.

Mass spectra of group I pigments, isolated using a Sep-Pak C_{18} cartridge (designated as Sep-Pak eluent 2), were obtained using a VG Thermospray interface on a VG TS250, double-focusing air-cored magnet mass spectrometer, at the VG Tritech Applications Laboratory (Manchester, UK). An untreated Hypersil ODS column was used with isocratic elution, the solvent being 2% (v/v) acetonitrile in 0.05% (v/v) aqueous trifluoroacetic acid, with a flow-rate of 0.8 ml min^{-1} and injection of 50 μl. The chromatogram was monitored with a UV detector at 280 nm. The mass spectrometer scanned the mass range m/z 2000–200. All mass spectra described in this paper were acquired in the positive-ion mode.

Mass spectra of group I pigments, isolated using a column of Amberlite CG-120 cation-exchange resin (designated the CG-120 fraction), were obtained using a Finnigan Thermospray interface on the Finnigan TSQ70, triple quadrupole mass spectrometer at the Finnigan Applications Labs. (Hemel Hempstead, UK). Loop injections were carried out with 2% aqueous (v/v) acetic acid, at a flow-rate of 0.8 ml min^{-1}. The flow into the ion source was made up to 2 ml min^{-1} by post-column addition of 0.1 *M* aqueous ammonium acetate at a flow-rate of 1.2 ml min^{-1}. Volumes of 20–50 μl were injected. The mass spectrometer scanned the mass range m/z 1000–100.

Mass spectra of group I pigments, isolated using a Bond-Elut SCX cation-exchange cartridge (designated anthocyanidin pigments), were obtained using a Kratos Thermospray inter-

face on a Kratos MS80RFA double focusing mass spectrometer, in the Department of Food Science and Technology, University of Reading. An untreated Hypersil ODS column, eluted isocratically with 30% (v/v) methanol in 0.1 *M* ammonium acetate at a flow-rate of 1.0 ml min^{-1}, was used, 20–50 μl being injected. The mass spectrometer scanned the mass range *m/z* 800–100.

Isolation of Roberts' SI and SII thearubigin fractions

A tea liquor was prepared (tea, 10 g; water, 100 ml) and allowed to cool. The liquor was extracted with ethyl acetate (50 ml, ×4), in a separating funnel. The combined extracts were evaporated to dryness, under vacuum on a rotary evaporator, to give a red oil. The red oil was dissolved in acetone (10 ml) and chloroform (90 ml) added to precipitate a buff solid, which was filtered off, washed with chloroform, washed with light petroleum (b.p. 60–80°C), and dried in a vacuum desiccator over phosphorus pentoxide, to give a crude, solid SI fraction (0.56 g). This was dissolved in acetone (5 ml) and diethyl ether (300 ml) added to precipitate a buff solid, which was filtered off, washed with diethyl ether, washed with light petroleum (b.p. 60–80°C), and dried in a vacuum desiccator over phosphorus pentoxide, to give the SI fraction (0.13 g).

The aqueous layer from the ethyl acetate extraction was extracted with isobutanol (50 ml, ×2) and the combined extracts evaporated to dryness, under vacuum on a rotary evaporator, to give a pale yellow solid, which contained traces of solvent. The pale yellow solid was dissolved in methanol (8–10 ml) and diethyl ether (300 ml) added to precipitate a buff solid, which was filtered off, washed with diethyl ether, washed with light petroleum (b.p. 60–80°C), and dried in a vacuum desiccator over phosphorus pentoxide. This filtrate was evaporated to dryness, the precipitation repeated, and the solids combined, to give a solid SII fraction (0.24 g).

The isolation of "polar" and "non-polar" fractions from a neutral Sep-Pak C_{18} cartridge

A Sep-Pak C_{18} cartridge was conditioned first with methanol and then with water. A tea liquor was prepared (tea, 4 g; water, 100 ml) and an aliquot (2–5 ml) applied to the cartridge. The cartridge was washed with 35% (v/v) aqueous methanol (2–5 ml) and then with 80% (v/v) aqueous methanol (2–5 ml), the eluents being collected as separate fractions.

Isolation of group I pigments using Sep-Pak C_{18} cartridges

Sep-Pak 1 was conditioned first with methanol and then with water, and Sep-Pak 2 was conditioned first with methanol and then with 0.01 *M* HCl. A tea liquor was prepared (tea, 4 g; water, 100 ml) and an aliquot (2 ml) applied to Sep-Pak 1, the eluent (eluent 1) being collected and the Sep-Pak set aside. Eluent 1 was then applied to Sep-Pak 2 and the eluent (eluent 2) collected. The material retained on Sep-Pak 2 was eluted from it with pure methanol (eluent 3).

Isolation of group I pigments using Sephadex LH-20

Sephadex LH-20 (25 g) was washed in 35% (v/v) aqueous acetone (150 ml, ×3), the suspension allowed to settle, the liquid containing fines decanted off, and the LH-20 allowed to stand overnight in the solvent. A column (30 × 1 cm) was packed and equilibrated with the same solvent (100 ml). The void volume of the column was measured with Dextran Blue and found to be 10.5 ml. A tea liquor was prepared (tea, 4 g; water 100 ml), made 35% (v/v) in acetone and an aliquot (2 ml) applied to the column. The chromatogram was developed with 35% aqueous acetone at a flow-rate of about 0.33 ml min^{-1}. Coloured bands eluting from the column were collected separately and the volume of the fractions measured.

Isolation of group I pigments using Whatman CF1 and microcrystalline cellulose

Columns of Whatman CF1 Cellulose and Whatman Microcrystalline Cellulose (35 × 3 cm) were packed in water and washed with methanol (500 ml) and 2% (v/v) aqueous acetic acid (500 ml). Tea liquor was prepared (tea, 4 g; water, 100 ml), an aliquot (10 ml) applied to each of the above columns, and each chromatogram developed stepwise with 1% (v/v) aqueous acetic acid (200 ml), methanol (200 ml) and 5% (v/v)

aqueous acetic acid (200 ml). Fractions were collected and monitored for an absorption maximum at 510 nm. The fractions showing such absorption were combined and concentrated under vacuum on a rotary evaporator. When the liquid had been reduced to about 2 ml, ethanol (10 ml) was added and the solution evaporated to dryness under vacuum on a rotary evaporator.

Isolation of group I pigments using a Bond-Elut SCX (sulfonic acid) cation-exchange cartridge

A Bond-Elut SCX cartridge was conditioned first with methanol and then with 1% (v/v) aqueous acetic acid. A tea liquor was prepared (tea, 4 g; water, 100 ml) and an aliquot (5 ml) applied to the cartridge. The cartridge was washed with water until the washings were colourless, and then with 2% (v/v) concentrated hydrochloric acid in methanol (5 ml), the latter eluent being collected.

Isolation of group I pigments using a Bond-Elut CBA (carboxylic acid) cation-exchange cartridge

A Bond-Elut CBA cartridge was conditioned first with methanol and then with 1% (v/v) aqueous acetic acid. A tea liquor was prepared (tea, 4 g; water, 100 ml) and an aliquot (5 ml) applied to the cartridge. The cartridge was washed with water until the washings were colourless, and then with 2% (v/v) concentrated hydrochloric acid in methanol (5 ml), the latter eluent being collected.

Isolation of group I pigments using Amberlite CG-120 (sulfonic acid) cation-exchange resin

Amberlite CG-120 resin was washed with 0.1 *M* hydrochloric acid (200 ml, ×3), the suspension allowed to settle and the liquid containing fines decanted off. A column (30 × 1 cm) was packed in 0.1 *M* HCl and washed with distilled water until the washings were the same pH as the water. A tea liquor was prepared (tea, 4 g; water, 100 ml) and an aliquot (10 ml) applied to the column. The chromatogram was developed, stepwise, with distilled water (100 ml), 20% (v/v) aqueous methanol (100 ml), 80% (v/v) aqueous methanol (100 ml) and 2% (v/v) conc. HCl in methanol (100 ml). Fractions (5 ml) were collected and their composition was monitored by UV–Vis spectroscopy and HPLC.

Paper chromatography of tea liquors and tea fractions

Squares (25.5 × 25.5 cm) of Whatman 3MM paper were used. The paper was held in plastic racks, separated by plastic spacers, and developed by upward displacement. The chromatograms were developed first in isobutanol–acetic acid–water (4:1:2.2, v/v/v), removed from the tank, dried, and developed in the second direction in 2% (v/v) aqueous acetic acid. The paper was removed from the tank, dried and sprayed with 2% (w/v) ferric chloride–2% (w/v) potassium ferricyanide reagent, to which a few drops of 1% (w/v) potassium permanganate solution had been added.

RESULTS AND DISCUSSION

The isolation and analysis of Roberts' SI and SII fractions and "polar" and "non-polar" fractions

Roberts' SI and SII thearubigin fractions were isolated by the method of Roberts *et al.* [8] (Table I). The 280 nm chromatograms of the SI and SII fractions on an EDTA–citrate-treated Hypersil ODS column showed peaks close to the void volume of the column, a convex broad band, and resolved and partially resolved peaks with the broad band as baseline. They showed that both fractions contained gallic acid, cinnamic acid derivatives, flavonol glycosides, flavanol gallates, caffeine and some theaflavins [1]. The corresponding 460 nm chromatograms (SI: Fig. 1; SII: Fig. 2) showed pigments from all three groups I–III [2] and clear differences between the two fractions. The Hamilton PRP-1 column gave better 460 nm chromatograms of the group III pigments (SI: Fig. 3; SII: Fig. 4), showing clearly that the broad band from the SI and SII fractions differed, the maximum of the former being at a longer retention time than that of the latter.

Photodiode-array UV–Vis spectra taken from a 460 nm chromatogram of the SI fraction on an EDTA–citrate-treated Hypersil ODS column showed the presence of the four main theaflavins

TABLE I

SUMMARY OF THE ISOLATION AND ANALYSIS OF THE FRACTIONS

Fraction	Ref.	HPLC column	Comments
SI	7, 8	Treated[a] Hypersil ODS and Hamilton PRP-1	Pigments from all three groups, distinguishable from SII
SII	7, 8	Treated Hypersil ODS and Hamilton PRP-1	Pigments from all three groups, distinguishable from SI
"Polar"	9	Treated Hypersil ODS and Hamilton PRP-1	SII-like
"Non-polar"	9	Treated Hypersil ODS and Hamilton PRP-1	SI-like
Sep-Pak C_{18}, eluent 2	2	Untreated Hypersil ODS	Group I pigments: first peak an anthocyanidin pigment, second and third peaks brown pigments
Sephadex LH-20, first brown band	2	Untreated Hypersil ODS	Group I pigments: first peak an anthocyanidin pigment, second, third and fourth peaks brown pigments
Bond-Elut, SCX fraction	2	Untreated Hypersil ODS	Anthocyanidin pigments: first peak a group I pigment and second peak tricetinidin
Bond-Elut CBA fraction	2	Treated Hypersil ODS and Hamilton PRP-1	Anthocyanidin pigments (as above) and SI-like thearubigins
Amberlite CG-120 fraction	2	Untreated Hypersil ODS	Anthocyanidin pigments (as above)

[a] Treatment of the Hypersil ODS column was with EDTA and citrate as described in ref. 2.

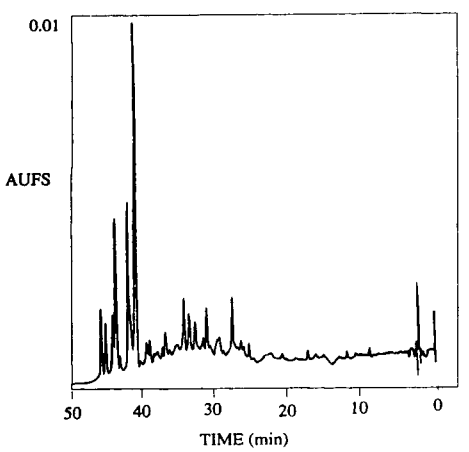

Fig. 1. The chromatogram (460 nm) of the SI fraction on an EDTA–citrate-treated 5-μm Hypersil ODS column. Solvent A = 2% (v/v) aqueous citrate buffer. Solvent B = acetonitrile. Gradient 8 to 31% solvent B over 50 min. Flow-rate = 1.5 ml min^{-1}.

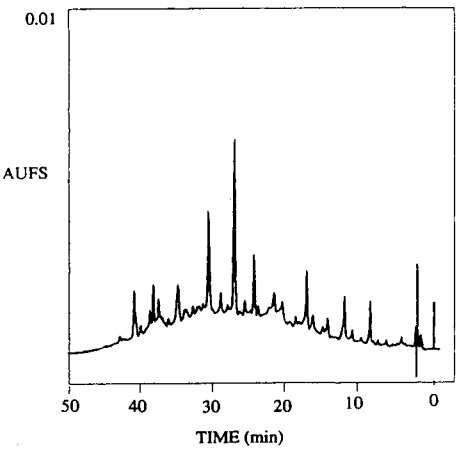

Fig. 2. The chromatogram (460 nm) of the SII fraction on an EDTA–citrate-treated 5-μm Hypersil ODS column. Solvent A = 2% (v/v) aqueous citrate buffer. Solvent B = acetonitrile. Gradient 8 to 31% solvent B over 50 min. Flow-rate = 1.5 ml min^{-1}.

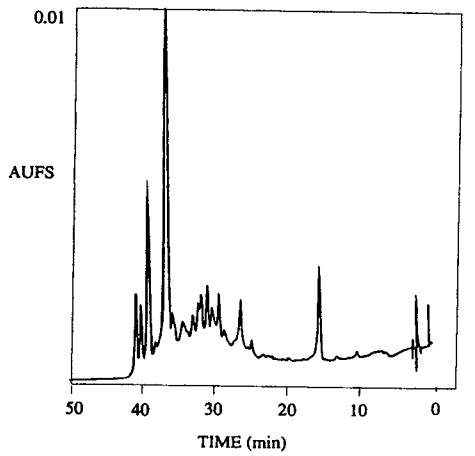

Fig. 3. The chromatogram (460 nm) of the SI fraction on a 5-μm Hamilton PRP-1 column. Solvent A = 2% (v/v) aqueous acetic acid. Solvent B = acetonitrile. Gradient 5 to 33% solvent B over 50 min. Flow-rate = 1.0 ml min^{-1}.

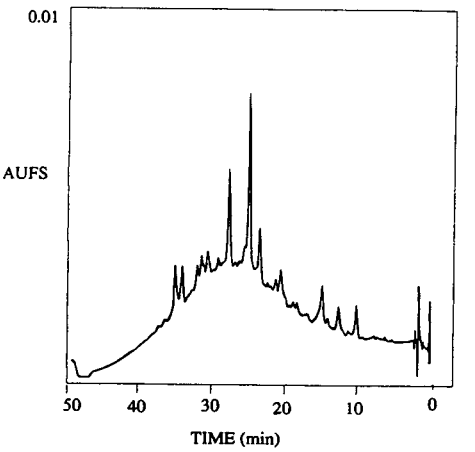

Fig. 4. The chromatogram (460 nm) of the SII fraction on a 5-μm Hamilton PRP-1 column. Solvent A = 2% (v/v) aqueous acetic acid. Solvent B = acetonitrile. Gradient 5 to 33% solvent B over 50 min. Flow-rate = 1.0 ml min^{-1}.

found in all black tea liquors [1,2], plus one other theaflavin [2], three theaflavic acids [2], three type I resolved pigments [2] and five type II resolved pigments [2]. It was not possible to obtain good quality spectra from all of the peaks due to the low solubility of the SI fraction in the solvents used. The collection of photodiode-array spectra from the SII fraction was more difficult, as the fraction was less soluble in the HPLC solvent than SI, and many of the spectra were noisy and difficult to classify. However, a few photodiode-array UV–Vis spectra from the chromatogram could be used for classification. The theaflavin levels were lower than in the SI fraction, and there were only two theaflavic acids. Four peaks were assigned to type II resolved pigments, and one to a type I resolved pigment. The remaining peaks were very small and did not give spectra good enough for classification.

Wellum and Kirby [9] obtained a "polar" fraction from a Sep-Pak C_{18} cartridge with 35% (v/v) aqueous methanol, and a "non-polar" fraction with 80% (v/v) aqueous methanol. Since Wellum and Kirby [9] did not publish details of the first-eluted "polar" fraction, the procedure was repeated and both fractions were analysed by HPLC (Table I). A black tea liquor was applied to a neutral Sep-Pak C_{18} cartridge and a polar fraction eluted from the cartridge with 35% (v/v) aqueous methanol, before a "non-polar" fraction consisting of flavonol glycosides and theaflavins and other pigments was eluted with 80% (v/v) aqueous methanol. The 280 nm chromatograms of the "polar" fraction on an EDTA–citrate-treated Hypersil ODS column were complex, with many polyphenols, caffeine, and a convex broad band [1]. The 460 nm chromatograms of the "polar" fraction on the EDTA–citrate-treated Hypersil ODS (Fig. 5)

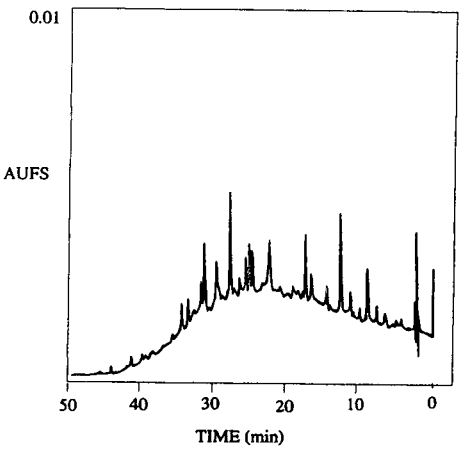

Fig. 5. The chromatogram (460 nm) of the "polar" Sep-Pak fraction on an EDTA–citrate-treated 5-μm Hypersil ODS column. Solvent A = 2% (v/v) aqueous citrate buffer. Solvent B = acetonitrile. Gradient 8 to 31% solvent B over 50 min. Flow-rate = 1.5 ml min^{-1}.

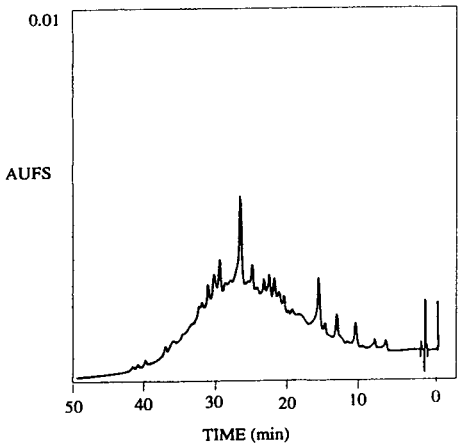

Fig. 6. The chromatogram (460 nm) of the "polar" Sep-Pak fraction on a 5-μm Hamilton PRP-1 column. Solvent A = 2% (v/v) aqueous acetic acid. Solvent B = acetonitrile. Gradient 5 to 33% solvent B over 50 min. Flow-rate = 1.0 ml min^{-1}.

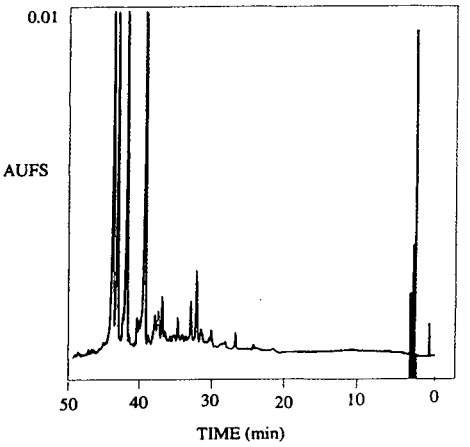

Fig. 7. The chromatogram (460 nm) of the "non-polar" Sep-Pak fraction on an EDTA–citrate-treated 5-μm Hypersil ODS column. Solvent A = 2% (v/v) aqueous citrate buffer. Solvent B = acetonitrile. Gradient 8 to 31% solvent B over 50 min. Flow-rate = 1.5 ml min^{-1}.

and a Hamilton PRP-1 columns (Fig. 6) were SII-like (*cf.* Figs. 1–4). The "non-polar" fraction was eluted from the cartridge with 80% (v/v) aqueous methanol. The 280 nm chromatograms of this fraction on an EDTA–citrate-treated Hypersil ODS column showed mainly flavonol glycosides and theaflavins [1], the broad band not being prominent. The 460 nm chromatograms of the "non-polar" fraction on an EDTA–citrate-treated Hypersil ODS and a Hamilton PRP-1 columns (Figs. 7 and 8) were SI-like.

Thus HPLC showed the Roberts' SI and SII thearubigin fractions to be mixtures of pigments from all three groups, similar to those found in black tea liquor, and showed them to be distinguishable. The "polar" and "non-polar" fractions isolated previously by Wellum and Kirby [9] were shown to be pigment fractions chromatographically similar to Roberts' SII and SI fractions, respectively.

The isolation and analysis of group I pigments

Since group I pigments were excluded from all the HPLC columns [2], it was thought that the fraction not retained by a Sep-Pak C_{18} cartridge would be enriched in these pigments (Table I). Jaworski and Lee [10] fractionated grape phenolics using Sep-Pak C_{18} cartridges, so a further fractionation of the group I pigments by this method was attempted. Using this method, a

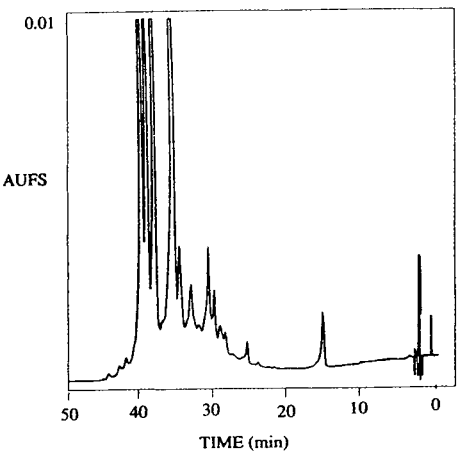

Fig. 8. The chromatogram (460 nm) of the "non-polar" Sep-Pak fraction on a 5-μm Hamilton PRP-1 column. Solvent A = 2% (v/v) aqueous acetic acid. Solvent B = acetonitrile. Gradient 5 to 33% solvent B over 50 min. Flow-rate = 1.0 ml min^{-1}.

fraction, not retained by a neutral cartridge, was collected for further fractionation on a second cartridge conditioned with 0.01 *M* HCl. The following designations are used below (*cf.* Materials and Methods): eluent 1 was not retained by a neutral Sep-Pak, eluent 2 was not retained by a Sep-Pak conditioned with 0.01 *M* HCl and eluent 3 was retained by the Sep-Pak conditioned with 0.01 *M* HCl.

The 280 nm chromatogram of eluent 1, on an untreated Hypersil ODS column, showed group I pigments, as well as gallic acid, theogallin, chlorogenic acid, *p*-coumaroylquinic acid, flavanol gallates, caffeine and some group III pigments [1,2]. Most, but not all, of the theaflavins and flavonol glycosides were retained on the cartridge. Thus eluent 1 was enriched in group I pigments, as expected, but was still a complex fraction. The 280 nm chromatogram of eluent 2, on an untreated Hypersil ODS column (Fig. 9), showed group I pigments, gallic acid and theogallin. Few group III pigments were present and the remaining peaks were very small. Thus eluent 2 was less complex than eluent 1. The 280 nm chromatograms of eluent 3, on an untreated Hypersil ODS column, showed group I pigments, polyphenols, caffeine and group III pigments.

Thermospray mass spectra of eluent 2 showed interesting high-mass ions, to which plausible ion compositions were assigned. The purity of the chromatographic peaks was not known, however, so more complete spectral interpretation was not attempted. Three peaks were observed on the UV trace in the first 3 min, but only the first peak (*ca.* 1 min) appeared on the ion chromatogram. Spectra extracted from the first peak, showed an ion at *m/z* 1822, for which two plausible compositions can be written, namely,

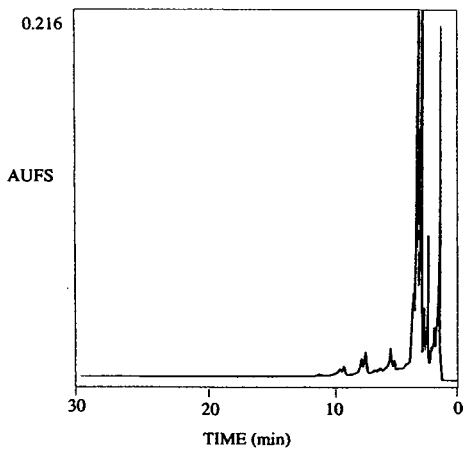

Fig. 9. The chromatogram (280 nm) of eluent 2 on an untreated 5-μm Hypersil ODS column. Solvent A = 2% (v/v) aqueous acetic acid. Solvent B = acetonitrile. Gradient 8 to 31% solvent B over 50 min. Flow-rate 1.5 ml min^{-1}.

[4GCG − 6H − 4] and [3GC + 2GCG − 8H − 4], where GCG and GC are the masses of gallocatechin gallate and gallocatechin monomer units, respectively. The formation of a tetramer would require the loss of six H atoms from the sum of the monomer masses, leaving a difference of four H atoms to explain. Oxidation of one monomer unit to the anthocyanidin level, would account for a further three H atoms, leaving only one H atom outstanding. Similar reasoning was applied to the pentameric ion. In a similar way, two compositions for an ion at *m/z* 1529 are [1C + 2GC + 1GCG − 6H + 23] and [1C + 1GC + 2GCG − 6H + 23], where C is the mass of a catechin monomer unit. The mass difference of +23 suggests that the fragment was cationised by sodium. Spectra taken from a small peak eluting after the first group showed an ion at *m/z* 1973, which could have been a pentamer [2GC + 3GCG − 8H − 5] or hexamer [5GC + 1GCG − 10H − 5], again with one unit oxidised to the anthocyanidin level. However, assignments for these two ions were treated with even more caution, as the peak on the ion-chromatogram was very small. Thus MS suggests that some of the group I pigments were charged flavanol oligomers with end-groups oxidised to the anthocyanidin level.

That only the first of the main group of peaks, visible on the UV trace, was observed on the ion chromatogram suggested that only the first of the main early running peaks (group I pigments) possessed such an anthocyanidin group, the charged species being detected efficiently by the thermospray interface. The first peak of the photodiode-array three-dimensional plot of tea liquor, on EDTA–citrate-treated Hypersil ODS and Hamilton PRP-1 columns, showed an absorption at *ca.* 510 nm, suggestive of anthocyanidin chromophore [1,2] and of pigments similar to the anthocyanidin pigments found in wine [11]. The present oligomers, detected by MS, could be pigments of this type. Immobile, pink pigments are also observed at the origin of paper chromatograms of black tea liquor run using the method of Roberts *et al.* [8]. Experiments arising from this observation are discussed later in this paper.

Pursuing this approach, it was decided to

collect fractions that were excluded from a column of Sephadex LH-20, so a black tea liquor was applied to a column of Sephadex LH-20, packed and equilibrated in 35% (v/v) aqueous acetone, and the chromatogram developed, isocratically, with the same solvent (Table I). Three discrete brown bands ran ahead of coloured material that was strongly retained at the top of the column. These bands were collected and analysed by HPLC. The photodiode-array three-dimensional plot of the chromatogram of the first brown band (Fig. 10) on an untreated Hypersil ODS column showed that the fraction contained group I pigments. Four peaks were present in the first 5 min of the chromatogram, each with a spectrum that tailed off into the visible region, suggestive of a brown pigment [2]. However, the first peak in the plot (*ca.* 1.5 min) also showed an absorption at *ca.* 510 nm, that could have been due to an anthocyanidin chromophore. Once again, this peak was similar to the peak on photodiode-array three-dimensional plots of black tea liquor tentatively assigned to an anthocyanidin pigment [1,2]. This material could also have been a flavanol oligomer or polymer with endgroups oxidised to the anthocyanidin level, analogous to the anthocyanidin pigments in wine [11], although further work is required to substantiate this suggestion. The other peaks appeared to be brown pigments but remain not otherwise characterised.

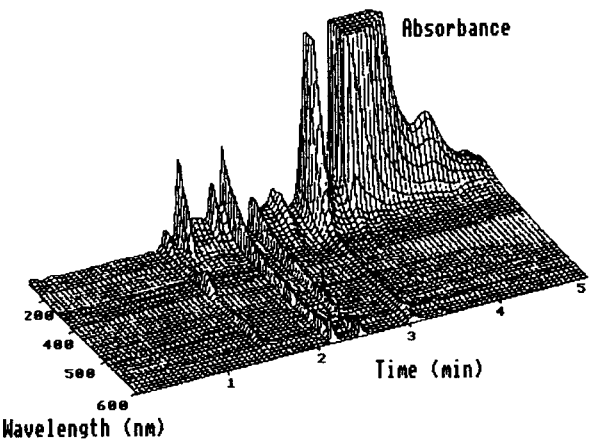

Fig. 10. The photodiode-array three-dimensional plot of the first brown band on an untreated 5-μm Hypersil ODS column. Solvent A = 2% (v/v) aqueous acetic acid. Solvent B = acetonitrile. Gradient 8 to 31% solvent B over 50 min. Flow-rate = 1.5 ml min^{-1}.

The photodiode-array three-dimensional plot of the second brown band on an untreated ODS Hypersil column showed group I pigments, chlorogenic acid, *p*-coumaroylquinic acid and caffeine. The observation of simple polyphenols co-eluting with the group I pigments does not rule out the possibility that group I pigments are excluded from the HPLC columns by size, as, with the solvents used, polyphenols show adsorption and/or partition as well as size exclusion, on Sephadex LH-20 [12]. The photodiode-array three-dimensional plot of the chromatogram of the third brown band on an untreated Hypersil ODS column showed group I pigments, polyphenols, caffeine and the broad band.

Since anthocyanidin pigments adsorbed strongly on paper, an attempt was made to isolate them from black tea liquor by selective adsorption on a column of cellulose. Columns of Whatman CF1 and microcrystalline cellulose were packed and equilibrated in 1% (v/v) aqueous acetic acid. Black tea liquor was applied to both columns, and the chromatograms were developed stepwise with 1% (v/v) aqueous acetic acid and methanol. Fractions were collected and analysed by UV–Vis spectroscopy and HPLC (on an untreated Hypersil ODS column). All the fractions were complex mixtures and none showed a band at 510 nm, suggestive of an anthocyanidin chromophore. Much coloured material remained on the columns after development with methanol, so the columns were washed with 5% (v/v) aqueous acetic acid, and this resulted in the elution of pink fractions with an absorption maximum at 510 nm. Fractions showing this band were combined and concentrated under vacuum on the rotary evaporator, ethanol being added to assist in the removal of the last traces of water. On addition of ethanol, the colour of the solution changed from light pink to purple and the absorption maximum shifted from 510 and 570 nm, the pink colour and the absorption maximum at 510 nm returning on addition of glacial acetic acid. This behaviour is typical of an anthocyanidin [13] and supported the suggestion that anthocyanidin pigments were present in the pink fraction. How-

ever, this method for the isolation of these pigments lacked reproducibility and much coloured material remained on the column.

To pursue the idea that some of the group I pigments possess anthocyanidin chromophores, their isolation using cation exchange was explored. Cation-exchange chromatography has been used to isolate polyphenolics and anthocyanidins from plant extracts [13]. Therefore, methods for the isolation of anthocyanidin pigments, using Bond-Elut cation-exchange cartridges, were explored (Table I). Black tea liquor was applied to a Bond-Elut SCX (sulfonic acid) cartridge, conditioned in turn with methanol and 1% (v/v) aqueous acetic acid. After washing with water until the washings were colourless, anthocyanidin pigments were eluted from the cartridge with 2% (v/v) concentrated hydrochloric acid in methanol. The UV–Vis spectrum of the anthocyanidin pigments showed a band with absorption maximum at about 505 nm.

The 280 nm chromatograms of the anthocyanidin pigments on an untreated Hypersil ODS column showed a peak at 1.8 min and a very small peak at 11.2 min. The 460 nm chromatogram on the Hamilton PRP-1 column showed two peaks, at 1.4 and 18.6 min. A photodiode-array three-dimensional plot of the chromatogram suggested that the peak at 18.6 min was an anthocyanidin, and the spectrum extracted for the peak confirmed this suggestion. This spectrum was the same as that of the first retained peak of the 460 nm chromatogram of black tea on the Hamilton PRP-1 column [2]. The photodiode-array UV–Vis spectrum of the peak at 1.4 min was difficult to interpret, as it was very close to the "refractive index peak" and showed much noise. The pigments were applied to paper and run using the method of Roberts *et al.* [8]; much of the material was completely immobile, remaining at the origin, supporting the suggestion that some of the pigments were polymeric anthocyanidin pigments. A faint coloured spot, mobile in butanol–acetic acid–water, but immobile in 2% (v/v) aqueous acetic acid, suggested the presence of Roberts' tricetinidin [7,8]. No standard was available to confirm this suggestion, but, in support of it, an ion was observed in a thermospray spectrum of the fraction at m/z 287, the correct mass for tricetinidin. On applying the fraction to an untreated Hypersil ODS column and eluting isocratically with 2% (v/v) aqueous acetic acid 0.1 *M* in ammonium acetate, ions at m/z 287 (M_r of tricetinidin = 287) and 403 [287 + 2NaCl] were observed. Fast atom bombardment spectra of anthocyanins show a peak at the mass of the flavylium ion [14,15], so the assignment of the ion at m/z 287 to the anthocyanidin tricetinidin is reasonable. Intense peaks due to clusters of sodium chloride were observed in this scan, showing the presence of sodium chloride in the sample.

Tea liquor was applied to a Bond-Elut CBA (carboxylic acid) cartridge, conditioned in turn with methanol and 1% (v/v) aqueous acetic acid (Table I). After washing with water until the washings were colourless, brown pigments were eluted from the cartridge with 2% (v/v) concentrated hydrochloric acid in methanol. The brown solution showed an absorption maximum at 510 nm. This suggested that the fraction was a mixture of anthocyanidin and thearubigin pigments. The 460 nm chromatograms of the fraction, on EDTA–citrate-treated Hypersil ODS and Hamilton PRP-1 columns, were SI-like. Thus the CBA cartridge gave a mixture of SI-like pigments and anthocyanidin pigments, and was less useful than the SCX cartridge. It is relevant to note the consistency of the presence of the anthocyanidin peak at *ca.* 18.5 min on the 460 nm chromatograms, on the Hamilton PRP-1 column, in the SI, Bond-Elut SCX and Bond-Elut CBA fractions, and in black tea liquor.

The Bond-Elut SCX cartridge isolation method was scaled up using a column of Amberlite CG-120 chromatographic grade sulfonic acid resin (Table I). The column was packed in distilled water, the tea liquor applied, and the column eluted, stepwise, with water, 20% (v/v) aqueous methanol, 80% (v/v) aqueous methanol and 2% (v/v) conc. HCl in methanol. The first three solvents were from a method of Ribéreau-Gayon [13], and the last solvent was chosen as one likely to elute anthocyanidin pigments from the column. The UV–Vis spectra of the pink fractions were similar to those of the pink fractions from the Bond-Elut SCX cartridges.

Similar pigments were obtained from the CG-120 column with 0.5% conc. HCl in methanol, suggesting that the pigments were unlikely to be merely degradation products. Paper chromatograms of these pigments, by the method of Roberts *et al.* [8], were similar to those isolated with Bond-Elut SCX cartridges. The fraction was heavily contaminated with sodium chloride, and ions consisting of clusters of tricetinidin, sodium chloride and water were observed in its thermospray spectrum.

CONCLUSIONS

This paper describes the isolation and HPLC analysis of fractions consisting of various black tea pigments, the results being summarised in Table I. HPLC showed the Roberts' SI and SII thearubigin fractions to be complex mixtures of pigments from all the groups I–III [2], including theaflavins, theaflavic acids, type I and type II resolved pigments (resolved thearubigins), and unresolved thearubigins. That both fractions are composed of pigments previously observed on black tea chromatograms gives increased confidence that the pigments observed on black tea chromatograms are, in fact, pigments previously designated as thearubigins. The SI fraction showed more theaflavins and a different distribution of group II and III pigments than SII. The convex broad bands from SI and SII were distinguishable by HPLC, their shapes being different, and their maxima at different retention times (Figs. 1 to 4).

"Polar" and "non-polar" fractions were isolated from black tea liquor using Sep-Pak C_{18} cartridges, following a method due to Wellum and Kirby [9]. HPLC showed the "polar" fraction to be SII-like, and the "non-polar" fraction (the fraction discussed by Wellum and Kirby [9]) SI-like. This provides a rapid, simple and robust method for the isolation SI-like and SII-like fractions for routine assessments, *e.g.*, as part of tea quality surveys. However, the relation of the SI-like and SII-like fractions to tea quality remains to be established.

Methods have been developed for the isolation of group I pigments, pigments that elute at the void volume of all the HPLC columns [2]. A similar group of pigments was also not retained by a Sep-Pak C_{18} cartridge or a Sephadex LH-20 column, and this enabled these pigments to be partially purified. A fraction of such pigments, designated eluent 1, was obtained from a Sep-Pak C_{18} cartridge. Further fractionation of these pigments gave eluent 2, a relatively simple fraction with an HPLC peak that gave thermospray ions at masses up to m/z 1973. These ions appeared to be from linear flavanol oligomers with one unit oxidised to the anthocyanidin level, and could be related to the anthocyanidin pigments discussed previously [1,2]. The chromatogram was monitored by UV and mass spectrometry, the 280 nm chromatogram showing a group of three peaks in the first 5 min, but the ion–chromatogram only the first peak of the group. These chromatograms were consistent with the chromatogram of the first brown band, excluded from a column of Sephadex LH-20, that showed only one peak with a UV–Vis absorption maximum at *ca.* 510 nm, the other three peaks having the spectra of brown pigments. The anthocyanidin pigments could be similar to the pink pigments found in wine [11].

Pink group I pigments were isolated from black tea using selective adsorption on a column of cellulose. However, the procedure lacked reproducibility, and coloured material was irreversibly adsorbed onto the cellulose. Anthocyanidin pigments were isolated using a Bond-Elut SCX (sulfonic acid) cation-exchange cartridge, the method being scaled up using a column of Amberlite CG-120 cation-exchange resin. HPLC, on the Hamilton PRP-1 column, showed these fractions to consist of an anthocyanidin, probably Roberts' tricetinidin [7,8], and a peak running close to the void volume of the column. The latter was similar to the pink pigments discussed above. The anthocyanidin was also prominent on black tea chromatograms run on the Hamilton PRP-1 column, but was not prominent on chromatograms run using an EDTA–citrate-treated Hypersil ODS column. An ion at m/z 287 in the thermospray mass spectra of the fraction provided evidence for the presence of tricetinidin. The Bond-Elut CBA cartridge was not as useful, as it gave a mixture of SI-like pigments and anthocyanidin pigments (460 nm

chromatograms on EDTA–citrate-treated Hypersil ODS and Hamilton PRP-1 columns). Thus the evidence is that the group I pigments are a mixture of pink anthocyanidin pigments and brown pigments.

The experiments described in this paper show the usefulness of our HPLC methods [1,2] for the qualitative analysis of black tea pigments. Used in conjunction with a range of separation methods, LC–MS, and photodiode-array detection, the methods have increased our knowledge of these pigments. However, much work remains to be done, particularly in the field of LC–MS. The long-term aim is to provide routine methods for the evaluation of tea quality for use in tea-producing countries. The Sep-Pak isolation methods could form the basis of a simple, rapid and robust method for the determination of thearubigin levels in black tea. However, this must await a better appreciation of the role of SI and SII thearubigins in tea quality.

ACKNOWLEDGEMENT

Financial support by the Natural Resources Institute is gratefully acknowledged.

REFERENCES

1 R.G. Bailey, I. McDowell and H.E. Nursten, *J. Sci. Food Agric.*, 52 (1990) 509.
2 R.G. Bailey, H.E. Nursten and I. McDowell, *J. Chromatogr.*, 542 (1991) 115.
3 I. McDowell and R.G. Bailey, *J. Chromatogr. Sci.*, 30 (1992) 330.
4 R.G. Bailey, H.E. Nursten and I. McDowell, *J. Sci. Food Agric.*, 59 (1992) 365.
5 R.G. Bailey, H.E. Nursten and I. McDowell, *J. Sci. Food Agric.*, (1993) in press.
6 R.G. Bailey, H.E. Nursten and I. McDowell, *J. Sci. Food Agric.*, 63 (1993) 455.
7 E.A.H. Roberts, in T.A. Geissman (Editor), *Chemistry of Flavonoid Compounds*, Pergamon, Oxford, 1962, pp. 468–512.
8 E.A.H. Roberts, R.A. Cartwright and M. Oldschool, *J. Sci. Food Agric.*, 8 (1957) 72.
9 D.A. Wellum and W. Kirby, *J. Chromatogr.*, 206 (1981) 400.
10 A.W. Jaworski and C.Y. Lee, *J. Agric. Food Chem.*, 35 (1987) 257.
11 T.C. Somers, *Phytochemistry*, 10 (1971) 2175.
12 C.K. Wilkins, *J. Chromatogr.*, 87 (1973) 250.
13 P. Ribéreau-Gayon, *Plant Phenolics*, Oliver & Boyd, Edinburgh, 1972, pp. 135–168.
14 N. Saito, M. Yokoi, M. Yamaji M and T. Honda, *Phytochemistry*, 26 (1987) 2761.
15 E. Idaka, T. Ogawa, T. Kondo and T. Goto, *Agric. Biol. Chem.*, 51 (1987) 2215.

Journal of Chromatography A, 662 (1994) 113–122
Elsevier Science B.V., Amsterdam

CHROM. 25 690

Assessment of peak origin and purity in one-dimensional chromatography by experimental design and heuristic evolving latent projections

Yi-zeng Liang

Department of Chemistry and Chemical Engineering, Hunan University, Changsha (China)

Markku D. Hämäläinen*

Department of Chemistry, Swedish University of Agricultural Sciences, Box 7015, S-750 07 Uppsala (Sweden)

Olav M. Kvalheim

Department of Chemistry, University of Bergen, N-5007 Bergen (Norway)

Roger Andersson

Department of Food Science, Swedish University of Agricultural Sciences, Box 7051, S-750 07 Uppsala (Sweden)

(First received June 25th, 1993; revised manuscript received October 20th, 1993)

ABSTRACT

A new procedure for assessing peak origin and purity in chromatographic calibration is presented. Chemical analytes were mixed according to an experimental design in order to achieve independent concentration patterns. One-dimensional chromatograms were analysed as digital profiles with the heuristic evolving latent projections (HELP) method after minimization of the retention time shifts between target peaks by a simplex technique. The origin of peaks was assessed by calculating the correlation between concentration patterns, obtained as the first loadings in HELP from principal component analysis (PCA) on selective chromatographic regions, and the patterns in the designed mixtures. Co-eluting impurities and overlapping peaks could be detected, resolved and quantified. Only a few non-overlapping data points were needed to assess the origin of peaks. Latent-variable correlation chromatograms are introduced as a powerful tool for the assignment of chromatographic areas with similar concentration patterns.

INTRODUCTION

Calibration in chromatographic analysis is commonly carried out by mixing all the chemical compounds in a stock standard solution, followed by sequential dilution to give working standard solutions of different concentrations. This creates a situation where all the chromatographic peaks from the standards are correlated. Chromatograms often contain different types of "ghost" peaks, for example from derivatization reagents, column bleed and carryover from previous samples or from partial decomposition of analytes. These peaks can overlap with the true peaks from the standards. The conventional method of calibration prevents the identification of peaks by correlation analysis as all the standards have the same concentration pattern. Cali-

* Corresponding author.

SSDI 0021-9673(93)E1143-N

bration is also usually based on area quantification. This is appropriate if the peaks are pure or overlapping impurities do not vary. However, real samples may not fulfil the above criteria, and this calls for a new strategy.

Retention time shifts and different background from one chromatogram to another make it difficult to utilize several chromatographic profiles jointly. Fortunately, in recent work [1], it was shown that by simplex optimization of the cross-correlation between selected target peaks, such retention time shifts could be minimized and the chromatographic profiles analysed by means of latent-variable projection methods [2–5]. Thus, the one-dimensional chromatograms from different runs can be made comparable by using this technique first. Fig. 1a and b show the gas chromatographic profiles for the nine calibration samples before and after baseline and retention time correction, respectively. The chromatograms from different runs can now be collected in a data matrix, in which each column represents the digital chromatographic profile of one sample and each row the chromatographic concentration of the different samples at a specific retention time point. Every region in chromatographic profiles can now be subjected to a local factor analysis as developed for coupled chromatography in heuristic evolving latent projections (HELP) methods [3–5].

In this study, we investigated a model system consisting of peracetylated aldoses. By mixing the standards according to a factorial design [6], the different chemical components are forced to

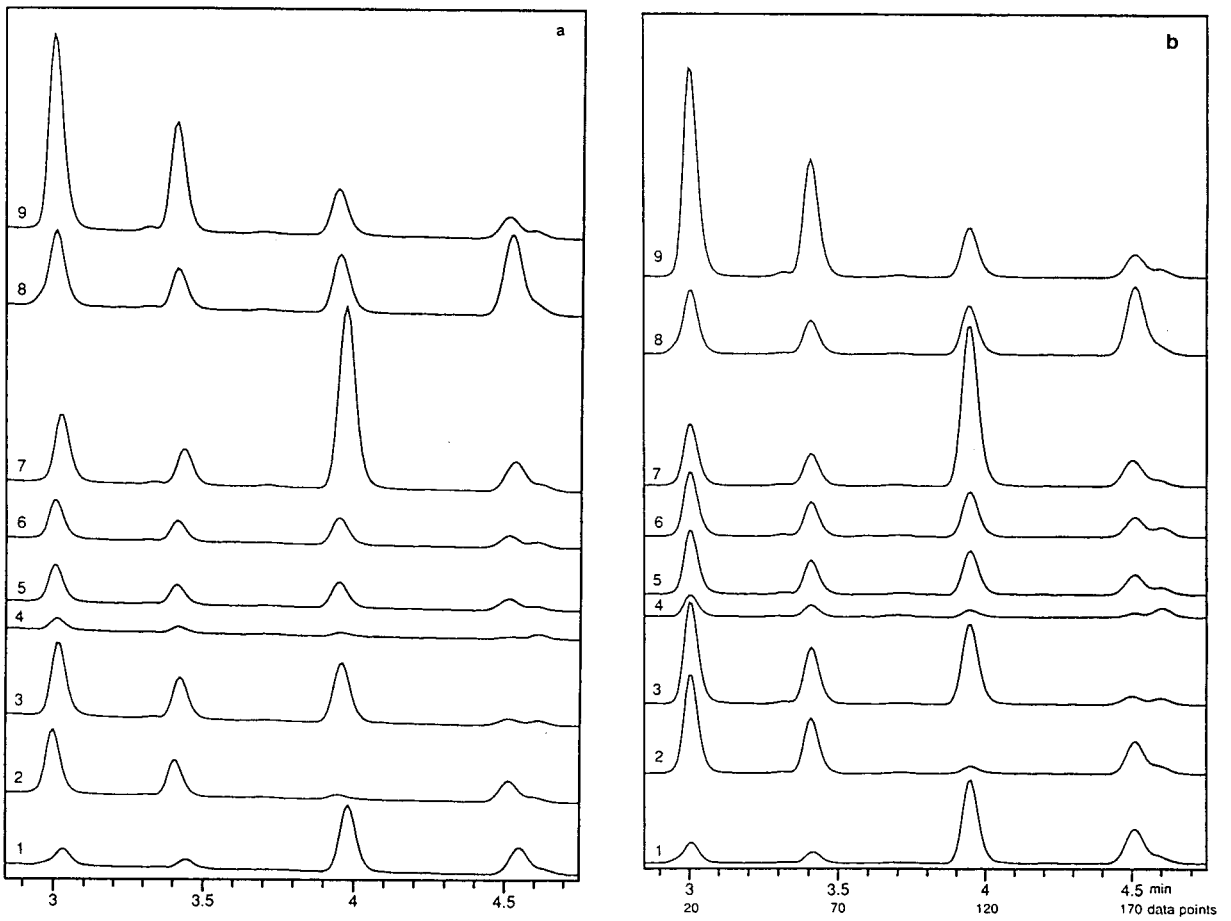

Fig. 1. Gas chromatographic profiles from peracetylated aldoses. (a) Raw data; (b) retention time, baseline and internal standard adjusted data. Time scale in min.

vary independently. The aldose standards equilibrate into anomeric isomers in acidic water, introducing several correlated peaks into the chromatograms. These correlations depict the decomposition of a compound and/or the existence of impurities in the standards, which give rise to correlated peaks in the chromatograms. There are also peaks from the derivatization reagents. Hence it should be possible to find three different kind of chromatographic areas: (i) non-correlated areas from the different experimentally designed aldoses, (ii) highly correlated areas derived from the isomerization of the aldoses and (iii) non-correlated areas, *e.g.*, from the derivatization reagents, which do not correlate with the designed concentration patterns. The first two types of areas should also correlate with the designed concentration patterns. In this paper, we present the advantages of using preprocessed chromatograms which are analysed as digital profiles by the HELP method. This provides a systematic way to find and identify the origin of chromatographic peaks in one-dimensional chromatography and to check the purity of each analyte.

THEORY

Rank analysis of a chromatographic profile

As discussed in the Introduction, a data matrix can be constructed by including different chromatographic profiles of calibration samples. For ease of comparison with the HELP resolution procedure developed for multi-detection chromatography, we let each column represent the digital chromatographic profile of one sample, and, consequently, each row the detector response of the different samples at a specific retention time point. Eigenstructure-tracking analysis (ETA) utilizing local principal component analysis (PCA) [7,8] can now be used for the analysis of the resulting matrix. This procedure performs PCA on local regions of the chromatographic profiles by moving a window of specified size from the first until the last retention time point and plotting the evolving eigenvalues in the retention time direction. The procedure starts with a window size of two and is repeated with a window of three, four, etc., until the window size exceeds by one the maximum number of co-eluting chemical components. With this window size, the last-evolving eigenvalue corresponds to the noise level over the entire elution region. The number of evolving eigenvalues above the noise level corresponds to the number of co-eluting chemical compounds in a local retention time region. For pure peaks only one eigenvalue is above the noise level. The plot of evolving eigenvalues can thus be used to assess the homogeneity of a peak [2].

In PCA the data matrix ($\boldsymbol{X}$) is decomposed into scores ($\boldsymbol{T}$) and loadings ($\boldsymbol{P}$) according to

$$\boldsymbol{X} = \boldsymbol{T}\boldsymbol{P}^{T} \tag{1}$$

For selective chromatographic regions, the concentrations for one chemical component from sample to sample are proportional to the elements in the first loading vector ($\boldsymbol{p}$). This may appear strange, since the score vector maps the chromatographic concentration profile for selective chromatographic regions [3]. However, this follows from the design and the organization of the data described above. Further details can be found in ref. 2.

Note that the HELP method works on uncentred data so that correlation is defined around the origin, not around the mean as is commonly done in factor analysis (see ref. 7, p. 40). The information on peak origin can therefore be obtained by comparing the first loadings from selective regions detected by the HELP method with the uncentred orthogonal concentration patterns from the experimental design. The procedure is illustrated in Fig. 2.

One-component and zero-component regions of chromatographic profiles

Chromatographic profiles possess an attractive feature: chemical compounds appear and disappear in a continuous manner during elution. Thus, signals at neighbouring retention time points tend to correlate. This gives an opportunity to perform correlation analysis by applying PCA on interesting chromatographic regions. Let $a_{i,j}$ be an element in a data matrix ($\boldsymbol{A}$) at the ith retention time point and from the jth calibration sample. The sub matrix $\boldsymbol{A}_{\text{sub}}$ including a

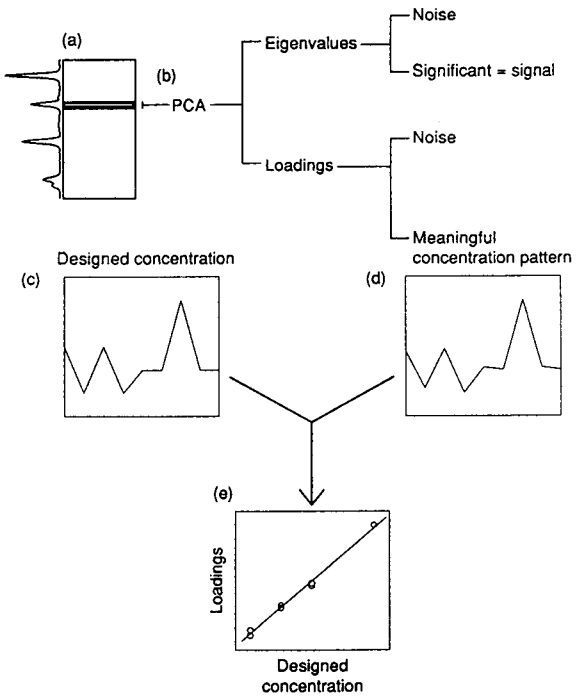

Fig. 2. Assessment of peak origin by the heuristic evolving latent projections method for one-dimensional chromatograms on several samples. (a) Pre-processed data matrix; (b) local principal component decomposition of the submatrix into loadings (eigenvectors) and eigenvalues; (c) designed concentration pattern; (d) first loading vector from a selective region; (e) assessment of peak origin by analysis of the correlation between the loadings from a selective region and the designed concentrations.

particular retention time interval (the shaded region in Fig. 2) can be expressed by

$$\boldsymbol{A}_{\text{sub}} = \begin{matrix} a_{i+1,1}a_{i+1,2}a_{i+1,3}\cdots a_{i+1,N} \\ a_{i+2,1}a_{i+2,2}a_{i+2,3}\cdots a_{i+2,N} \\ \vdots \qquad\qquad \vdots \\ a_{i+k,1}a_{i+k,2}a_{i+k,3}\cdots a_{i+k,N} \end{matrix} \tag{2}$$

Let us take a simple situation as example where there is only one chemical species, say component β, eluting from retention time point $i+1$ to $i+k$. In this case the chromatographic values for sample g, a_i+1, g, a_i+2, g, ..., a_i+k, g, should all be proportional to the designed concentration of component β in sample g. That is,

$$a_{i+j,g} \propto c_{\beta,g} \text{ or } a_{i+j,g} = r_j c_{\beta,g}$$
$$(j = 1, 2, \ldots, k,\ g = 1, 2, \ldots, N) \tag{3}$$

where $c_{\beta,g}$ indicates the designed concentration of component β in sample g and r_j is a proportionality constant.

Note that eqn. 3 implies that all the rows, $\boldsymbol{a}_j = (a_{i+j,1}a_{i+j,2}a_{i+j,3}\cdots a_{i+j,N})$, in the submatrix $\boldsymbol{A}_{\text{sub}}$ can be linearly expressed by one vector, $\boldsymbol{c}_\beta = (c_{\beta,1}\, c_{\beta,2}c_{\beta,3}\cdots c_{\beta,N})$. In mathematical terms, the rank of the matrix $\boldsymbol{A}_{\text{sub}}$ is one. Such a one component region is called a selective region in the HELP method [3,4].

Because of the measurement error from the instrument, eqn. 3 should include an error term:

$$a_{i+j,g} = r_j c_{\beta,g} + e_{i+j,g} \tag{4}$$

For this reason, ETA is used for resolving significant signals from noise, *i.e.*, for finding the "chemical rank" (number of components under a studied peak). The task is completed by comparing the eigenvalues obtained from the matrix $\boldsymbol{A}_{\text{sub}}$ with the first eigenvalue from the regions with no chemical signals above the baseline, *i.e.*, the so-called zero-component regions [2–5]. The rationale for this comparison has been published recently [9].

Loading pattern and designed concentration pattern

As discussed in the last section, a submatrix $\boldsymbol{A}_{\text{sub}}$ containing only one chemical component can be decomposed to provide a loading vector, $\boldsymbol{p}_\beta = (p_{\beta,1}p_{\beta,2}p_{\beta,3}\cdots p_{\beta,N})$, with the concentrations of the chemical components as elements. This vector can be used to find the origin of the peak. It is the experimental design with independent concentration patterns for different chemical analytes, which permits such identification. If the studied peak originates from the calibration set, the first loading vector from a selective region is proportional to one of the designed concentration vectors, *i.e.*, $\boldsymbol{p}_\beta \propto \boldsymbol{c}_\beta$. On the other hand, if the first loading vector obtained from PCA for a one-component region does not correlate with any designed concentration pattern, the peak is a so-called "ghost" peak.

Latent-variable correlation chromatograms

A noise-reduced evolving correlation pattern, latent-variable correlation chromatogram (LVCC), can be constructed in the following way:

(1) Selective regions are identified by ETA.

(2) Target concentration profiles are calculated with a local PCA, one for each selective region. The whole selective regions are used to provide maximum noise reduction. The first loadings vector in a selective region defines the target concentration profile, $\boldsymbol{p}_t$, for a chemical component.

(3) A local PCA is performed, starting from the three first retention time points, moving in step by one until the end of elution. The first evolving loading vector, $\boldsymbol{p}_e$, is stored. Step 3 provides a further noise reduction.

(4) The latent-variable correlation chromatograms are finally constructed by calculating and displaying the evolving correlation coefficients between the target loading vectors in step 2 and the evolving loading vectors in step 3, *i.e.*, $\boldsymbol{p}_t^T \boldsymbol{p}_e$.

EXPERIMENTAL

Sample description

The sample set used in this work was mixed from individual standards of xylose, arabinose and rhamnose. A four-level factorial design (Table I) was used in the mixing of the standards in order to define their concentration patterns. The first four experiments are half of a two-level factorial design for three factors followed by two centre points. The last three experiments are the high star points of a star design. This design is not orthogonal by the common definition used in experimental design if the columns are mean-centred. However, as discussed under Theory, the PCA modelling in the HELP method is based on uncentred data and therefore the concentration patterns between the aldoses are totally independent (orthogonal; $x_i^T x_j = 0$). Table II shows the amounts of the three aldoses in the mixture samples. The aldoses were peracetylated with acetic anhydride using 1-methylimidazole as catalyst [10]. All samples were analysed on a Packard Model 427 gas chromatography equipped with a flame ionization detector and a CP-SIL 88 (9 m × 0.22 mm I.D.) capillary column with helium as carrier gas at 150 cm/min (splitting ratio 1:20). Detailed conditions are given in ref. 7. Nelson 2600 chromatography software was used for collecting digital chromatographic elution profiles. The first 200 data points (retention time range 2.85–4.75 min, sampling interval 0.6 s) from the profiles were used in this paper.

TABLE I

EXPERIMENTAL DESIGN MATRIX USED IN THE MIXING OF STANDARDS

The true amounts can be found in Table II.

Standard No.	Xylose	Arabinose	Rhamnose
1	+1	+1	−1
2	−1	+1	+1
3	+1	−1	+1
4	−1	−1	−1
5	0	0	0
6	0	0	0
7	+3	0	0
8	0	+3	0
9	0	0	+3

Data pretreatment and analysis

Retention time adjustment, baseline correction and intensity normalization were first performed on a IBM PC-486 compatible computer

TABLE II

AMOUNTS OF SUGARS (IN mg) AT THE DIFFERENT DESIGN LEVELS

The coded design levels correspond to the amounts in Table I.

Sugar	Design level			
	−1	0	+1	+3
Xylose	1	4.75	8.5	16
Arabinose	1	4.75	8.5	16
Rhamnose	1	3.25	5.5	10

by means of ChromPro software (BioTriMark, Björkkulla, Funbo, Uppsala, Sweden). The chromatograms were normalized in regions with high intensities in order to correct for the effect of increased noise with increased signal, *i.e.*, heteroscedasticity [4,11]. The data were then analysed by means of the HELP method. The software used for data analysis was written in VAX FORTRAN and implemented on a VAX-station 2000 [3].

RESULTS AND DISCUSSION

Defining peak purity by local PCA

PCA can be used for resolving signals from noise. If a region of a chromatographic area contains only one pure chemical component, the chemical rank of the submatrix A_{sub} (representing the chromatographic signal intensity for the region of elution of that peak) is one and the data contain only one principal component above the noise level. Such a region is referred to as a selective region [3–5]. The eigenvalues from PCA obtained from the matrix A_{sub} are compared with the first eigenvalue from the zero-component regions [3,4]. If the second eigenvalue of the studied region is significantly smaller than the first eigenvalue obtained from the zero-component region (noise level), the studied region can be considered to have chemical rank one. Fig. 3 shows the results from an ETA obtained with window sizes three and two. This will give a rank map for every local retention time region [5]. For instance, Fig. 3 shows that the second eigenvalue is larger than the noise level around data points 18, 57, 110 and 182. Hence the number of co-eluting chemical components is two in these regions.

A comparison of eigenvalues between the zero-component regions and the selective regions is shown in Table III. The first eigenvalues from the selective regions are all significantly larger than those from the zero-component regions (noise level or detection limit), showing the presence of chemical substances. In selective regions the second eigenvalues are all smaller than the first eigenvalues from the zero-component regions, indicating the presence of only *one* compound in the regions. If the second

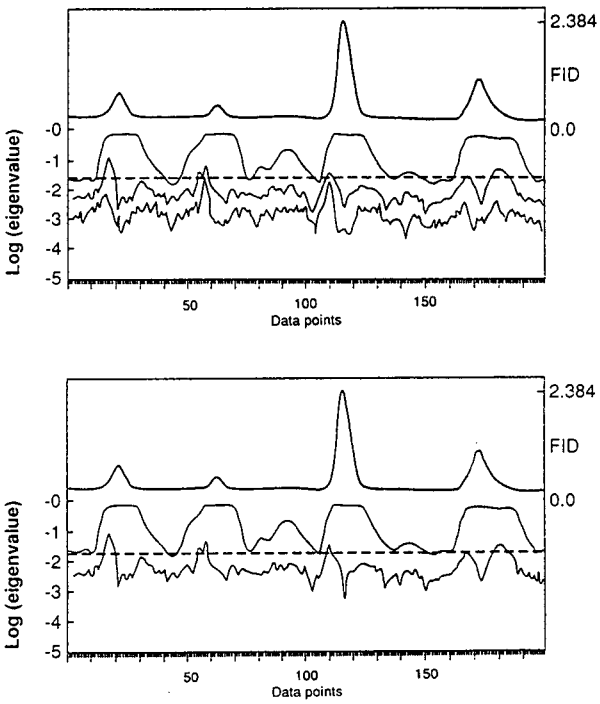

Fig. 3. Eigenstructure-tracking analysis of the data using window sizes three (top) and two (bottom). The upper trace in both parts is one of the chromatograms, followed by the first, second and (in the top part) third eigenvalues. The dashed horizontal lines indicate the noise level.

eigenvalues from some regions are larger than the zero-component region and the third eigenvalue smaller, these regions are two-component regions.

Concentration patterns, peak origin and resolution

The first loading vector in the selective regions obtained by local PCA displays the chromatographic concentration pattern (Fig. 4). These loadings should be proportional to some of the designed concentration vectors if the chemical components in these regions are derived from the standards or their decomposition products (illustrated by anomeric isomers). By comparing the loading vectors (Fig. 4) with the designed concentration profiles for the three standards (Fig. 5), the origin of the peaks can be established. The region denoted *C* in Fig. 4 is noisy as this chromatographic peak is very small, but one can still easily identify its origin (rhamnose). It is

TABLE III

EIGENVALUE COMPARISON BETWEEN THE ZERO-COMPONENT REGIONS AND SELECTIVE REGIONS

Retention time points	First eigenvalue	Second eigenvalue	Peak in Fig. 4
Zero-component regions			
4–6	0.0254	0.0082	
44–47	0.0250	0.0064	
156–159	0.0269	0.0076	
Selective regions			
12–15	0.2138	0.0151	A
23–26	0.8037	0.0058	B
48–51	0.1351	0.0136	C
62–65	0.8154	0.0101	D
117–120	0.8414	0.0108	E
171–173	0.6931	0.0053	F

interesting to look at the peaks at retention time 3 min. The first peak can, with some difficulty, be visually detected in sample 1 and sample 8 (Fig. 1b). However, the loading pattern from local PCA based on four retention time points (Table III) in the beginning of the peak cluster, denoted A in Fig. 4, correlates well with the concentration profile of arabinose (Fig. 5). This

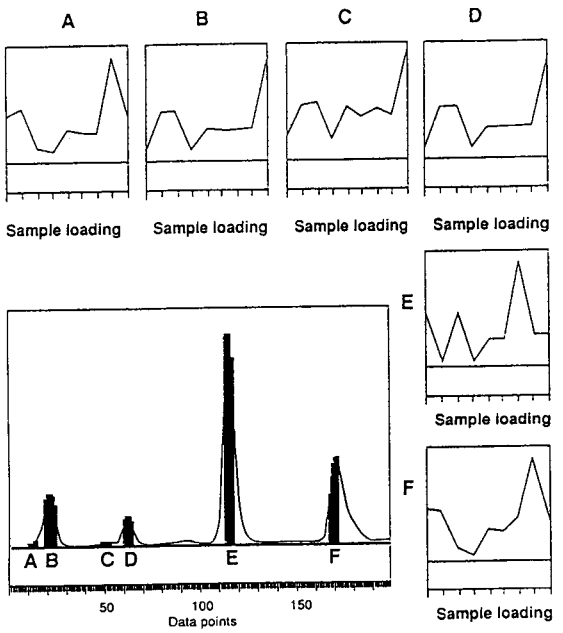

Fig. 4. Sample loading pattern (concentration) in selective areas (A–F) which correlates with the designed concentrations (Fig. 5).

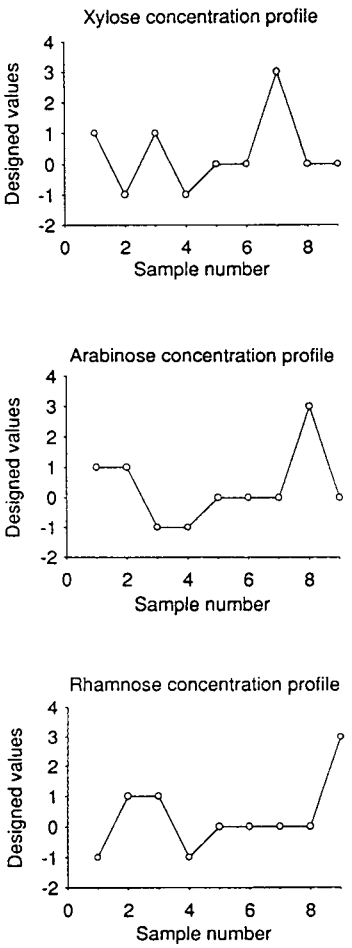

Fig. 5. Designed concentration pattern in the nine calibration mixtures.

is a clear advantage in comparison with the older integration approaches where the correlation can only be analysed between integrated peak areas (one needs at least ten data points for good integration results). Fig. 6 shows the first loading vectors for three other selective regions where the concentration patterns are far away from the designed ones. These peaks are impurities from the derivatization step.

The above-mentioned methods provide good tools for the detection of peak impurities and for the assessment of peak origin. Calibration results can be improved by eliminating the influence of impurities. This can be done by first resolving the peaks by the HELP method [3,5] and then using the resolved peak of the analytes for calibration. For example, the peak cluster around retention time 4.4–4.7 min contains two peaks (figs. 1b and 4), where the latter is an impurity (denoted C in Fig. 6). These peaks were resolved with the HELP method (Fig. 7).

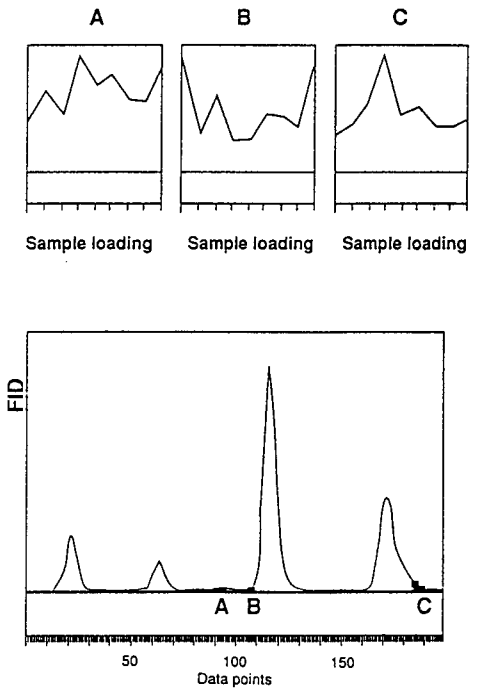

Fig. 6. Sample loading pattern (concentration) in selective areas derived from "ghost" peaks.

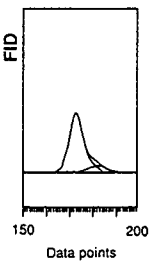

Fig. 7. Two-peak cluster at 4.5 min resolved by the HELP method.

Latent-variable correlation chromatography

In order to investigate thoroughly the correlation between one selected peak and all the other areas in the chromatogram, we introduce here the concept of latent-variable correlation chromatograms (LVCC). A chemical compound which is in equilibrium with different isomers, or a minor decomposition product, or an impurity in a standard, should have the same concentration profile with only differences in magnitude. The simplest way to assess similarities in concentration profiles is to calculate the correlation coefficient between two data points in the different chromatograms. However, a simple correlation coefficient is noise sensitive and we therefore use the loadings from principal component analysis for the calculation of the correlations (see Theory). A correlation coefficient near 1.0 indicates that the compounds have the same origin, whereas two compounds with independent concentration patterns have a correlation close to zero. It is also possible to obtain a correlation coefficient close to -1 if a single sample is run several times and a compound in the mixture decomposes giving a new, perhaps highly overlapped peak in the chromatogram. This is useful, for example, when studying the stability of compounds.

Fig. 8a shows three selected pure one-component areas (1, 2 and 3). These areas were selected by the ETA proceduce (at the minimum of the second eigenvalue at the bottom of Fig. 8a). Each of the three areas consists of three data points and are centred around retention times 3.0, 3.95 and 4.5 min, respectively (Fig.

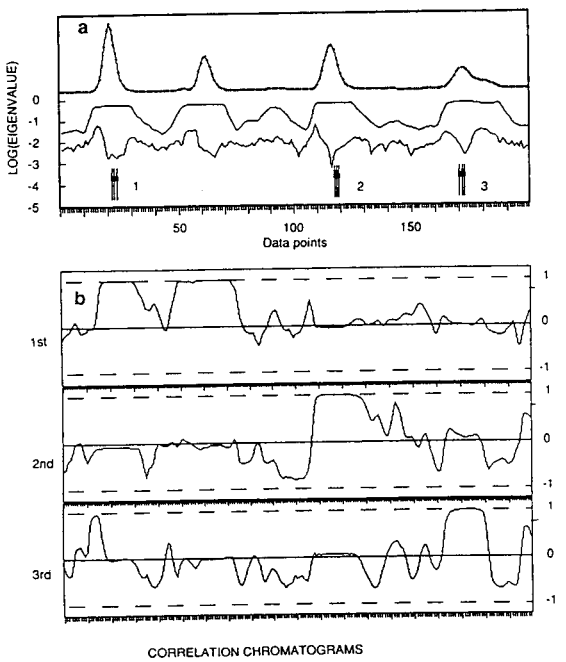

Fig. 8. (a) ETA using two retention time points as the window size. The top trace is one of the chromatograms, followed by the first and second eigenvalues. Three pure one-component areas (1–3) were selected as the target concentration patterns. (b) Three latent-variable correlation chromatograms (1st, 2nd and 3rd) calculated for each selected area.

1b), corresponding to the data point intervals 22–24, 117–119 and 170–172 in Fig. 8. Three separate PCAs are applied to these areas and the first loading vector is used as the target concentration patterns. A concentration profile chromatogram is constructed by ETA using three retention time points as the window size. For each of the three target areas an LVCC is constructed by a sequential calculation and display of the correlation between the first loading vector from the target area and all the loadings in the concentration profile chromatogram (Fig. 8b 1st–3rd). In the first LVCC, we can see that the correlation coefficients are close to one between data points 18–30 and 50–70. The first interval (18–30) includes the first target window and the second (50–70) a peak with a highly correlated concentration pattern. In the second LVCC (Fig. 8b, 2nd), only the target area has a correlation close to 1, which shows that the second target area has a unique concentration. The last LVCC (Fig. 8b, 3rd) indicates that the minor peak, with the maximum at data points 13–15, strongly correlates with the third target concentration profile. This small peak has only a few pure data points at the beginning of the peak cluster and it is notable that it was possible to identify its origin.

CONCLUSIONS

The following stepwise procedure is proposed for improved control of the calibration process in one-dimensional chromatography:

(1) In the calibration step, the standards are mixed according to an experimental factorial design, Plackett–Burman design [12], an orthogonal array or a response surface design to create uncorrelated concentration patterns.

(2) The chromatograms are made comparable by adjustment of retention time and baseline shifts.
This allows the analysis of the chromatograms as digital profiles.

(3) Heuristic evolving latent projections is applied on the profiles using the following steps:

(a) the noise level is determined from baseline regions (zero-component regions);

(b) ETA is performed in order to distinguish between pure one-component regions (peak purity check) and areas with overlapping peaks;

(c) the peak origin is established by analysis of the congruence between the sample loadings from pure one-component areas and designed concentration patterns;

(d) if a peak from a standard overlaps with other peaks which have a different concentration pattern, it can be resolved with the HELP method and the resolved areas are used in the calibration.

(4) Latent variable correlation chromatograms provide a powerful tool for finding chromatographic regions with similar concentration patterns. This method can also be used without calibration.

ACKNOWLEDGEMENTS

Y.L. is grateful for a postdoctoral fellowship from the Royal Norwegian Council for Scientific and Industrial Research (NTNF). M.D.H. thanks the Swedish Council for Technical Research for financial support.

REFERENCES

1 R. Andersson and M.D. Hämäläinen, *Chemom. Intell. Lab. Syst.*, in press.
2 M.D. Hämäläinen, Y. Liang, O.M. Kvalheim and R. Andersson, *Anal. Chim. Acta*, 271 (1993) 101–114.
3 O.M. Kvalheim and Y. Liang, *Anal. Chem.*, 64 (1992) 936–945.
4 Y. Liang, O.M. Kvalheim. H.R. Keller, D.L. Massart, P. Kiechle and F. Erni, *Anal. Chem.*, 64 (1992) 946–953.
5 Y. Liang, O.M. Kvalheim, A. Rahmani and R.G. Brereton, *J. Chemom.*, 7 (1993) 15–43.
6 S.N. Deming and S.L. Morgan, *Experimental Design: a Chemometric Approach*, Elsevier, Amsterdam, 1987, pp. 214–215.
7 E.R. Malinowski and D.G. Howery, *Factor Analysis in Chemistry*, Wiley, New York, 2nd ed., 1991.
8 S. Wold, K. Esbensen and P. Geladi, *Chemom. Intell. Lab. Syst.*, 2 (1987) 37–52.
9 Y. Liang, O.M. Kvalheim, and A. Höskuldsson, *J. Chemom.*, 7 (1993) 277–290.
10 M.D. Hämäläinen, I.-E. Ternrud, E. Nordkvist and O. Theander, *Carbohydr. Res.*, 207 (1990) 167–175.
11 H.R. Keller, D.L. Massart, Y. Liang and O.M. Kvalheim, *Anal. Chim. Acta*, 263 (1992) 29–36.
12 R.L. Plackett and J.P. Burman, *Biometrica*, 33 (1946) 305.

Journal of Chromatography A, 662 (1994) 123–137
Elsevier Science B.V., Amsterdam

CHROM. 25 675

Methylation reagents for the direct on-column derivatisation of veterinary residues

Masooma Amijee and Robert J. Wells*

Australian Government Analytical Laboratories, 1 Suakin Street, Pymble, NSW 2073 (Australia)

(First received September 14th, 1993; revised manuscript received October 22nd, 1993)

ABSTRACT

It has been demonstrated that judicious choice of the derivatisation reagent used for direct on-column methylations can have a profound effect of the products produced, often with little effect on the overall methylation efficiency of the process.

MethElute (PTMA-OH) and MethPrep (TTMA-OH) are perfectly satisfactory in the derivatisation of mono-functional compounds but produce mixtures, often very complex, when used for methylation of multi-functional substances.

Phenyltrimethylammonium cyanide (PTMA-CN) is readily prepared and is a far more selective alternative to MethElute for direct on-column methylation whilst still providing good yields of methylation products. Overall methylation efficiency is also dependent on the GC injector temperature whilst the condition of the injection liner can exert a significant effect on both methylation efficiency and selectivity.

INTRODUCTION

The analyses of many biologically active substances are routinely performed by HPLC because such substances are not suitable for analysis by gas chromatography (GC) or gas chromatography–mass spectrometry (GC–MS) without prior derivatisation. A wide range of these are acidic and can be converted into methylated derivatives which are more volatile and therefore far more amenable to GC–MS analysis. Analytical results obtained by HPLC are frequently required to be confirmed by the GC–MS analysis of a methylated derivative. Examples of drug groups which require methylation to be satisfactorily detected and quantified by GC or GC–MS are: sulfonamide antimicrobials (**1**, see Fig. 1), benzimidazole anthelmintics (**2**, **3**, see Figs. 2 and 3), thiouracil thyrostatics (**4**, see Fig. 4) and thiazide diuretics.

In addition to these examples may be added acidic herbicides such as 2,4-D and wood preservatives such as pentachlorophenol which are often analysed by GC as their methylated derivative.

Derivatisation may be achieved by a number of methods of which reaction with diazomethane [1], methylation with methyl iodide–potassium carbonate [2] or phase-transfer methylation with methyl iodide–tetrahexylammonium bromide [3–5] are typical examples. Although many of these procedures are simple and give high product yields, they add an extra step and often involve the use of toxic or hazardous reagents.

Phenyltrimethylammonium hydroxide (PTMA-OH) and 3-trifluoromethylphenyltrimethylammonium (TTMA-OH) hydroxide are commercially available analytical reagents which are sold under the trade names of MethElute and MethPrep, respectively. They have been widely used for the on-column derivatisation of acidic substances in GC [6,7]. Trimethylsulfoxonium hydroxide (TMSO-OH) [8,9] has also been used for the same purpose. These sub-

* Corresponding author.

0021-9673/94/$07.00
SSDI 0021-9673(93)E1123-H

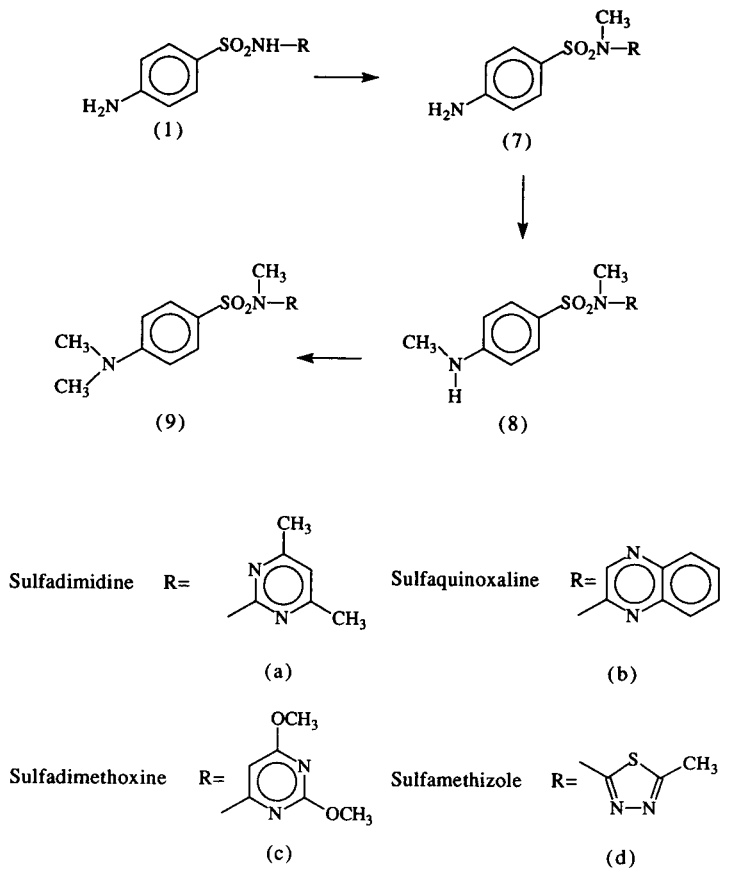

Fig. 1. Methylation products of sulfonamides.

stances all offer the advantage of *in situ* formation of the methylated derivative in the GC injection port but, in our hands, have proved somewhat non-selective in the methylation of some compound classes as illustrated later in this paper.

During studies on methylation under phase transfer conditions or using ion-exchange resins it has been found that the use of tetraalkylammonium salts or resins converted to the fluoride rather than the hydroxide form often offer advantages in terms of yield and selectivity [10]. This work suggested the replacement of the hydroxide anion of PTMA-OH with an alternative counter ion such as fluoride or cyanide could give greater selectivity.

We now report the investigation of phenyltrimethylammonium fluoride (PTMA-F) and phenyltrimethylammonium cyanide (PTMA-CN) as reagents for the direct on-column derivatisation of a series of substances used in veterinary treatments. Emphasis was placed on various sulfonamides (**1**), benzimidazoles (**2**, **3**) and thyrostatic substances (**4**). There are significant differences between the products formed when different methylation reagents are used.

EXPERIMENTAL

Reagents

MethElute (PTMA-OH) and Methprep-II (TTMA-OH) were commercial analytical reagents obtained from Pierce (Rockford, IL, USA) and Alltech (Deerfield, IL, USA), respectively.

Phenyltrimethylammonium iodide was prepared by refluxing a 20% solution of dimethyl-

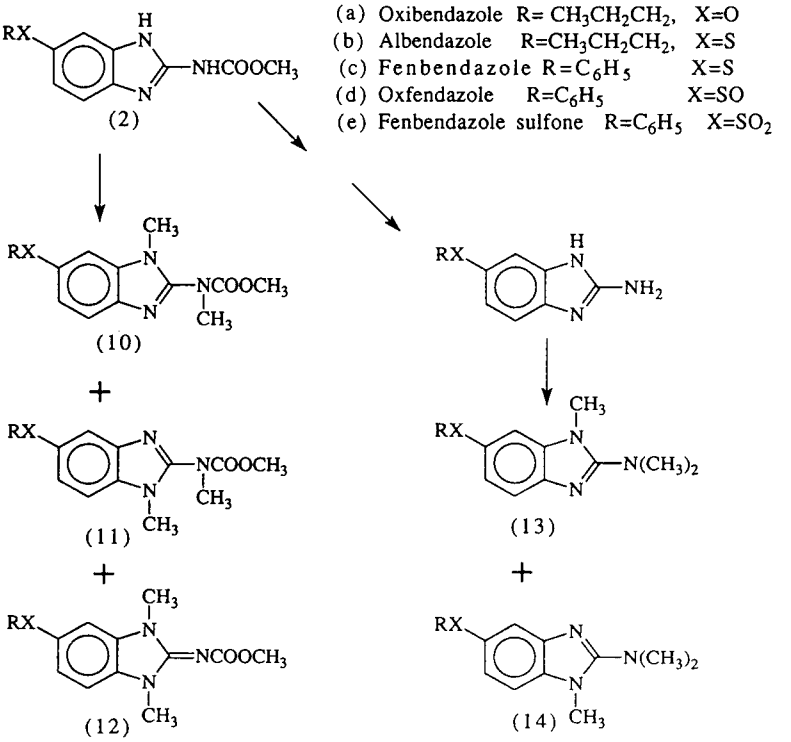

Fig. 2. Methylation products of benzimidazoles.

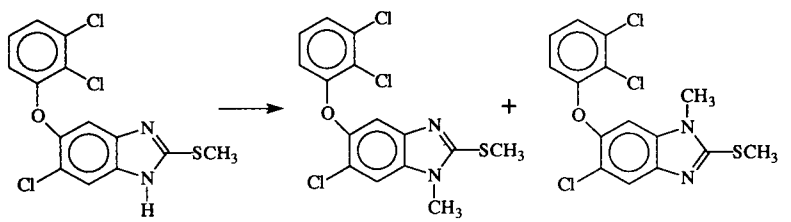

Fig. 3. Methylation products of triclabendazole.

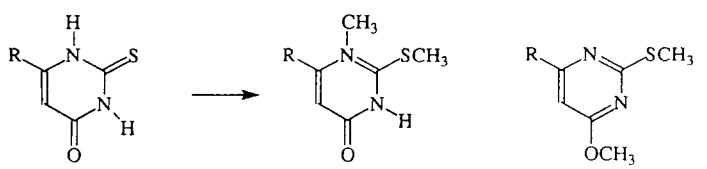

R = H, CH_3, $CH_3CH_2CH_2$, C_6H_5

Fig. 4. Methylation products of thiouracils.

aniline in acetonitrile with methyl iodide, followed by recrystallisation from acetonitrile–ethyl acetate. It was converted to the respective hydroxide, fluoride or cyanide derivatives by the following general procedure:

A chromatographic column containing 500 ml of AG 1-X8 anion-exchange resin [200–400 mesh (38–75 μm wet bead size), Bio-Rad Labs.] was percolated with a 0.1 *M* solution of either sodium hydroxide, sodium fluoride or sodium cyanide. The column was then washed with water (1000 ml) and methanol (2000 ml). A 0.5 *M* solution of the quaternary ammonium salt in methanol (20 m*M* total) was applied to the column and eluted with methanol. The emergence of the quaternary derivative was monitored by frequent testing of small aliquots of column eluent with aqueous silver nitrate. When all the quaternary derivative had been eluted, enough methanol was added to the combined fractions to bring the concentration to 0.2 *M*. This stock solution was used for on-column derivatisation experiments.

Trimethyloxysulfonium hydroxide was prepared as a 0.2 *M* solution in methanol by stirring a suspension of trimethyloxysulfonium iodide (4.4 g) in methanol (800 ml) with silver oxide, freshly prepared from silver nitrate (3.4 g) and well washed with water and methanol, until the solids changed colour from brown to pale yellow. The solution was filtered, the residual silver iodide washed with methanol (100 ml) and the combined solutions adjusted to 1000 ml with methanol.

Trimethyloxysulfonium fluoride (0.2 *M* in methanol) was prepared by neutralisation of the hydroxide to pH 7 with 40% hydrofluoric acid.

Standards

Sulfonamide standards were obtained from Sigma (St. Louis, MO, USA) and benzimidazole and thiouracil standards were provided by the Curator of Standards, Australian Government Analytical Laboratories (Pymble, Australia).

On-column derivatisation studies

Unless otherwise stated, on-column methylations were investigated by injection of a 1:1 mixture of a solution of the analyte (100 μg ml^{-1}) and a 0.2 *M* methanolic solution of the requisite quaternary ammonium salt.

Equipment operation

Gas chromatography–mass spectrometry

GC analyses were conducted on a Hewlett-Packard 5890 gas chromatograph, operating in the split injection mode, equipped with a Hewlett-Packard 7673A autosampler and a Hewlett-Packard mass-selective detector (Model 5971A). The column was a Hewlett-Packard HP-1 12 m × 0.22 mm fused-silica capillary column with a film thickness of 0.33 μm (Hewlett-Packard, Palo Alto, CA, USA). Helium was used as the carrier gas. The data were analysed using the software supplied with the 5971A mass-selective detector.

Injector inserts were cleaned and prepared by washing with methanol.

Acquisition of GC data

All GC analyses and on-column methylation studies were conducted employing the following standard conditions for the analyses of sulphonamides and benzamidazoles:

GC. Injection temperature 250°C, detector temperature 280°C, injection volume 2 μl (with three washes between injections), oven equilibration time between runs 0.5 min, oven program: initial temperature 140°C (0.5 min) then 20°C/min to 300°C and hold at 300°C for 3 min.

MS. Solvent delay 3.5 min, scan parameters *m/z* 50–450, threshold 1500.

On-column methylation studies for thiouracils employed the following standard conditions:

GC. Injection temperature 250°C, detector temperature 280°C, injection volume 2 μl (with three washes between injections), oven equilibration time between runs 0.5 min, oven program: initial temperature 60°C (1.0 min) then 15°C/min to 140°C, 25°C/min to 280°C and hold at 280°C for 2 min.

MS. Solvent delay 2 min, scan parameters *m/z* 50–500, threshold 1000.

Mass spectra of methylated analytes

Sulfonamides

N_1-Methylsulfadimidine (**7a**). *m/z* 228 ($M^+ - 64$, 73%), 227 ($M^+ - 65$, 100%), 136 ($C_6H_2N_2Me_2NMe-$, 12%), 121 ($H_2NC_6H_4$-NMe–, 12%), 108 ($C_6H_2N_2Me_2-$, 28%), 107 ($C_4HN_2Me_2-$, 13%), 107 ($C_6H_6N_2-$, 13%), 92 ($H_2NC_6H_4-$, 24%), 67 (10%), 65 (20%).

N_1,N_4-Dimethylsulfadimidine (**8a**). *m/z* 242 ($M^+ - 64$, 100%), 241 ($M^+ - 65$, 93%), 136, ($C_6H_2N_2Me_2NMe-$, 5%), 136 ($H_2NC_6H_4NMe-$, 12%), 108 ($C_6H_2N_2Me_2-$, 28%), 122 ($C_4HN_2Me_2-$, 13%), 107 ($C_6H_6N_2-$, 13%), 92 ($H_2NC_6H_4-$, 24%), 67 (10%), 65 (20%).

N_1,N_4,N_4-Trimethylsulfadimidine (**9a**). *m/z* 256 ($M^+ - 64$, 100%), 255 ($M^+ - 65$, 70%), 242 (5%), 241 (11%), 136 ($C_6H_2N_2Me_2NMe-$, 35%), 135 (12%), 134 (20%), 121 (12%), 120 (17%), 108 ($C_6H_2N_2Me_2-$, 8%), 107 ($C_6H_6N_2-$, 7%), 105 (9%), 104 (13%), 79 (7%), 78 (5%), 77 (11%), 67 (10%).

N_1-Methylsulfadimethoxine (**7c**). *m/z* 260 ($M^+ - 64$, 96%), 259 ($M^+ - 65$, 100%), 140 (29%), 92 (55%), 65 (39%).

N_1,N_4-Dimethylsulfadimethoxine (**8c**). *m/z* 274 ($M^+ - 64$, 100%), 273 ($M^+ - 65$, 71%), 259 (7%), 154 (9%), 140 (21%), 122 ($C_4HN_2Me_2-$, 25%), 121 (14%), 120 (21%), 107 (10%), 106 (28%), 82 (10%), 79 (17%), 78 (14%), 77 (25%), 65 (7%).

N_1,N_4,N_4-Trimethylsulfadimethoxine (**9c**). *m/z* 288 ($M^+ - 64$, 100%), 287 ($M^+ - 65$, 32%), 274 (11%), 273 (11%), 168 (7%), 140 (15%), 136 (31%), 135 (15%), 134 (14%), 122 (6%), 121 (11%), 120 (19%), 108 (5%), 105 (11%), 104 (9%), 83 (5%), 82 (6%), 79 (7%), 78 (5%), 77 (16%), 68 (5%).

N_1-Methylsulfaquinoxaline (**7b**). *m/z* 250 ($M^+ - 64$, 84%), 249 ($M^+ - 65$, 100%), 159 (8%), 158 (8%), 157 (5%), 156 (20%), 140 (7%), 131 (10%), 130 (17%), 129 (11%), 117 (5%), 116 (6%), 108 ($C_6H_2N_2Me_2$–37%), 107 ($C_6H_6N_2-$, 12%), 106 (8%), 102 (11%), 93 (8%), 92 (54%), 91 (8%), 90 (26%), 66 (5%), 65 (25%), 64 (7%).

N_1,N_4-Dimethylsulfaquinoxaline (**8b**). *m/z* 265 (19%), 264 ($M^+ - 64$, 100%), 263 ($M^+ - 65$, 63%), 170 (12%), 158 (5%), 154 (7%), 131 (8%), 130 (8%), 129 (9%), 122 ($C_4HN_2Me_2-$, 66%), 121 (24%), 120 (9%), 107 (6%), 106 (43%), 105 (7%), 104 (8%), 102 (8%), 91 (5%), 90 (17%), 79 (17%), 78 (9%), 77 (19%), 76 (5%), 66 (5%), 65 (9%), 64 (7%), 63 (9%).

N_1,N_4,N_4-Trimethylsulfaquinoxaline (**9b**). *m/z* 279 (21%), 278 ($M^+ - 64$, 100%), 277($M^+ - 65$, 35%), 264 (33%), 263 (19%), 207 (12%), 137 (9%), 136 (76%), 135 (21%), 134 (6%), 131 (9%), 130 (5%), 129 (5%), 122 ($C_4HN_2Me_2-$, 13%), 121 (7%), 120 (45%), 118 (7%), 115 (5%), 106 (12%), 105 (12%), 104 (13%), 103 (6%), 102 (75), 92 (6%), 91 (6%), 90 (20%), 79 (15%), 78 (7%), 77 (23%), 76 (7%), 65 (7%), 64 (5%), 63 (6%).

N_1-Methylsulfamethizole (**7d**). *m/z* 284 (M^+ 83%), 156 (66%), 108 (58%), 92 (100%), 70 (63%), 65 (47%), 51 (35%).

N_1,N_4-Dimethylsulfamethizole (**8d**). *m/z* 299 (15%), 298 (M^+ 100%), 207 (13%), 176 (26%), 170 (21%), 138 (10%), 122 (74%), 117 (13%), 107 (12%), 106 (51%), 90 (16%), 79 (17%), 77 (31%), 69 (12%), 65 (15%).

N_1,N_4,N_4-Trimethylsulfamethizole (**9d**). *m/z* 314 (14%), 313 (M^+ 20%), 312 (100%), 311 (8%), 298 (14%), 207 (11%), 184 (14%), 136 (84%), 120 (50%), 119 (9%), 118 (11%), 105 (14%), 104 (14%), 92 (8%), 79 (11%), 78 (9%), 77 (12%), 70 (11%), 69 (14%), 59 (13%).

Benzimidazoles

Dimethyloxibendazole (**10a**). *m/z* 278 (11%), 277 (M^+ 88%), 235 (10%), 234 (27%), 218 (14%), 178 (19%), 177 (32%), 176 (100%), 175 (7%), 174 (7%), 162 (7%), 148 (11%), 147 (14%), 134 (5%), 119 (5%), 106 (7%), 105 (5%), 90 (5%), 80 (6%), 79 (5%), 72 (64%), 59 (9%).

Dimethyloxibendazole (**11**). *m/z* 278 (8%), 277 (M^+ 85%), 235 (14%), 234 (17%), 219 (5%), 218 (21%), 177 (15%), 176 (100%), 175 (6%), 162 (7%), 161 (7%), 149 (7%), 148 (12%), 147 (10%), 134 (5%), 106 (6%), 92 (7%), 79 (5%), 72 (5%), 66 (7%), 59 (8%).

Dimethyloxibendazole (rearranged) (**12**). *m/z* 278 (10%), 277 (M^+ 71%), 247 (13%), 246 (100%), 234 (15%), 233 (8%), 219 (11%), 205 (5%), 204 (61%), 203 (12%), 189 (9%), 188

(5%), 187 (5%), 177 (15%), 176 (8%), 174 (8%), 161 (6%), 160 (5%).

Trimethyldecarbomethoxyoxibendazole (**13**). *m/z* 234 (9%), 233 (M^+ 48%), 204 (7%), 191 (12%), 190 (100%), 176 (9%), 162 (11%), 148 (9%), 147 (12%).

Trimethyldecarbomethoxyoxibendazole (**14**). *m/z* 234 (14%), 233 (M^+ 100%), 218 (21%), 204 (34%), 191 (13%), 190 (16%), 189 (7%), 176 (44%), 163 (7%), 162 (59%), 161 (12%), 160 (12%), 159 (5%), 149 (6%), 148 (27%), 147 (31%), 145 (5%), 134 (6%), 121 (6%), 106 (7%), 71 (5%).

Dimethylalbendazole (**10**). *m/z* 295 (9%), 294 (16%), 293 (M^+ 100%), 250 (14%), 235 (10%), 234 (36%), 194 (7%), 193 (23%), 192 (30%), 191 (14%), 164 (7%), 163 (8%), 159 (6%), 150 (5%), 149 (5%), 72 (19%), 59 (5%).

Dimethylalbendazole (**11**). *m/z* 294 (18%), 293 (M^+ 100%), 264 (8%), 250 (8%), 234 (28%), 193 (9%), 192 (54%), 191 (15%), 164 (10%), 163 (7%), 106 (5%), 90 (10%), 83 (5%).

Dimethylalbendazole (rearranged) (**12**). *m/z* 294 (14%), 293 (M^+ 63%), 264 (6%), 263 (15%), 262 (100%), 250 (11%), 249 (7%), 235 (10%), 220 (19%), 219 (29%), 218 (6%), 207 (5%), 205 (6%), 204 (12%), 192 (8%), 186 (5%), 59 (6%).

Trimethyldecarbomethoxyalbendazole (**13**). *m/z* 250 (14%), 249 (M^+ 86%), 234 (15%), 220 (16%), 207 (15%), 206 (100%), 205 (9%), 192 (17%), 178 (6%), 177 (7%), 176 (10%), 165 (6%), 164 (18%), 163 (14%), 162 (6%), 131 (6%), 118 (6%), 95 (5%).

Trimethyldecarbomethoxyalbendazole (**14**). *m/z* 250 (15%), 249 (M^+ 100%), 234 (24%), 220 (29%), 207 (8%), 206 (19%), 205 (17%), 192 (21%), 178 (22%), 177 (15%), 176 (13%), 165 (8%), 164 (19%), 163 (23%), 161 (5%), 132 (6%), 131 (5%), 122 (6%), 109 (5%), 91 (5%), 65 (7%).

Dimethylfenbendazole (**10**). *m/z* 328 (19%), 327 (M^+ 100%), 270 (11%), 269 (25%), 268 (88%), 239 (19%), 90 (6%).

Dimethylfenbendazole (**11**). *m/z* 328 (14%), 327 (M^+ 100%), 270 (10%), 269 (19%), 268 (63%), 239 (9%), 207 (11%), 82 (6%), 77 (9%).

Dimethylfenbendazole (rearranged) (**12**). *m/z* 328 (21%), 327 (90%), 297 (22%), 296 (100%), 270 (15%), 269 (10%), 207 (37%), 148 (18%).

Trimethyldecarbomethoxyfenbendazole (**13**). *m/z* 284 (18%), 283 (M^+ 100%), 269 (5%), 268 (10%), 255 (5%), 254 (20%), 253 (9%), 241 (7%), 240 (13%) 239 (35%), 225 (5%), 224 (5%), 159 (5%), 142 (11%), 134 (9%), 131 (7%), 109 (6%), 77 (6%).

Trimethyldecarbomethoxyfenbendazole (**14**). *m/z* 284 (14%), 283 (M^+ 100%), 269 (8%), 268 (48%), 255 (6%), 254 (33%), 253 (7%), 241 (6%), 240 (16%) 239 (47%), 224 (6%), 207 (5%), 184 (5%), 142 (14%), 134 (8%), 132 (5%), 127 (6%), 118 (7%), 109 (5%).

Dimethyloxfenbendazole (**10**). *m/z* 344 (16%), 343 (M^+ 51%), 328 (35%), 327 (100%), 295 (70%), 281 (41%), 270 (16%), 269 (24%), 268 (98%), 267 (21%), 266 (53%), 240 (17%), 239 (20%), 236 (72%), 234 (37%), 225 (12%), 209 (32%), 208 (27%), 207 (73%), 191 (18%), 159 (44%), 158 (12%), 147 (20%), 131 (19%), 118 (19%), 95 (19%), 78 (14%), 72 (47%), 59 (27%).

Dimethyloxfenbendazole (**11**). *m/z* 344 (12%), 343 (M^+ 39%), 328 (15%), 327 (95%), 295 (48%), 282 (18%), 281 (32%), 269 (32%), 268 (88%), 266 (56%), 250 (27%), 240 (11%), 240 (11%), 239 (18%), 236 (45%), 234 (40%), 208 (22%), 207 (100%), 191 (18%), 159 (30%), 147 (15%), 131 (13%), 119 (1%), 118 (23%), 73 (38%).

Dimethyloxfenbendazole (rearranged) (**12**). *m/z* 344 (16%), 343 (M^+ 51%), 328 (35%), 327 (100%), 295 (70%), 281 (41%), 270 (16%), 269 (24%), 268 (98%), 267 (21%), 266 (53%), 240 (17%), 239 (20%), 236 (72%), 234 (37%), 209 (32%), 208 (27%), 207 (73%), 191 (18%), 159 (44%), 158 (12%), 147 (20%), 131 (19%), 118 (19%), 96 (19%), 77 (26%), 272 (47%), 59 (27%).

Trimethyldecarbomethoxyoxfenbendazole (**13**). *m/z* 299 (14%), 284 (22%), 283 (100%), 282 (6%), 269 (9%), 268 (36%), 254 (27%), 253 (12%), 240 (21%), 239 (30%), 222 (35%), 207 (11%), 192 (5%), 191 (6%), 190 ((%), 159 (10%), 142 (9%), 134 (10%), 133 (6%), 132 (8%), 131 (9%0, 118 (9%), 77 (12%), 51 (7%).

Trimethyldecarbomethoxyoxfenbendazole (**14**).

m/z 300 (18%), 299 (95%), 284 (23%), 283 (100%), 281 (11%), 270 (8%), 269 (9%), 268 (46%), 254 (28%), 253 (9%), 251 (14%), 240 (20%), 239 (47%), 236 (17%), 223 (10%), 222 (75%), 221 (11%), 209 (8%), 208 (18%), 207 (48%), 206 (15%), 193 (19%0, 191 (7%), 190 (23%), 163 (13%), 162 (15%), 159 (27%), 147 (12%), 145 (24%), 141 (14%), 134 (12%), 133 (10%), 131 (13%), 130 (11%), 118 (15%), 104 (11%), 77 (22%), 51 (10%).

Monomethyltriclabendazole (**4**). *m/z* 378 (8%), 376 (27%), 375 (20%), 374 (M^+ 100%), 373 (17%), 372 (99%), 370 (7%), 357 (9%), 343 (23%), 342 (15%), 341 (88%), 340 (22%), 339 (93%), 328 (5%), 325 (7%), 302 (6%), 269 (8%), 256 (9%), 229 (9%), 227 (13%), 207 (13%), 198 (6%), 196 (9%), 169 (7%), 168 (9%), 166 (9%), 164 (6%), 154 (8%), 153 (6%), 152 (13%), 151 (14%), 111 (10%), 110 (8%), 109 (22%), 100 (7%), 97 (8%), 85 (8%), 75 (11%), 74 (8%), 73 (10%).

Monomethyltriclabendazole (**5**). *m/z* 377 (10%), 376 (40%), 375 (25%), 374 (M^+ 100%), 373 (21%), 372 (100%), 357 (6%), 343 (15%), 342 (10%), 341 (55%), 340 (10%), 339 (53%), 327 (13%), 326 (7%), 325 (9%), 304 (5%), 303 (14%), 302 (13%), 269 (8%), 256 (9%), 255 (10%), 227 (10%), 208 (10%), 207 (12%), 198 (8%), 196 (8%), 170 (7%), 169 (7%), 168 (14%), 152 (26%), 151 (20%), 109 (17%), 102 (6%), 101 (9%), 76 (12%), 75 (11%), 74 (8%), 73 (6%), 66 (13%), 63 (14%).

RESULTS AND DISCUSSION

Effect of injection temperature

The effect of the injection temperature on methylating power and efficiency was compared for PTMA-OH and PTMA-F using the methylation of sulfadimidine (**1a**) and oxibendazole (**2a**) at different injector block temperatures as a general guide. A 100 μg ml^{-1} solution of oxibendazole and sulfadimidine in 0.2 *M* methanolic PTMA-F was analysed using injector block temperatures between 180 and 280°C. The methylation efficiency was estimated from the combined total ion current produced by GC–MS monitoring of methylated products. The results of this study are shown in Table I.

These results indicate an injection temperature of 240–260°C is optimal for maximum derivatisation efficiency of both oxibendazole and sulfadimidine. This injection temperature is also optimal for both derivatising agents as is the overall methylation efficiency. At lower injection temperatures there is little difference in methylation efficiency of sulfadimidine for either of the two reagents. By contrast, methylation efficiency of oxibendazole is better with PTMA-OH than with PTMA-F at temperatures below 250°C. However, in general, total derivatisation efficiency decreases with decrease in temperature and is very poor below 200°C.

In terms of selectivity, it is clear from Table I that the hydroxide is a more vigorous and non-selective methylation reagent than is the corresponding fluoride. However, with either reagent there is very little variation of methylation selectivity with increasing injection block temperature above a temperature of 200°C although the ratios of various products are subject to some variation as the injection temperature is increased. At 180°C oxibendazole gave only two dimethylated products (**10** and **11**) but this selectivity was associated with a methylation efficiency of only 20% that obtained at 250°C. Above 200°C, the formation of a third rearranged dimethylated product in the methylation of oxibendazole becomes important and constitutes about 40% of the combined derivatives at 250°C.

Methylation efficiency

Effect of injector insert

It was found during this work that following the replacement of an unclean injector liner with a fresh one, a maximum reproducible value for overall methylation efficiency and selectivity was attained only after about 20 on-column methylation injections. Thus the methylation of oxibendazole (**2a**) with PTMA-CN gave 67% of a monomethyl derivative together with a combined yield of 33% of two dimethyl derivatives at 250°C when a fresh injector insert was used. After 20 further injections involving a variety of methylation reagents, the same methylation mix-

TABLE I

EFFECT OF INJECTION TEMPERATURE ON THE METHYLATION EFFICIENCY OF OXIBENDAZOLE AND SULFADIMIDINE BY TMPA-OH AND TMPA-F

The structures of products formed are numbered and are discussed in detail later in the paper. TIC = Total ion current.

Methylation agent	Analyte	Injector temp (°C)	No. of products	Ratio of products %					Combined TIC × 10^3
				13a	**14a**	**10a**	**11a**	**12a**	
PTMA-F	Oxibendazole	180	2			50	50		181
		200	3			37	37	26	270
		220	3			35	30	35	295
		260	3			28	28	44	580
		280	3			30	23	47	380
PTMA-OH	Oxibendazole	180	3			30	30	40	260
		200	3			45	35	20	415
		220	3	18	16	16	16	34	440
		250	5	21	18	14	14	33	550
		280	5	21	20	13	13	33	625

Derivatising agent	Analyte	Injector temp. (°C)	No. of products	Ratio of products %			Combined TIC × 10^3
				7a	**8a**	**9a**	
PTMA-F	Sulfadimidine	180	2	80	20		100
		200	2	80	20		294
		220	2	83	17		380
		250	2	83	17		450
		280	2	83	17		520
PTMA-OH	Sulfadimidine	180	3	48	31	21	86
		200	3	37	27	36	230
		220	3	30	30	40	350
		250	3	27	25	48	408
		280	3	27	25	48	456

ture of oxibendazole and PTMA-CN gave combined yield of 100% of the two dimethyl derivatives. Both the selectivity and overall methylation efficiency was subsequently maintained for the lifetime of the injector insert. Similar behaviour was found for other methylation reagents. For example, the methylation of sulfadimidine (**1a**) with PTMA-OH gave 33% of the trimethylated derivative with a fresh insert. This value rose to and was maintained at 55% as the insert was subsequently used.

Comparison of the efficiencies of on-column and phase transfer methylations

Information on the efficiency of direct on-column methylation was obtained by a direct comparison of the methylation of triclabendazole (**3**) using a phase-transfer procedure [3–5] and on-column methylation with PTMA-F. The phase-transfer methylation reaction has previously been reported to give yields in the range of 70–80% [3–5]. Triclabendazole was the chosen analyte because it methylated in good yield using either method and produced only two products (**5** and **6**) in approximately the same ratio.

In order to assess the comparability of phase transfer and direct methylation a standard solution of triclabendazole in methanol was mixed 1:1 with 2 *M* methanolic PTMA-F for direct injection. A parallel phase-transfer methylation was conducted on the same amount of triclabendazole standard solution. This solution was then evaporated to near dryness, methylated by published procedures [4] and the product made up to the same concentration as the triclabendazole in the direct injection experiment.

TABLE II

COMPARISON OF THE METHYLATION EFFICIENCY OF TRICLABENDAZOLE BY TMPA-F AND PHASE TRANSFER AT DIFFERENT ANALYTE CONCENTRATIONS

The concentration of injection solutions were adjusted to ensure that the concentration of the analytes were equivalent for either derivatisation method. The total ion current (TIC) for each of the two possible monomethylated products **4** and **5** are listed together with the combined TIC for **4** plus **5**

Concentration of analyte (in solution injected) $\mu g\ ml^{-1}$	Phase transfer, TIC $\times 10^3$			PTMA-F, TIC $\times 10^3$		
	Peak 1	Peak 2	Total	Peak 1	Peak 2	Total
110	2366	1173	3539	2744	1650	4394
55	872	401	1273	1108	631	1739
28	260	112	372	243	128	371
5	–	–	–	14	–	14

The results shown in Table II demonstrate that derivatisation using on-column injection with PTMA-F is at least as efficient as phase-transfer methylation at higher analyte concentrations, at an intermediate level both methods give comparable results whilst at 5 $\mu g\ ml^{-1}$ only PTMA-F gives a detectable product using the MS in full scan mode. Thus, not only is direct on-column methylation a very convenient technique but it appears to give methylated derivatives in yields comparable to alternative methods.

Effect of variation of methylation reagent on selectivity

Sulfonamides

Work on the derivatisation of sulfonamides has been reviewed previously [11]. On-column derivatisation of sulfonamides (**1**) with PTMA-OH gave significantly different results than those obtained by use of PTMA-F or PTMA-CN. Thus, with PTMA-OH, all sulfonamides tested gave a mixture of three derivatives consisting of monomethylated (**7**), dimethylated (**8**) and trimethylated (**9**) substances as judged from the mass spectrum of each peak (see Fig. 5). Very little variation of derivatisation pattern was obtained by alteration of injector temperature.

By contrast, PTMA-F gave predominantly mono- and dimethyl derivatives which were identical to those obtained by phase-transfer alkylation [3–5] and PTMA-CN yielded the monomethyl derivative almost exclusively. Phase-transfer methylation of sulfonamides produced the monomethyl derivative, however it was found that the phase-transfer methylation of three out of the four sulfonamides tested gave unsatisfactory yields. The direct on-column methylation efficiencies of PTMA-F and PTMA-CN were comparable to that obtained with the PTMA-OH but PTMA-CN showed far greater methylation selectivity than the corresponding fluoride or hydroxide. Therefore PTMA-CN appears to be the reagent of choice for the on-column derivatisation of sulfonamides. It is interesting to note that methylation using TTMA-OH gave predominantly dimethylated and monomethylated derivatives and therefore possesses a methylation selectivity similar to that of PTMA-F.

Methylation of sulfadimethoxine (**1c**) and sulfamethizole (**1d**) by both TMSO-OH and TMSO-F gave predominantly monomethyl derivatives but methylation efficiency was lower than that obtained for PTMA-F or PTMA-CN.

The variation in product patterns with various methylation reagents is shown in Fig. 6. The products and the apparent relative yields obtained from on-column methylation of a series of different sulfonamides at 250°C with PTMA-OH, PTMA-F, PTMA-CN, TTMA-OH, TMSO-OH and TMSO-F is shown in Table III.

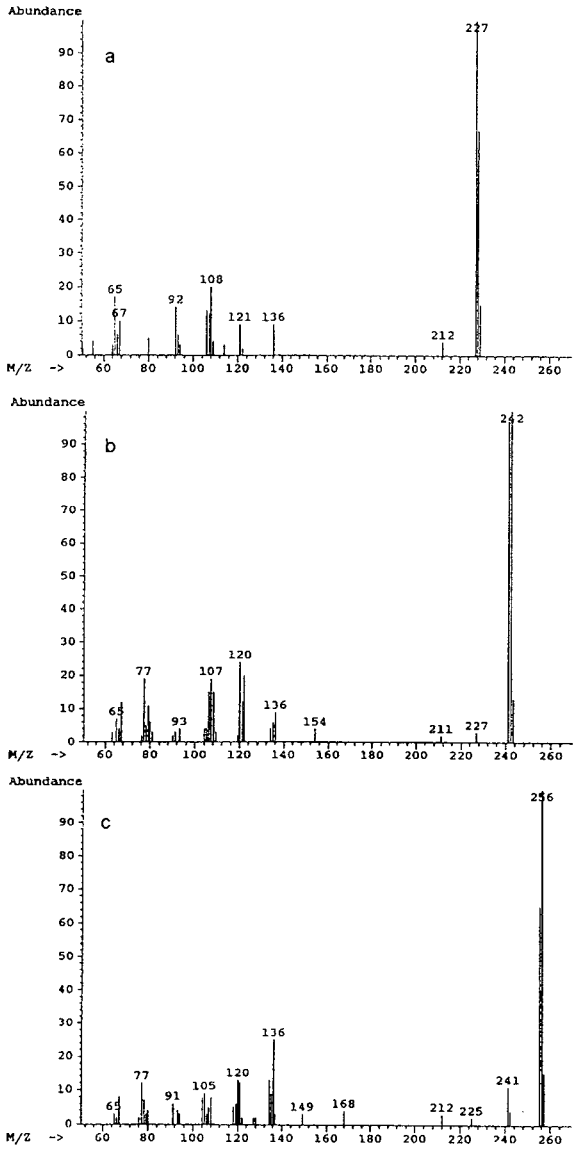

Fig. 5. The mass spectra of methylated sulfadimidines (monomethyl, **7a**, dimethyl, **8a** and trimethyl, **9a**).

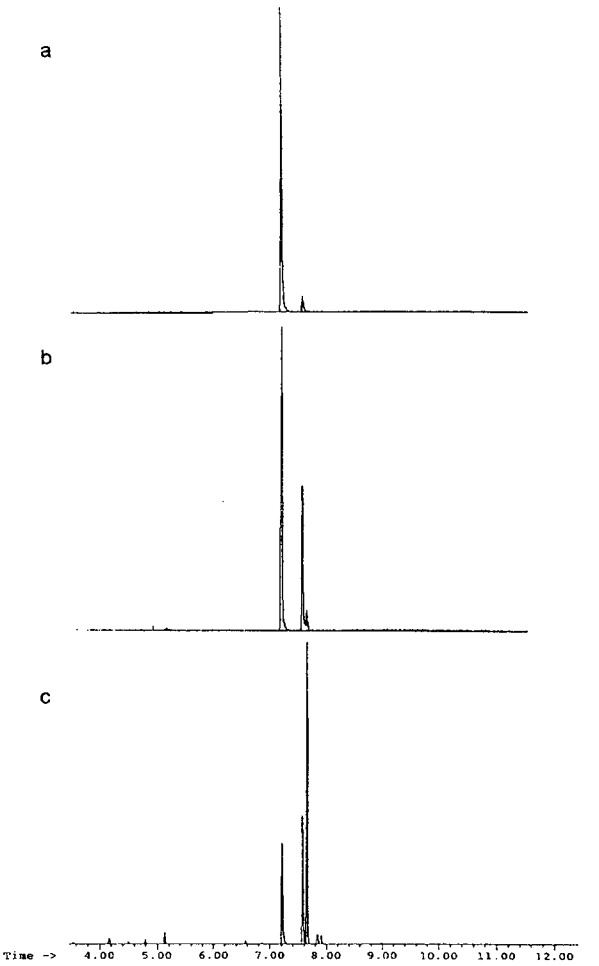

Fig. 6. The variation in product patterns in the methylation of sulfadimidine with three methylation reagents (PTMA-OH, PTMA-F and PTMA-CN). The three products in increasing retention time are **7a**, **8a** and **9a** (mono-, di- and trimethylation products). (a) PTMA-CN, (b) PTMA-F, (c) PTMA-OH. Time scale in min.

Benzimidazoles

In previous work [2] on the confirmation of the HPLC analysis of benzimidazoles by methylation with methyl iodide–potassium carbonate in acetone followed by GC–MS detection, the formation of two dimethyl benzimidazole derivatives was reported. The mass spectra of these derivatives were very similar and, although GC peaks were completely separated, the GC retention times were close and the alternative N,N′-dimethyl structures **10** and **11** were assigned to these substances.

We have studied the direct on-column methylation of a series of typical benzimidazoles with several different methylation reagents including phenyltrimethylammonium hydroxide, fluoride and cyanide salts. The results of this study are summarised in Table IV together with data on

TABLE III

COMPARISON OF THE METHYLATION OF SOME SULFONAMIDES WITH DIFFERENT ON-COLUMN METHYLATION REAGENTS

Sulfonamide	Monomethyl	Dimethyl	Trimethyl
Sulfadimidine (**1a**) (retention time, min)	7.26	7.62	7.70
PTMA-OH (% formed)	27	25	48
TTMA-OH (% formed)	40	32	28
PTMA-F (% formed)	63	29	8
PTMA-CN (% formed)	94	6	
TMSO-OH	100	low yield	
TMSO-F	100	low yield	
Extractive Me (%)	100	(good yield)	
Sulfaquinoxaline (**1b**) (retention time, min)	8.63	8.97	9.01
PTMA-OH (% formed)	36	36	28
TTMA-OH (% formed)	56	24	6
PTMA-F (% formed)	41	59	
PTMA-CN (% formed)	99	1	
TMSO-OH	96	4	(moderate yield)
Phase transfer Me (%)	100	(very poor yield)	
Sulfadimethoxine (**1c**) (retention time, min)	7.93	8.24	8.28
PTMA-OH (% formed)	13	32	55
TTMA-OH (% formed)	38	48	14
PTMA-F (% formed)	41	59	
PTMA-CN (% formed)	98	2	
TMSO-OH	100	25% yield of TMSO-F	
TMSO-F	95	5	(moderate yield)
Phase transfer Me (%)	100	(very poor yield)	
Sulfamethizole (**1d**) (retention time, min)	7.96	8.35	8.47
PTMA-OH (% formed)	13	38	49
TTMA-OH (% formed)	19	51	30
PTMA-F (% formed)	25	53	23
PTMA-CN (% formed)	91	9	
TMSO-OH	100		
TMSO-F	87	17	
Phase transfer Me (%)	100	(very poor yield)	

methylation using TTMA-OH, TMSO-OH and TMSO-F, respectively.

Methylations of benzimidazoles with PTMA-OH, PTMA-F and TTMA-OH are complex and produced up to six products. By contrast, PTMA-CN, TMSO-OH and TMSO-F yielded predominantly two dimethylated products suitable for confirmation purposes. TMSO-OH and TMSO-F are less aggressive methylation reagents than PTMA-OH and TTMA-OH and give similar product mixtures to those given by PTMA-CN, however the methylation efficiencies of the TMSO-derived reagents are less than that of PTMA-CN and therefore the use of TMSO-OH and TMSO-F offers no advantages over PTMA-CN either in methylation efficiency or

TABLE IV

COMPARISON OF THE METHYLATION OF SOME BENZIMIDAZOLES WITH DIFFERENT ON-COLUMN METHYLATION REAGENTS

Benzimidazole	Trimethyldecarbomethoxy-		Dimethyl		Dimethyl (rearranged)
Oxibendazole (retention time, min)	5.24	5.37	6.23	6.31	7.95
PTMA-OH (% formed)	21	18	14	14	33
TTMA-OH (% formed)	16	13	23	19	29
PTMA-F (% formed)	14	13	19	17	37
PTMA-CN (% formed)			48	52	
TMSO-F (% formed)	Monomethyl 5.83 min, m/z 263(M +)		Very poor yield		
Phase transfer Me (%)			49	51	
Albendazole (retention time, min)	6.12	6.29	6.96	7.11	8.11
PTMA-OH (% formed)	27	25	11	10	27
TTMA-OH (% formed)	20	19	20	23	18
PTMA-F (% formed)	19	16	19	18	28
PTMA-CN (% formed)			45	46	9
TMSO-OH (% formed)	Poor yield		45	55	
Phase transfer Me (%)			45	55	
Fenbendazole (retention time, min)	7.85	8.05	8.52	8.75	9.63
PTMA-OH (% formed)	29	32	12	14	13
TTMA-OH (% formed)	16	17	25	30	12
PTMA-F (% formed)	18	17	21	27	17
PTMA-CN (% formed)			45	55	
TMSO-OH (% formed)	Poor yield		45	55	
Phase transfer Me (%)			49	51	
Oxfendazole (retention time, min)	9.03	9.35	9.52	9.95	11.10
PTMA-OH (% formed)	32	28	14	13	10
TTMA-OH (% formed)	14	9	27	31	10
PTMA-F (% formed)	4	4	41	39	12
PTMA-CN (% formed)			48	52	
Phase transfer Me (%)			54	46	
Fenbendazole sulfone (retention time, min)			9.74	10.27	11.30
PTMA-F (% formed)			47	46	7
PTMA-CN (% formed)			70	48	
Phase transfer Me (%)			61	39	
Triclabendazole (retention time, min)			8.94	9.10	
PTMA-OH (% formed)			52	48	
TTMA-OH (% formed)			52	48	
PTMA-F (% formed)			50	50	
PTMA-CN (% formed)			51	49	
TMSO-OH			54	46	
Phase transfer Me (%)					

selectivity although optimum conditions for derivatisation by these reagents were not explored in this work.

Methylation of benzimidazoles with PTMA-CN gave the same two dimethylated products as those obtained by phase transfer methylation. These dimethyl derivatives produced almost identical mass spectra which were consistent with the alternative structures **10** and **11** whilst a third later eluting dimethyl benzimidazole produced during methylation with PTMA-OH, PTMA-F and TTMA-OH was assigned the symmetrical structure **12** on the basis of its mass spectrum. Thus, for oxibendazole, each derivative had predominant ions at m/z 277 (M^+) and 176 ($M^+ - C_3H_6 - COOCH_3$) with more minor fragments at m/z 235 ($M^+ - C_3H_6$), 234 ($M^+ - C_3H_7$) and 218 ($M^+ - COOCH_3$) consistent with structures **10a** and **11a**. By contrast, the third dimethyl derivative had a mass spectrum containing only three ions at m/z 277 (M^+), 246 ($M^+ - OCH_3$) and 204 ($M^+ - OCH_3 - C_3H_6$) which is more consistent with structure **12a** than with **10a** and **11a**.

In addition to the three dimethyl derivatives discussed above, direct on-column methylation of benzimidazoles with either PTMA-OH or TTMA-OH yield two additional products which elute earlier than the dimethyl derivatives discussed above. Thus oxfendazole gave two additional products with molecular ions at m/z 299 and similar mass spectra which corresponded to trimethyldecarbomethoxy derivatives. Both of these substances had the same major fragment ions. On this basis the unsymmetrical structures **13a** and **14a** were assigned to these products.

It can be seen in Table IV that there is a significant difference in methylation pattern obtained from direct on-column derivatisation which is dependent on the methylation reagent employed. Reagent selectivity increases in the order PTMA-OH < TTMA-OH < PTMA-F < PTMA-CN ≥ TMSO-OH(F). However, whilst PTMA-OH, TTMA-OH, PTMA-F and PTMA-CN give the same methylation efficiency, TMSO-OH and TMSO-F give lower methylation yields. Thus in terms of efficiency and selectivity PTMA-CN is the reagent of choice for the on-column methylation of benzimidazoles. The exception is triclabendazole which cannot undergo the rearrangement or degradation reactions of the other benzimidazoles and PTMA-OH, TTMA-OH or PTMA-F are equally satisfactory derivatising reagents for this substance. The results of methylation of albendazole (**2b**) and fenbendazole (**2c**) with three different methylation reagents are shown in Figs. 7 and 8 and the mass spectra of the three classes of methylated derivatives of oxibendazole (**10a**, **12a** and **13a**) are illustrated in Fig. 9.

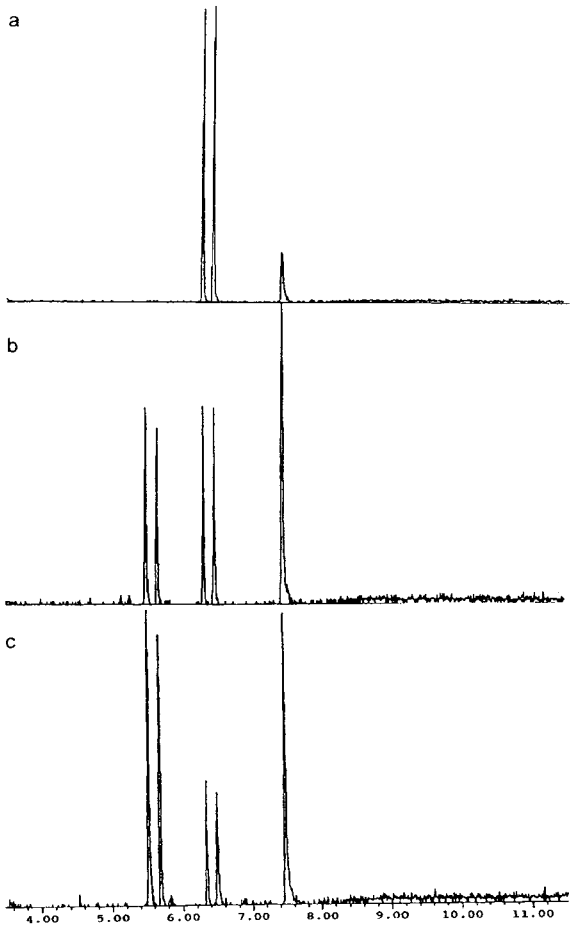

Fig. 7. The variation in product patterns in the methylation of albendazole with three methylation reagents (PTMA-OH, PTMA-F and PTMA-CN). The five products in increasing retention time are **13b**, **14b**, **10b**, **11b** and **12b**. (a) PTMA-CN, (b) PTMA-F, (c) PTMA-OH. Time scale in min.

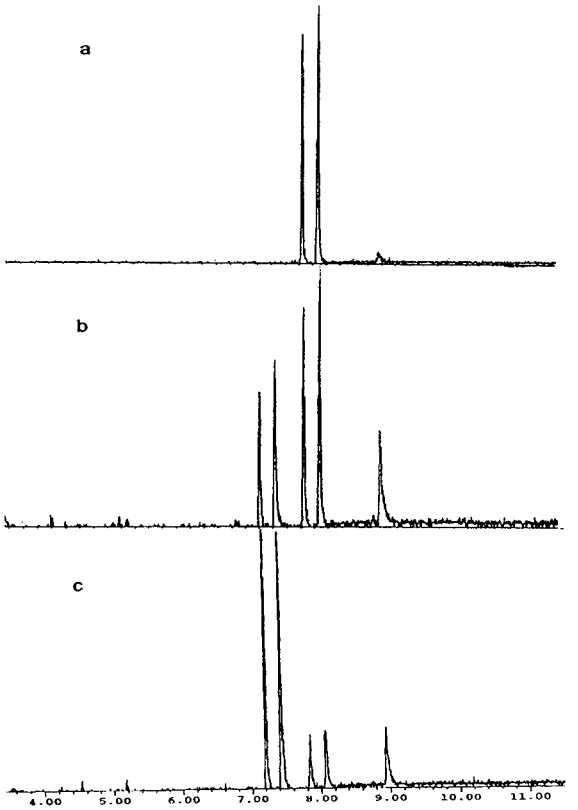

Fig. 8. The variation in product patterns in the methylation of fenbendazole with three methylation reagents (PTMA-OH, PTMA-F and PTMA-CN). The five products in increasing retention time are **13c**, **14c**, **10c**, **11c** and **12c**. (a) PTMA-CN, (b) PTMA-F, (c) PTMA-OH. Time scale in min.

Thiouracils

On-column derivatisation of thiouracils gave two dimethylated derivatives with all reagents whereas phase transfer methylation gave a single product identical to the later eluting dimethyl derivative. The structure **15** has been previously assigned to the phase transfer methylation product [12] but the structure of the second dimethylated derivative formed in on-column methylation is tentatively assigned the structure **16**. The results obtained from on-column methylation of thiouracils are shown in Table V. Although some methylation selectivity can be achieved by variation of the on-column derivatisation reagent, such selectivity is not great and no reagent is clearly superior for *in situ* derivatisation of this class of substances.

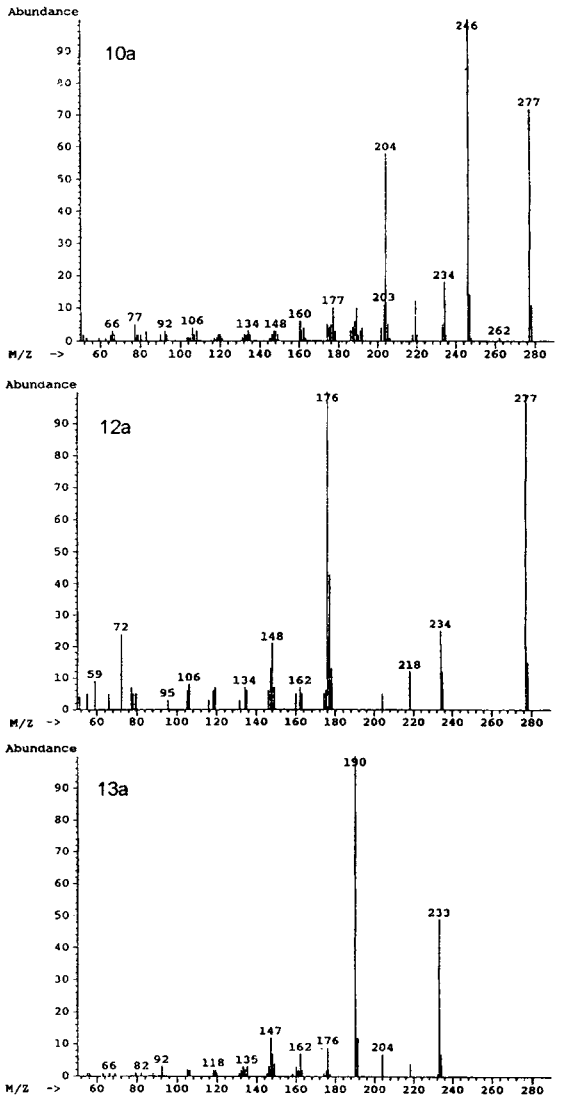

Fig. 9. The mass spectra of dimethylated oxibendazole (**10a**), the isomeric dimethylated oxibendazole (**12a**) and the trimethylated degradation product (**13a**).

CONCLUSIONS

It has been demonstrated that judicious choice of the derivatisation reagent used for direct on-column methylations can have a profound effect on the products produced, often with little effect on the overall methylation efficiency of the process.

MethElute (PTMA-OH) and MethPrep

TABLE V

COMPARISON OF THE METHYLATION OF SOME THIOURACILS WITH DIFFERENT ON-COLUMN METHYLATION REAGENTS

Derivatising agent	Thiouracil substituent	Product **15**		MS Fragmentation	Product **16**		MS Fragmentation
		%	Time (min)		%	Time (min)	
TMPA-OH	None	60	4.73	156 (100%), 141 (42), 126 (3), 125 (3), 111 (10), 110 (47), 95 (18)	40	6.18	156 (40%), 141 (5), 123 (4), 112 (15), 111 (100), 110 (28), 109 (73)
TMPA-F		45			55		
TMPA-CN		40			60		
TTPA-OH		45			55		
Phase transfer					100		
TMPA-OH	5-Methyl		5.80	170 (100%), 155 (37), 125 (9), 124 (39), 109 (14)		6.71	170 (66%), 155 (9), 127 (9), 126 (22), 125 (100), 124 (35), 123 (36), 109 (8), 95 (22)
TMPA-F		66			34		
TMPA-CN		33			67		
TTPA-OH		60			40		
Phase transfer					100		
TMPA-OH	5-Propyl	55	8.42	198 (100%), 183 (18), 170 (12), 169 (50), 110 (11), 96 (88)	45	9.50	198 (47%), 197 (20), 183 (30), 169 (100), 153 (16), 88 (15), 83 (25)
TMPA-F		45			55		
TMPA-CN		70			30		
TTPA-OH		45			55		
Phase transfer					100		
TMPA-OH	5-Phenyl	80	9.28	232 (100%), 217 (28), 186 (35), 171 (20), 145 (17), 129 (15), 128 (15), 102 (16)	20	10.16	232 (68%), 217 (8), 188 (10), 187 (60), 186 (28), 185 (25), 145 (18), 116 (20), 102 (18), 83 (100)
TMPA-F		45			55		
TTPA-OH		67			33		
Phase transfer					100		

(TTMA-OH) are perfectly satisfactory in the derivatisation of mono-functional compounds but produce mixtures, often very complex, when used for methylation of multi-functional substances.

PTMA-CN is readily prepared and is a far more selective alternative to MethElute for direct on-column methylation whilst still providing good yields of methylation products. Overall methylation efficiency is also dependent on the GC injector temperature whilst the condition of the injection liner can exert a significant effect on both methylation efficiency and selectivity.

ACKNOWLEDGEMENTS

The authors are grateful to Angelo Lisi for discussions on phase-transfer methylations and Robyn Clark for discussions on resin-assisted methylations of thiouracils. Thanks are also gratefully extended to the Australian Government Analyst, Dr. C.J. Dahl, for permission to publish.

REFERENCES

1 A.J. Manuel and W.A. Steller, *J. Assoc. Off. Anal. Chem.*, 64 (1981) 794.
2 A.M. Marti, A.E. Mooser and H. Koch, *J. Chromatogr.*, 498 (1990) 145.
3 A.M. Lisi, G.J. Trout and R. Kazlauskas, *J. Chromatogr.*, 563 (1991) 257.
4 A.M. Lisi, R. Kazlauskas and G.J. Trout, *J. Chromatogr.*, 581 (1992) 57.
5 O. Gyllenhaal, U. Tjarnlund, H. Ehrsonn and P. Hartvig, *J. Chromatogr.*, 156 (1978) 275.
6 I. Brondz and I. Olsen, *J. Chromatogr.*, 598 (1992) 309.
7 R.L. Crackel, D.J. Buckley, A. Asghar, J.I. Grayn and A.M. Booren, *J. Food Sci.*, 53 (1988) 1220.
8 H. Farber, S. Petdszus and H.F. Scholer, *Vom Wasser*, 76 (1991) 13.
9 H. Farber and H.F. Scholer, *J. Agric. Food Chem.*, 41 (1993) 217.
10 G. Gelbard and S. Colonna, *Synthesis*, (1977) 113.
11 D. Guggisberg, A.E. Mooser and H. Koch, *J. Chromatogr.*, 624 (1992) 425.
12 L. Laiten and P. Gaspar, *J. Chromatogr.*, 140 (1977) 266.

Journal of Chromatography A, 662 (1994) 139–146
Elsevier Science B.V., Amsterdam

CHROM. 25 667

Determination of pesticides in water by capillary gas chromatography with splitless injection of large sample volumes

Toshinari Suzuki*, Kumiko Yaguchi, Kazuo Ohnishi and Tatsunori Yamagishi

Tama Branch Laboratory, Tokyo Metropolitan Research Laboratory of Public Health, 3-16-25, Shibazaki-cho, Tachikawa-shi, Tokyo 190 (Japan)

(First received June 23rd, 1993; revised manuscript received October 21st, 1993)

ABSTRACT

A large-volume injection for a capillary gas chromatograph equipped with an electron-capture, nitrogen–phosphorus-selective (NPD) or flame photometric detector is proposed for the determination of pesticides. The cold-trap column, a deactivated fused-silica column (3 m × 0.53 mm I.D.), was attached to the analytical column (30 m) and the regulation column (3 cm), DB-5, both of 0.25 mm I.D. with film thickness 0.25 μm, with a dual-outlet splitter. The regulation column was connected with the solvent-diversion column, a deactivated fused-silica column (2 m × 0.53 mm I.D.), which was led out of the column oven and attached to an electromagnetic valve. By opening the valve in the splitless mode, the pesticides slowly injected in *n*-hexane in a volume from 25 to 150 μl were trapped in the cold-trap column, and a large volume of *n*-hexane was almost all diverted from the gas chromatograph through the diversion column. The trapped pesticides were introduced to the analytical column by closing the valve. Twenty-five pesticides, scattered on a golf course in Japan, were determined at concentrations from 1 to 100 ng/ml in *n*-hexane. The reproducibility of separation of the pesticides by the proposed method was similar to that of normal splitless (1-μl) injection. The proposed method was applied to the screening of the pesticides in groundwater after liquid–liquid extraction with dichloromethane; the pesticides could be determined at levels lower than 1 μg/l in a 20-ml water sample.

INTRODUCTION

Many contaminants in environmental waters that are thermally stable and volatile have been determined by capillary gas chromatography (GC) after sample enrichment by liquid–liquid [1–4] or solid-phase extraction [3–5]. If they contain a high-polarity group such as carboxyl or hydroxyl, they are determined by capillary GC after appropriate derivatization of those groups. The merits of capillary GC are high resolution, reasonable analysis times and sensitive and specific detection.

Various types of apparatus and techniques have been developed for the determination of the contaminants in water at trace levels, such as increasing the concentration factor from 500 to 1000 [1,2] and introduction of selected ion monitoring in GC–mass spectrometry [1,6]. In addition, injection of large sample volumes in capillary GC has been studied in the past decade. One of the major problems in this regard is the removal of the large volume of solvent from the capillary column and the quantitative retention of analyte compounds in the column. The injection techniques for large-volume sample injection are classified into several groups. In one of them, the separation of analytes from the solvent (*ca.* 100 μl) is performed in the capillary column, which is called on-column injection. This technique is mainly used in capillary GC coupled with liquid chromatography (LC–GC) [7–10]. In another, the separation of analytes from the solvent (*ca.* 200 μl) is performed before

* Corresponding author.

0021-9673/94/$07.00
SSDI 0021-9673(93)E1118-J

the capillary column using a programmed-temperature vaporizer [11], which is called a PTV injector, and a modified system [12,13]. These methods are mainly applied for the determination of alkanes [9–12] or polyaromatics [8]. Further, splitless injection for large sample volumes (*ca.* 30 μl) in capillary GC was recently reported [14]. In the method utilizing a splitless injector, complicated apparatus such as valve switching systems and remodelling of the GC set-up is unnecessary, and contamination in the capillary column by high-boiling compounds is less than that with on-column injection for large sample volumes.

The object of this work was the development of a large-volume (>100 μl) sample injection system for capillary GC to determine pesticides at the level of a few ng/ml. We designed a capillary GC system with splitless injection of large sample volumes and established the optimum conditions. The application of an analytical method involving this GC system coupled with liquid–liquid extraction could reduce the sample volume and organic solvent volume in the screening of the pesticides in groundwater.

EXPERIMENTAL

Apparatus

The GC system consisted of an HP 5890 gas chromatograph (Hewlett-Packard, Sunnyvale, CA, USA) equipped with a split–splitless injector and electron-capture (ECD), nitrogen–phosphorus-selective (NPD) or flame photometric detection (FPD) systems and a Shimadzu CR-4A integrator (Shimadzu, Kyoto, Japan). For the capillary inlet system, a glass insert of 1-ml volume was installed and the carrier gas was helium. The cold-trap column, a deactivated column (3 m × 0.53 mm I.D.) (GL Science, Tokyo, Japan) was connected to the analytical column (30 m) and the regulation column (3 cm), DB-5, both of 0.25 mm I.D. with film thickness 0.25 μm (J&W Scientific, Rancho Cordova, CA, USA), with a dual-outlet splitter (J&W Scientific) as shown in Fig. 1. The solvent diversion column, deactivated (2 m × 0.53 mm I.D.) (GL Science), was connected to the regulation column with a universal-type glass union

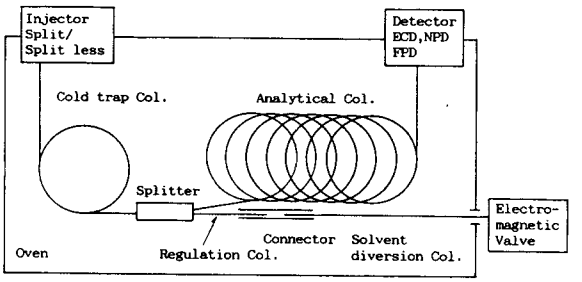

Fig. 1. Schematic diagram of the capillary GC system to divert large solvent volumes. Cold-trap column, deactivated fused-silica column, 3 m × 0.53 mm I.D.; analytical column, DB-5, 30 m × 0.25 mm I.D., film thickness 0.25 μm; solvent diversion column, deactivated fused-silica column, 2 m × 0.53 mm I.D.; splitter, dual-outlet type; connector, universal-type glass union.

(J&W Scientific) which was led out of column oven and connected to a three-way electromagnetic valve (GL Science) with a $\frac{1}{4}$-in. nut and graphite ferrule.

Chemicals

Butamifos, isoprothiolane, isoxathion and pyridaphenthion were purchased from GL Science and other pesticides from Hayashi Pure Chemical (Osaka, Japan), as listed in Table I. Organic solvents of pesticide grade were purchased from Wako (Osaka, Japan). Each of the 25 pesticides was dissolved in ethyl acetate–*n*-hexane (50:50, v/v) at a concentration of 1000 μg/ml, and then a pesticide mixture at a concentration of 10 μg/ml was diluted to ng/ml levels with *n*-hexane.

Chromatographic conditions

The oven temperature was always programmed as follows: held for 1 min at 40°C, increased from 40 to 180°C at 20°C/min and from 180 to 270°C at 4°C/min, and held for 2 min at 270°C. The injector was operated in the splitless mode with a splitless time of 1 min. The column head pressure was set at 100 kPa by the total mass flow controller of the gas chromatograph when the electromagnetic valve was closed. The injector temperature was set at 220°C. The temperatures for ECD, NPD and FPD were set at 300, 250, and 270°C, respectively. The septum purge flow-rate was 5 ml/min.

Injection procedures

The electromagnetic valve was set open and the head pressure was kept constant at the desired pressure by controlling the total mass flow controller of the gas chromatograph. Pesticide solution was slowly injected (manually) with a 250-μl gas-tight glass syringe in the splitless mode. The capillary GC and integrator operation were started when the electromagnetic valve had been closed after sample injection.

Sample preparation for groundwater

A 20-ml volume of groundwater spiked with pesticides standard was dispensed into a 30-ml separating funnel and 2 g of sodium chloride were added. The pesticides were extracted twice with 1 ml of dichloromethane, vigorously shaking for 1 min. The dichloromethane solution was dried with sodium sulphate and gradually evaporated off under a stream of nitrogen at room temperature. The extract obtained was dissolved in 1 ml of *n*-hexane.

RESULTS AND DISCUSSION

Diversion of solvent

We designed a solvent diversion system with splitless injection based on the difference in resistance (trapping efficiency) depending on the length of two DB-5 columns. When the electromagnetic valve was opened in the splitless mode with an injector temperature of 220°C and a column oven temperature of 40°C, the flow-rates of the carrier gas at the exits of the solvent diversion and analytical columns changed with the column head pressure, as shown in Fig. 2. The ratios of the flow-rate of the carrier gas in the analytical column to that in the diversion column were 1:200 and 1:240 at head pressures of 40 and 80 kPa, respectively. The total flow-rate which were fixed at the splitting ratio did not change during the injection of 100 μl of *n*-hexane at about 2.5 μl/s at any head pressure examined. The septum purge flow-rate, 5 ml/min, was also unchanged during injection of *n*-hexane in the splitless mode. Therefore, with the construction of the columns as shown in Fig. 1, the large amount of solvent vaporized in the injector could be passed through the cold-trap

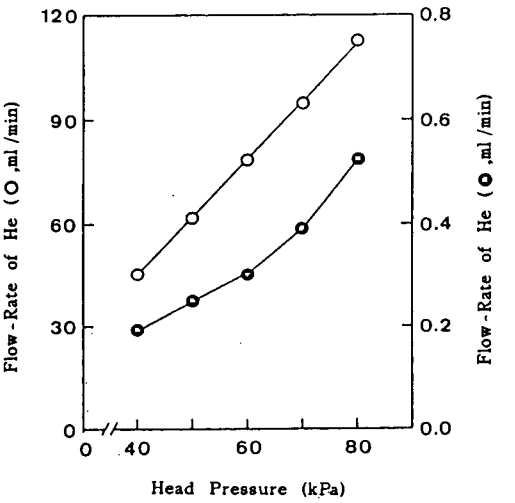

Fig. 2. Flow-rate of carrier gas at the exits of (●) analytical and (○) solvent diversion columns. Injection temperature, 220°C; oven temperature, 40°C; other conditions as in Fig. 1.

column and diverted from the analytical column through the solvent diversion column outside the gas chromatograph. In practice, the peak areas of the solvent on the FPD and NPD chromatograms with large-volume injection, as shown in Fig. 3B and C, respectively, corresponded to the peak areas from the splitless injection of about 3 μl of *n*-hexane.

Trapping of pesticides

The effect of the flow-rate of the carrier gas on the retention of analytes in the cold-trap column was examined. As shown in Fig. 4A, the retentions of dichlorvos, which is the most volatile of the pesticides examined (Table I), diazinone and butamifos decreased with increasing carrier gas flow-rate. The proposed method utilized recondensation of the analytes vaporized in the injector on the cold-trap column in the GC oven. When the flow-rate of the carrier gas in the column is high, the analytes may escape from the solvent diversion column. For trapping dichlorvos, the optimum flow-rate of the carrier gas, which was that of the solvent diversion column plus that of the analytical column, ranged from 40 to 60 ml/min.

The effect of varying the solvent diversion time on the retention of the analytes was examined. When the electric valve was opened for

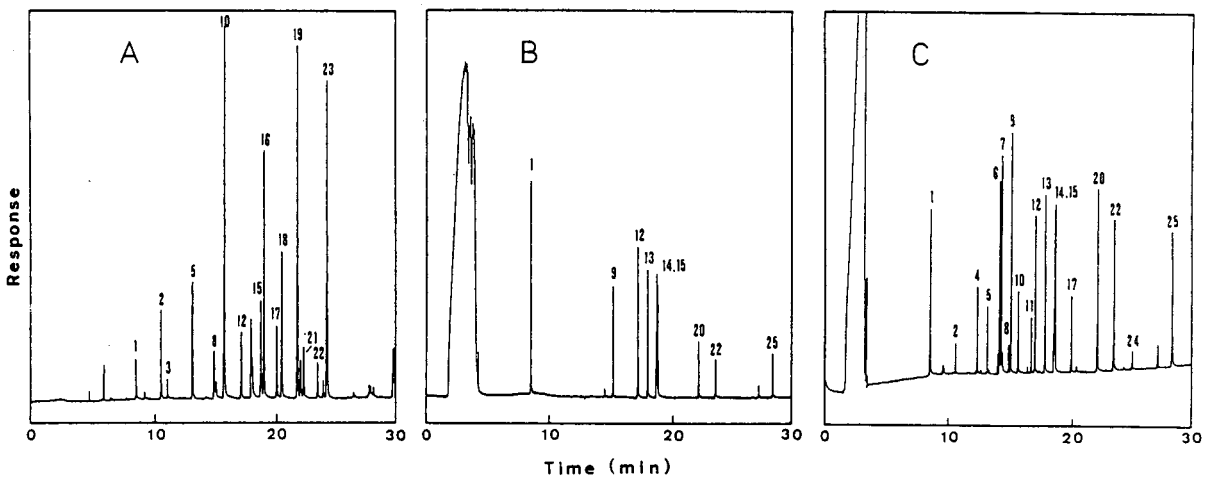

Fig. 3. Chromatograms obtained by large-volume injection of the extract from 20 ml of groundwater spiked with pesticides at 0.5 μg/l. Injection volume, 100 μl. (A) ECD; (B) FPD; (C) NPD. Injection conditions as in Fig. 5B. Numbers refer to Table I.

15 s after injection of 100 μl of the pesticide solution, dichlorvos was hardly detected (Fig. 4B). The retention of diazinon gradually decreased with increasing diversion time. Butamifos and pyridaphenthion were not affected by the diversion time. Hiller *et al.* [9] examined the effect of solvent diversion time with large-volume on-column injection, in which the optimum solvent diversion time was 0.25 min to trap hydrocarbons such as *n*-heptane and *n*-octane in

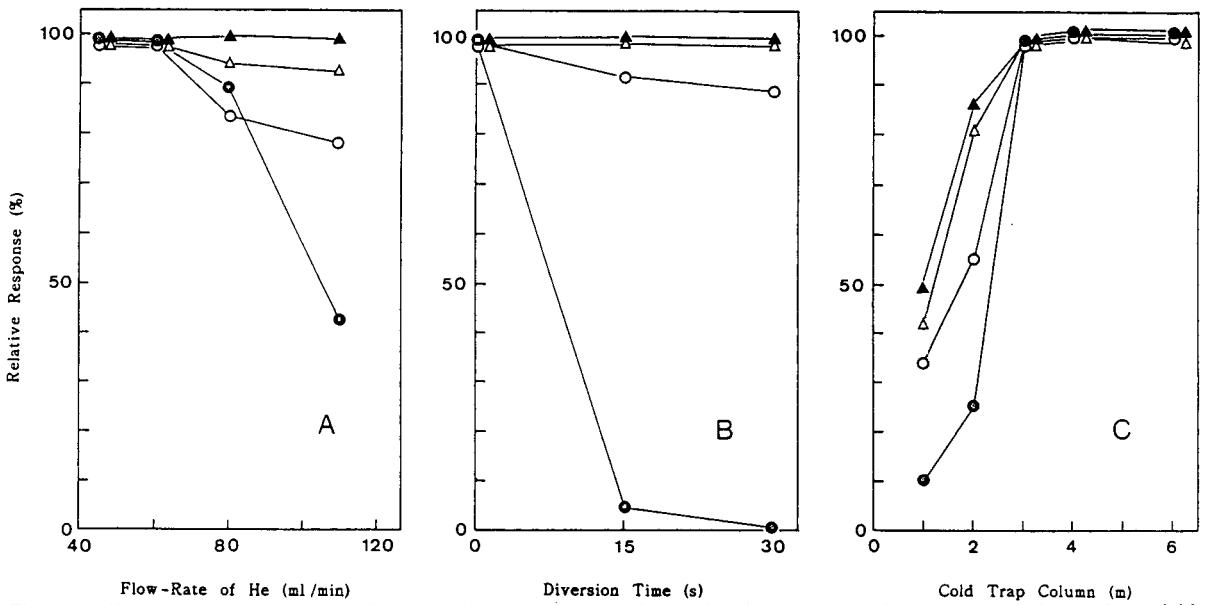

Fig. 4. Effects of flow-rate of carrier gas, diversion time and length of cold-trap column on retentions of pesticides. ● = Dichlorvos; ○ = diazinon; △ = butamifos; ▲ = pyridaphenthion. Injection temperature, 220°C; oven temperature, 40°C; injection volume, 100 μl; pesticide concentration, 10 ng/ml; injection speed, 2.5 μl/s; detection, FPD. (A) Cold-trap column, 3 m; diversion time, 0 s; (B) cold-trap column, 3 m; carrier gas flow-rate, 60 ml/min; (C) carrier gas flow-rate, 60 ml/min; diversion time, 0 s.

hexane [9]. With the splitless injection of large-volume samples reported by Tajima *et al.* [14], the optimum solvent diversion time was 0.3 min to trap *n*-dodecane in *n*-hexane. With the present method, to trap dichlorvos, etridiazole and chloroneb, it is necessary to close the valve immediately after sample injection.

The effect of the length of the cold trap column on the retentions of the analytes were examined. As shown in Fig. 4C, the retention of most of the pesticides examined was poor when using column lengths of 1 and 2 m. When the column length ranged from 3 to 6 m, trapping of the pesticides examined was not changed. In the splitless injection method of Tajima *et al.* [14] with the introduction of an SPB-1 precolumn (0.5 m × 0.53 mm I.D.; film thickness 0.5 μm) (Supelco, Bellefonte, PA, USA) to reconcentrate the analytes between the cold-trap and analytical columns, the optimum length of the cold-trap column was 2 m. For trapping low-volatility pesticides using only the cold-trap column, at least a 3-m length of deactivated fused-silica column is needed.

The effect of injection temperature on the retentions of the analytes was examined. An injector temperature of 180°C was insufficient to volatilize pyridaphenthion. With injector temperatures from 200 to 240°C, dichlorvos and pyridaphenthion, the first and last compounds on the chromatogram, respectively, were quantitatively recovered.

The effects of column oven temperature and injection speed on the trapping and separation of the pesticides are shown in Fig. 5. For trapping of the pesticides, the optimum oven temperature was 40°C (Fig. 5B). At 50°C, dichlorvos, etridiazole, chloroneb and benfluralin showed poor responses (Fig. 5C). When oven temperature was 30°C, the peak shape of each compound was distorted (Fig. 5A). Noy *et al.* [10] stated that this is due to recondensation of the solvent in the cold-trap column by means of a vaporizer as an LC–GC interface [10].

When the injection of a 100-μl sample was performed for 15 s (6.7 μl/s), the separation of each pesticide was incomplete, as shown in Fig. 5D. The optimum sample injection speed ranged from 2 to 3 μl/s under the conditions adopted.

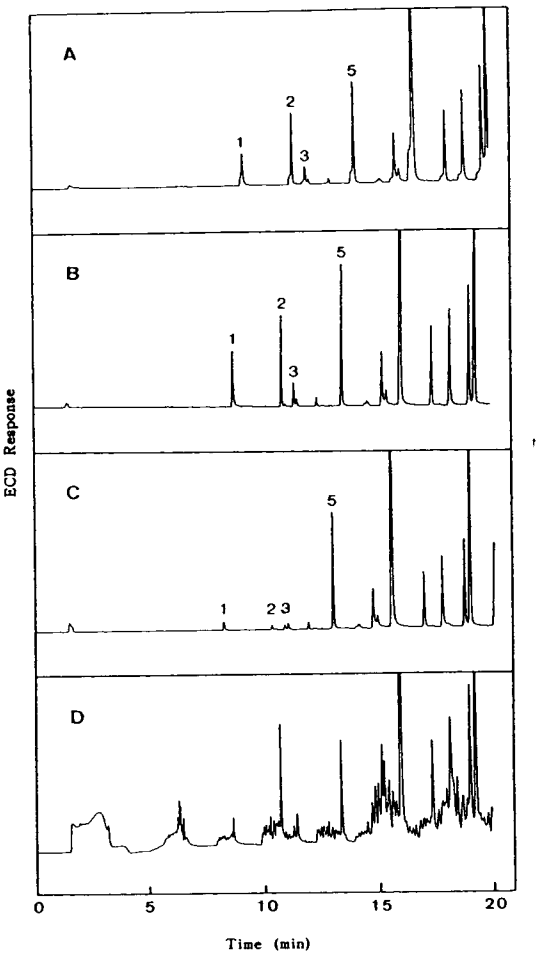

Fig. 5. Separation of pesticides by large-volume injection at altered GC oven temperature and injection speed. Cold trap column, 3 m; injection temperature, 220°C; injection volume, 100 μl; pesticide concentration, 10 ng/ml; carrier gas flow-rate, 60 ml/min; injection speed, 2.5 μl/s except for (D) 6.7 μl/s; diversion time, 0 s; detection, ECD. Oven temperature: (A) 30; (B) 40; (C) 50; (D) 40°C. Numbers refer to Table I.

Reproducibility of separation

The optimum conditions with large-volume injection to determine the pesticides were set as follow: injection temperature, 220°C; oven temperature, 40°C; cold-trap column length, 3 m; carrier gas (helium) flow-rate, 60 ml/min; valve close time, immediately after sample injection; and injection speed, *ca.* 2.5 μl/s. Under these conditions, the reproducibility of the separation of the pesticides was as reported in Table I. The

TABLE I

REPRODUCIBILITY OF SEPARATION OF PESTICIDES BY THE LARGE-VOLUME INJECTION METHOD COMPARED WITH THAT FROM THE SPLITLESS INJECTION METHOD[a]

No.	Pesticide[b]	Large-volume injection[d]			Splitless injection[e]		
		t_R (s)	$A \times 10^3$	$N \times 10^3$	t_R (s)	$A \times 10^3$	$N \times 10^3$
1	Dichlorvos	517.3(0.09)	21.7(9.8)	119	531.6(0.09)	42.0(2.0)	125
2	Etridiazole	642.0(0.05)	3.7(15.5)	226	659.6(0.20)	7.3(5.5)	239
3	Chloroneb[c]	675.1(0.05)	19.1(16.5)	202	686.0(0.09)	24.6(2.2)	200
4	Propoxur	749.0(0.02)	10.7(12.6)	249	768.5(0.12)	10.7(5.4)	262
5	Benfluralin	799.5(0.03)	8.4(8.6)	315	820.9(0.12)	10.4(5.8)	331
6	Simazine	860.1(0.02)	31.2(5.5)	327	881.5(0.12)	30.5(5.2)	344
7	Atrazine	869.2(0.02)	32.8(4.3)	336	890.8(0.12)	30.9(6.2)	352
8	Propyzamide	905.3(0.02)	4.3(7.4)	364	928.1(0.12)	3.2(6.3)	382
9	Diazinon	916.9(0.01)	34.3(6.1)	374	940.9(0.12)	41.3(3.9)	392
10	Chlorothalonil	953.4(0.01)	14.2(5.0)	404	977.0(0.11)	12.6(6.1)	423
11	Terbucarb	1017.0(0.02)	8.6(5.3)	460	1042.4(0.11)	8.0(4.5)	482
12	Tolclophosmethyl	1035.3(0.02)	26.2(4.9)	305	1061.0(0.11)	34.3(3.8)	320
13	Fenitrothion	1083.0(0.01)	31.5(5.3)	231	1108.9(0.10)	37.2(4.0)	242
14	Fenthion	1126.8(0.02)	27.9(3.2)	361	1153.4(0.09)	36.0(4.5)	378
15	Chlorpyrifos	1132.2(0.01)	28.3(5.3)	365	1159.5(0.09)	32.2(3.8)	382
16	Dactal[c]	1146.8(0.03)	220.0(5.2)	191	1173.0(0.05)	227.8(1.4)	195
17	Pendimethalin	1210.5(0.02)	13.7(6.3)	417	1238.1(0.09)	12.2(4.2)	435
18	Captan[c]	1236.2(0.03)	138.0(5.3)	302	1263.8(0.05)	77.8(5.8)	444
19	α-Endosulfan[c]	1313.9(0.03)	351.1(4.6)	192	1343.8(0.05)	358.0(2.0)	256
20	Butamifos	1330.4(0.01)	37.2(5.9)	350	1359.6(0.08)	40.1(4.8)	364
21	Isoprothiorane[c]	1345.3(0.03)	49.9(6.2)	357	1374.9(0.05)	43.0(1.8)	365
22	Isoxathion	1411.7(0.01)	29.7(6.6)	394	1441.6(0.07)	14.9(13.1)	410
23	β-Endosulfan[c]	1458.2(0.03)	325.9(4.5)	236	1489.9(0.05)	306.0(1.8)	242
24	Mepronil	1503.2(0.03)	3.2(8.0)	446	1532.2(0.07)	2.7(8.8)	463
25	Pyridaphenthion	1691.5(0.03)	26.8(6.2)	318	1721.6(0.06)	24.1(11.0)	329

[a] t_R = Retention time; A = peak area; N = plate number. Values in parentheses are relative standard deviations (%) ($n = 4$).
[b] Data from NPD ($n = 4$), except where indicated otherwise.
[c] Data from ECD ($n = 4$).
[d] 100 μl of 10 ng/ml solution in *n*-hexane.
[e] 1 μl of 1000 ng/ml solution in *n*-hexane.

theoretical plate number (N) and the relative standard deviation (R.S.D.) of the retention time (t_R) of each pesticide examined were similar to those using normal splitless (1 μl) injection. For the peak areas with large-volume injection, the R.S.D.s for dichlorvos, etridiazole, chloroneb, propoxur and benfluralin ranged from 9 to 17%, which is a poorer reproducibility than with the splitless method. In this experiment, injection of the sample and valve closing were performed manually; if these processes are carried out automatically, the R.S.D.s could be improved. The resolutions of simazine and atrazine for large-volume and splitless injection were 1.05 and 1.03, respectively, and those of fenthion and chlorpyrifos were 0.71 and 0.74, respectively.

The effect of injection volume on the retentions of the analytes was examined. Each plot of injection volume against peak area for each pesticide was linear from 25 to 150 μl at pesticides concentrations of 10 ng/ml ($r = 0.991$–0.999). Tajima *et al.* [14] reported that the maximum injection volume in the splitless mode was 30 μl when the sample was injected automatically at high speed and with a carrier gas flow-rate of 20 ml/min. Owing to the decrease of sample injection speed, the maximum injection volume in the proposed method is improved.

The present model is useful for injecting more than 100 μl of sample without a decrease in plate number and resolution of the pesticides, although the R.S.D.s of the retention of low-volatility pesticides such as dichlorvos, etridiazole, chloroneb and propoxur were more than 10%.

Screening of pesticides in groundwater

The application of the large-volume injection method to the determination of pesticides in groundwater samples was examined. The recovery data are reported in Table II. The recoveries of the pesticides were more than 73% at any pesticide concentration. The R.S.D.s of the recoveries of dichlorvos, etridiazole, chloroneb and propoxur ranged from 10 to 19% at 0.1 and 1.0 μg/l. Fig. 3 shows typical chromatograms obtained by injection of 100 μl of the extract from groundwater spiked with pesticides at a concentration of 0.5 μg/l. The chromatograms of the extracts were similar to those from pesticides standard solutions with respect to the plate number and retention time for each pesticide.

As environmental pollution by chemicals, including organic solvents, is of great public concern, it is preferable to be able to reduce the amounts of organic solvents used in laboratories when screening for levels of contaminants. With the normal splitless injection of a few microlites of sample, to determine pesticides at concen-

TABLE II

RECOVERY OF PESTICIDES (%) IN 20 ml OF GROUNDWATER BY THE LARGE-VOLUME INJECTION METHOD AFTER LIQUID–LIQUID EXTRACTION WITH DICHLOROMETHANE[a]

No.	Pesticide[b]	Fortification level (μg/l)		
		0.1	1.0	10.0
1	Dichlorvos	77.3 ± 16.4	85.4 ± 14.0	83.1 ± 5.2
2	Etridiazole	79.2 ± 18.9	76.7 ± 13.3	92.3 ± 1.9
3	Chloroneb[c]	90.2 ± 16.8	90.2 ± 17.1	100 ± 3.4
4	Propoxur	86.7 ± 11.5	83.4 ± 10.0	96.9 ± 1.2
5	Benfluralin	84.8 ± 10.3	87.0 ± 5.3	95.4 ± 3.9
6	Simazine	81.7 ± 10.4	86.1 ± 6.0	96.4 ± 2.1
7	Atrazine	84.1 ± 12.2	88.5 ± 5.2	92.1 ± 1.4
8	Propyzamide	73.3 ± 11.5	82.5 ± 9.2	98.2 ± 1.3
9	Diazinon	85.7 ± 10.0	90.9 ± 6.7	92.0 ± 3.9
10	Chlorothalonil	85.8 ± 9.4	91.0 ± 5.1	94.4 ± 4.9
11	Terbucarb	91.7 ± 14.4	91.1 ± 5.3	91.1 ± 1.4
12	Toluclophosmethyl	85.7 ± 7.2	92.8 ± 6.3	101 ± 2.4
13	Fenitrothion	82.4 ± 8.9	90.4 ± 4.2	94.2 ± 1.3
14	Fenthion	85.9 ± 11.0	93.5 ± 4.3	94.8 ± 1.6
15	Chlorpyrifos	85.9 ± 8.0	91.8 ± 4.3	92.9 ± 4.1
16	Dactal[c]	97.2 ± 2.9	91.9 ± 1.9	96.3 ± 1.5
17	Pendimethalin	90.0 ± 10.0	90.1 ± 6.4	99.5 ± 1.8
18	Captan[c]	87.2 ± 7.8	96.4 ± 4.9	102 ± 2.6
19	α-Endosulfan[c]	99.8 ± 3.0	89.3 ± 1.3	99.5 ± 1.7
20	Butamifos	93.0 ± 10.0	89.0 ± 3.6	96.1 ± 1.4
21	Isoprothiolane[c]	85.0 ± 6.4	98.0 ± 5.9	94.0 ± 3.0
22	Isoxathion	87.5 ± 16.0	87.8 ± 4.1	92.4 ± 1.6
23	β-Endosulfan[c]	89.4 ± 5.8	90.7 ± 4.0	102 ± 4.3
24	Mepronil	88.9 ± 9.6	86.9 ± 3.0	98.9 ± 3.5
25	Pyridaphenthion	93.8 ± 6.3	89.2 ± 8.0	89.8 ± 2.4

[a] Values are means ± S.D. ($n = 4$).
[b] Data from NPD, except where indicated otherwise.
[c] Data from ECD.

trations of 0.1 μg/l, a concentration factor from 500 to 1000 by liquid–liquid extraction with dichloromethane is needed. The injection of 100 μl of the extract from a water sample permits pesticide determinations at concentrations of 0.1 μg/l with a concentration factor of 20. In addition, this system is efficient with a capillary GC system equipped simply with a split–splitless injector without the need for complicated apparatus.

REFERENCES

1 V. Lopez-Avila, P. Hirata, S. Kraska, M. Flanagan, J.H. Taylor, Jr., and S.C. Hern, *Anal. Chem.*, 57 (1985) 2979–2801.
2 H.-B. Lee and Y.J. Stokker, *J. Assoc. Off. Anal. Chem.*, 69 (1986) 568–571.
3 A.M. Dietrich, D.S. Millington and Y.-H. Seo, *J. Chromatogr.*, 436 (1988) 229–241.
4 T. Okumura and K. Imanura, *Jpn. J. Water Pollut. Res.*, 14 (1991) 109–122.
5 A. Bacaloni, G. Goretti, A. Lagana, B.M. Petronio and M. Rotatori, *Anal. Chem.*, 52 (1980) 2033–2036.
6 H.-J. Stan, *J. Chromatogr.*, 467 (1989) 85–98.
7 E. Noroozian, F.A. Maris, M.W.F. Nielen, G.J. de Jong and U.A.Th. Brinkman, *J. High Resolut. Chromatogr. Chromatogr. Commun.*, 10 (1987) 17–24.
8 I.L. Davies, K.D. Bartle, P.T. Williams and G.E. Andrews, *Anal. Chem.*, 60 (1988) 204–209.
9 J.F. Hiller, T. McCabe and P.L. Morabito, *J. High Resolut. Chromatogr.*, 16 (1993) 5–12.
10 T. Noy, E. Weiss, T. Herps, H.V. Cruchten and J. Rijks, *J. High Resolut. Chromatogr. Chromatogr. Commun.*, 11 (1988) 181–186.
11 W. Vogt, K. Jacob, A.-B. Ohnesorge and H.W. Obwexer, *J. Chromatogr.*, 186 (1979) 197–205.
12 K. Grob and S. Brem, *J. High Resolut. Chromatogr.*, 15 (1992) 715–722.
13 K. Grob, S. Brem and D. Frohlich, *J. High Resolut. Chromatogr.*, 15 (1992) 659–664.
14 M. Tajima, N. Shimarura and M. Aoki, *J. Environ. Chem.*, 3 (1993) 446–447.

Journal of Chromatography A, 662 (1994) 147–152
Elsevier Science B.V., Amsterdam

CHROM. 25 698

Small-scale multi-residue method for the determination of organochlorine and pyrethroid pesticides in vegetables

H.B. Wan, M.K. Wong*, P.Y. Lim and C.Y. Mok

Department of Chemistry, National University of Singapore, Lower Kent Ridge Road, Singapore 0511 (Singapore)

(First received June 9th, 1993; revised manuscript received October 28th, 1993)

ABSTRACT

A simple and inexpensive multi-residue method is described for the determination of organochlorine and pyrethroid pesticides in vegetables. Pesticides in vegetables were extracted with ethanol and partitioned into toluene. A mini-column packed with 0.5 g of Florisil was used for further clean-up prior to gas chromatographic determination. The detection limits were 0.02–0.05 μg/g without concentrating the extract, which are below the maximum residue limits set by the Singapore government. The recoveries of the pesticides from fortified samples were 65–97% at the 0.1 μg/g level and 87–114% at the 0.5 μg/g level. The amounts of the reagents required for analysing one sample are only 100 ml of ethanol, 6 ml of toluene and 0.5 g of Florisil. Among fifteen vegetable samples collected from the Singapore local market and were analysed by this method, five were found to contain detectable amount of organochlorine pesticides. One sample contained 22 μg/g of endosulfan but the residue levels in other four samples were below 1 μg/g.

INTRODUCTION

A multi-residue method is required for a survey of pesticide residues in vegetables produced in Singapore and neighbouring countries. General methods for the determination of pesticide residues in plant samples require several hundred millilitres of organic solvents for one sample [1,2], leading to high analysis costs. Since the early 1980s, several methods that consume much less solvents have been reported. Consumption of solvents is considerably reduced by simplifying the analytical procedures [3] or by miniaturizing the scale of conventional methods [4–8]. Miniaturization is achieved either by replacing liquid–liquid extraction with solid-phase extraction [4] or by replacing the conventional column chromatographic clean-up with small cartridge clean-up [5–8]. As most of the reported small-scale methods for plant samples deal with only three to five pesticides [5–7], modification is required to obtain a small-scale method that can analyse for more pesticides simultaneously. In this work, we evaluated a small-scale multi-residue method for the determination of thirteen organochlorine and pyrethroid pesticides in vegetables. The method uses less toxic solvents and the solvent consumption is considerably decreased by adopting small-scale partitioning and mini-column clean-up. Some vegetable samples collected from the local market were analysed by this method.

EXPERIMENTAL

Materials

Technical-grade toluene and ethanol were redistilled before use. Florisil particle size 0.15–0.25 mm was heated at 400°C for 12 h and then deactivated by mixing with 4% (w/w) distilled

* Corresponding author.

0021-9673/94/$07.00
SSDI 0021-9673(93)E1145-P

water. Pesticide standards were of purity above 96% and were dissolved in toluene to prepare standard solutions. The chromatographic mini-column (12 × 0.5 cm I.D.) was of a similar size to a Pasteur pipette. An HP-5890A gas chromatograph (Hewlett-Packard) equipped with an electron-capture detector and a Megabore HP-5 column (12 m × 0.53 mm I.D., 2.65 μm film thickness) was used for the residue analysis.

Methods

A vegetable sample (60 g) was blended for 6 min with ethanol (100 ml) and extract was filtered through a Büchner funnel by suction. An aliquot of the filtrate (6 ml) was mixed with toluene (4 ml) in a 20-ml test-tube by bubbling the liquid for 3 min using a Pasteur pipette. The test-tube was allowed to stand for 20 min to obtain phase separation. The lower, ethanol layer was removed using a Pasteur pipette. The toluene layer was washed with saturated sodium sulphate solution (5 ml) by mixing the two phases using a Pasteur pipette. The upper, toluene layer was transferred to a chromatographic mini-column packed with Florisil (0.5 g) followed by anhydrous sodium sulphate (1 g). The column was eluted with toluene until 5 ml of the eluate had been collected. The eluate was analysed by gas chromatography under following conditions: injection port temperature, 270°C; detector temperature, 280°C; column temperature, programmed from 160°C (held for 10 min) to 235°C at 2°C/min; carrier gas, nitrogen; flow-rate, 13 ml/min.

Recovery study

Measured amounts of 10 μg/ml pesticide solution were added to 60 g of finely chopped vegetable in the blender jar to final concentrations of 0.1 and 0.5 μg/g (wet mass). The fortified sample was well mixed and blended for 6 min with 100 ml of ethanol. The extract was partitioned, cleaned up and measured gas chromatographically following the above procedures. The moisture content (W_m) of the vegetable was determined by heating 20 g of chopped vegetable at 105°C for 4 h and measuring the mass before and after the heating. The amount of the vegetable equivalent to 1 ml of extract (W_{eq}) was calculated using the equation

$$W_{eq} = 60/(100 + 60W_m)$$

If the moisture content is 90%, 6 ml of extract will be equivalent to 2.3 g of vegetable sample.

Sample analysis

Vegetable samples were purchased from a wholesale centre near the University. Most of the vegetables sold in Singapore are imported and redistributed at this centre. Some of the collected samples, such as lettuce, spring onion, spinach, leaf mustard and celery, were from the Cameron Highlands, West Malaysia, whereas cabbage mustard was from Johor, Malaysia.

The samples were analysed following the proposed procedures. The analysis of each sample was unreplicated. The identification of the chromatographic peaks was based on a comparison of the retention times with those for known compounds. Because a GC–MS system for confirmation was not available, samples with detectable amounts of pesticides were also analysed using an HP Ultra-2 capillary column (25 m × 0.32 mm I.D.). In addition, the samples were also examined using flame ionization detection (FID). The identity of each peak on the chromatogram with electron-capture detection (ECD) was further confirmed by comparing the response change between unknown and known samples where the detection, method was changed from ECD to FID.

RESULTS AND DISCUSSION

Evaluation of the method

Under the GC conditions, all the pesticides studied were well separated from each other on the wide-bore column (Fig. 1). Fenvalerate gave two overlapped peaks because of its geometric isomers. Its quantification was based on the sum of the heights of the two peaks. In addition to the wide-bore HP-5 column, an Ultra-2 capillary column (25 m × 0.32 mm I.D., 0.52 μm film thickness) was also tested. Although the Ultra-2

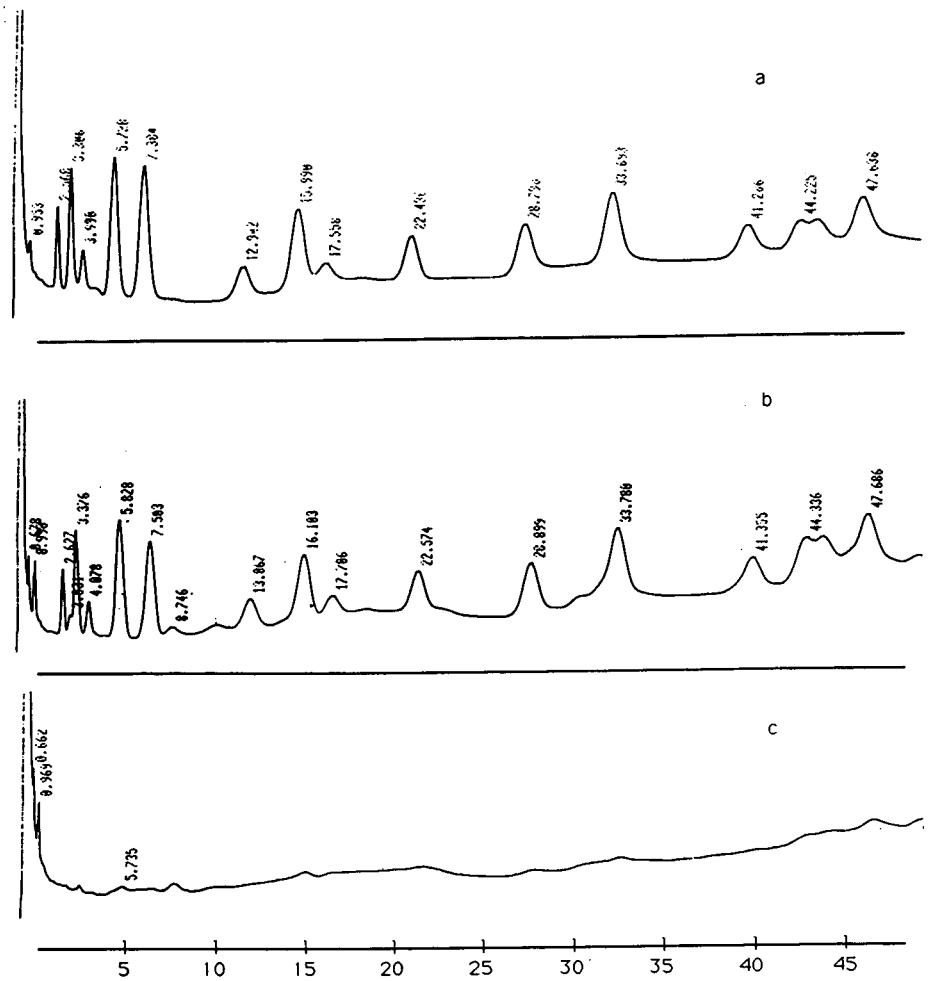

Fig. 1. Chromatograms of (a) standard solution containing α-BHC (2.6 min), γ-BHC (3.3 min), heptachlor (5.7 min), aldrin (7.4), α-endosulfan (12.9 min), DDE (16.0 min), endosulfan (17.6 min), DDT (22.4 min), biphenthrin (28.8 min), cyhalothrin (33.7 min), cypermethrin (41.3 min), fenvalerate (44.2 min) and deltamethrin (47.6 min) (0.1 ng each), (b) cabbage mustard fortified with pesticides at the 0.1 μg/g level and (c) cabbage mustard without adding pesticides. Injection volume: 2 μl. Time scale in min.

column gave better separations and peak shapes for the pesticides, the reproducibility of the analysis was much better when the wide-bore column was used. Therefore, in subsequent analyses the widebore column was used for quantitative analysis and the capillary column was used for confirmation.

The results of the recovery study are given in Tables I and II. The recoveries from Chinese cabbage were 65–95% at the 0.1 μg/g level and 87–113% at the 0.5 μg/g level. For cabbage mustard, the recoveries were 82–164% at the 0.1 μg/g level and 75–92% at the 0.5 μg/g level. The relative standard deviations were generally less than 10%. The recovery of fenvalerate from cabbage mustard at the 0.1 μg/g level was extraordinarily high (164%). A similar phenomenon has been reported with some organophosphorous pesticides [9,10], and the higher recoveries were attributed to matrix-induced re-

TABLE I

RECOVERIES OF PESTICIDES FROM CHINESE WHITE CABBAGE AND THE MAXIMUM RESIDUE LIMITS OF THE PESTICIDES IN LEAFY VEGETABLES SET BY THE SINGAPORE GOVERNMENT

Pesticide	Recovery (%)[a]		MRL[b] (mg kg^{-1})
	0.1 μg/g level	0.5 μg/g level	
α-BHC	79 ± 4	91 ± 9	
γ-BHC	81 ± 3	94 ± 10	0.5
Heptachlor	78 ± 4	89 ± 8	0.05
Aldrin	78 ± 3	91 ± 8	
α-Endosulfan	77 ± 9	92 ± 4	
β-Endosulfan	95 ± 3	112 ± 7	2
DDE	70 ± 3	91 ± 5	
DDT	69 ± 6	87 ± 21	0.2
Biphenthrin	80 ± 8	102 ± 4	
Cyhalothrin	67 ± 4	101 ± 7	
Cypermethrin	68 ± 8	110 ± 18	1
Fenvalerate	95 ± 11	113 ± 26	5
Deltamethrin	65 ± 4	104 ± 23	0.1

[a] Mean ± S.D. for three replicates.
[b] The MRL for DDT includes DDE and the MRL for endosulfan includes the two isomers and the corresponding sulphates.

sponse enhancement, in which the matrix protects the analytes from adsorption and/or decomposition in the hot injector [11]. In the present instance, the high recovery of fenvalerate was obtained only at low residue levels (0.1 μg/g). Therefore, the high recovery is probably due to the effects of some co-extractives with similar retention times. When the residue level of fenvalerate was very low, these effects became very significant.

TABLE II

RECOVERIES OF PESTICIDES FROM CABBAGE MUSTARD

Pesticide	Recovery (%)[a]	
	0.1 μg/g level	0.5 μg/g level
α-BHC	84 ± 4	81 ± 7
γ-BHC	85 ± 3	84 ± 6
Heptachlor	96 ± 1	83 ± 8
Aldrin	82 ± 2	85 ± 5
α-Endosulfan	112 ± 5	87 ± 8
β-Endosulfan	145 ± 4	92 ± 17
DDE	93 ± 2	79 ± 6
DDT	91 ± 5	76 ± 10
Biphenthrin	121 ± 3	85 ± 4
Cyhalothrin	115 ± 3	79 ± 7
Cypermethrin	115 ± 15	75 ± 11
Fenvalerate	164 ± 13	80 ± 11
Deltamethrin	123 ± 8	74 ± 9

[a] Mean ± S.D. for three replicates.

Typical chromatograms of fortified vegetable samples and blank vegetable samples are shown in Fig. 1. The results show that the clean-up procedure can remove most of the co-extractives affecting the GC determination. The detection limits calculated from the chromatograms of fortified samples were 0.02–0.05 μg/g, without concentrating the eluates. These detection limits are below the maximum residue limits (MRL) of the pesticides set by the Singapore government (Table I).

Compared with existing small-scale methods for plant samples, the present procedures are more similar to those reported by Joia *et al.* [6], except that the concentration step is omitted in the present method and the eluent benzene is replaced with the less toxic toluene. Joia's *et al.* method and the present method use Florisil mini-columns for clean-up, whereas other small-

TABLE III

ANALYTICAL RESULTS FOR COMMERCIAL VEGETABLE SAMPLES

Sample No.	Vegetable type	Pesticide detected	Residue level[a] (μg/g)
1	Chili (*Capsicum annum* var. *longum*)	α-Endosulfan	0.13
		β-Endosulfan	0.10
		DDE	0.29
2	Chinese boxthorn (*Lysium chinense*)		N.D.
3	Chinese celery (*Apium graveolens*)	α-BHC	0.12
		γ-BHC	0.82
		α-Endosulfan	0.57
		β-Endosulfan	0.16
		DDT	0.09
4	Chinese celery		N.D.
5	Chinese white cabbage (*Brassica chinensis*)		N.D.
6	Chinese white cabbage		N.D.
7	Chinese mustard (*Brassica juncea* var. *rugosa*)	α-Endosulfan	0.03
		β-Endosulfan	0.05
8	Choi-sam (*Brassica chinensis* var. *parachinensis*)	α-BHC	0.06
		γ-BHC	0.51
		α-Endosulfan	17.4
		β-Endosulfan	5.2
		DDT	0.09
9	Choi-sam		N.D.
10	Cowpea (*Vigna sinensis*)		N.D.
11	Cabbage mustard (*Brassica alboglabra*)		N.D.
12	Cabbage mustard		N.D.
13	Lettuce (*Lactuca sativa*)		N.D.
14	Spinach (*Spinacea oleracea*)		N.D.
15	Spring onion (*Allium fistulosum*)	α-Endosulfan	0.73
		β-Endosulfan	0.23

[a] N.D. = Residue level is below the detection limit (0.02–0.05 μg/g).

scale methods use cartridges prepacked with chemically bonded adsorbents. As this kind of cartridge is sometimes not affordable or not readily available in many Asian countries, a method that uses Florisil mini-columns is more practicable.

Analysis of vegetable samples

Among the fifteen vegetable samples collected and analysed, five were found to contain organochlorine pesticides (Table III). The pesticides found were endosulfan, benzene hexachloride (BHC), DDT and DDE. The residue levels were below 1.0 μg/g, except for one sample, which contained 22 μg/g of endosulfan. Such a high residue level could have been due to the short interval between spraying and harvest. No pyrethroid pesticides were found in any of the samples. It should be pointed out that the method used in this work is not sufficient for positive confirmation, although it can give reliable results for negative confirmation. Other methods, such as GC–MS, are required to produce more reliable results for the pesticides detected in the five samples.

ACKNOWLEDGEMENT

H.B. Wan thanks the National University of Singapore for the award of a research scholarship.

REFERENCES

1 E. Papadopoulou-Mourkido, *Residue Rev.*, 89 (1983) 179.
2 H.A. Moye, *Analysis of Pesticide Residues*, Wiley, New York, 1981, p. 263.
3 W. Liao, T. Joe and W.G. Gasick, *J. Assoc. Off. Anal. Chem. Int.*, 74 (1991) 554.
4 Y. Odanaka and N. Tomiyama, *J. Pestic. Sci.*, 16 (1991) 247.
5 S. Forbs, *Pestic. Sci.*, 16 (1985) 404.
6 B.S. Joia, L.P. Sarna and G.R.B. Webster, *Int. J. Environ. Anal. Chem.*, 21 (1985) 179.
7 C. Bicchi, A. D'Amato, I. Tonutti and M.T. Barbina, *Chromatographia*, 20 (1985) 219.
8 R.Z. Sapp, *J. Agric. Food Chem.*, 37 (1989) 1313.
9 L.J. Carson, *J. Assoc. Off. Anal. Chem.*, 64 (1981) 714.
10 A.M. Gillespie and S.M. Walters, *Anal. Chim. Acta*, 245 (1991) 259.
11 D.R. Erney, A.M. Gillespie and D.M. Gilvydis, *J. Chromatogr.*, 638 (1993) 57.

Journal of Chromatography A, 662 (1994) 153–166
Elsevier Science B.V., Amsterdam

CHROM. 25 692

System peaks and disturbances to the baseline UV signal in capillary zone electrophoresis

J.L. Beckers

Laboratory of Instrumental Analysis, Eindhoven University of Technology, P.O. Box 513, 5600 MB Eindhoven (Netherlands)

(Received September 15th, 1993)

ABSTRACT

Non-steady-state processes in capillary electrophoresis can be estimated by applying a steady-state mathematical model. Calculations with a steady-state model indicate that in capillary electrophoresis, moving boundary zones can originate from discontinuities in the concentration of the co-ions and/or the pH of the background electrolyte. Calculations showed that cationic moving boundaries with high mobilities originate with low system pH values. If the separation capillary and anode compartment are filled with electrolytes, different in concentration or pH, a shift of the baseline UV signal can occur. Block-shaped discontinuities in pH and/or concentrations split up in a migrating part with a mobility determined by the composition of the background electrolyte and a part migrating with the velocity of the electroosmotic flow at the position of the original disturbance. As a result, dips of the electroosmotic flow marker (low background concentration) split up and a negative system peak migrates through the system at low system pH values. Injections of high concentrations of background electrolyte or samples at high ionic strength lead to positive system peaks. These system peaks are, of course, only visible if the background electrolyte shows UV-absorbing properties. Experimentally determined data match the calculated values for these mobilities and baseline shifts.

INTRODUCTION

In the performance of electrophoretic experiments, mixed-mode effects can often be observed. In capillary zone elecrophoresis (CZE), *e.g.*, isotachophoretic (ITP) effects can act, and a specific choice of the electrolyte systems results in, *e.g.*, on-column transient and coupled column ITP preconcentration [1,2] and ITP/CZE [3]. Also other curious phenomena, linked with pH and concentration disturbances, are evident in CZE. Because UV detectors are often applied in CZE, phenomena related to concentration disturbances are only observable on applying background electrolytes with UV-absorbing properties (indirect UV mode). Often pH and concentration disturbances originate from a different composition of the electrolytes in the capillary and electrode compartments and cause system peaks, baseline shifts and unstable baselines. Vinther *et al.* [4] observed a jump in the baseline UV absorbance signal from one stable level to another at the position of the electroosmotic flow (EOF) marker. Beckers and Ackermans [5] reported a reversed migration behaviour due to pH disturbances in CZE as a result of an imbalance of the hydrogen mass balance. Disturbances by an imbalance of the hydrogen mass balance can be expected on applying background electrolytes at low or high pH. In this paper, the presence of system peaks and shifts in the baseline of the UV signal originating from discontinuities in pH and concentration of the co-ions in background electrolytes are discussed.

EXPERIMENTAL

For all CZE experiments, a P/ACE System 2000 HPCE instrument (Beckman, Palo Alto, CA, USA) was used. All experiments were carried out applying a Beckman eCAP capillary tubing (75 μm I.D.) with a total length of 46.7

0021-9673/94/$07.00
SSDI 0021-9673(93)E1150-X

cm and a distance between injection and detection of 40.0 cm. The wavelength of the UV detector was set at 214 nm. The operating temperature was 25°C and all experiments were carried out applying 15 kV, unless stated otherwise. Sample injection was performed by applying pressure injection where a 1-s pressure injection equals an injection amount of *ca.* 6 nl and an injected length of 0.136 cm. Data analysis was performed using the laboratory-written data analysis program CAESAR.

RESULTS AND DISCUSSION

System peaks

In CZE experiments, in the indirect UV mode, peaks of the electrosmotic flow marker split up on applying background electrolytes at low pH and a system peak appears. As an example, in Fig. 1A the electropherogram is given of the separation of the 5-s pressure injection of a mixture of 0.0001 *M* potassium, sodium, tetramethyl- (TMA), tetraethyl-(TEA) and tetrabutylammonium (TBA) ions applying a background electrolyte of 0.005 *M* histidine adjusted to pH 5.0 by adding formic acid. The system peak (sharp at the front and diffuse at the rear) is also present on injecting pure water (see Fig. 1B). Such a system peak can be characterized by a mobility with a value determined by the composition of the background electrolyte. In Fig. 2, some electropherograms are given 5-s pressure injections of pure water applying background electrolytes of 0.01 *M* histidine adjusted to different pHs by adding acetic acid. It can be seen that the mobilities of the system peaks increase at low pH. To demonstrate the effect of the composition of the injected solution, in Fig. 3 the electropherograms are given for 5-s pressure injections of several dilutions of the background elecrolyte 0.01 *M* histidine adjusted to pH 3.8 by adding formic acid. The system and the EOF peaks are always present on injecting dilute background electrolytes, whereas on injecting pure background electrolytes small baseline disturbances mark the positions of these peaks. Although the migration times of the peaks can vary, owing to varying mobilities of

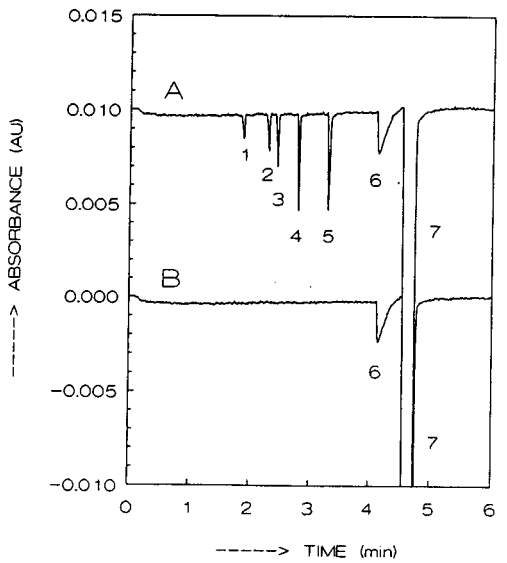

Fig. 1. Electropherograms of (A) the separation of the 5-s pressure injection of a mixture of 0.0001 *M* (1) potassium, (2) sodium, (3) tetramethyl-, (4) tetraethyl- and (5) tetrabutylammonium ions and (B) the 5-s pressure injection of pure water, applying a background electrolyte of 0.005 *M* histidine adjusted to pH 5.0 by adding formic acid. The EOF peak (7) splits up and a system peak (6) appears.

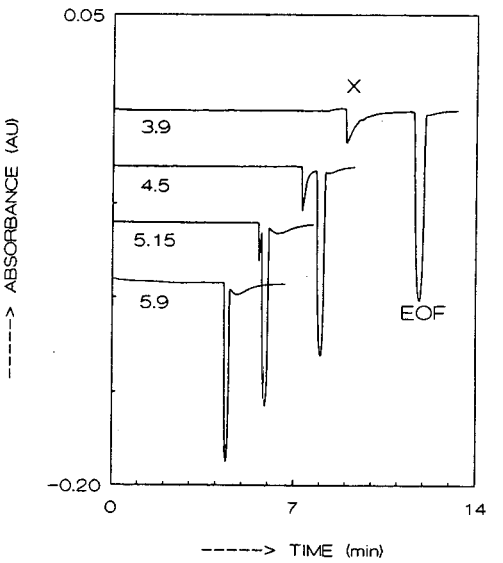

Fig. 2. Electropherograms for 5-s pressure injections of water in background electrolytes of 0.01 *M* histidine adjusted to different pHs by adding acetic acid. The numbers refer to the pH of the background electrolyte solutions. System peaks X show higher and EOF peaks show lower mobilities at lower pH.

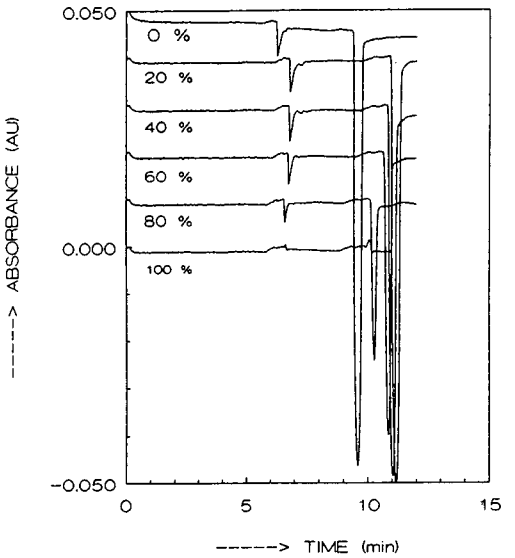

Fig. 3. Electropherograms for 5-s pressure injections of several dilutions of background electrolyte. The percentages are the concentrations of background electrolyte used for the injection. The background was 0.01 *M* histidine adjusted to pH 3.8 by adding formic acid.

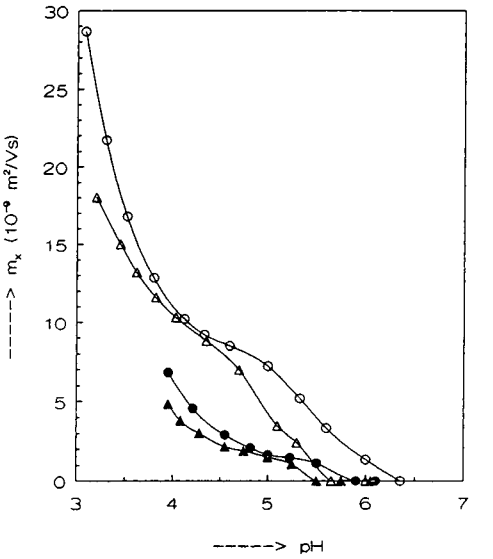

Fig. 4. Measured mobilities of system peaks X as function of the pH of background electrolytes consisting of 0.01 *M* imidazole with the pH adjusted by adding (○) formic acid and (●) acetic acid and of 0.01 *M* histidine with the pH adjusted by adding (△) formic acid and (▲) acetic acid.

the EOF, the mobilities of the system peaks were constant. In Fig. 4 the measured mobilities of the system peaks, for 5-s pressure injections of water, are given for background electrolytes of 0.01 *M* histidine and 0.01 *M* imidazole adjusted to different pH values by adding formic and acetic acid. The mobilities increase at lower pH and with formic acid. On applying background electrolytes without UV-absorbing properties such as 0.01 *M* potassium formate and acetate at different pHs, such system peaks cannot be observed.

In ITP experiments hydrogen ions can act as a terminator [6–8]. Sharp zone boundaries are typical for ITP zones. Because the system peaks are sharp at the front and diffuse at the rear, in the first instance the origin of these peaks was ascribed to a local disturbance of the zone electrophoretic process and a local ITP terminating effect was assumed. With a mathematical, model, described previously [8], the mobilities of terminating hydrogen zones for the electrolyte systems used in Fig. 4 were calculated. In Fig. 5 the calculated mobilities of the terminating hydrogen zones are given and it can be concluded

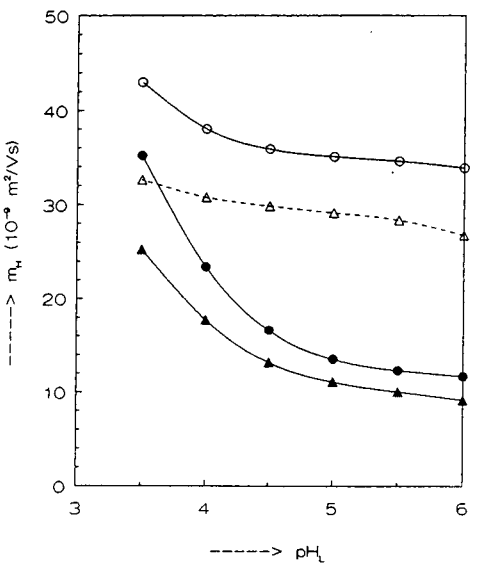

Fig. 5. Calculated mobilities of terminating hydrogen zones in ITP as function of the pH of the leading electrolyte for the systems used in Fig. 4. The dashed line indicates a non-steady-state ITP.

that these values are much higher than those of the measured system peaks from Fig. 4, indicating that the system peaks are caused by another effect.

Disturbances to baseline UV signal

Because the system peaks are only present at low pHs of the background electrolytes and their mobilities increase at lower pH, we thought that the system peaks were related to a pH shift migrating through the capillary. To study the effect of a pH shift, electropherograms were measured on applying a background electrolyte at the inlet side (anode) consisting of the same concentration of the cationic species in the separation capillary but at a different pH. In Fig. 6 the electropherograms are given for 5-s pressure injections of water, filling the cathode compartment and capillary with the background electrolyte 0.01 *M* histidine adjusted to pH 3.8 by adding formic acid and filling the anode compartment (inlet side) with 0.01 *M* histidine

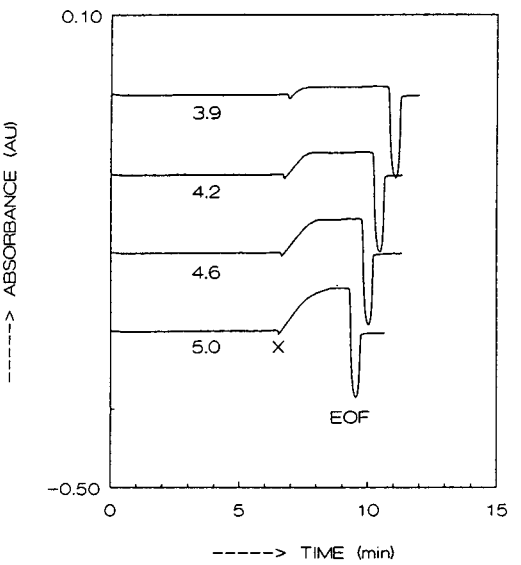

Fig. 6. Electropherograms for 5-s pressure injections of water, filling the cathode compartment and separation capillary with the background electrolyte of 0.01 *M* histidine adjusted to pH 3.8 by adding formic acid and filling the anode compartment (inlet side) with 0.01 *M* histidine adjusted to different pHs by adding formic acid. The numbers refer to the pH in the anode compartment. Shifts in baseline UV signal are obtained from the position of system peaks X to EOF marker.

adjusted to different pHs by adding formic acid. Surprisingly, diffuse disturbances of the baseline were present, between the system peaks X as described earlier (and with the same mobility) and the EOF marker. The UV absorbances of the leading and terminating electrolytes are nearly equal. Without the injection of water the dip of the system peak disappeared, but the shift of the baseline started at the same position. The migration times of the system and EOF peaks differ for larger differences between the pHs of electrolytes in the separation capillary and anode compartment, because the mobility of the EOF of the electrolyte in the anode compartment is higher, ultimately resulting in a higher overall EOF in the separation capillary. The disturbance to the baseline (increase in UV signal) is stronger for larger differences in pH of the electrolytes in the capillary and anode compartment. Because the measurements show that the UV absorbances for equimolar solutions of histidine at different pHs between 3 to 6 are nearly equal, the increase in the UV signal of the baseline must be caused by an increase in the concentration of histidine. This means that on applying electrolytes at different pH values ($pH_L < pH_T$) in the capillary and anode compartment a diffuse zone of increasing concentration of histidine appears between the position of the system peak and the EOF marker.

Mathematical model

The electrophoretic separation mechanism can approximately be described by Kohlrausch's regulation function, originally derived for strong monovalent ions [9]. Dismukes and Alberty [10] showed that this regulating function also can be applied for weak monovalent ionic species and is often applied for electrophoretic calculations in the form

$$\sum_i \frac{\bar{c}_i}{m_i} = \omega \qquad (1)$$

where $\bar{c}_i$ and m_i represent the total concentrations and absolute values of the effective ionic mobilities of all components present in the electrolyte solution and the numerical value of the Kohlrausch's function ω is locally invariant with time [11], under certain conditions.

In isotachophoresis, sample components are separated using a leading and terminating electrolyte and the application of Kohlrausch's law gives, for strong monovalent ionic species,

$$c_A = c_L \cdot \frac{m_A(m_L + m_C)}{m_L(m_A + m_C)} \quad (2)$$

where c and m represent the ionic concentrations and absolute values of the ionic mobilities of the sample component A, leading ions L and buffering counter ions C.

Often a steady-state model [8], including corrections for the effect of pH and relaxation and retardation effects on the mobilities, is used and generally four equations are needed to calculate all parameters of the zones, *viz.*, the modified Ohm's law, the buffer balance, the electroneutrality equation (EN) and the isotachophoretic condition (IC). In such a model it is assumed that all parameters of the proceeding zones are determined by the composition of the leading electrolyte, via the buffer balance and isotachophoretic condition. Original compositions of terminating and sample solutions are of no importance. Applying the steady-state model, Kohlrausch's law is implicitly obeyed and ω values are fairly constant for all zones both for cationic and anionic systems.

Considering the electrophoretic experiments in Fig. 6, where the separation capillary is filled with a leading electrolyte L and the anode compartment with a terminating electrolyte T, consisting of the leading ion at the same concentration but at a higher pH (see Fig. 7), an adapted zone L′ should be formed between the zones T and L with exactly the same composition as L, applying the steady-state model for ITP, *i.e.*, the shift of the baseline of the UV signal cannot be explained with the steady-state model. Also, the application of Kohlrausch's law, under the assumption that the pH in zone L′ is high (a low hydrogen concentration), resulting in a small increase in the concentration of histidine, cannot explain the large increase in histidine concentration.

However, the increase in histidine concentration in the extra zone X can be fairly easily explained. The contribution of the hydrogen ions

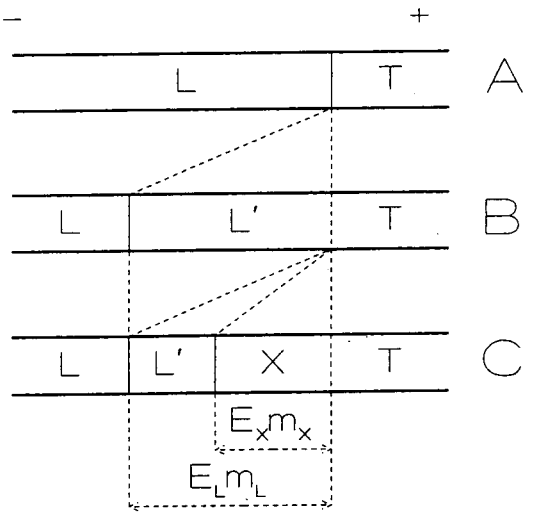

Fig. 7. (A) If the cathode compartment and the separation capillary are filled with a leading electrolyte L and the anode compartment with a terminating electrolyte T with the same co-ion at the same concentration but at a higher pH, (B) an adapted zone L′ with a composition identical with that of the leading electrolyte L should be formed between the leading and terminating zones, according to the steady-state model in ITP. (C) In practice, an extra zone X at higher concentration is formed if there is an imbalance between the mass transport of the co-ions between the leading and terminating zones due to a large difference in pH.

in zone T to the conductivity is much smaller than that in zone L and because the ionic concentrations of histidine and counter ions are nearly constant, the zone resistance and hence the electric field strength E are higher in zone T. Therefore, the amount of histidine coming from zone T is higher than needed to substitute the histidine ions of the moving zone L and an extra zone X at higher histidine concentration is created (see Fig. 7C). This zone X can be characterized by a mobility m_X depending on several parameters. From the experiments it appeared that the value of m_X is smaller than that of m_L, therefore it is assumed in the model that the moving zone L is partly elongated with a zone L′ with the same composition as that of zone L and partly substituted by zone X.

In the first instance, a steady-state model was set up for the calculation of the parameters of zone X. The reduced number of parameters is five for zone X, *viz.*, the total concentrations of the histidine and counter ions, E, pH and m_X.

The equations are the EN, modified Ohm's law and the mass balances of histidine, counter ions and hydrogen ions. Calculations with this model did not give significant results. Because the length of zone X increases with time and can be very long, it is unlikely that a surplus of histidine at the T side will influence the mobility of zone X at the L side. Therefore, a model was set up with the same five parameters, but not handling mass balances over the whole of zone X but only over the front side of zone X and assuming that the X–T boundary is a concentration boundary. Also with this model it was not possible to satisfy the hydrogen balance. Bearing in mind that also in the steady-state calculation of ITP the mass balance of the hydrogen ions is not used, the parameters of zone X are approximately calculated in the following way. The total concentration of histidine is assumed in zone X, through which the unknown parameters are only four, *viz.*, the total concentration of the counter ions, pH, m_X and the E gradient. For the calculation of these parameters the mass balances of the buffer and the co-ions, the modified Ohm's law and the EN are used. The mass balance of the hydrogen ions was not taken into account. In the calculations the following equations are used.

Mass balance of the co-ions. For the derivation of the mass balance only the effect in front of zone X is taken into account (see Fig. 8A) and the equations are given for two adjacent zones with total concentrations of the co-ions A of $\bar{c}_{A,L}$ and $\bar{c}_{A,X}$, respectively. The zone boundary z is assumed to move over a distance $E_X m_X$ in unit time. Co-ions A at time $t = 0$ present at point 1 will just reach the boundary z at time $t = 1$ and move a distance $E_X m_{A,X}$. Co-ions A at time $t = 0$ present at the zone boundary z will reach point 2 at $t = 1$ and migrate a distance $E_L m_{A,L}$. The amount of co-ions A present between point 1 and zone boundary z in zone X, at $t = 0$ (amount Q_1) will be present in zone L at $t = 1$ between the zone boundary z and point 2 (Q_2). The mass balance of the co-ions A will therefore be

$$(E_X m_{A,X} - E_X m_X)\bar{c}_{A,X} = (E_L m_{A,L} - E_X m_X)\bar{c}_{A,L} \quad (3)$$

Mass balance of the counter ions C. The migration paths for the counter ions C are given in Fig. 8B. Counter ions C present at $t = 0$ at point 3 will just reach the zone boundary z at $t = 1$ and the counter ions C present at the zone boundary z at $t = 0$ will reach point 4 at $t = 1$. The migration distances are $E_L m_{C,L}$ and $E_X m_{C,X}$, respectively. The amount of counter ions C between point 3 and z in zone L at $t = 0$ (Q_1) will be present between z and point 4 in zone x at $t = 1$ (Q_2) and the mass balance of the counter ions C will therefore be

$$(E_L m_{C,L} + E_X m_X)\bar{c}_{C,L} = (E_X m_X + E_X m_{C,X})\bar{c}_{C,X} \quad (4)$$

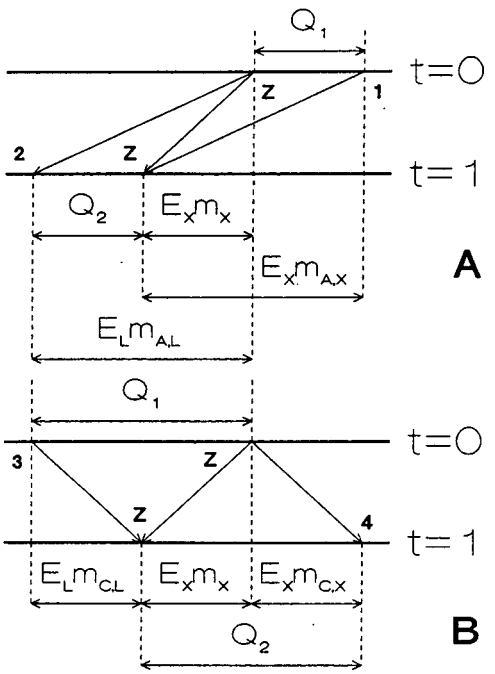

Fig. 8. Migration paths for (A) co-ions A and (B) counter ions C over a zone boundary z between leading zone L and zone X. For further explanation, see text.

The principle of electroneutrality. In accordance with the principle of electroneutrality, the arithmetic sum of all products of the concentration of all forms for all species and the corresponding valences, present in each zone, much be zero [8].

Modified Ohm's law. According to Ohm's law, the product of E and σ must be constant for all zones. The overall electrical conductivity, σ,

of a zone is the sum of the values $c|mz|F$, where z and F represent the valency of the ionic species and Faraday constant.

Procedure of calculation. The parameters of zone X are calculated in the following way. The concentration $\bar{c}_{A,X}$ is assumed. Then a pH is taken whereby all effective mobilities can be calculated and with the EN the total concentration of the counter ions $\bar{c}_{C,X}$ can be found. The zone conductivity can be calculated and with Ohm's law E can be obtained. With the mass balance of the co-ions A a value for m_X can be calculated and also with the mass balance of the counter ions C an m_X value can be obtained. For the correct pH the m_X values must be identical.

Significance of the model. In Fig. 9 the values of m_X and the ratio E_X/E_B of the electric field strengths in zone X and the background electrolyte B (right-hand scale), calculated with this model, are given as function of assumed $c_{HIST,X}$ values varying from 0.005 to 0.007 M histidine for a background electrolyte consisting of 0.006 M histidine adjusted to pH 3.5 by adding formic acid. From Fig. 9 some interesting conclusions can be drawn. If in the background electrolyte a zone is present where the co-ions have a concentration different from that of the background electrolyte, this concentration disturbance migrates through the system with a specific mobility m_X. Note that this means that the ω value according to Kohlrausch's law is locally not invariant with time. The mobilities m_X of zones with concentrations lower than that of the background electrolyte are higher than those of zones with higher concentrations. For lower concentrations the E gradient is higher than E_B and for high concentrations it is lower. This means that zones with lower concentrations will move showing a sharp step in front of the disturbance (usually with a lower UV absorbance than the background electrolyte, because its concentration is lower), whereas disturbances at higher concentrations will be diffuse. Further, the mobilities m_X decrease for increasing concentrations. Hence the diffuse fronts in Fig. 6 can be explained. The extra zone X is not block-shaped, but diffuse at the front, through which a steady-state model over the whole zone is not significant. To calculate the shift of the baseline, zone X is thought to be built up of small steps of increasing concentrations of histidine (see Fig. 10). The mathematical model was applied in the following way. In first instance a very small increase in concentration $\bar{c}_{A,X}$ was assumed and this zone was calculated using the parameters from the background electrolyte. Then calculations were carried out whereby concentrations steps were related to the parameters of the preceding zones. These calculations were repeated until zone X, whereby

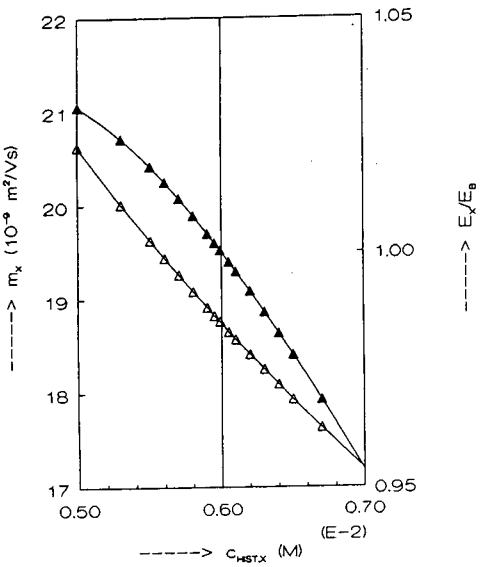

Fig. 9. Calculated values of (△) m_X of the zone X and (▲) ratio of the electric field strengths of zone X and of the background electrolyte, E_x/E_B (right-hand scale), as a function of the assumed concentration of histidine, $c_{HIST,X}$, in zone X, applying a background electrolyte consisting of 0.006 M histidine adjusted to pH 3.5 by adding formic acid. For further explanation, see text.

$$E_X m_{A,X} \bar{c}_{A,X} = E_T m_{A,T} \bar{c}_{A,T} \quad (5)$$

because a concentration boundary between the rear of the concentration disturbance and the terminating electrolyte is assumed.

Check of the model. To compare calculated and experimentally obtained values, concentrations must be deduced from measured steps in the UV signal. Therefore, in the first instance the UV absorbances were measured for several background electrolytes at different concentrations and different pHs. As an example, in Fig. 11 the relationship is given between the measured UV absorbances and the concentrations of solutions

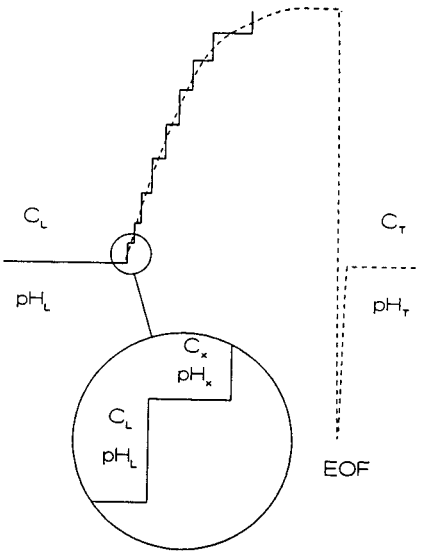

Fig. 10. For the calculation of the diffuse front of the disturbance of the baseline UV signal the shift in the baseline is thought to be built up of small steps of increasing concentrations of histidine. Calculations are started from the leading zone with a concentration c_L and pH_L. For each step the total concentration of histidine, c_X, is assumed and the other parameters are calculated using the given mathematical model.

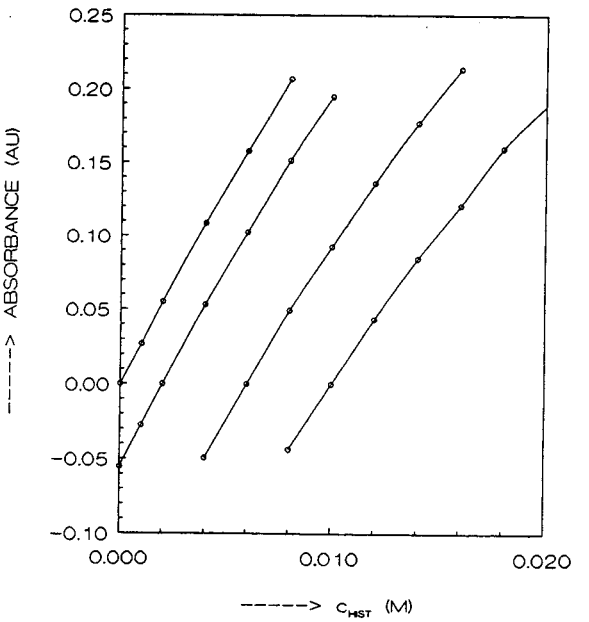

Fig. 11. Measured UV absorbances for several solutions of histidine adjusted to pH 4 by adding formic acid. Different curves were measured using different solutions for the zero setting of the UV detector. The relationships are not completely linear and the measured values differ slightly depending on the choice of the solution used for the zero setting of the UV detector.

of histidine adjusted to pH 4 by adding formic acid. Because the relationship is not completely linear and the measured values differ slightly, depending to the choice of the solution used for the zero setting of the UV detector, the relationship between absorbance and concentration is always applied using the same electrolyte for zero setting in both the calibration graph and electrophoretic experiments. From the calibration graph, shifts in the UV signal can be recalculated to concentration differences. In Fig. 12 the measured UV signals (lines) are given for leading and terminating electrolytes consisting of 0.006 *M* histidine at (A) pH 3.5 and 4, respectively, and (B) at pH 3.5 and 4.5, respectively, and the calculated values (Δ) for the concentrations, recalculated to UV values using Fig. 11. In the calculations the m_{EOF} values calculated from the experimental results are used. In practice, the m_{EOF} is not constant in such systems and the m_{EOF} is, in the first instance, determined by the composition of the leading electrolyte (low pH, low m_{EOF} value) whereas during the analysis the m_{EOF} increases because the terminating electrolyte (high pH, high m_{EOF} value) is migrating into the separation capillary. This means that in the calculations the m_{EOF} values are too high at the beginning of the analysis, through which the calculated migration times are too low, as can be seen in Fig. 12. Nevertheless, the calculations seem to be a good approximation of the measured values.

As a second check of the model, in Fig. 13 the calculated m_X values for (A) 0.01 *M* histidine and (B) 0.006 *M* histidine adjusted to different pHs by adding formic acid (lines) are compared with the measured values. The measured values were calculated from the negative dip in the UV signal applying 5-s pressure injections of water. According to the theory, these values are slightly too high, through which the measured values are higher than the calculated values, but the measured values fit the calculated lines. As a third check, calculated values of the maximum concentration of the diffuse UV signal shifts were

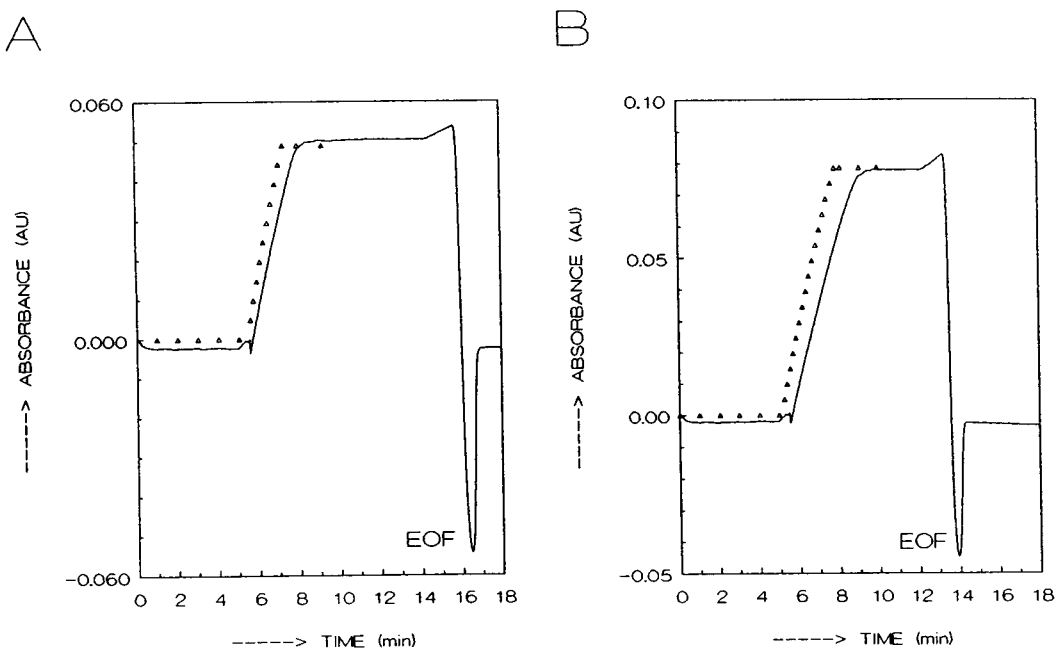

Fig. 12. Measured UV signals (lines) for leading and terminating electrolytes consisting of 0.006 *M* histidine at (A) pH 3.5 and 4, respectively, and (B) pH of 3.5 and 4.5, respectively, and (△) calculated values for the concentrations, recalculated to UV values using Fig. 11. In the calculations the m_{EOF} values calculated from the experimental results were used (applied voltage 20 kV).

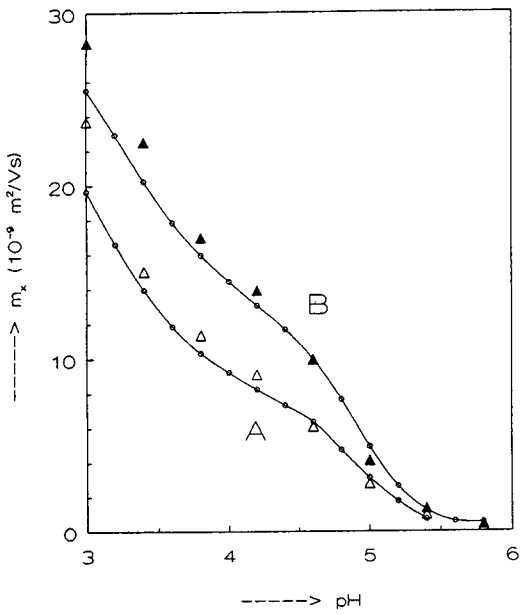

Fig. 13. Calculated (○) m_X values and measured values for (A) 0.01 *M* histidine and (B) 0.006 *M* histidine adjusted to different pHs by adding formic acid. The measured values were calculated from the negative dip in the UV signal applying 5-s pressure injections of water.

compared with measured values for several systems of histidine adjusted to pH 3.5 for the leading electrolyte by adding formic acid and to pH (A) 5, (B) 4.5 and (C) 4 for the terminating electrolyte for several concentrations of histidine. The measured UV shifts were recalculated to concentrations using Fig. 11. In Fig. 14, the calculated values (lines) and measured values are given. The calculated and measured values agree well although both the calculated and measured values increase strongly for high concentrations of histidine and a large difference between the pHs of the leading and terminating electrolyte. In that case no steady state is reached.

Moving boundary zones in LT systems. On applying in electrophoresis a terminating electrolyte, different in pH or concentration of the co-ions of the leading electrolyte, an extra zone X can be obtained migrating with a mobility m_X, determined by the composition of the leading electrolyte. In fact, a moving boundary zone is created. If the supply of co-ions coming from the terminating solution is larger than needed to

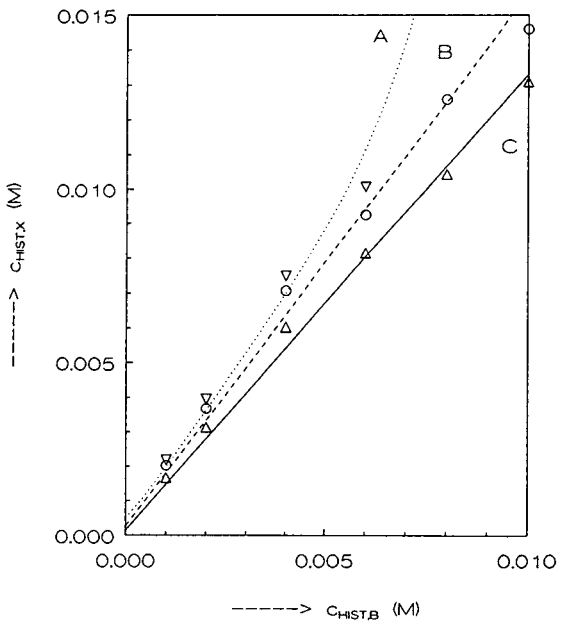

Fig. 14. Calculated values (lines) and measured values for shifts in concentrations ($c_{HIST,X}$) due to the fact that the capillary and anode compartment are filled with background electrolytes of the same concentration of histidine ($c_{HIST,B}$) but at different pH. In all experiments the leading electrolyte was at pH 3.5, whereas the pH of the terminating electrolyte was (A) 5.0 (measured values ▽), (B) 4.5 (○) and (C) 4.0 (△).

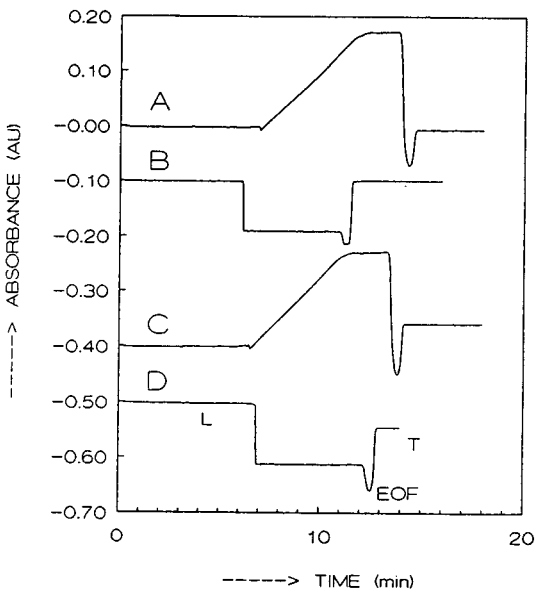

Fig. 15. Electropherograms for moving boundary zones in electrophoresis. In all instances the leading and terminating electrolytes were solutions of histidine formate. The concentrations and pH of the leading electrolytes were respectively (A) 0.01 *M* and pH 3.25, (B) 0.01 *M* and pH 4.8, (C) 0.01 *M* and pH 3.25 and (D) 0.012 *M* and pH 4.8 and in the terminating zone (A) 0.01 *M* and pH 4.8, (B) 0.01 *M* and pH 3.25, (C) 0.012 *M* and pH 4.8 and (D) 0.01 *M* and pH 3.25. For further explanation, see text.

substitute the moving co-ions of the leading electrolyte, a diffuse zone at a higher co-ion concentration than that of the leading electrolyte is obtained. If the supply is smaller, a sharp zone at lower concentration is obtained. To illustrate these effects, in Fig. 15 some of these moving boundary zones are shown. In all instances the terminating and leading electrolyte were solutions of histidine formate.

In Fig. 15A the electropherogram is given for a leading electrolyte of 0.01 *M* at pH 3.25 and a terminating electrolyte of 0.01 *M* at pH 4.8. Because the *E* gradient in the terminating zone is large compared with that in the leading zone, owing to the small contribution to the conductivity of the hydrogen ions, the supply of histidine from the terminating zone is high and a diffuse moving boundary zone can be observed. Note the small dip in front of the moving boundary zone originating from the EOF dip. The UV absorbances in the leading and terminating electrolytes are nearly equal. In Fig. 15B the concentrations and pH of the histidine formate were respectively 0.01 *M* and 4.8 in the leading zone and 0.01 *M* and 3.25 in the terminating zone. Because the supply of histidine from the terminating electrolyte is much too small, a large, sharp moving boundary zone at a lower concentration than that of the leading electrolyte migrates in front of the EOF dip. The UV signals of the leading and terminating zones are equal again. In Fig. 15C the leading electrolyte was 0.01 *M* histidine formate at pH 3.25 and the terminating electrolyte was 0.012 *M* histidine formate at pH 4.8. Analogously to Fig. 15A, a diffuse moving boundary zone is present coming to a steady state (flat profile). In Fig. 15D the leading electrolyte was 0.012 *M* at pH 4.8 and the terminating electrolyte 0.01 *M* at pH 3.25. The UV absorbance of the terminating

electrolyte is lower than that of the leading electrolyte and is preceded by a large dip of a sharp moving boundary zone.

It is clear that the use of electrolytes at different pHs or concentrations must be handled carefully, because it can result in moving boundary zones with different pHs and concentrations, not observable if the background electrolytes do not have UV-absorbing properties.

Block-shaped discontinuities in composition of background electrolytes. If a block-shaped discontinuity in pH and/or concentration of the co-ions of the background electrolytes is introduced, a steady-state discontinuity could be expected according to the simplified Kohlrausch law of eqn. 1. In practice, such a block-shaped discontinuity can show a totally different character. It can be considered as a combination of two leading–terminating systems, with opposite behaviour. For example, the introduction of 0.012 *M* histidine formate at pH 4.8 in a background electrolyte of 0.01 *M* histidine formate at pH 3.25 is the combination of the systems from Fig. 15C and D. It can be expected that in front of the discontinuity a diffuse zone at higher concentration is formed and at the rear side a sharp zone at lower concentration. To study this behaviour, a long block-shaped zone (50-s pressure injection) of 0.012 *M* histidine formate at pH 4.8 was injected in the background electrolyte 0.01 *M* histidine formate at pH 3.25 in such a way that this discontinuity was introduced at various distances from the detector. In this way several intermediate stages in the separation procedure can be observed. In Fig. 16 the measured electropherograms obtained in this way are given. In Fig. 16A the discontinuity was introduced just before the detector, whereas the distance to the detector increases from Fig. 16A to D. In Fig. 16A the formation of a diffuse zone with a higher UV absorbance than that of the original 0.012 *M* histidine formate solution starts, whereas at the rear side a large, sharp dip is present. From the UV absorbance it can be deduced that the concentration in the dip is about 0.006 *M*. For longer separation times (Fig. 16B and C) the fronting zone increases in height, the original 0.012 *M* zone disappears and the dip elongates. In Fig. 16D the fronting diffuse zone separates

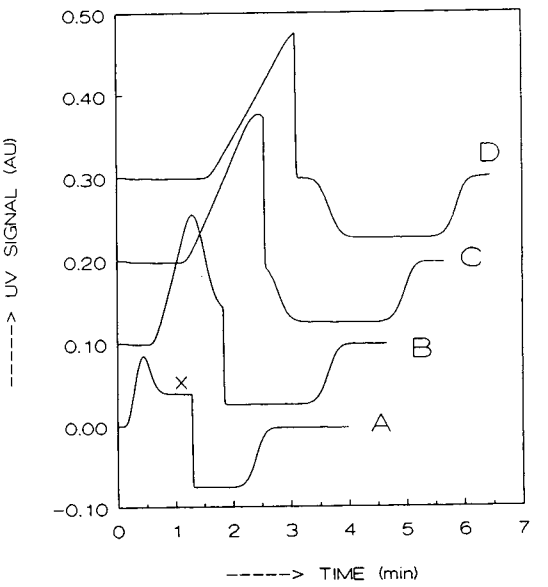

Fig. 16. Electropherograms for 50-s pressure injection of 0.012 *M* histidine formate at pH 4.8 in a background electrolyte of 0.01 *M* histidine formate at pH 3.25. The distance between the injected solution of 0.012 *M* histidine formate and the detector increases from A to D. In (A) the original 0.012 *M* histidine formate plug (X) is partially visible. In front of X a moving boundary zone at higher histidine concentration is formed, whereas at the rear side of X a sharp zone at low concentration is formed. Zone X splits into a migrating system peak and a zone at low concentration at the original position of zone X. In (D) zone X has disappeared and the system peak and dip are released.

from the dip. The fronting diffuse zone migrates with a mobility determined by the composition of the background electrolyte whereas the dip remains at the position of the original block-shaped discontinuity and migrates with the velocity of the EOF.

To illustrate some of these effects, in Fig. 17 some electropherograms are shown for the 20-s pressure injections of several block-shaped discontinuities, followed by a 3-s pressure injection of water as EOF marker in a background electrolyte of 0.01 *M* histidine formate at pH 3.25. For the electropherogram in Fig. 17A, 0.012 *M* histidine formate at pH 4.8 was injected. Although a solution at higher histidine concentration (higher UV absorbance) was injected, a dip just before the EOF marker position and a migrating diffuse peak are the result. Even the

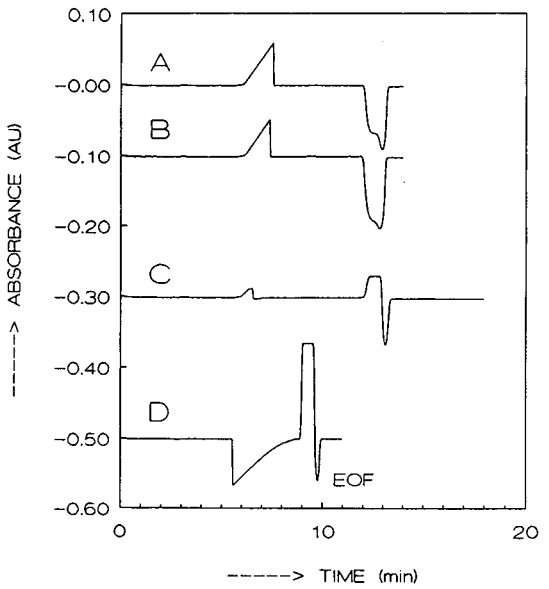

Fig. 17. Electropherograms for 20-s pressure injections of block-shaped discontinuities and 3-s pressure injection of water. The background electrolyte and block-shaped discontinuity were always solutions of histidine formate. The concentration of histidine formate and the pH of the solution for the background electrolytes were respectively (A, B and C) 0.01 *M* and pH 3.25 and (D) 0.01 *M* and pH 4.8 and for the discontinuity (A) 0.012 *M* and pH 4.8, (B) 0.01 *M* and pH 4.8, (C) 0.012 *M* and pH 3.25 and (D) 0.01 *M* and pH 3.25. In all systems system peaks were present.

introduction of 0.01 *M* histidine formate at pH 4.8, where a straight baseline could be expected, results in a positive system peak and a dip just before the EOF dip (Fig. 17B). On injecting a 0.012 *M* solution at pH 3.25, the supply of histidine from the discontinuity is smaller and at the EOF marker position a positive peak remains, but a small positive system peak migrates through the system (Fig. 17C). In Fig. 17D the leading electrolyte was 0.01 *M* histidine formate at pH 4.8 and the discontinuity was 0.01 *M* histidine formate at pH 3.25. Although a straight baseline could be expected, the electropherogram shows a large migrating diffuse dip and a large positive peak at the EOF marker position.

From all these experiments, it can be concluded that the introduction of discontinuities in zone electrophoresis can result in system peaks, with a mobility determined by the background electrolyte.

CONCLUSIONS

Non-steady-state processes in capillary electrophoresis can be estimated with a steady-state mathematical model. Calculations with a steady-state model indicate that in CZE, moving boundary zones can be created by the presence of discontinuities in concentrations of the co-ions and/or pH of the background electrolyte.

The moving boundary zones migrate with a mobility determined by the composition and pH of that background electrolyte, *i.e.*, the ω value of Kohlrausch's regulating function according to eqn. 1 is not locally invariant with time. If the concentration in the moving boundary zone is lower than that of the background electrolyte (negative disturbance), the local E is higher than that of the background electrolyte, through which the zone boundary is sharp. If the concentration is higher than that of the background electrolyte (positive disturbance), the zone is diffuse owing to the fact that the lower concentrations of the zone migrate at a higher mobility than the increasing concentrations of the diffuse zone. Block-shaped discontinuities in pH and/or concentration of the co-ions split up in a migrating part with a velocity determined by the background electrolyte composition and a part migrating with the velocity of the EOF.

To illustrate all these effects, in Fig. 18 the electropherograms are given for 3-s pressure injections of (1) water, (2) a solution of 0.01 *M* histidine adjusted to pH 5 by adding formic acid, (3) a solution of 0.02 *M* KCl and (4) applying a terminating electrolyte of 0.01 *M* histidine formate at pH 5, applying a leading electrolyte of 0.006 *M* histidine adjusted to pH (A) 6 and (B) 4 by adding formic acid. The mobilities of the concentration disturbances are nearly zero at pH 6. For this reason, no special effects can be observed in the electropherograms in Fig. 18A. In electropherogram 1, the EOF peak is present. In electropherogram 2 a positive peak is present at the EOF position, because owing to Kohlrausch's law the initial ω value is high. In electropherogram 3 a negative peak of potassium is present (indirect UV mode), whereas at the EOF position a positive peak is present because the histidine concentration is adapted to the

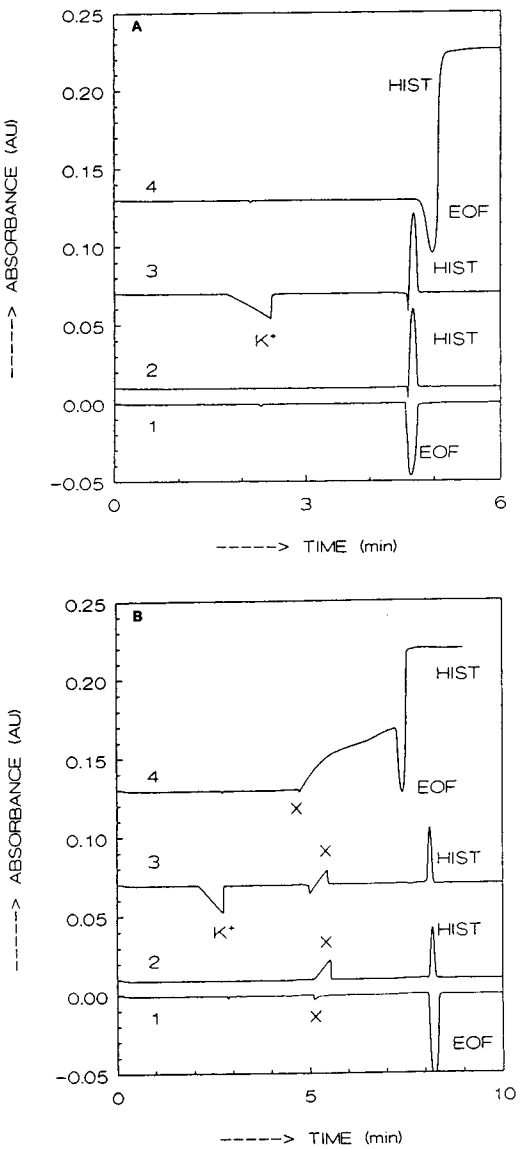

Fig. 18. Electropherograms for the separations of 3-s pressure injections of (1) water, (2) 0.01 *M* histidine adjusted to pH 5 by adding formic acid, (3) 0.02 *M* KCl and (4) the application of a terminating solution of 0.01 *M* histidine formate at pH 5 applying a background electrolyte of 0.006 *M* histidine adjusted to pH (A) 6 and (B) 4 by adding formic acid.

original ω value of the KCl solution. In electropherogram 4 a strong shift in the UV signal is present after the EOF dip due to the migration of the original terminating solution at a higher histidine concentration than the background electrolyte (note that the baseline UV signal is constant before the EOF dip). In Fig. 18B some typical effects are visible on applying a background electrolyte at low pH. In electropherogram 1, the EOF peak splits and a system peak X occurs. In electropherogram 2, a solution of high histidine concentration (positive disturbance) is injected and this peak splits, giving a positive peak X just beginning at the same position of the negative peak in electropherogram 1. The resulting peak at the position of the EOF is smaller than that of the corresponding peak in Fig. 18A. On injecting a 0.02 *M* KCl solution the potassium peak can be observed, a histidine peak at the position of the EOF according to Kohlrausch's law and a system peak X, consisting of a small negative dip followed by a positive peak. This system peak can be explained as follows. In the first instance the KCl solution migrates from the EOF position. According to Kohlrausch's law, the EOF position will be filled with histidine (at a high concentration). Because this process lasts for some time, in the first instance a negative disturbance migrates through the system, followed by the positive disturbance. According to the mathematical model the mobility of the negative disturbance is higher than that of the positive disturbance and migrates with a sharp front. Because the supply of histidine from the terminating solution is small, the positive peak has a limited length. If the terminating electrolyte has a much higher concentration of histidine and the supply from the terminating electrolyte is high (electropherogram 4), a continuous shift of baseline UV signal is obtained. Kohlrausch's law is not valid, showing that this law must not be applied at low pH.

The character of the different kinds of moving boundary zones and their effects on systems peaks and separations is under investigation.

REFERENCES

1 F. Foret, E. Szoko and B.L. Karger, *J. Chromatogr.*, 608 (1992) 3.
2 C. Schwer and F. Lottspeich, *J. Chromatogr.*, 623 (1992) 345.
3 J.L. Beckers, *J. Chromatogr.*, 641 (1993) 363.
4 A. Vinther, F.M. Everaerts and H. Søberg, *J. High Resolut. Chromatogr.*, 13 (1990) 639.

5 J.L. Beckers and M.T. Ackermans, *J. Chromatogr.*, 629 (1993) 371.
6 P. Bocek, P. Gebauer and M. Deml, *J. Chromatogr.*, 217 (1981) 209.
7 P. Bocek, P. Gebauer and M. Deml, *J. Chromatogr.*, 219 (1981) 21.
8 J.L. Beckers and F.M. Everaerts, *J. Chromatogr.*, 480 (1989) 69.
9 F. Kohlrausch, *Ann. Phys. (Leipzig)*, 62 (1897) 209.
10 E.B. Dismukes and R.A. Alberty, *J. Am. Chem. Soc.*, 76 (1954) 191.
11 F.E.P. Mikkers, *Thesis*, University of Technology, Eindhoven, 1980.

Journal of Chromatography A, 662 (1994) 167–172
Elsevier Science B.V., Amsterdam

CHROM. 25 681

Analysis of snake venoms by sodium dodecyl sulfate–polyacrylamide gel electrophoresis and two-dimensional electrophoresis

T. Marshall* and K.M. Williams

School of Health Sciences, The University of Sunderland, Fleming Building, Sunderland SR2 7EE (UK)

(First received June 11th, 1993; revised manuscript received October 19th, 1993)

ABSTRACT

The protein composition of snake venom has been analysed by sodium dodecyl sulfate–polyacrylamide gel electrophoresis (SDS-PAGE) and high-resolution two-dimensional electrophoresis (2-DE). SDS-PAGE suggests differences between species and similarities between related species. As expected, silver staining greatly enhanced detection sensitivity whilst 2-DE dramatically improved separation to reveal multiple strings of spots indicative of molecular heterogeneity. It is recommended that similarities (or differences) in the SDS-PAGE patterns of venoms from the same (or different) species of snake should be further characterized by 2-DE.

INTRODUCTION

The pharmacological/toxicological properties of snake venom are mainly associated with proteins particularly enzymes [1–3]. The protein composition of venom has been studied for the purpose of species comparison/development of anti-venoms [3] and sodium dodecyl sulfate–polyacrylamide gel electrophoresis (SDS-PAGE) has been widely applied [4–10]. Recently, Mendoza *et al.* [10] compared the SDS-PAGE profiles of 21 snake venoms and demonstrated individual patterns with shared characteristics. We have investigated additional factors affecting electrophoretic analysis of snake venoms and have extended previous work to include the application of high-resolution two-dimensional electrophoresis (2-DE).

* Corresponding author.

EXPERIMENTAL

Sample preparation

The following snake venoms were supplied by Sigma (Poole, UK): *Agkistrodon contortrix mokason* (Northern Copperhead), *Bothrops jararacussu* (Jararacussu river snake), *Crotalus molossus molossus* (Black-tailed rattlesnake), *Crotalus horridus horridus* (Timber rattlesnake), *Crotalus ruber* (Red diamond rattlesnake), *Bitis arietans* (Puff adder), *Naja haje* (Egyptian cobra), *Enhydrina schistosa* (Common sea snake) and *Dispholidus typus* (Boomslang). The lyophilized venoms were dissolved (final concentration 5–10 mg/ml) by carefully adding an appropriate volume of 0.0625 *M* Tris–HCl pH 6.8 containing 2% SDS and 20% glycerol. 2-Mercaptoethanol (final concentration 5%) was added to an aliquot of each solubilized venom and the sample mixtures (both reduced and non-reduced) heated at 95°C for 10 min. In subsequent experiments selected venoms were di-

0021-9673/94/$07.00
SSDI 0021-9673(93)E1156-T

luted to 0.2–5.0 mg/ml for Coomassie blue staining and 0.002–0.10 mg/ml for silver staining.

Electrophoresis

SDS-PAGE. The denatured venoms (5 μl) were loaded in agarose wells precast on the upper surface of 6–20% (w/v) polyacrylamide gradient gels (75 × 75 × 3 mm) and electrophoresed at 70 mA/gel for 1 h in precooled (4°C) 0.025 *M* Tris, 0.2 *M* glycine containing 0.1% (w/v) SDS [11]. M_r was estimated by co-electrophoresis of Pharmacia-LKB calibration proteins (2.5 μl).

2-DE. The denatured venoms (200 μg for Coomassie blue staining; 10 μg for silver staining) were analysed by the simplified method [12] of high-resolution 2-DE [13]. Isoelectric focusing (IEF, first dimension) in 4% (w/v) polyacrylamide gel rods containing 9 *M* urea, 0.5% Nonidet P-40 and 2% ampholine (pH 2.5–4.0, pH 5.0–7.0, pH 3.5–10.0; 2:3:6, v/v/v) was followed by SDS-PAGE (second dimension) as described above. Co-electrophoresis of a human serum and a serum/venom mixture were used for calibration of p*I* and M_r.

Staining

Coomassie blue. The SDS-PAGE gels were fixed in aqueous 20% (w/v) trichloroacetic acid (TCA) and the proteins stained at 60°C for 30 min in methanol–acetic acid–water (50:10:40, v/v/v) containing 0.1% (w/v) Serva Blue R prior to destaining in methanol–acetic acid–water (10:10:80, v/v/v) [11]. The 2-DE gels were fixed in methanol–acetic acid–water (50:10:40, v/v/v) prior to staining as above —this eliminates "shadow effects" associated with the staining of ampholytes.

Silver. The SDS-PAGE and 2-DE gels were fixed in methanol–acetic acid–water (50:10:40, v/v/v) prior to silver staining as previously described [14] and outlined in Table I.

RESULTS

Fig. 1 shows the SDS-PAGE patterns of a range of venoms following sample preparation in the presence (Fig. 1A) or absence (Fig. 1B) of 2-mercaptoethanol ("reducing" and "non-reducing" conditions, respectively). The optimal sample load for CBB staining was 50 μg. Higher amounts (100 μg) resulted in smearing but lower

TABLE I

THE METHYLAMINE-INCORPORATING SILVER STAIN

(1) Wash in two changes of water (10 min each)[a].
(2) Incubate in aqueous 0.1% (w/v) formaldehyde (30 min); cool in water (20°C, 10 min).
(3) Incubate in silver methylamine[b] (10 min).
(4) Quickly rinse in water (2 changes) and developer [formaldehyde, 0.02% (w/v) containing 0.005% (w/v) citric acid]. Change developer at 5-min intervals till gel blackens (*ca.* 30 min).
(5) Rinse in three changes of water (10 min each).
(6) Incubate in destaining solution[c] till gel background is golden yellow (*ca.* 1–4 min).
(7) Rinse in water, incubate in aqueous 2.5% (w/v) Kodak hypo clearing agent[d] (30 min) and wash in three changes of water (10 min each).

[a] Perform all steps with gentle shaking in a fume cupboard; steps 1, 2 at 60°C (with reagent volume of 200 ml/gel) and steps 3–7 at room temperature (100 ml/gel).
[b] For 100 ml (1 gel): mix commercial methylamine solution (30%) with 0.36% (w/v) sodium hydroxide (1:5, v/v), add (*ca.* 10 ml) to 4 ml of a stirring solution of 20% (w/v) silver nitrate till it just clears and dilute to 100 ml with water.
[c] For 800 ml (8 gels): solution A, dissolve 11.1 g sodium chloride and 11.1 g cupric sulphate in 285 ml water and add ammonia solution (25%) till the precipitate clears to a deep blue solution (final volume *ca.* 300 ml). Solution B, dissolve 44 g sodium thiosulfate pentahydrate in 85 ml water (final volume 100 ml). Mix solutions A and B (3:1, v/v) and dilute to 800 ml with water.
[d] Gels may be photographed at this stage.

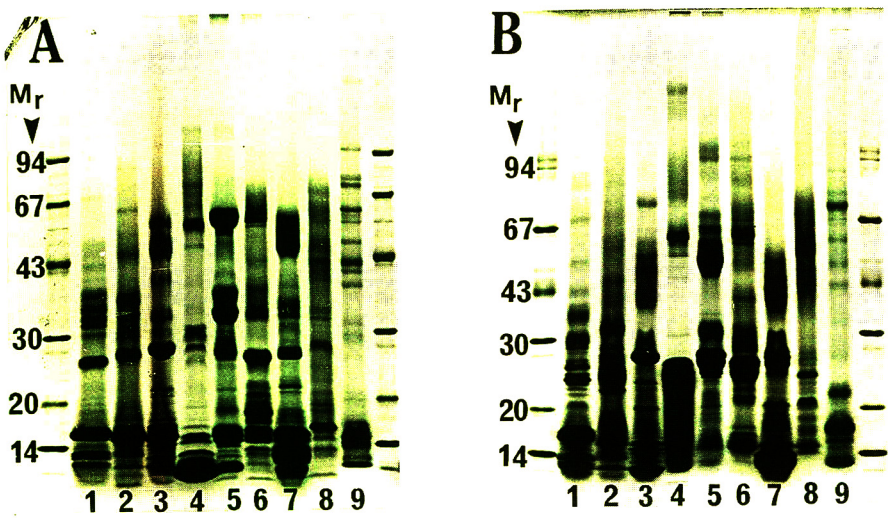

Fig. 1. SDS-PAGE of snake venom (50 μg) analyzed following sample preparation in the presence (A) or absence (B) of 2-mercaptoethanol ("reducing" and "non-reducing" conditions, respectively). Venoms: 1 = *Agkistrodon contortrix mokason*; 2 = *Bothrops jararacussu*; 3 = *Crotalus molossus molossus*; 4 = *Naja haje*; 5 = *Crotalus horridus horridus*; 6 = *Bitis arietans*; 7 = *Crotalus ruber*; 8 = *Dispholidus typus*; 9 = *Enhydrina schistosa*. M_r indicates relative molecular mass × 10^{-3}. Protein was detected with Coomassie brilliant blue.

loads (5–10 μg) were useful for improving the resolution of the major protein constituents. The lower-molecular-mass proteins showed a tendency to diffuse upon destaining —this was minimized by fixing the gels in aqueous 20% TCA [rather than methanol–acetic acid–water (50:10:40)] and destaining in methanol–acetic acid–water (10:10:80) [rather than methanol–acetic acid–water (5:7:88)]. Comparison of "reducing" *versus* "non-reducing" conditions indicated optimal resolution under "reducing" conditions with detection of up to 30 polypeptide bands. "Non-reducing" conditions revealed a greater proportion of high-molecular-mass proteins (presumably oligomers) but the low-molecular-mass proteins were less well defined with a tendency to smear (Fig. 1B). The patterns obtained for individual venoms were distinctly different irrespective of the sample preparation (Fig. 1).

Silver staining enhanced detection sensitivity 100- and 200-fold ["reducing" (Fig. 2A, B) and "non-reducing" (Fig. 2C, D), respectively]. The detection limit for CBB staining was approximately 1 μg of snake venom (Fig. 2A, C), whilst the respective values for silver staining were 10 ng ("reducing" conditions, Fig. 2B) and 5 ng ("non-reducing" conditions, Fig. 2D).

Fig. 3 demonstrates 2-DE of snake venom and compares the detection sensitivity of Coomassie brilliant blue and silver staining. Fixation of the gels in 20% TCA prior to Coomassie brilliant blue staining resulted in a background "shadow" of ampholyte staining in the low-molecular-mass cathodal region of the gel. Fixation in 20% TCA prior to silver staining impaired detection sensitivity. Whilst fixation in methanol–acetic acid–water (50:10:40) eliminated these staining problems the spots were less sharp suggesting an increased tendency for the protein to diffuse. In contrast to the 30 polypeptide bands detected by SDS-PAGE (Fig. 1), 2-DE revealed up to 400 polypeptide spots in microgram amounts of snake venom (particularly when combined with silver staining). The higher-molecular-mass protein bands ($M_r > 30\,000$, Fig. 1A) were separated into strings of up to 10 spots reflecting microheterogeneity whilst the lower-molecular-mass bands ($M_r < 30\,000$, Fig. 1A) were shown to consist of apparently unrelated spots.

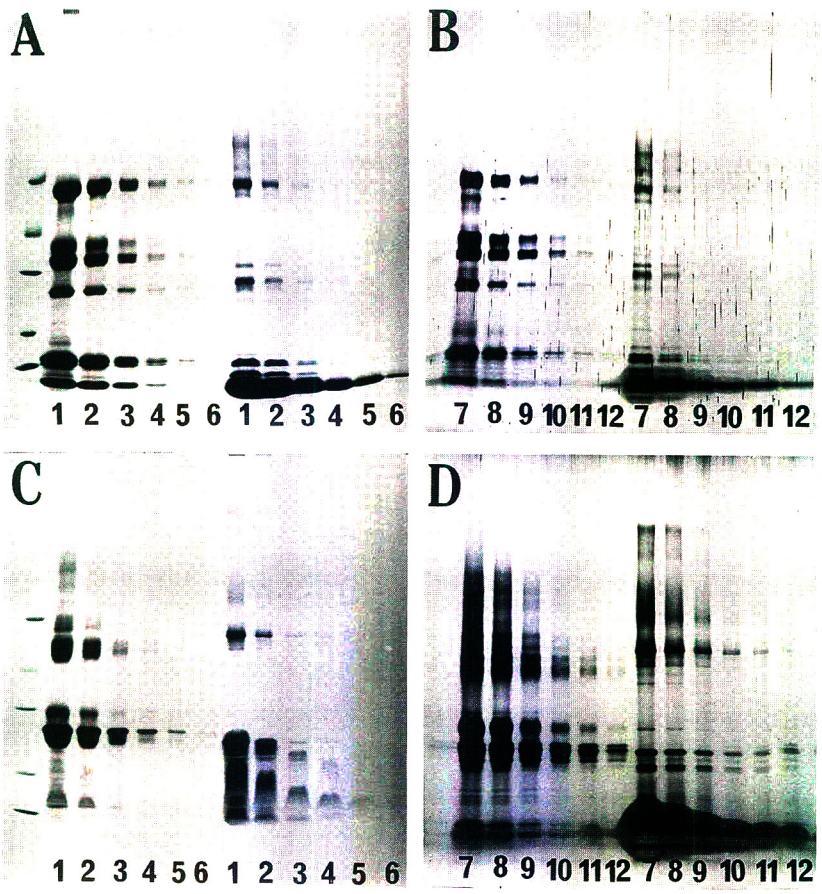

Fig. 2. Comparison of Coomassie brilliant blue (A, C) and silver (B, D) staining following SDS-PAGE of decreasing amounts of two venoms (*Crotalus horridus horridus* and *Naja haje*) after sample preparation in the presence (A, B) or absence (C, D) of 2-mercaptoethanol ("reducing" and "non-reducing" conditions, respectively). Venom amounts: 1 = 50 μg; 2 = 25 μg; 3 = 10 μg; 4 = 5 μg; 5 = 2.5 μg; 6 = 1 μg; 7 = 0.5 μg; 8 = 0.25 μg; 9 = 0.1 μg; 10 = 0.05 μg; 11 = 0.025 μg; 12 = 0.01 μg.

DISCUSSION

The present study suggests that one-dimensional SDS-PAGE may be of limited value for inter-species comparison of the polypeptide constituents of snake venoms. 2-DE clearly indicates that individual SDS-PAGE bands consist of multiple strings of related spots and/or numerous unrelated spots. This overlap is a common problem when applying one-dimensional electrophoretic methods to complex proteins mixtures. In this respect, 2-DE demonstrates a previously unknown degree of complexity in the polypeptide constituents of snake venom. This complexity may be partly explained by microheterogeneity whereby minor differences in the charge or molecular size of a polypeptide manifests itself as delicate trails of closely packed spots. Thus, apparent similarities in the SDS-PAGE banding patterns of different snake venoms need to be confirmed by techniques of higher resolution, including 2-DE. Such comparisons should also include 2-DE using non-equilibrium pH gradient electrophoresis [15] to account for additional proteins of a more basic nature.

Mendoza *et al.* [10] recently suggested that "certain proteins from native venoms and polypeptides derived from SDS-treated venoms do

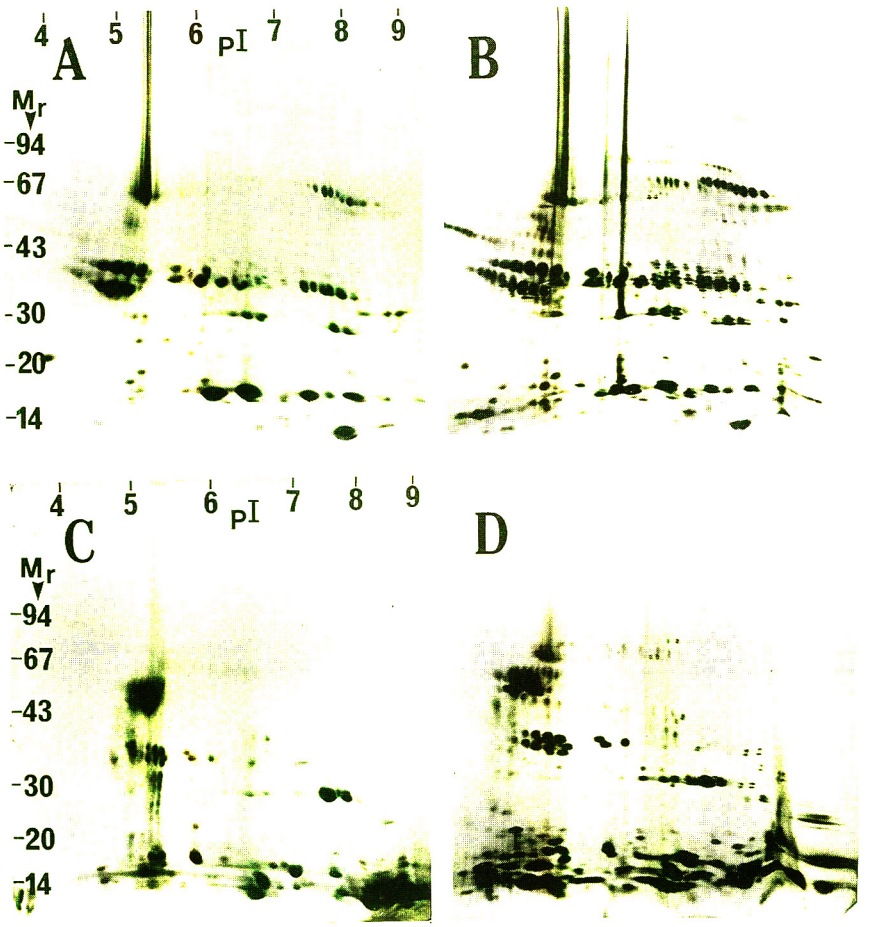

Fig. 3. 2-DE of snake venom from *Crotalus horridus horridus* (A, B) and *Crotalus ruber* (C, D) as detected by Coomassie brilliant blue staining (A, C; 200 μg venom) or silver staining (B, D; 10 μg venom). Co-electrophoresis of human serum and a serum/venom mix were used to calibrate p*I* and M_r.

not react strongly with the silver nitrate stain and are not readily detectable. In contrast, they produce an intense reaction with the Coomassie brilliant blue stain and are readily detectable". We have found no evidence to support this claim. On the contrary, our silver staining method consistently improved the detection sensitivity of Coomassie brilliant blue staining at least 100-fold. This discrepancy may arise from the choice of silver stain as different methods vary widely in their response and commercially available stains often sacrifice sensitivity for improved reproducibility.

REFERENCES

1 C.Y. Lee (Editor), *Venoms*, Springer, New York, 1979.
2 C.Y. Lee (Editor), *Handbook of Experimental Pharmacology*, Vol. 52, Springer, Berlin, 1979.
3 A.T. Tu (Editor), *Reptile Venoms and Toxins: Handbook of Natural Toxins*, Vol. 5, Marcel Dekker, New York, 1991.
4 S.E. Pollack, K. Uchida and U.S. Auld, *J. Protein Chem.*, 2 (1983) 1.
5 P. Lollar, C.G. Parker, P.J. Karjenski, R.D. Litwiller and D.N. Sass, *Biochemistry*, 26 (1987) 7627.
6 L.C. Evans and F.J. Torre, *J. Chem. Educ.*, 65 (1988) 1011.
7 G.P. Jayanthi and T.V. Gowda, *Toxicon*, 26 (1988) 257.

8 L. Chinonavanig, P.B. Billings, P. Matangkasombut and K. Ratanabanangkoon, *Toxicon*, 26 (1988) 883.
9 M.F.D. Furtado, M. Maruyama, A.S. Kamiguti and L.C. Antonio, *Toxicon*, 29 (1991) 219.
10 C.E.C. Mendoza, T. Bhatti and A.R. Bhatti, *J. Chromatogr.*, 580 (1992) 355.
11 T. Marshall, *Clin. Chem.*, 30 (1984) 475.
12 T. Marshall and K.M. Williams, *Electrophoresis*, 12 (1991) 461.
13 P.H. O'Farrell, *J. Biol. Chem.*, 250 (1975) 4007.
14 T. Marshall, *Anal. Biochem.*, 136 (1984) 340.
15 P.Z. O'Farrell, H.M. Goodman and P.H. O'Farrell, *Cell*, 12 (1977) 1133.

Journal of Chromatography A, 662 (1994) 173–177
Elsevier Science B.V., Amsterdam

CHROM. 25 757

Short Communication

Comparison of high-performance liquid chromatography with radioimmunoassay for the determination of domoic acid in biological samples

James F. Lawrence*, Chantal Cleroux and John F. Truelove

Bureau of Chemical Safety, Food Directorate, Health Protection Branch, Banting Research Centre, Ottawa, Ontario K1A 0L2 (Canada)

(First received August 11th, 1993; revised manuscript received November 22nd, 1993)

ABSTRACT

A reversed-phase liquid chromatographic method employing UV absorption detection at 242 nm was compared to a radioimmunoassay technique for the determination of the marine toxin, domoic acid, in several types of seafood and biological samples. Agreement between the two methods for spiked samples of mussels and rat serum was very good over a range of concentrations of 0.15–7.3 μg/g domoic acid. Also, a very good correlation was observed between the two methods for naturally incurred residues of domoic acid in razor clams, anchovies and crab meat over a concentration range of 0.6–43 μg/g domoic acid.

INTRODUCTION

Domoic acid is a marine toxin (produced by the phytoplankton species, *Nitzschia pungens*), that has been identified in various types of shellfish on the Atlantic and Pacific coasts of the USA and Canada [1]. Methods most commonly employed for determining the compound in contaminated samples involve high-performance liquid chromatography (HPLC) with a variety of sample extraction techniques [2–8]. The procedure most commonly used at present employs methanol–water extraction [6] with or without a cleanup step involving disposable solid-phase extraction (SPE) cartridges filled with strong anion-exchange (SAX) resin.

Only one report has appeared in the literature describing the application of immunoassay techniques for the determination of domoic acid [9]. This work compared enzyme-linked immunosorbent assay (ELISA) with radioimmunoassay (RIA) for the determination of the toxin in urine and serum of experimental animals (monkeys, rats). The methods were found to be very sensitive enabling the detection of domoic acid at low ng/ml levels in the samples. Immunoassay methods are particularly advantageous because they are capable of rapidly screening many samples at a time, at a relatively low cost. This approach can be particularly useful for screening samples for toxic chemicals for regulatory purposes. This prompted us to evaluate the approach for the determination of domoic acid in shellfish and to compare it to HPLC in terms of accuracy and ease of analysis. The comparison to HPLC is important since immunoassay techniques are

* Corresponding author.

0021-9673/94/$07.00
SSDI 0021-9673(93)E1235-R

susceptible to giving false positives or false negative results due to the presence of coextractives which may bind to enzymes or to matrix effects which may inhibit binding of the domoic acid. HPLC in this regard can act as an extremely useful confirmation technique for samples found to be positive by immunoassay. The comparison of the two techniques was also applied to rat urine, serum and feces in animal feeding studies for which the RIA method was initially developed. Confirmation by HPLC of the values found by RIA adds important information to the metabolism of domoic acid in animals.

EXPERIMENTAL

Reagents

Standard solutions of domoic acid (DACS-1, National Research Council of Canada, Halifax, Canada) were prepared in doubly deionized water. All solvents and chemicals were HPLC- or analytical-grade materials. All solutions of standards and samples were refrigerated when not in use. [^{3}H]Domoic acid (specific activity 165 GBq/nmol) was obtained from Amersham Labs., UK. Prior to use the [^{3}H]domoic acid was purified by HPLC.

Sample extraction

The extraction procedure was based on the methanol–water extraction method described elsewhere [6,7] with modifications. For shellfish, 10 g homogenized tissue were mixed with 10 ml water in a 50-ml centrifuge tube for 1 min using a vortex mixer. Following this, 20 ml methanol were added and the contents mixed again for 1 min. The mixture was centrifuged and the clear supernatant decanted into a clean tube. A 10-ml volume of methanol was added to the residue and the contents mixed and centrifuged as above. The clear supernatant was combined with the first and the total volume adjusted to 50.0 ml. A 5-ml aliquot of this was used for SPE cleanup and HPLC while a 1.0-ml aliquot was diluted with phosphate-buffered saline (PBS) for RIA.

Serum and urine samples were diluted ten times with methanol–water (50:50, v/v) before SPE cleanup and HPLC. A 2-ml volume of diluted serum and 2.5 ml of diluted urine were used for SPE cleanup. For RIA, 0.1 ml sample was diluted with PBS. Feces samples (2 g) were extracted with methanol–water (50:50, v/v) as described above for the shellfish samples. A 2.0-ml aliquot (0.1 g equivalent feces) of the supernatant was used for SPE cleanup.

Solid-phase extraction cleanup

All HPLC determinations were performed after SPE cleanup either with a SAX resin [6] for shellfish and serum samples or with a strong cation-exchange (SCX) cartridge followed by a C_{18} (reversed-phase) cartridge [8] for urine and feces samples.

For SPE-SAX cleanup an aliquot of sample extract was passed though a 3-ml Supelclean LC-SAX cartridge (Supelco, USA) preconditioned with 6 ml methanol, 3 ml water and 3 ml methanol–water (50:50, v/v). The effluent was discarded and the cartridge washed with 5 ml acetonitrile–water (10:90, v/v) which was discarded. Domoic acid was eluted with 3 ml acetonitrile–formic acid–water (10:2:88, v/v/v). A 20-μl aliquot was analysed by HPLC.

The SPE-SCX cleanup was carried out by passing 2.5 ml of diluted urine or feces extract (adjusted to pH 3–4) through a 3-ml Bond Elut SCX cartridge (Baker, USA) preconditioned with 6 ml methanol and 6 ml 0.1 *M* HCl. The effluent was discarded and the cartridge washed with 3 ml water which was also discarded. Domoic acid was eluted with 6 ml 0.7 *M* HCl directly onto a 3 ml SPE-C_{18} cartridge (Baker) preconditioned with 6 ml methanol and 6 ml 0.7 *M* HCl. The effluent was discarded and the cartridge washed with 3 ml water which was also discarded. Domoic acid was eluted with 4 ml acetonitrile–acetic acid–water (20:1:79, v/v/v). A 20-μl aliquot was analysed by HPLC.

High-performance liquid chromatography

The HPLC system consisted of a ternary low-pressure gradient pump (Eldex, Model 9600) connected to a rotary loop injector (Rheodyne, Model 8125) with a 20-μl sample loop and a reversed-phase C_{18} column (Supelco LC-18, 150 × 2.1 mm I.D., 5 μm). The column effluent was monitored with a diode array UV absorb-

ance detector (Hewlett-Packard, Model 1040A) set to 242 nm. The mobile phase was 0.2% (v/v) formic acid plus 12% (v/v) acetonitrile in water (pH 3.0). The flow-rate was set to 0.5 ml/min.

Radioimmunoassay

RIA was carried out exactly as described earlier using polyclonal antibodies generated from rabbits [9]. Briefly, domoic acid standards were prepared at concentrations of 1.0–8.0 ng/ml in PBS, pH 7.0. Samples were diluted with PBS to fall within the same domoic acid concentration range. To 200-μl aliquots of standards or diluted samples in small glass test tubes were added 100-μl volumes of antiserum in PBS. The tubes were mixed using a vortex mixer and then incubated overnight at 4°C. A 500-μl volume of[^{3}H]domoic acid (ice cold) in PBS was added to each tube and mixed and allowed to equilibrate for 30 min at 4°C. Free and bound domoic acid were separated by adding 500 μl of a suspension consisting of 10 mg/ml charcoal and 1 mg/ml dextran in PBS. After mixing, the tubes were allowed equilibrate for 10 min at 4°C and then centrifuged. The supernatant was removed to a scintillation vial, mixed with scintillator (Aquasol) and placed in a liquid scintillation counter (LKB) for tritium quantitation. Non-specific binding was determined by substituting PBS for the antibody. A zero point on the standard curve was determined by substituting PBS for the standard.

RESULTS AND DISCUSSION

The HPLC system functioned well for all analyses. The narrow-bore (2.1 mm I.D.) column was selected for this work because of the very good mass detection limits obtained and the low flow-rates employed. The methanol–water extraction procedure was found to be satisfactory for the seafood samples and the serum and urine samples. However, for rat feces only 2.0 g of material could be extracted with the volumes of solvents employed. Also, only 0.1 g equivalent feces could be applied to the SPE cartridges without causing overloading and poor cleanup efficiency.

The SPE-SAX cartridges provided very good cleanup of the seafood samples. Fig. 1 shows typical results obtained for mussels, razor clams, crabmeat and anchovies at a variety of domoic acid concentrations. Recoveries of domoic acid through this extraction and cleanup procedure were usually >90% ($n = 6$) over the range of 0.2–40 μg/g domoic acid with good repeatability similar to that described earlier [6]. The detection limits were estimated to be about 0.1 μg/g (3:1, signal-to-noise) under the conditions employed. The same cleanup procedure was also found to be very satisfactory for the monkey and rat serum samples. The resulting chromatograms were very clean and good recoveries (>90%) and repeatability (11% relative standard deviation, R.S.D., $n = 5$) obtained from spiked samples over the concentration range of 0.2–5 μg/g. Detection limits were *ca.* 0.05 μg/g under the conditions employed in the experimental.

The urine and feces samples were found to be more difficult to purify. The SPE-SAX cleanup was not effective in removing interfering coextractives from the samples, making the determination of domoic acid at low μg/g levels difficult. However, the SPE-SCX-C_{18} combination cleanup produced cleaner chromatograms and permitted the detection of domoic acid at levels of about 0.1 μg/g. Fig. 2 shows chromatograms obtained for rat urine spiked with domoic acid using the SPE-SCX-C_{18} cleanup. The recoveries averaged 81% from 0.2–1.0 μg/g spiking levels with a R.S.D. of 13% ($n = 3$). For feces, recoveries at a spiking level of 1 μg/g were 82 and 90% for duplicate samples.

Table I compares results obtained by the HPLC procedure to those obtained by RIA. As can be seen there is a good correlation between the two methods for the seafood samples and for spiked rat serum over a range of about 0.15–43 μg/g domoic acid. The correlation coefficient was calculated to be 0.9897 with a slope of 1.014, indicating a very good quantitative agreement between the two methods. Under the conditions of the analysis the two methods produced similar detection limits (approximately 0.05–0.1 μg/g) in the samples analysed. However, the RIA method has the potential for detecting lower amounts by reducing the dilution of the samples before analysis. An additional advantage of the

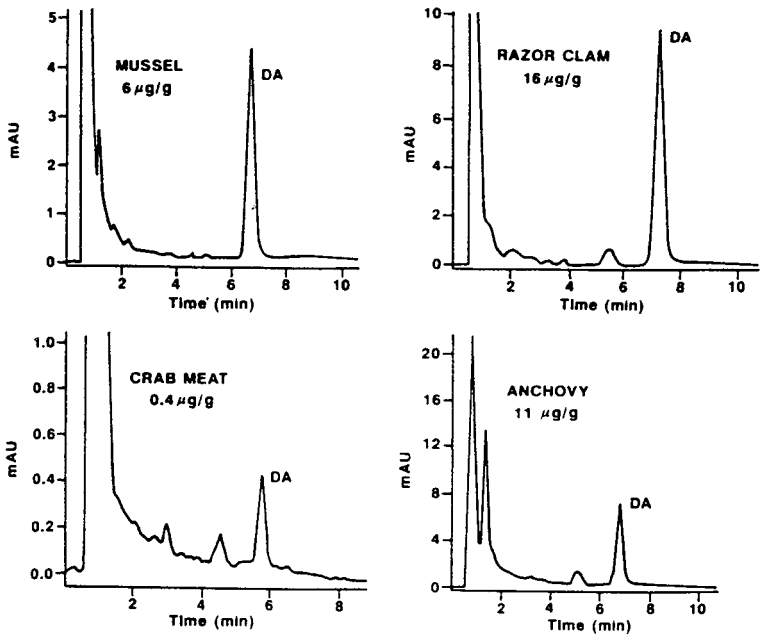

Fig. 1. Chromatograms of seafood samples containing domoic acid. Cleaned up using SPE-SAX. Razor clam, (16 μg/g domoic acid), anchovy (11 μg/g), mussel (6 μg/g, spiked) and crabmeat (0.4 μg/g). DA = Domoic acid. Chromatograms obtained on different days with slight changes in domoic acid retention time.

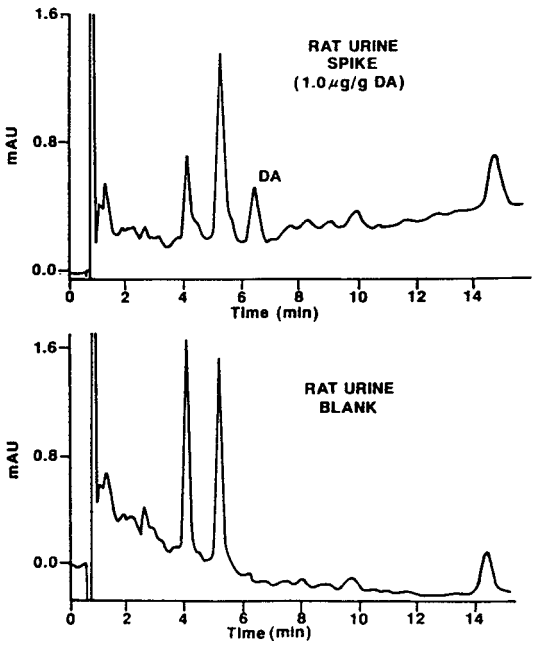

Fig. 2. Chromatograms of blank and spiked (1.0 μg/g domoic acid) extracts of rat urine cleaned up using SPE-SCX-C_{18}.

TABLE I

COMPARISON OF RESULTS BY HPLC AND RIA

Sample[d]	Domoic acid concentration (μg/g)	
	HPLC[a]	RIA
Razor clam (1)	43	38, 49[b]
Razor clam (2)	15	16
Anchovy	11	11
Crab meat	0.60	0.73
Mussel (1) blank	nd[c]	nd
Mussel (1) spiked	7.3	6.5
Mussel (2) blank	nd	nd
Mussel (2) spiked	5.3	4.8, 5.3[b]
Rat serum blank	nd	nd
Rat serum spiked	0.15	0.14, 0.17[b]
Rat serum spiked	0.39	0.39
Rat serum spiked	7.1	7.9

[a] Corrected for recovery. Values in the text.
[b] Duplicate determinations.
[c] Not detected (< 0.1 μg/g, HPLC; < 0.05 μg/g, RIA).
[d] (1) and (2) indicate different samples.

RIA method for the samples analysed was that the SPE cleanup procedure was not required. However, the linear range of the immunoassay technique is rather limited (about a 10-fold range) which requires re-analysis of unknown samples, if the domoic acid concentration falls outside the linear range.

There is always the possibility that cross-reactivity with other chemicals can lead to false results in RIA and other immunoassay methods. In the present case, no false positives (greater than 0.05 μg/g) were found in any of the samples. The good agreement between the HPLC and RIA methods for both spiked and naturally incurred domoic acid shellfish samples clearly indicates that cross-reactivity and matrix effects are not significant in the immunoassay method.

In a further comparison, the HPLC method was applied to the determination of domoic acid in serum and urine samples from rats and monkeys that had received domoic acid either orally or by intravenous injection. The samples had been frozen for about a year. The overall results correlated well although the HPLC values were only 64% (average of 11 samples), of the RIA values (0.5–11 μg/g) obtained at the time of the study. (The RIA analysis was not repeated at the time of the HPLC analysis.) It is likely that this difference is due to the long time between RIA and HPLC analyses. Domoic acid is known to be unstable in biological extracts even when frozen. We have observed that domoic acid degrades substantially (by 50% or more) in extracts or tissue homogenates of shellfish which had been stored frozen for 6 months. Domoic acid is not metabolized by the rat or monkey [10] ruling out the possibility that the RIA method detected a domoic acid metabolite which might account for the difference.

This study has shown that HPLC and RIA provide similar results for domoic acid in seafood and biological fluids. It indicates the potential of immunoassay for rapid screening and quantitation of domoic acid with confirmation by HPLC.

ACKNOWLEDGEMENT

The technical assistance of L. Martin for the RIA analyses is greatly appreciated.

REFERENCES

1 *Proceedings of the Domoic Acid Workshop, San Pedro, CA, Feb. 6–8, 1992,* Food and Drug Administration, Washington, DC, 1992.
2 J.F. Lawrence, C.F. Charbonneau and C. Ménard, *J. Assoc. Off. Anal. Chem.*, 74 (1991) 68.
3 M.A. Quilliam, P.G. Sim, A.W. McCullogh and A.D. McInnes, *Int. J. Environ. Anal. Chem.*, 36 (1989) 139.
4 M.S. Nijjar, B. Grimmelt and J. Brown, *J. Chromatogr.*, 568 (1991) 393.
5 J.R.T. Blanchard and R.A.R. Tasker, *J. Chromatogr.*, 526 (1990) 546.
6 M.A. Quilliam, M. Xie and W.R. Hardstaff, *Tech. Report 64, NRCC 33001*, Inst. Marine Biosciences, Halifax, 1991.
7 J.F. Lawrence and C. Ménard, *J. Chromatogr.*, 550 (1991) 595.
8 J.F. Lawrence, C.F. Charbonneau, B.D. Page and G.M.A. Lacroix, *J. Chromatogr.*, 462 (1989) 419.
9 H. Newsome, J. Truelove, L. Hierlihy and P. Collins, *Bull. Environ. Contam. Toxicol.*, 47 (1991) 329.
10 C.A.M. Suzuki and L. Hierlihy, *Food Chem. Tox.*, (1993) in press.

Journal of Chromatography A, 662 (1994) 178–184
Elsevier Science B.V., Amsterdam

CHROM. 25 732

Short Communication

Instability of tetryl to Soxhlet extraction

Thomas F. Jenkins* and Marianne E. Walsh

US Army Cold Regions Research and Engineering Laboratory, Hanover, NH 03755-1290 (USA)

(First received September 7th, 1993; revised manuscript received October 21st, 1993)

ABSTRACT

The stability of tetryl (N-methyl-N,2,4,6-tetranitroaniline) to Soxhlet extraction with methanol was examined by refluxing tetryl in methanol and extracting a tetryl-contaminated soil using Soxhlet, ultrasonic bath and wrist-action shaker methods. The results indicate that tetryl is unstable to Soxhlet extraction. If wet soils are Soxhlet-extracted with methanol, tetryl hydrolyzes to N-methylpicramide (N-methyl-2,4,6-trinitroaniline). If extracted dry, methanolysis products are formed. Ultrasonic bath extraction with acetonitrile is recommended instead.

INTRODUCTION

Tetryl (N-methyl-N,2,4,6-tetranitroaniline) was used as a common component of USA military high explosives from 1916–1979 [1,2]. While it has been largely replaced by RDX (hexahydro-1,3,5-trinitro-1,3,5-triazine) in modern explosives formulations, residues of tetryl have been found at a number of military facilities [3–5]. Concerns about the health effects of tetryl have led to interest in its fate under environmental conditions [6].

Tetryl (Fig. 1a) is a solid at normal environmental temperature and the neat material is known to be thermally unstable at temperatures above 131°C [7]. Tetryl has a water solubility of about 80 mg/l [8] and an estimated octanol–water partition coefficient of 45 [9], indicating it is relatively mobile in the soil and has a potential to contaminate ground water.

Analytical methods for the determination of tetryl and other nitroaromatics and nitramines in environmental samples have generally relied on solvent extraction followed by gas chromatography (GC) with electron-capture detection [10], GC–mass spectrometry (MS) [11], reversed-phase high-performance liquid chromatography (RP-HPLC) [12–14], or supercritical fluid chromatography [15]. Because of the facile thermal conversion of tetryl to N-methylpicramide (Fig. 1b) during GC analysis [11], most routine analyses of tetryl in soil extracts have been conducted using RP-HPLC [16–18].

A comparison of extraction techniques for nitroaromatics and nitramines in soil showed that ultrasonic bath and Soxhlet extraction were superior to other methods examined and approximately equivalent in extraction efficiency, and that acetonitrile was superior to methanol due to its more rapid extraction of nitramines [19]. Tetryl was not studied, but the authors cautioned that thermally labile compounds can be a problem with the Soxhlet method because the extract is maintained at the boiling point of the solution

* Corresponding author.

SSDI 0021-9673(93)E1189-7

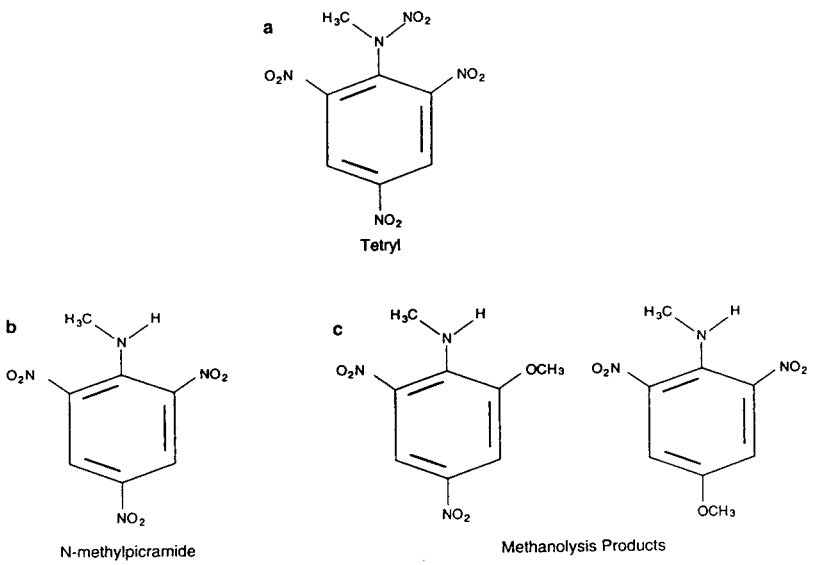

Fig. 1. Molecular structures of (a) tetryl, (b) N-methylpicramide and (c) tetryl methanolysis products.

in the receiver for an extended period. In a collaborative study of the ultrasonic bath extraction method, low recovery of tetryl was traced to high sonic bath temperatures ($>45°C$) [20]; for this reason, standard methods based on this procedure now specify that the sonic bath be maintained at or below room temperature [16–18].

In a recent study, wet, tetryl-fortified soils were extracted using methanol in a Soxhlet extractor for 48 h [21]. Care was taken to wrap the Soxhlet with aluminum foil to eliminate light. To test the stability of tetryl to Soxhlet extraction, a 15 mg/l solution of tetryl in methanol was refluxed for 48 h and the resulting solution analyzed by gradient elution RP-HPLC. After reflux, although the color of the solution changed from yellow to green (indicating that some tetryl degradation had occurred), a recovery of 82% of unaltered tetryl was reported. Because of the thermal lability of tetryl in GC–MS analysis [11], the conclusion that tetryl was unaltered by this process was based on RP-HPLC retention time using a gradient elution separation.

The objective of this work is to verify the stability of tetryl during Soxhlet extraction relative to its stability in the standard ultrasonic bath method [16–18].

EXPERIMENTAL

Chemicals

Standard analytical reference material (SARM) for tetryl was obtained from the US Army Environmental Center, Aberdeen Proving Ground, MD, USA. Water used in the preparation of HPLC eluent was reagent grade from a Milli-Q Type-1 reagent-grade water system (Millipore, Bedford, MA, USA). Methanol used in the preparation of eluent and for soil extraction was Alltech (Deerfield, IL, USA) HPLC grade. Acetonitrile used for soil extraction and for preparation of eluent was Baker (Phillipsburg, NJ, USA) analyzed HPLC grade. Eluent used for isocratic separations was prepared daily by combining the appropriate volumes of water, acetonitrile and methanol and vacuum filtering through a nylon-66 membrane (0.45 μm) to degas the solvent and remove particulate matter.

Instrumentation

RP-HPLC analyses were obtained on a modular system composed of the following: (1) Spectra-Physics (San Jose, CA, USA) Model 8800 ternary HPLC pump; (2) Spectra-Physics Spectra 100 variable-wavelength UV detector set at 254 nm with a cell path length of 0.6 cm; (3) Hewlett-Packard (Avondale, PA, USA) Model

HP 3393A digital integrator equipped with a Hewlett-Packard Model HP911B disk drive; (4) Linear (Reno, NV, USA) Model 500 strip chart recorder.

RP-HPLC separations

All separations were accomplished on either a Supelco (Bellefonte, PA, USA) LC-18 (octadecyldimethylsilyl) or LC-CN (cyanopropylmethylsilyl) column (25 cm × 4.6 mm, 5 μm particle size, 100 Å pore diameter) using either binary or ternary eluents composed of water, methanol and acetonitrile. The first was the gradient elution separation reported elsewhere [21], where an LC-18 column was eluted with 1.0 ml/min of water–acetonitrile, and the acetonitrile percentage was programmed from 35 to 100% at 1%/min. The second separation was isocratic on LC-18 using water–methanol (1:1) at 1.5 ml/min [13,16–18]. The third separation, also isocratic, was obtained on LC-CN eluted with water–acetonitrile–methanol (65:23:12) [22] at a flow-rate of 1.5 ml/min.

GC–MS analysis

All GC–MS analyses were conducted on an Hewlett-Packard 5992 mass-selective detector. Samples (1 μl) were introduced into the mass-selective detector through a Hewlett-Packard 5890 Series II gas chromatograph operated in the splitless mode. An HP-1 (cross-linked methyl silicone, 12 m × 0.20 mm, 0.33 μm film thickness) column was maintained at 45°C for 2 min and then the oven was temperature-programmed at 20°C/min to 240°C and held for 10 min.

Field-contaminated soil

Tetryl-contaminated soil collected at the Nebraska Ordnance Plant, Mead, NE, USA, was used to test various extraction techniques. Soil was air-dried, ground with a mortar and pestle, and mixed thoroughly to obtain as homogeneous a test sample as possible. Because the reported method [21] utilized undried soil, water was added to one test portion (2.0 ml to 10.0 g of soil) prior to Soxhlet extraction to examine the effect of the presence of water on the stability of tetryl during Soxhlet extraction.

RESULTS AND DISCUSSION

Instability of tetryl under reflux conditions

An initial experiment was conducted to examine the stability of tetryl during reflux in methanol reported elsewhere [21]. In this experiment a 2.02 mg/l solution of tetryl was prepared in methanol from a freshly opened bottle, and the solution was refluxed for 48 h in a Soxhlet extractor. The device was wrapped with aluminum foil to eliminate light. A drying tube was attached to the top of the condenser to minimize the incorporation of atmospheric moisture in the methanol during the 48-h reflux. After the extract cooled, a portion was analyzed using the three separations described above. A tetryl standard not subjected to reflux was analyzed as well. Analysis using the gradient elution separation [21] revealed one large peak that eluted at the same retention time as tetryl, a small peak eluting just prior to the retention time of tetryl that was identified as N-methylpicramide, and several other small peaks not present prior to refluxing, which were apparent degradation products caused by the instability of tetryl to reflux conditions (Fig. 2). The apparent recovery of tetryl was 59% compared with 82% reported in the earlier work [21]. However, when this extract was analyzed using an isocratic LC-18 separation [13,16–18], again one large

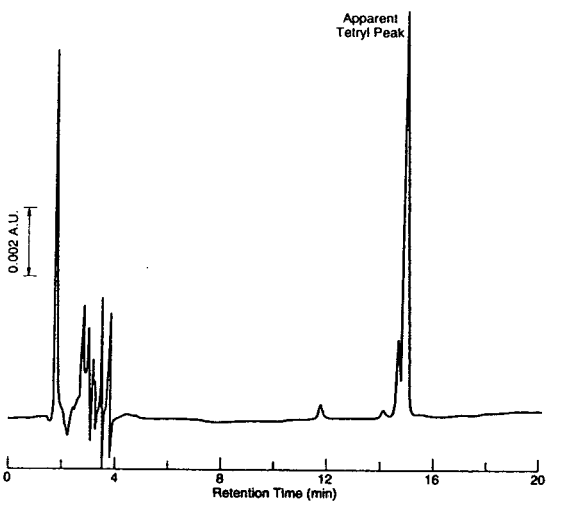

Fig. 2. HPLC chromatogram obtained by gradient elution of an LC-18 column of a tetryl solution refluxed in methanol.

peak was observed, but the retention time was longer than that for tetryl (Fig. 3). Very small peaks were observed at the retention time for tetryl and N-methylpicramide. These results were confirmed using a second isocratic separation on LC-CN [22], which resolved the single major peak observed on LC-18 into two peaks, neither of which had the characteristic retention time of tetryl (Fig. 4). The presence of two major degradation products was confirmed by GC–MS analysis of the extract. These peaks eluted from GC about a minute apart, but had very similar mass spectra. Their mass spectra are consistent with the structures of 2-methoxy-N-methyl-4,6-dinitroaniline and 4-methoxy-N-methyl-2,6-dinitroaniline (Fig. 1c). These compounds may be formed by methanolysis of N-methylpicramide, the initial degradation product of tetryl, or from methanolysis of tetryl followed by loss of the nitramine nitro group during GC–MS analysis in an analogous manner to the loss of NO_2 from tetryl under identical conditions. Thus our results indicate that tetryl is not stable when refluxed in methanol in the dark, even when the solution contains minimal water. These results conflict with those reported elsewhere [21] relative to the stability of tetryl to the reflux conditions typical of Soxhlet extraction.

Comparison of extraction methods for tetryl

An experiment was run to compare the stability of tetryl during Soxhlet extraction with the standard ultrasonic bath procedure using a soil collected at the Nebraska Ordnance Works that was field-contaminated with tetryl. A field-contaminated soil was selected for this study since earlier work indicated a difference in behavior between fortified and field-contaminated soil during extraction [13]. Two subsamples of 10.0 g each were placed in extraction thimbles and refluxed in Soxhlet extractors with methanol in the dark for 48 h, as described elsewhere [21]. Because this procedure uses undried soil, 2.0 ml of reagent-grade water were added to one subsample prior to extraction, and a drying tube was attached to the top of the condenser for the other, as described above. Two additional 2.0-g subsamples of dried soil were also extracted using an ultrasonic bath procedure for 18 h as

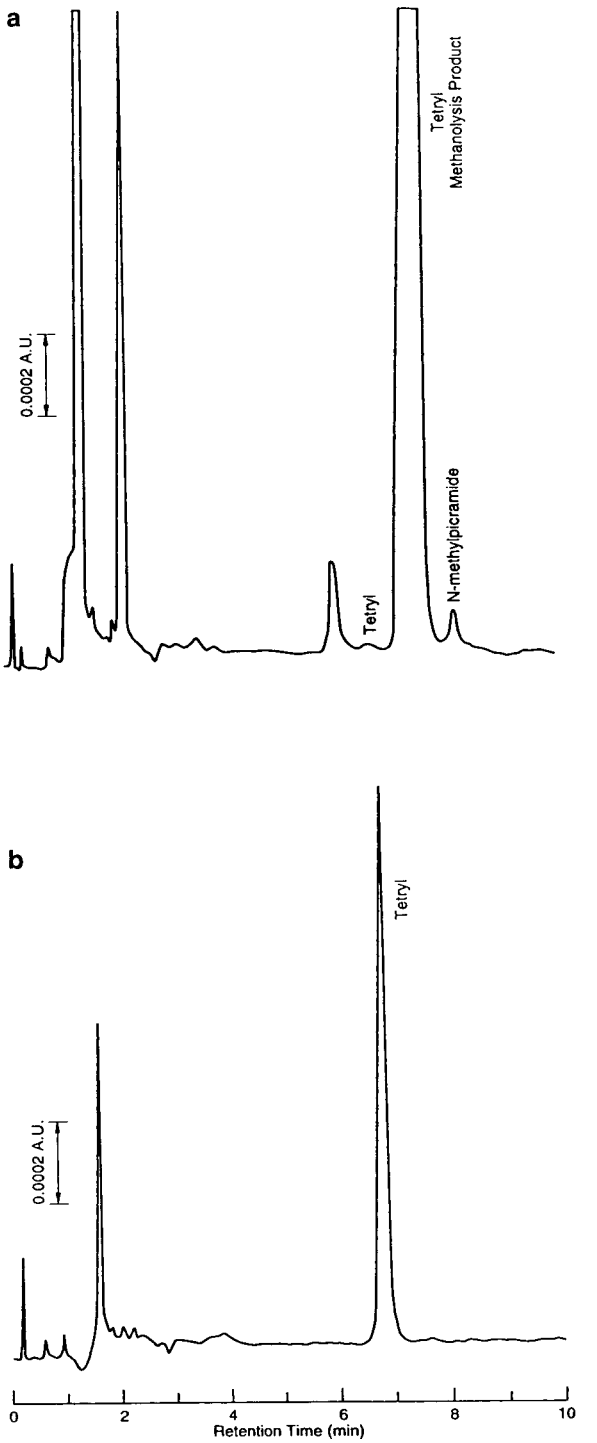

Fig. 3. HPLC chromatograms obtained by isocratic elution of an LC-18 column of (a) a tetryl solution refluxed in methanol and (b) a tetryl standard in methanol.

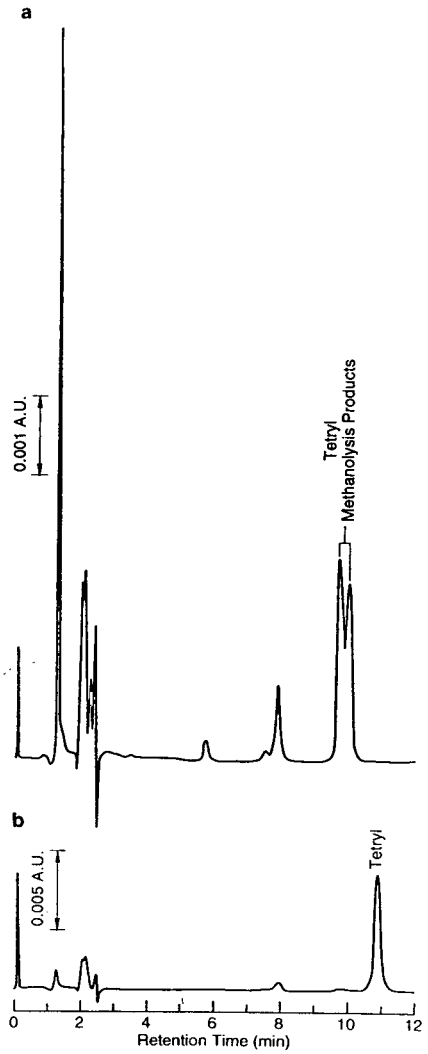

Fig. 4. HPLC chromatograms obtained by isocratic elution of an LC-CN column of (a) a tetryl solution refluxed in methanol and (b) a tetryl standard in methanol.

described elsewhere [13,16–18]. One portion was extracted using methanol and one using acetonitrile. The ultrasonic bath was maintained at or below room temperature to minimize thermal degradation of tetryl [20]. Because the ultrasonic bath procedure also imparts considerable energy into the sample during extraction and could also result in tetryl degradation, two portions of this dried soil were also extracted using a gentler wrist-action shaker procedure. These extractions were also conducted for 18 h at room temperature (about 22°C), one portion using methanol and one using acetonitrile.

The extracts from the Soxhlet, ultrasonic bath and wrist-action shaker were analyzed using the three RP-HPLC separations described above. Fig. 5 presents the chromatograms obtained for the methanol extracts from the Soxhlet, with and without addition of water, and the methanol extract from the ultrasonic bath procedure using the isocratic LC-18 separation. Recovery of tetryl, compared to the methanol extract from the wrist-action shaker, was only 0.2% for the Soxhlet extract of the wet soil and 60% for the Soxhlet extract of dry soil. In addition, the peak area for N-methylpicramide for the extract from the Soxhlet with wet soil was 19 times that found for the wrist-action shaker while the major degradation products from the dry soil were the methanolysis products (Fig. 1c). This behavior is consistent with the hypothesis of Davis and Allen [23], who attributed the conversion of tetryl to N-methylpicramide in refluxing capryl or *n*-butanol to hydrolysis from water present in these alcohols. Thus, the rapid loss of tetryl and immediate production of N-methylpicramide reported elsewhere, when tetryl was spiked onto wet soils and then extracted using the Soxhlet method, were probably artifacts of the Soxhlet extraction procedure [21]. The two chromatograms from extractions using the ultrasonic bath and wrist-action shaker with methanol are nearly identical, showing equivalent recovery of tetryl and a similar pattern of smaller peaks. They are considerably less complicated and qualitatively quite different from the chromatograms from the Soxhlet, particularly the one for wet soil. Chromatograms from the two other separations are consistent with these conclusions.

The methanolysis products discussed in our reflux experiments were also observed, although to a much lesser degree, in the methanol extracts from the ultrasonic bath and wrist-action shaker. As expected, these peaks do not appear in either acetonitrile extract. Instability of tetryl in methanol solution has been observed elsewhere [24], although the products were not reported. Because extracts are often held for many days prior to determination, we recommend the use

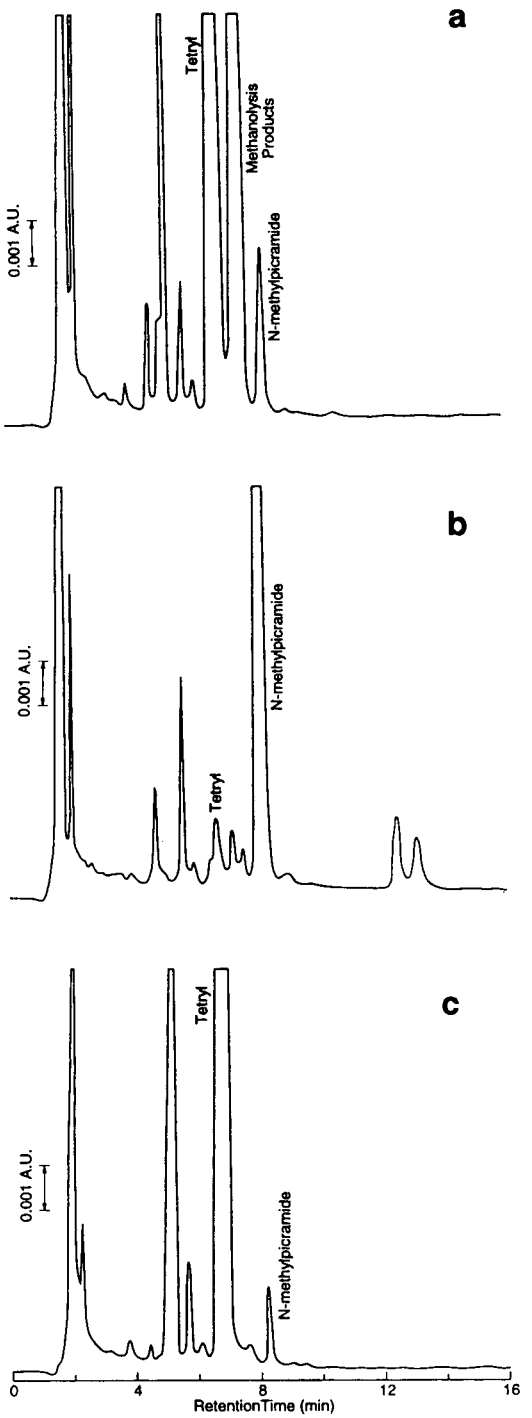

Fig. 5. HPLC chromatograms obtained by isocratic elution of an LC-18 column of extracts of a tetryl contaminated soil. (a) Soxhlet: dry soil (methanol); (b) Soxhlet: wet soil (methanol); (c) ultrasonic bath (methanol).

of acetonitrile rather than methanol for extraction of tetryl-contaminated soils.

CONCLUSIONS

The results of this study indicate that tetryl is not stable to Soxhlet extraction with methanol, particularly for undried soils, and we recommend ultrasonic bath extraction with acetonitrile. Tetryl's instability during Soxhlet extraction casts doubt on the validity of the conclusions presented elsewhere [21] relative to the kinetics of transformation of tetryl in soil and their identification of microbiological transformation products. Research is needed to determine the fate of tetryl in the environment, as was evident from the observation of large concentrations of tetryl remaining in soils contaminated with tetryl many years ago and the presence of a variety of unknown environmental transformation products in the extracts of these field-contaminated soils. The results of this study also demonstrate the need to use second column confirmation when analyte identification is accomplished by RP-HPLC retention time alone.

ACKNOWLEDGEMENTS

The authors acknowledge Dr. C.L. Grant, Professor Emeritus, University of New Hampshire, and D.C. Leggett of the US Army Cold Regions Research and Engineering Laboratory (CRREL) for useful comments and suggestions on the manuscript. S.M. Golden of the Science and Technology Corporation and P.G. Thorne of CRREL are acknowledged for conducting several of the experiments described. Funding for this research was provided jointly by the US Army Corps of Engineers Waterways Experiment Station, Vicksburg, MS, USA, Ann B. Strong, Project Monitor, and the US Army Environmental Center (formerly the US Army Toxic and Hazardous Materials Agency), Aberdeen Proving Ground, MD, USA, Martin H. Stutz, Project Monitor.

This publication reflects the personal views of the authors and does not suggest or reflect the policy, practices, programs, or doctrine of the US Army or Government of the USA.

REFERENCES

1 E.G. Kayser, N.E. Burlinson and D.H. Rosenblatt, *Report NSWC TR 84-68*, Naval Surface Weapons Center, Silver Spring, MD, 1984.
2 Department of the Army, Military Explosives, *Department of the Army Technical Manual TM9-1300-214*, Headquarters, Department of the Army, Washington, DC, September 1984.
3 M.N. Keirn, C.L. Stratton, J.J. Mousa, J.D. Bonds, D.L. Winegardner, H.S. Prentice, W.D. Adams and V.J. Powell, *USATHAMA Report DRXTH-AS-CR-81104*, US Army Toxic and Hazardous Materials Agency, Aberdeen Proving Ground, MD, 1981.
4 J. Batzer, S. Haverl, S. Frostman and J. Retzlaff, *USATHAMA Report DRXTH-AS-CR-82143A*, US Army Toxic and Hazardous Materials Agency, Aberdeen Proving Ground, MD, 1982.
5 M.E. Walsh, T.F. Jenkins, P.S. Schnitker, J.W. Elwell and M.H. Stutz, *Special Report 93-5*, US Army Cold Regions Research and Engineering Laboratory, Hanover, NH, 1993.
6 W.-Z. Whong, N.D. Speciner and G.S. Edwards, *Toxicol. Lett.*, 5 (1980) 11.
7 K. Raha, P.S. Makashir and E.M. Kurian, *J. Thermal Anal.*, 35 (1989) 1173.
8 E.P. Burrows, D.H. Rosenblatt, W.R. Mitchell and D.L. Palmer, *Report 8901*, US Army Biomedical Research and Development Laboratory, Frederick, MD, 1989.
9 T.F. Jenkins, *Dissertation*, Department of Chemistry, University of New Hampshire, Durham, NH, 1989.
10 F. Belkin, R.W. Bishop and M.V. Sheely, *J. Chromatogr. Sci.*, 24 (1985) 532.
11 T. Tamiri and S. Zitrin, *J. Energ. Mater.*, 4 (1986) 215.
12 T.F. Jenkins, D.C. Leggett, C.L. Grant and C.F. Bauer, *Anal. Chem.*, 58 (1986) 170.
13 T.F. Jenkins, M.E. Walsh, P.W. Schumacher, P.H. Miyares, C.F. Bauer and C.L. Grant, *J. Assoc. Off. Anal. Chem.*, 72 (1989) 890.
14 M.A. Major, R.T. Checkai, C.T. Phillips, R.S. Wentsel and R.O. Nwanguma, *Int. J. Environ. Anal. Chem.*, 48 (1992) 217.
15 W.H. Greist, C. Guzman and M. Dekker, *J. Chromatogr.*, 467 (1989) 423.
16 *Method for Analysis of Nitroaromatic and Nitramine Explosives in Soil by High Performance Liquid Chromatography, Method D5143–90*, American Society for Testing and Materials, Philadelphia, PA, 1991.
17 *Munition Residues in Soil, Liquid Chromatographic Method; Official First Action, September, 1990; Method 991.09, Second Supplement to the 15th Edition of Official Methods of Analysis*, Association of Official Analytical Chemists, Arlington, VA, 1990, pp. 78–80.
18 *Nitroaromatics and Nitramines by HPLC; Second Update SW846 Method 8330*, US Environmental Protection Agency, Washington, DC, 1992.
19 T.F. Jenkins and C.L. Grant, *Anal. Chem.*, 59 (1986) 1326.
20 C.F. Bauer, S.M. Koza and T.F. Jenkins, *J. Assoc. Off. Anal. Chem.*, 73 (1990) 541.
21 S.D. Harvey, R.J. Fellows, J.A. Campbell and D.A. Cataldo, *J. Chromatogr.*, 605 (1992) 227.
22 T.F. Jenkins and S.M. Golden, *Special Report 93-14*, US Army Cold Regions Research and Engineering Laboratory, Hanover, NH, 1993.
23 T.L. Davis and C.F.H. Allen, *J. Am. Chem. Soc.*, 36 (1924) 1063.
24 T.F. Jenkins, P.H. Miyares and M.E. Walsh, *Special Report 88-23*, US Army Cold Regions Research and Engineering Laboratory, Hanover, NH, 1988.

Journal of Chromatography A, 662 (1994) 185–190
Elsevier Science B.V., Amsterdam

CHROM. 25 687

Short Communication

Simultaneous microdetermination of chlorine, bromine and phosphorus in organic compounds by ion chromatography

Rosanna Toniolo and Gino Bontempelli*

Department of Chemical Sciences and Technology, University of Udine, via Cotonificio 108, I-33100 Udine (Italy)

Mirella Zancato and Agostino Pietrogrande

Department of Pharmaceutical Sciences, University of Padova, via Marzolo 5, I-35131 Padova (Italy)

(First received August 9th, 1993; revised manuscript received October 25th, 1993)

ABSTRACT

A procedure for the simultaneous microdetermination of chlorine, bromine and phosphorus in organic compounds is described. It consists of ion chromatographic analysis, after suitable dilution, of the solution resulting from the collection in water containing hydrogen peroxide of the combustion products obtained by decomposition of the sample in a Schöniger flask. Before analysis, this solution undergoes a post-combustion procedure involving further hydrolysis of the combustion products which allows a nearly quantitative recovery of phosphorus to be achieved even in the presence of other heteroatoms such as chlorine and bromine. This post-combustion step avoids negative errors in the microdetermination of phosphorus by ion chromatography owing to the minor but not insignificant amounts of both pyrophosphate and a cyclic metaphosphate which are formed together with the predominant orthophosphate in the conventional Schöniger combustion of organophosphorus compounds. The accuracy and precision of the overall procedure were evaluated.

INTRODUCTION

A great deal of work conducted over many years has produced a number of procedures for the accurate determination of the chlorine, bromine and phosphorus contents of organic compounds. These procedures usually involve converting the organically bound heteroatoms into the corresponding chloride, bromide and phosphate ions by a suitable sample decomposition procedure and then determination of the amounts of these ions by volumetric or gravimetric procedures [1].

Because the ions mentioned can be readily detected by ion chromatography, the application of this instrumental technique to microanalysis appears to be particularly advantageous. Indeed, ion chromatography is an attractive alternative to classical volumetric or gravimetric procedures as it is a selective technique able both to provide the simultaneous determination of a series of heteroatoms by using the same instrumentation, procedure and sample, and to remove many known interferents that usually affect their de-

* Corresponding author.

0021-9673/94/$07.00
SSDI 0021-9673(93)E1142-M

termination. In addition, the chromatographic portion of the analysis can be readily automated and requires no extensive operator training. A further significant advantage of this approach over the traditional chemical methods is a decrease in the time required for analysis.

Several papers suggesting ion chromatographic determination following Schöniger combustion of heteroatoms (F, Cl, Br, P, S) frequently present in organic compounds have been published [2–10]. However, when this type of procedure is applied to the determination of phosphorus present in organic molecules together with other heteroatoms, problems are often encountered that arise from the complexity of phosphorus chemistry. In fact, speciation of combustion products obtained using a conventional hydrogen peroxide absorption solution (3–4% w/w) suggests the formation of at least three oxyanions of phosphorus. The desired product (orthophosphate) is formed predominantly, but significant amounts of pyrophosphate and a cyclic metaphosphate are also detected [10]. This is not a real problem when phosphorus determination is subsequently performed by volumetric or gravimetric procedures, as the equilibria between these species shift towards the orthophosphate form thanks to its sequestration occurring in the quantitative reaction involved. In contrast, the formation of the mentioned less oxygenated species leads to negative errors when the phosphorus determination is performed by an ion chromatographic separation of the combustion products which does not perturb substantially the slow, spontaneous solution equilibria, so that the phosphorus content turns out to refer only to the recorded orthophosphates. Consequently, the problem of avoiding the formation of the undesired oxyanions of phosphorus was practically ignored as no real alternative to volumetric or gravimetric determination methods was available. Such a problem is also the probable reason why the ion chromatographic determination of phosphorus following Schöniger combustion has been considered, to our knowledge, only in two [2,10] of the several papers reporting the application of this procedure to elemental microanalysis. In particular, only in the most recent of these papers [10] was the minimization of the relevant error tackled.

To overcome this drawback, we propose here a post-combustion procedure involving further hydrolysis of the combustion products which allows a nearly quantitative recovery of phosphorus to be achieved even in the presence of other heteroatoms. This procedure was evaluated in detail for the routine ion chromatographic microdetermination of chlorine, bromine and phosphorus in organic compounds following the Schöniger combustion procedure. This evaluation also included the determination of the accuracy and precision of the method.

EXPERIMENTAL

Chemicals

All the chemicals used were of analytical-reagent grade and were used as received. In all instances, water purified with a Millipore Milli-Q system ("Milli-Q water") was used as the solvent.

Stock standard solutions of chloride, bromide and phosphate ions ($1 \cdot 10^{-3}$ *M*) were prepared by dissolving suitable amounts of the corresponding salts (NaCl, NaBr and NaH_2PO_4, respectively) in Milli-Q water. They were standardized by titration using the conventional Volhard method for chlorides and bromides and by titration with NaOH after precipitation as quinoline–phosphomolybdate for phosphates [11]. These solutions were then diluted to the desired concentration with Milli-Q water containing 1.8 m*M* Na_2CO_3 and 1.7 m*M* $NaHCO_3$ and in which the absence of Cl^-, Br^- and phosphates at concentrations higher than 10^{-7} *M* was first checked by ion chromatography.

Procedure

The procedure adopted for organic compounds involves the decomposition of known amounts of pure organic samples (2–10 mg) in a 500-ml Schöniger flask by collecting the combustion products in 10 ml of Milli-Q water containing 0.8 ml of 30% (w/w) H_2O_2. The samples were weighed, wrapped in a piece of Schleicher and Schüll No. 589-2 paper and then placed in the platinum basket. Oxygen was blown into the flask and the samples were burned in the usual way. Following combustion, the solutions obtained were boiled gently for 10 min while their

TABLE I

ION CHROMATOGRAPHIC CONDITIONS ADOPTED

Column	5-cm Dionex AG4 guard column plus 25-cm Dionex AS-4A separation column
Mobile phase	0.0018 *M* Na_2CO_3 + 0.0017 *M* $NaHCO_3$ in Milli-Q water
Flow-rate	2 ml min^{-1}
Temperature	Ambient
Detection	Suppressed conductivity at 30 μS using 0.0125 *M* H_2SO_4 as regenerant
Injection volume	50 μl

initial volume was continuously restored by adding small drops of Milli-Q water as required.

This boiling step was added to the usual procedure with the aim of facilitating the hydrolysis reactions and allowing the conversion of the less oxygenated oxyanions of phosphorus to the desired ortophosphate product.

The solutions thus obtained were transferred into volumetric flasks where they were diluted with a solution of 1.8 m*M* Na_2CO_3 and 1.7 m*M* $NaHCO_3$ in milli-Q water, *i.e.*, the mobile phase adopted in the subsequent ion chromatographic analysis (see later). By this dilution step, solutions containing the analyte elements in the concentration range $5 \cdot 10^{-5}$–$3 \cdot 10^{-4}$ *M* were obtained.

Ion chromatography was carried out by injecting a 50-μl sample of these solutions into a Dionex Model 2000i chromatograph equipped with a Dionex AS-4A anion-exchange column at room temperature. All determinations were performed by using a Dionex AMMS-1 micro-membrane suppressor continuously regenerated with 0.0125 *M* H_2SO_4 and a conductance detector. The chromatographic conditions adopted are reported in Table I.

Calibration

A preliminary calibration of the instrumental responses was performed by using standard solutions of NaCl, NaBr and NaH_2PO_4. Table II gives the retention times, detection limits calculated for a signal-to-noise ratio of 3 and the dynamic ranges explored. In fact, linearity extends over a much wider range but it was intentionally limited to take into account the amount of organic sample usually applied in the Schöniger combustion step. All peak areas found were characterized by good reproducibility, the relative standard deviation being 1.3%.

RESULTS

The reliability of the proposed procedure, aimed at making nearly quantitative the hydrolysis of the combustion products obtained from phosphorus-containing organic compounds, was first tested by application to the analysis of different organic samples each containing only a single heteroatom. Such a test was designed to check not only if the extended boiling step was really advantageous for phosphorus but also

TABLE II

RESULTS OBTAINED IN THE CALIBRATION OF INSTRUMENTAL RESPONSES

Analyte	Retention time (min)[a]	Detection limit (*M*)	Dynamic range explored (*M*)
Cl^-	1.86 (±0.02)	$1.05 \cdot 10^{-7}$	$5 \cdot 10^{-6}$–$5 \cdot 10^{-4}$
Br^-	3.65 (±0.05)	$1.45 \cdot 10^{-7}$	$5 \cdot 10^{-6}$–$5 \cdot 10^{-4}$
HPO_4^{2-}	6.61 (±0.06)	$1.51 \cdot 10^{-7}$	$5 \cdot 10^{-6}$–$5 \cdot 10^{-4}$

[a] Standard deviations ($n = 5$) in parentheses.

whether it is able to interfere in the determination of other heteroatoms.

The results obtained in these preliminary tests are reported in Table III, where each value found was calculated as the average of five replicate measurements. The good agreement between the experimental and theoretical values indicates that the proposed modification of the conventional procedure leads to satisfactory results for phosphorus without affecting the results relating to other heteroatoms.

Subsequently, to evaluate the accuracy and precision attainable by the suggested procedure, multiple analyses were performed on high-purity, crystalline samples of known composition. For this purpose, suitably dosed mixtures of chemically stable and non-hygroscopic organic compounds, each containing a single heteroatom, were employed. This was because the use of commercially available organic compounds containing simultaneously chlorine, bromine and phosphorus is not advisable because they are almost always characterized by poor stability and purity.

A typical chromatogram obtained after combustion of these samples is reported in Fig. 1. Peaks 1, 3 and 5 relate to chlorides, bromides and phosphates, respectively, *i.e.*, the ions corresponding to the analyte heteroatoms. Peaks 2, 4 and 6 relate to nitrites, nitrates and sulphates, respectively, which are contaminants generated in the combustion step. In fact, as demonstrated by comparison with blanks of sample wrapper and absorption solution, which were analysed in the same way as the organic sample, nitrites and nitrates arise from combustion of atmospheric nitrogen whereas the combustion of the sample wrapper leads both to sulphates and to a rather small and reproducible chloride response, which was subtracted from the peak area due to chlorides from the samples (the same correction was also made to the chloride determinations summarized in Table III). In contrast, no peak due to the carbonate generated from the carbonaceous portion of the organic sample plus the sample wrapper was observed. This is because the concentration of carbonate coming from the

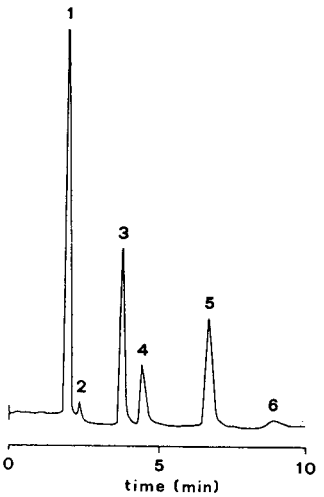

Fig. 1. Typical chromatogram obtained for organic samples containing simultaneously chlorine, bromine and phosphorus. Peaks: 1 = chloride; 2 = nitrite; 3 = bromide; 4 = nitrate; 5 = phosphate; 6 = sulphate.

TABLE III

COMPARISON BETWEEN EXPERIMENTAL AND THEORETICAL RESULTS FOR ORGANIC COMPOUNDS CONTAINING A SINGLE HETERO ATOM

Sample[a]	Chlorine (%)		Bromine (%)		Phosphorus (%)	
	Theoretical	Found[b]	Theoretical	Found[b]	Theoretical	Found[b]
PCBA	22.65	23.05 (0.36)	–	–	–	–
PBBA	–	–	39.75	39.92 (0.24)	–	–
TPP	–	–	–	–	11.81	11.72 (0.27)

[a] PCBA = *p*-Chlorobenzoic acid; PBBA = *p*-bromobenzoic acid; TPP = triphenylphosphine.
[b] Standard deviations ($n = 5$) in parentheses.

sample combustion does not exceed, under our experimental conditions, that present in the eluent, owing to the dilution of the combusted sample with the eluent which precedes the injection step. In fact, by simple calculations, such an additional concentration could be estimated to be typically *ca.* 20% of the background carbonate eluent.

Typical results obtained for the analysis of some of the mentioned sample mixtures, utilizing the peak areas for the various elements, are summarized in Table IV, which reports both accuracy and precision. Precision is expressed as the standard deviation calculated for five measurements relative to independent combustions of the same sample. These results appear to be satisfactory in that both their accuracy and precision compare fairly well with those expected by the classical methods.

CONCLUSIONS

The suggested procedure for the simultaneous microdetermination of chlorine, bromine and phosphorus in organic compounds is characterized by satisfactory accuracy. A maximum absolute difference with respect to the corresponding theoretical values of ±0.45% is observed, so that a relative error within 5% can in general be estimated. Good precision is also obtained, the relative standard deviation generally being within 4%. This performance is also comparable to (or only slightly worse than) that provided by gravimetric or volumetric methods for the same elements. However, the short analysis time and simplicity of the ion chromatographic analysis more than compensate for the slight difference.

The major advantages of this type of analysis are the selectivity, which eliminates possible

TABLE IV

COMPARISON BETWEEN EXPERIMENTAL AND THEORETICAL RESULTS FOR MULTIPLE HETEROATOM ORGANIC SAMPLES

Sample[a]	Chlorine (%)		Bromine (%)		Phosphorus (%)	
	Theoretical	Found[b]	Theoretical	Found[b]	Theoretical	Found[b]
2.892 mg PCBA 2.131 mg PBBA 4.327 mg TPP	7.00	7.39 (0.45)	9.06	9.15 (0.47)	4.86	4.78 (0.09)
1.991 mg PCBA 4.063 mg PBBA 3.851 mg TPP	4.55	4.80 (0.35)	16.30	16.48 (0.10)	4.63	4.60 (0.14)
4.099 mg PCBA 2.822 mg PBBA 2.813 mg TPP	9.54	9.46 (0.37)	11.52	11.96 (0.45)	3.41	3.25 (0.09)
2.847 mg CDEC 3.971 mg BAP 2.630 mg TPP	6.37	6.66 (0.45)	10.62	10.98 (0.28)	3.29	2.98 (0.28)
3.355 mg CDEC 3.073 mg BAP 2.730 mg TPP	7.74	7.75 (0.13)	8.48	8.67 (0.23)	3.52	3.24 (0.08)
2.840 mg CDEC 3.030 mg BAP 3.941 mg TPP	6.11	6.56 (0.42)	7.81	8.12 (0.05)	4.74	4.63 (0.38)

[a] PCBA = *p*-Chlorobenzoic acid; PBBA = *p*-bromobenzoic acid; TPP = triphenylphosphine; CDEC = chlordiazepoxide hydrochloride; BAP = bromazepan.

[b] Standard deviations ($n = 5$) in parentheses.

interferences without additional sample preparation, and the ability to perform simultaneous determinations using a single procedure which requires total analysis times of no longer than about 30 min.

ACKNOWLEDGEMENTS

The authors thank Mr. A. Valentino of the University of Udine for skilful experimental assistance. Financial aid from the Italian National Research Council (CNR) and the Ministry of University and of Scientific and Technological Research (MURST) is gratefully acknowledged.

REFERENCES

1 F. Ehrenberger, *Quantitative Organische Elementaranalyse*, VCH, Weinheim, 1991.
2 J.F. Colaruotolo and R.S. Eddy, *Anal. Chem.*, 49 (1977) 884.
3 T. Hara, K. Fujinaga and F. Okui, *Bull. Chem. Soc. Jpn.*, 54 (1981) 2956.
4 H. Saitoh and K. Oikawa, *Bunseki Kagaku*, 31 (1982) E375.
5 C.Y. Wang, S.D. Bunday and J.G. Tarter, *Anal. Chem.*, 55 (1983) 1617.
6 M. Kan, K. Ohnishi and M. Shintani, *Yakagaku Zasshi*, 104 (1984) 763.
7 A.M. Quinn, K.W.M. Siu, G.J. Gardner and S.S. Berman, *J. Chromatogr.*, 370 (1986) 203.
8 J.R. Kreling, F. Block, G.T. Louthan and J. De Zwaan, *Microchem. J.*, 34 (1986) 158.
9 G. Brandt and A. Kettrup, *Fresenius' Z. Anal. Chem.*, 327 (1987) 213.
10 J.P. Senior, *Anal. Proc.*, 27 (1990) 116.
11 A.I. Vogel, *A Text-Book of Quantitative Inorganic Analysis*, Longmans, London, 1961.

Journal of Chromatography A, 662 (1994) 191–197
Elsevier Science B.V., Amsterdam

CHROM. 25 662

Short Communication

Reduction/elimination of sulfur interference in organochlorine residue determination by supercritical fluid extraction

R. Tilio

Department of Chemistry and Center for Environmental Science and Technology, University of Missouri–Rolla, Rolla, MO 65401 (USA) and European Communities Joint Research Center, Ispra (Italy)

S. Kapila * and K.S. Nam

Department of Chemistry and Center for Environmental Science and Technology, University of Missouri–Rolla, Rolla, MO 65401 (USA)

R. Bossi

Sea Marconi Technologies, Collegno (TO) (Italy)

S. Facchetti

European Communities Joint Research Center, Ispra (Italy)

(First received May 4th, 1993; revised manuscript received October 18th, 1993)

ABSTRACT

Supercritical fluid extraction (SFE) was used for selective extraction of polychlorinated biphenyls and chlorinated pesticides from sediment samples fortified with elemental sulfur. The results obtained showed that use of SFE in static mode can lead to significant reduction in sulfur interference.

INTRODUCTION

Organochlorines as a class are some of the most persistent organic contaminants in the environment. These chemicals have found wide application in the past; however, due to adverse effect of these chemicals on human health and the environment, their use has been severely curtailed during the past decade. Despite the discontinuation of their use, these compounds are still prevalent in all compartments of the environment. Due to direct link of aquatic systems to human exposure, the contamination of aquatic systems is of special concern. In aquatic systems sediments are the primary reservoir of all hydrophobic compounds and monitoring pro-

* Corresponding author.

0021-9673/94/$07.00
SSDI 0021-9673(93)E1100-E

grams for environmental quality of aquatic systems generally involve measurements of contaminants in sediments. The traditional analytical methodologies employed for this purpose are quite laborious, a major problem in the sediment residue monitoring being the interference caused by elemental sulfur. The elemental sulfur in sediments results from degradation of biological materials, especially under anoxic conditions. The interference is quite serious when electron-capture detection (ECD) is used. The sulfur interference is linked to three factors.

(1) Aggregates of elemental sulfur exhibit partition behavior similar to organochlorine compounds in system where the fluid phase is a non-polar or a moderately polar organic solvent. As a result, elemental sulfur aggregates are extracted and carried through most adsorbent-based clean-up techniques.

(2) Sulfur aggregates exhibit chromatographic characteristics similar to a number of organochlorine compounds of interest in gas chromatography.

(3) Sulfur aggregates possess high affinity for thermal electrons and give strong ECD responses, which continues to be the primary detection method for polychlorinated organics.

In traditional analytical schemes, the sulfur interference problem has been dealt with using three different approaches. The first approach involves removal through size-exclusion chromatography (SEC). SEC is used extensively for removal of large interfering and/or other problematic molecules such as lipids. The technique has also been used to remove low levels of sulfur from extracts containing organochlorine compounds [1]. The removal is based on the fact that the most prevalent sulfur aggregates, such as S_8, possess a condensed cyclical structure and can exhibit total penetration on a selected SEC column. By proper selection of column gel packing, sulfur can be separated from the organochlorine compounds of environmental concern. Since the technique is based on physical separation, no artifacts or anomalies are introduced by its use. The primary limitation of the technique is due to the small column capacity which leads to the overloading of the column; this results in loss of separation between analytes of interest and sulfur.

The other techniques for removal of sulfur involve either reaction with metallic copper, mercury or tetrabutylammonium sulfite. The treatment with metallic copper is perhaps the most frequently used method and results in precipitation of sulfur as sulfide [2]. The methodology is very effective; however, its use results in degradation of a number of analytes of environmental interest.

It is quite logical that the performance of analytical methodology can be enhanced if a selective extraction procedure is employed to decrease the amount of sulfur in the extract. Supercritical fluid extraction (SFE) offers selectivity and has been shown to be applicable for a variety of small non-polar analytes in different matrices [3–5]. The present study was designed to monitor the effectiveness of SFE for reducing sulfur interference during organochlorine residues determinations.

Studies were also undertaken to improve the SFE process by optimization of adsorbent material for trapping extracted components.

EXPERIMENTAL

All SFE experiments were carried out with a multichamber SFE system, the details of which have been provided elsewhere [4]. The system consists of a pneumatic amplifier, extraction vessels [capable of withstanding up to 400 atm (1 atm = 101 325 Pa) pressure] and adsorbent traps. A schematic of the system is given in Fig. 1.

All experiments were conducted with sediment samples collected from streams in Missouri, USA. All evaluations were carried out with the material balance approach, which involved fortification of samples aliquots with known concentrations of elemental sulfur (0.15%) and organochlorines of interest, such as hexachlorobenzene, hexachlorocyclohexanes, chlordane, heptachlor, heptachlor epoxide, *p,p'*-DDT (and metabolites) and polychlorinated biphenyls (PCBs). The concentration of pesticides in the experiments was varied from 20 to 200 parts per billion (ppb, w/w). A 1-kg batch of samples was

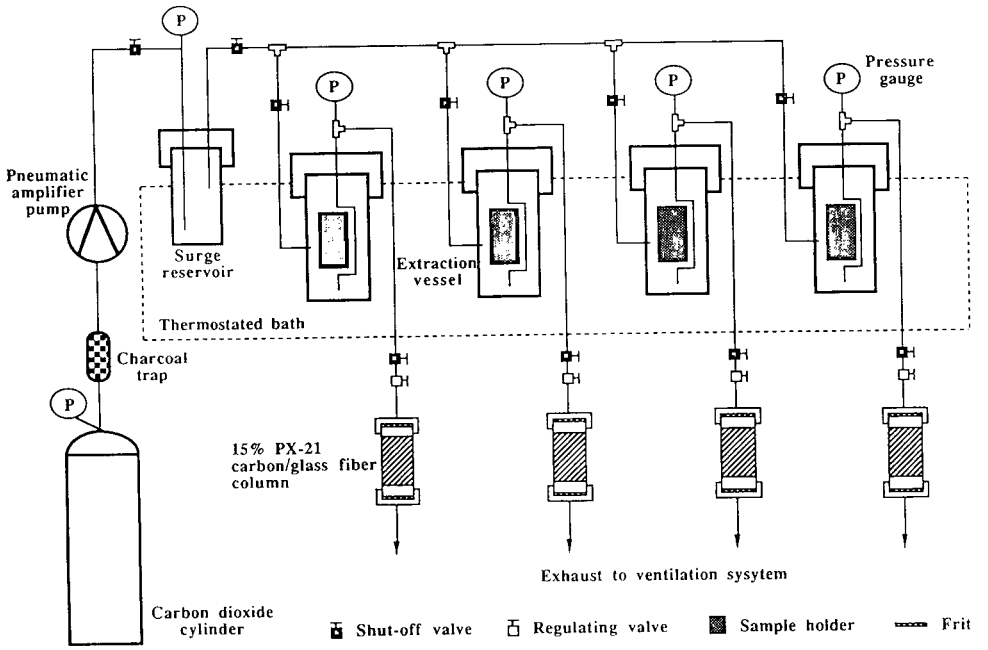

Fig. 1. Schematic diagram of SFE system.

homogenized, air dried, and sieved to remove stones and aggregates larger than 2 mm. Aliquots (5–10 g) were used for organochlorines residue determination. The samples were homogenized with anhydrous sodium sulfate and clean Pyrex wool, and the mixture was placed in a stainless-steel wire mesh sample holder. The sample holders were placed in the SFE vessels which were submerged in a thermostated water bath. The vessels were sealed and pressurized with either CO_2 or N_2O. All extractions were carried out in the static mode. Effects of density, temperature and equilibration period on extractability and the selectivity were monitored.

The extracted sediment components were trapped in solid adsorbent traps. Experiments to optimize the composition of adsorbent materials were carried out independently. The criteria for selection of optimal adsorbent material were minimum breakthrough and high desorption efficiency. To ascertain the breakthrough a series configuration was employed. The high-pressure cartridges used as adsorbent traps, were of an easy-to-operate snap-on/snap-off type, designed in our laboratories. A number of adsorbent materials were used, including silica gel Davidson grade 923, Florisil and graphitized carbon.

For comparative purposes, samples were also extracted in Soxhlet and subjected to classical clean-up steps including chromatographic fractionation on Florisil, size-exclusion and silica gels.

When required, the Cu metal treatment was used for removing elemental sulfur. Cu for this purpose was obtained by rinsing fine granular Cu with diluted nitric acid, followed by thoroughly rinsing with water, acetone and hexane. Approximately 0.6 g of the clean Cu was added to each sample extract, the contents were shaken for 10 min, the supernatant was separated and a 2-μl portion injected into a gas chromatograph. The gas chromatographic analyses were performed on a capillary gas chromatograph, Perkin-Elmer Model 8500 equipped with a split–splitless injector and an electron-capture detector. Gas chromatographic separations were carried out with a 30 m $\times$ 0.25 mm fused-silica capillary column coated with 95% methyl and 5% phenyl polysiloxane; helium was used as the carrier gas.

Gas chromatographic conditions were: injector

temperature 255°C; oven temperature program 1 min isothermal at 80°C, then at 10°C min^{-1} to 180°C, then at 3°C min^{-1} to 255°C, isothermal for 9 min. Determinations of polychlorinated dibenzo-*p*-dioxins (PCDDs) were carried out with a quadruple mass spectrometer (Hewlett-Packard MSD Model 5970B) interfaced with a gas chromatograph (Hewlett-Packard Model 5890). The mass spectrometer was operated in selected ion monitoring mode. The quantitation of PCDDs was accomplished with ^{13}C-labeled internal standards.

RESULTS AND DISCUSSION

The applicability of supercritical fluids for the extraction of non-polar and moderately polar analytes from soils or sediments has been demonstrated by a number of researchers [6–9]. Extraction efficiencies approaching 100% can be obtained even under moderate operating parameters, in the near critical region, especially in the presence of polar modifiers/wetting agents [6]. However, the acceptance of this technique for routine applications has been slow due to the relatively high cost of the extraction systems and poor precision. The latter problem is related to inefficient trapping of extracted analytes. An ideal trapping system is one which retains all analytes while allowing all of the extracting fluid to escape. The most common approach involves expansion of condensed fluid through a restrictor, where the expansion leads to a drop in the solubility of analytes. Analytes are then collected either on the walls of an expansion vessel or in an adsorbent trap or liquid impingers. The breakthrough of analytes in condensed CO_2 aggregates is the most severe problem in all trapping systems. The problem can be alleviated by using low-volume thermostated restrictors; however, this results in long decompression periods. For large extraction vessels, decompression periods often exceed extraction equilibration periods. The proper selection of trapping system is thus an important consideration for analytical SFE.

Application of adsorbent traps, in cases where the trap can serve a dual purpose of fractionation and clean-up, is quite attractive. For the present application, a dual adsorbent trap was found to give the best results. The trap consisted of a stainless steel tube (150 mm × 9 mm I.D.) designed to fit into a Swagelok quick-connecting fitting. The trap was packed with a 20-mm layer of Florisil and topped with a 20-mm layer of graphitized carbon PX-21 (10%, w/w, on glass fiber).

The choice of adsorbent combination was made to facilitate fractionation of PCDDs, PCBs, chlorinated pesticides and polar co-extractants. This fractionation was accomplished by forward elution with hexane, hexane–dichloro-

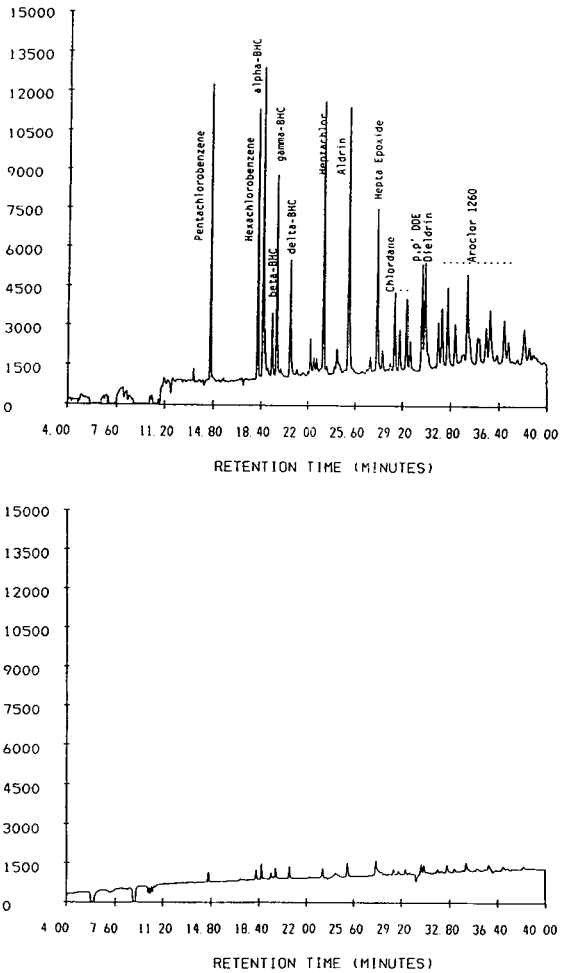

Fig. 2. Gas chromatographic output for SFE breakthrough experiment: chlorinated pesticides and PCBs. Hexane–diethyl ether (94:6); top: trap 1, bottom: trap 2. BHC = Benzene hexachloride.

methane (50:50) followed by a reverse extraction with toluene. Further fractionation into subclasses is feasible but was not optimized for the present study. The evaluation of traps included breakthrough and recovery experiments.

The breakthrough experiments were carried out by assembling two traps in a series. The carbon layer in the first trap was spiked with a mixture containing PCDDs, pesticides and PCBs. The extraction system was assembled and pressurized with CO_2 to 200 atm at 50°C. The fluid was then released through the serial trap. Both traps were eluted with hexane and hexane–dichloromethane mixture in the forward direction followed by extraction with toluene in the reverse direction. All components of the mixture were quantitatively recovered from the first trap indicating essentially zero breakthrough. The results are shown in Figs. 2 and 3, which depict the chromatographic traces of pesticides/PCBs extracts (hexane–dichloromethane fraction) and PCDDs extract (toluene fraction), respectively. The total concentration of components in the second trap extract was $\leq 2.0\%$ indicating minimal breakthrough.

The SFE experiments were carried out after optimization of trapping systems. The fortified sediment, containing 20–200 ppb of pesticides and PCBs and 0.15% (w/w) elemental sulfur, was placed in the extraction vessel. Results of extraction carried out at different densities (constant temperature) are given in Table I. The results show that all analytes were extracted quantitatively; recoveries were generally better

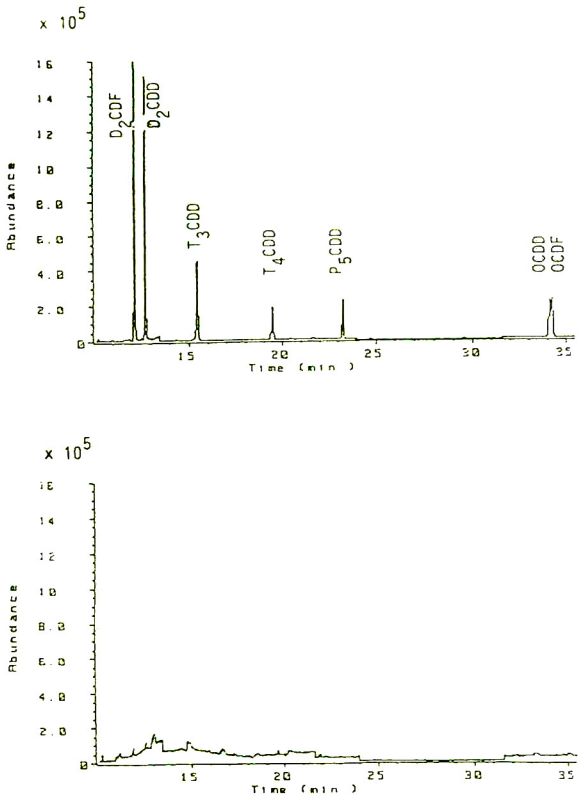

Fig. 3. Gas chromatographic output for SFE breakthrough experiment: polychlorinated dibenzo-*p*-dioxins. Reverse toluene extract; top: trap 1, bottom: trap 2. D_2CDF = dichlorodibenzofuran; D_2CDD = dichlorodibenzodioxin; T_3CDD = trichlorodibenzodioxin; T_4CDD = tetrachlorodibenzodioxin; P_5CDD = pentachlorodibenzodioxin; OCDD = octachlorodibenzodioxin; OCDF = octachlorodibenzofuran.

TABLE I

RECOVERY AT DIFFERENT EXTRACTION PRESSURES AND CONSTANT TEMPERATURE (323 K)

Results are averages of five determinations. Standard deviation for the recovery was 3.6.

Analyte	Recovery (%)			
	Extraction pressure (atm)			
	136	156	177	197
γ-Benzene hexachloride	98	98	92	93
Hexachlorobenzene	92	95	98	93
Heptachlor	105	96	96	95
Heptachlor epoxide	89	96	98	97
trans-Chlordane	98	96	96	96
cis-Chlordane	95	94	95	98
Dieldrin	98	93	91	94
p,p'-DDE	95	92	93	93
p,p'-DDD	89	85	84	83
p,p'-DDT	85	86	94	87
2,3,7,8-Tetrachlorodibenzo-*p*-dioxin	78	73	85	92
2,3,6,7,8-Pentachlorodibenzo-*p*-dioxin	73	76	81	90
Octachlorodibenzo-*p*-dioxin	65	66	78	85

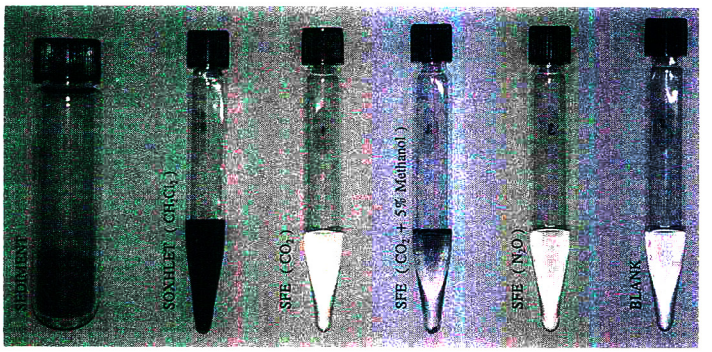

Fig. 4. Photograph of supercritical fluid and liquid solvent extracts of sulfur- and organochlorine-fortified soil.

than 85%, while the recovery for fortified sulfur ranged between 1–3%. By contrast, ≥90% of the fortified sulfur was recovered with liquid solvent extraction. The results of relative extractability of sulfur and other contaminants from soil/sediment samples are shown in Fig. 4. Quantitation of sulfur content in liquid extract and supercritical extract reveal that a 50-fold increase in selectivity for organochlorines over sulfur was obtained. However, the residual sulfur in SFE extract still caused considerable interference problems (Fig. 5). The interference problem was easily eliminated by mild treatment with Cu or SEC. The results obtained are shown in Fig. 6. By contrast, the sulfur content in fortified samples extracted in liquid solvent remained high even after Cu treatment and pre-

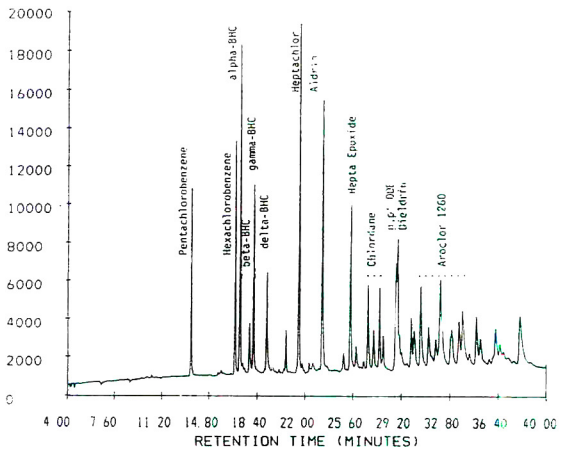

Fig. 6. Chromatographic output of Cu-treated SFE extract. Extraction fluid CO_2, 136 atm, 50°C.

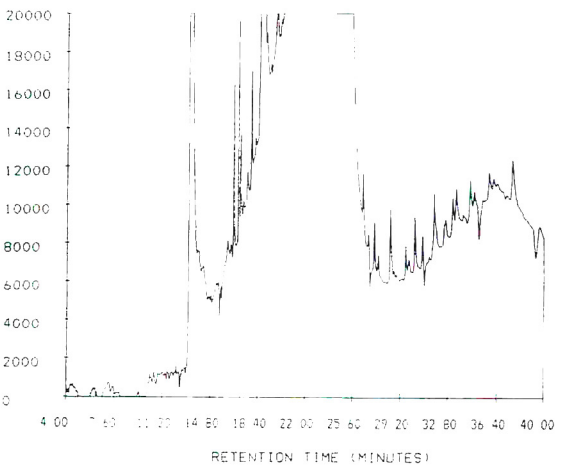

Fig. 5. Chromatographic output of supercritical fluid extract of sulfur-fortified soil. Extraction fluid CO_2, 136 atm, 50°C.

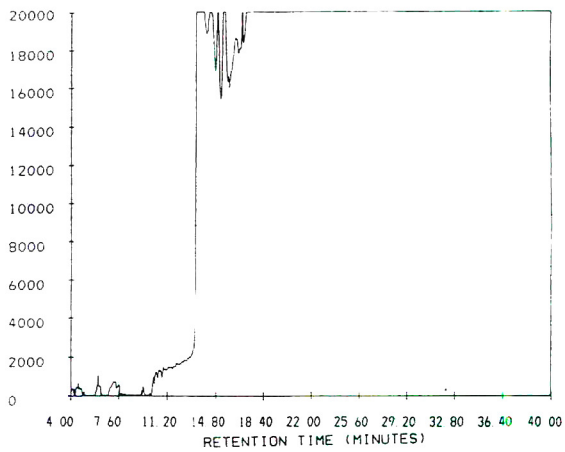

Fig. 7. Chromatographic output of liquid solvent extract after Cu treatment.

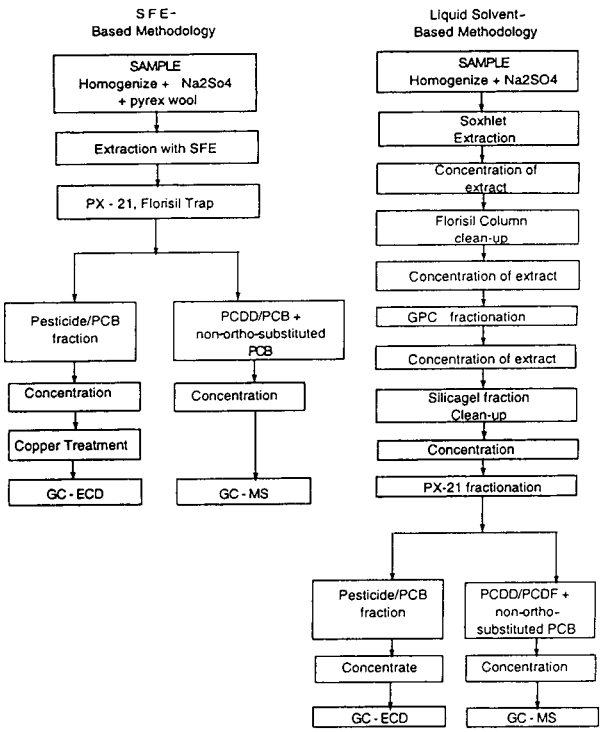

Fig. 8. Flow schematic of analytical methodologies. PCDD = Pentachlorodibenzodioxin; PCDF = pentachlorodibenzofuran.

vented detection and quantitation of any analytes. Chromatographic results obtained for a sample extracted in liquid are shown in Fig. 7. The results clearly demonstrate the superiority of SFE in reducing interference problems associated with the presence of elemental sulfur. Furthermore, the SFE and associated clean-up methodology is considerably faster. The methodology is essentially a two-step process compared to multi-step liquid solvent-based methodologies. The flow diagrams of the two approaches are given in Fig. 8.

ACKNOWLEDGEMENTS

The study was supported, in part, by grants from the Environmental Affairs Division of Southern California Edison, Rosemead, CA, USA and US Environmental Protection Agency Hazardous Substances Research Center, Kansas State University, Manhattan, KS, USA, under assistance agreement R-815709. Contents of the article have, however, not been subjected to the agency's peer review system.

REFERENCES

1 R.J. Marider, V. Taylor and M.R. Kennedy, *Evaluation of Method 3640 Gel Permeation Cleanup, Contract No. 69-03-3375*, US Environmental Protection Agency, Cincinnati, OH, 1987.
2 *US EPA Test Method for Evaluating Solid Waste Physical/Chemical Method, Test Number 3600, SW846*, US Environmental Protection Agency, Cincinnati, OH, 1990.
3 K.S. Nam, S. Kapila, D.S. Viswanath, T.E. Clevenger, J. Johansson and A.F. Yanders, *Chemosphere*, 19 (1989) 33–38.
4 K.S. Nam, S. Kapila, A.F. Yanders and R.K. Puri, *Chemosphere*, 20 (1990) 879–880.
5 K.S. Nam, S. Kapila, A.F. Yanders and R.K. Puri, *Chemosphere*, 23 (1991) 1109–1116.
6 D.J. Entholt, K. Thrun and C. Eppig, *Int. J. Environ. Anal. Chem.*, 13 (1983) 219.
7 K.M. Dooley, C.P. Kao, R.P. Gambrell and F.C. Knopf, *Ind. Eng. Chem. Res.*, 26 (1987) 261–268.
8 S.B. Hawthorne, D.J. Miller and M.S. Krieger, *Fresenius' Z. Anal. Chem.*, 330 (1988) 211–216.
9 F.I. Onuska and K.A. Terry, *J. High Resolut. Chromatogr.*, 12 (1989) 527–531.

Journal of Chromatography A, 662 (1994) 198–199
Elsevier Science B.V., Amsterdam

CHROM. 25 755

Book Review

Chromatography of mycotoxins — Techniques and applications (*Journal of Chromatography Library*, Vol. 54), edited by V. Betina, Elsevier, Amsterdam, 1993, XIII + 440 pp, price Dfl. 315.00, ISBN 0-444-81521-X

This volume is entirely devoted to techniques used in analytical chemistry. It consists of two parts; part A contains six separate chapters that covers the basic techniques commonly used in analytical chemistry and part B is devoted to applications/methods to mycotoxins.

In part A, most of the techniques are well enumerated and are compiled with adequate references at the end of each chapter. Techniques in thin-layer chromatography are illustrated with the description of small instruments or devices such as the U chamber, the Nanomat III with a semi automatic spotting instrument, the Camag TLC auto sampler, which can be useful for routine or semi-routine analysis. The following chapter is devoted to column chromatography of different types (silica gel) from the classical applications to the flash chromatography these types of column are extended to the HPLC column with different types of silica bonded and HPLC equipment along with different types of injectors and detector (UV, fluorescent). It would have been important to mention the chemiluminescent detectors available even if applications to mycotoxins have not yet been done. The theoretical basis of gas chromatography and the different detection methods commercially available (flame ionization, electron-capture, mass spectrometry) complete the description of this chapter. The next chapter on immuno-affinity technique is very well documented for the preparation, separation and various type of commercially available ligands. Following this chapter the enzyme-linked immunosorbent assay for mycotoxins is well presented. Since mycotoxins are haptens to be bound to a neutral protein to produce polyclonal antibodies or the monoclonals depending on the technique used. Applications for the aflatoxins and trichothecenes are adequately illustrated theses procedures. It would have been useful to mention the new technique using supercritical fluid extraction with or without coupling to gas chromatography detection as a separation technique.

Part B is mainly devoted to applications to mycotoxins. The first chapter is devoted to thin-layer chromatography with extensive examples and procedures given (extraction and clean-up, adsorbents and solvent system, and applications to aflatoxins, sterigmatocystin and related compounds, trichlothecenes, penicillic acid, tremorgenic mycotoxins, altenaria toxins, α-cyclopiazonic acid, mycotoxins produced by *Fusarium moniliforme*, etc.).

The following chapter deals with liquid column chromatography and over 20 pages are an enumeration of all fungal metabolites and over 30 pages on UV data for fungal metabolites. Examples are also given on the application of column chromatography and HPLC of aflatoxin, zearalenone, ochratoxins and related compounds and application of HPLC–MS. The last chapter deals with gas chromatography of mycotoxins for example the trichothecenes and the most common reagents used to derivatize the hydroxyl function of the trichothecenes. Detection using flame ionization, electron-capture or MS and the corresponding levels of sensitivity are given for each trichothecene. The preferred GC method is the capillary GC–MS. Mass spectra are essential to identify the trichothecenes species, applications for biological fluids, detection of T-2 toxin metabolities and *in vitro* studies on fungal culture, in grains foods and feeds. Applications for

SSDI 0021-9673(93)E1288-B

moniliformin, to the alternaria toxins, salframine and swainsonine, patulin, penicillic acid, sterigmatocystin, aflatoxins, ergot alkaloids, fumosinine, butenolide, fusarin C, griseofulvine, ochratoxin and fusarochromone are listed.

In conclusion this book is a very useful book an very well presented with information that will be useful to any laboratory wishing to initiate work in the area of mycotoxins or as reference book for more experienced workers.

Ottawa (Canada) Huguette Cohen

Journal of Chromatography A, 662 (1994) 200–201
Elsevier Science B.V., Amsterdam

CHROM. 25 736

Book Review

Gel electrophoresis: proteins, by M.J. Dunn, ßIOS Sci. Publ., Oxford, 1993, price £15, ISBN 1-872-74821-X.

I am sitting at my desk staring at a cheque which I just received from Butterworth Heinemann for a total of £1.74 (from an original £1.97 minus £0.23 personal income tax). I do not seem to be able to cash it. My bank claims that it will cost £3 to change it. I sent it to the Salvation army as a gift, but they returned it to me: they seem to have the same problem. This lavish sum seems to be my royalty for a chapter I wrote for an extremely good book: *Gel Electrophoresis of Proteins*, edited by M.J. Dunn (Wright, Bristol, 1986). This book was really well written, with very comprehensive chapters on all aspects of gel electrophoresis, a deep theoretical treatment and the like. Dunn has now rewritten the earlier book, stripping it down to the bare bones: this time, it is purely practical, with not even a single equation! The theoretical section, in fact, is more title lines than any real contents. Is this approach correct? Well, I am not sure: I am afraid that if the approach to science is stripped down to a cook book, we will be confronted with a generation of scientists who will insist they understand electrophoresis even though they might not be able to distinguish it from electroendosmosis. If we continue like that, we might end up with the big discovery of an Italian publisher (Etas Compass) who, 2 years ago, launched a series of books (available at news stands) called "mille lire" (from the price: 1000 lire, less than the cost of a newspaper!). Well, I wonder what would happen if tomorrow our new generation of scientists will be able to stop at a news stand and ask, "please give me 1000 lire worth of electrophoresis (or chromatography or genetic engineering. . .)".

Thus, with the present book, I am afraid it has a feeling of déjà vu throughout. It contains the same information available in all other books [such as the *Practical Approach Series*, *e.g.*, *Protein Structure*, edited by T.E. Creighton (IRL Press, Oxford, 1989) and *Gel Electrophoresis of Proteins*, by B.D. Hames and D. Rickwood (IRL Press, Oxford, 1990), the *Advances in Electrophoresis* series and the *Paper Symposia* in the journal *Electrophoresis*]. What I really cannot accept is the fact that there is no mention of capillary zone electrophoresis (CZE): this is truly the emerging novel technique and not to mention it seems to be rather crude. There is no excuse with the title, which is limited to gel electrophoresis of proteins: there is plenty of gel electrophoresis one can perform in CZE and, in addition, the novel revolution is even for more sophisticated matrices: polymer networks, a subtle concept promulgated already in 1979 by Nobel Laureate De Gennes and finally coming of age. If I were to recommend a book in this area today, sorry, but I would rather select *Elektrophorese-Prakticum* by R. Westermeier. Published in 1990, it was a delight of fresh and sparkling and very instructive drawings (done by Reiner himself on endless nights at the computer). Now that the *Prakticum* has become *Practice* (English translation from the German in 1993, by VCH, Weinheim), it is truly enjoyable reading, and the drawings have the charm that only Reiner could invent, such as Fig. 33 (p. 54), where the overnight blotting is seen against a starry sky and a moon slice, or Fig. 10 (p. 118) [repeated as Fig. 7 (p. 151)] in which again pressure blotting is seen with a rigorous load of 1 litre of good German beer—let us drink double to that!

Therefore, unfortunately, I cannot recommend Dr. Dunn's book this time.

SSDI 0021-9673(93)E1212-I

Post Scriptum: Reiner's book is 2 cm thick and weighs 673 g (worth every ounce of it!) and seems to be printed on acid-free, low-chlorine paper (ISBN 3-572-30012-0 in Weinheim and 81705 in New York). Reiner is one of the disappearing species belonging to the genus "Blue Finger" (also suspected to be a secret society). In 1979, upon a visit to my laboratory, I had to rescue him from the police in Corso Buenos Aires, where he had taken a shopping break. It turned out that he had just finished staining a focusing gel with Coomassie Blue, and sure enough he had blue fingers. But the shop owner, suspicious of his thick Ostrogote accent, suspected him of being a money forger and called the police. Well, with this book the Blue Finger secret sect strikes again!

Milan (Italy) Pier Giorgio Righetti

PUBLICATION SCHEDULE FOR THE 1994 SUBSCRIPTION

Journal of Chromatography A and *Journal of Chromatography B: Biomedical Applications*

MONTH	O 1993	N 1993	D 1993	J	F	M	A	
Journal of Chromatography A	652/1 652/2 653/1	653/2 654/1 654/2 655/1	655/2 656/1 + 2 657/1 657/2	658/1 658/2 659/1 659/2	660/1 + 2 661/1 + 2 662/1 662/2	663/1 663/2 664/1	664/2 665/1 665/2 666/1 + 2 667/1	The publication schedule for further issues will be published later.
Bibliography Section						681/1		
Journal of Chromatography B: Biomedical Applications				652/1	652/2 653/1	653/2 654/1	654/2 655/1	

INFORMATION FOR AUTHORS

(Detailed *Instructions to Authors* were published in *J. Chromatogr. A*, Vol. 657, pp. 463–469. A free reprint can be obtained by application to the publisher, Elsevier Science B.V., P.O. Box 330, 1000 AH Amsterdam, Netherlands.)

Types of Contributions. The following types of papers are published: Regular research papers (full-length papers), Review articles, Short Communications and Discussions. Short Communications are usually descriptions of short investigations, or they can report minor technical improvements of previously published procedures; they reflect the same quality of research as full-length papers, but should preferably not exceed five printed pages. Discussions (one or two pages) should explain, amplify, correct or otherwise comment substantively upon an article recently published in the journal. For Review articles, see inside front cover under Submission of Papers.

Submission. Every paper must be accompanied by a letter from the senior author, stating that he/she is submitting the paper for publication in the *Journal of Chromatography A* or *B*.

Manuscripts. Manuscripts should be typed in **double spacing** on consecutively numbered pages of uniform size. The manuscript should be preceded by a sheet of manuscript paper carrying the title of the paper and the name and full postal address of the person to whom the proofs are to be sent. As a rule, papers should be divided into sections, headed by a caption (*e.g.*, Abstract, Introduction, Experimental, Results, Discussion, etc.). All illustrations, photographs, tables, etc., should be on separate sheets.

Abstract. All articles should have an abstract of 50–100 words which clearly and briefly indicates what is new, different and significant. No references should be given.

Introduction. Every paper must have a concise introduction mentioning what has been done before on the topic described, and stating clearly what is new in the paper now submitted.

Experimental conditions should preferably be given on a *separate* sheet, headed "Conditions". These conditions will, if appropriate, be printed in a block, directly following the heading "Experimental"

Illustrations. The figures should be submitted in a form suitable for reproduction, drawn in Indian ink on drawing or tracing paper. Each illustration should have a caption, all the captions being typed (with double spacing) together on a *separate sheet*. If structures are given in the text, the original drawings should be provided. Coloured illustrations are reproduced at the author's expense, the cost being determined by the number of pages and by the number of colours needed. The written permission of the author and publisher must be obtained for the use of any figure already published. Its source must be indicated in the legend.

References. References should be numbered in the order in which they are cited in the text, and listed in numerical sequence on a separate sheet at the end of the article. Please check a recent issue for the layout of the reference list. Abbreviations for the titles of journals should follow the system used by *Chemical Abstracts*. Articles not yet published should be given as "in press" (journal should be specified), "submitted for publication" (journal should be specified), "in preparation" or "personal communication".

Vols. 1–651 of the *Journal of Chromatography*; *Journal of Chromatography, Biomedical Applications* and *Journal of Chromatography, Symposium Volumes* should be cited as *J. Chromatogr.* From Vol. 652 on, *Journal of Chromatography A* (incl. Symposium Volumes) should be cited as *J. Chromatogr. A* and *Journal of Chromatography B: Biomedical Applications* as *J. Chromatogr. B.*

Dispatch. Before sending the manuscript to the Editor please check that the envelope contains four copies of the paper complete with references, captions and figures. One of the sets of figures must be the originals suitable for direct reproduction. Please also ensure that permission to publish has been obtained from your institute.

Proofs. One set of proofs will be sent to the author to be carefully checked for printer's errors. Corrections must be restricted to instances in which the proof is at variance with the manuscript.

Reprints. Fifty reprints will be supplied free of charge. Additional reprints can be ordered by the authors. An order form containing price quotations will be sent to the authors together with the proofs of their article.

Advertisements. The Editors of the journal accept no responsibility for the contents of the advertisements. Advertisement rates are available on request. Advertising orders and enquiries can be sent to the Advertising Manager, Elsevier Science B.V., Advertising Department, P.O. Box 211, 1000 AE Amsterdam, Netherlands; courier shipments to: Van de Sande Bakhuyzenstraat 4, 1061 AG Amsterdam, Netherlands; Tel. (+31-20) 515 3220/515 3222, Telefax (+31-20) 6833 041, Telex 16479 els vi nl. *UK*: T.G. Scott & Son Ltd., Tim Blake, Portland House, 21 Narborough Road, Cosby, Leics. LE9 5TA, UK; Tel. (+44-533) 753 333, Telefax (+44-533) 750 522. *USA and Canada*: Weston Media Associates, Daniel S. Lipner, P.O. Box 1110, Greens Farms, CT 06436-1110, USA; Tel. (+1-203) 261 2500. Telefax (+1-203) 261 0101.

Ovomucoid Bonded Column for Direct Chiral Separation

ULTRON ES-OVM

Narrow-Bore Column (2.0 I.D. x 150 mm) for Trace Analyses
Analytical Column (4.6 I.D. , 6.0 I.D. x 150 mm) for Regular Analyses
Semi-Preparative Column (20.0 I.D. x 250 mm) for Preparative Separation

Analysis of Trace FLURBIPROFEN in Metabolite with NARROW-BORE COLUMN

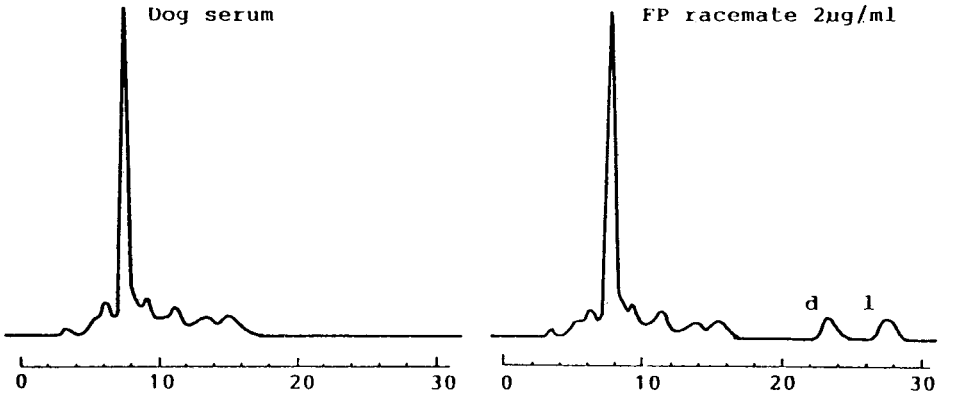

Conditions

Column: ULTRON ES-OVM(2.0I.D. x 150mm)
Mobile Phase: 20mMPhosphate Buffer(pH=3.0)/CH3CN =100/15
Flow Rate: 0.1ml/min
Temperature: 25°C
Injection: 5µl
Detection: UV- 247nm(0.05AUFS)

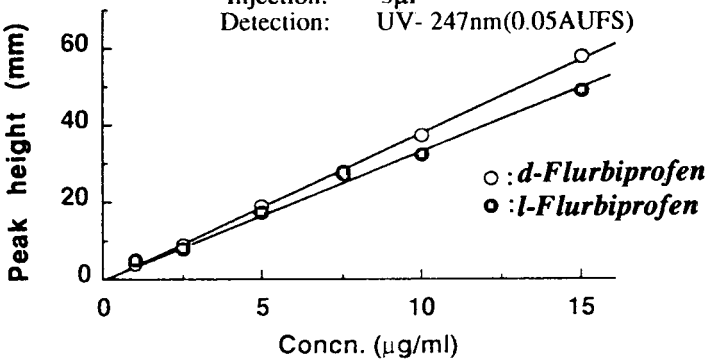

Calibration Curve for Each Enantiomer of Flurbiprofen

SHINWA CHEMICAL INDUSTRIES, LTD.

50 Kagekatsu-cho, Fushimi-ku, Kyoto 612, JAPAN
Phone:+81-75-621-2360 Fax:+81-75-602-2660

In the United States and Europe, please contact:

Rockland Technologies, Inc.

538 First State Boulevard, Newport, DE 19804, U.S.A.
Phone: 302-633-5880 Fax: 302-633-5893

This product is licenced by Eisai Co., Ltd.